FOREWORD

This report was prepared by Manufacturing Laboratories, Inc., Cambridge, Mass., under USAF Contract No. AF33(616)-6838. This contract was initiated under Project No. 7351, "Metallic Materials," Task No. 735101, "Refractory Metals." The work was administered under the direction of the Directorate of Materials and Processes, Deputy Commander/Technology, Aeronautical Systems Division, with Lt. J. Bitzer acting as project engineer.

The period covered by this report is 1 April 1961 to 31 March 1962.

The following personnel are the principal research investigators involved in this program:

Laboratory	Research Personnel
Manufacturing Laboratories, Inc.	B. S. Lement, Morris Cohen, Steven Allen, E. M. Passmore, J. E. Boyd, C. Andersson and I. Vilks
Massachusetts Institute of Technology	D. A. Thomas, M. F. Comerford, E. S. Meieran, J. F. Peck and C. M. Shine, Jr.
Rutgers, the State University	S. Weissman and N. Hosokawa
University of Liverpool	W. S. Owen, D. Hull, C. N. Reid, A. Gilbert, I. McIvor, and T. Ellison
University of Cambridge	P. B. Hirsch and E. Levin

ABSTRACT

Considerable progress has been made by the five research participants in elucidating the relation of substructure to the mechanical properties of tungsten, molybdenum, tantalum and columbium.

ManLabs has shown that during recovery of heavily deformed tungsten wire there is an initial increase in hardness accompanied by increased delineation of etch-pit subboundaries, which may be associated with segregation of interstitials to dislocations. Micro-twinning, which is indicated by a decrease in the effective particle size as determined by x-ray line shape analysis, may also contribute to the initial hardening. The sharp drop in room temperature ductility on annealing above about 1100°C was correlated with the rise of the transition temperture (T_d) above room temperature. Since the crack propagation energy (γ^*) as calculated by the Cottrell-Petch equation does not change appreciably with annealing temperature, it appears that the rise of T_d is mainly due to the increase in width of the fibrous grains. Microstructural observations and x-ray diffraction particle size determinations were also made of substructure in molybdenum, tantalum, and columbium.

M.I.T. has shown by transmission electron microscopy of thin films that competing processes of polygonization and strain induced fiber boundary migration occur on annealing 30-mil tungsten wire up to 1400°C. The texture of tungsten sheet was found to sharpen on recovery-annealing which is attributable to subgrain growth. Determination of textural and microstructural changes during drawing of columbium wire has provided further confirmation of the proposed mechanism of formation of ribbon-like grains in b.c.c. metals which involves restricted slip at high deformations. Measurements made on iron-3.19% silicon indicate that most of the changes in mechanical properties occur during recovery rather than the recrystallization stage.

Rutgers has shown by transmission electron microscopy of thin films of plastically deformed tantalum that the following substructural phenomena occur: a) dislocation pinning by superjogs, b) isolated dislocation loops left behind as debris of moving dislocations, and c) dislocation entanglement to form cells. The tangles appear to be formed by the interactions of dislocations moving on different slip systems. Quantitative strain analyses of tantalum single crystals were carried out using the x-ray back reflection divergent beam method. The maximum principal strain was found to change from positive to negative values as deformation in compression is carried out below and above the upper yield point respectively. This indicates that extensive slip occurs on many systems and results in increased complexity of dislocation tangles. In the case of molybdenum single crystals, the low ductility relative to tantalum is partly attributed to restriction of slip to a limited number of active planes.

Liverpool has shown that a variety of dislocation densities and arrangements can be formed in tantalum by annealing. In a narrow annealing range above the recrystallization temperature, <111>/<100> dislocation network subboundaries are formed; at high temperatures a low density of random dislocations is

observed. The aging of tantalum containing oxygen, nitrogen and carbon can be divided into three stages: a) Snoek-ordering of interstitials in the strain field of the dislocation resulting in an increase in the difficulty of slip propagation, b) long-range diffusion of interstitials to dislocations giving weak locking, and c) strong temperature-independent locking of dislocations. The binding energy, as determined by quenching experiments, is about 0.53 e.v. If the total interstitial content is low (less than about 50 ppm), the locking parameter (k_y) increases as the dislocation density is decreased by annealing at higher temperatures; for higher contents, the dislocations are apparently saturated at all annealing temperatures and k_y is unaffected. The stress for slip propagation (σ_i) can be altered by changes in substructure and interstitial content but the effect is small. All the yield data can be explained satisfactorily by a modified Cottrell-Petch theory in which it is assumed that the necessary local stress concentration is achieved near the tip of a slip band blocked at a grain boundary. Slip in the neighboring grain is nucleated by unlocking of annealed-in dislocations provided that these are weakly locked; if strongly locked, these dislocations play no part in the yield process and the slip dislocations form from virgin crystal at or near a grain boundary. Transmission electron-micrographic evidence of the latter process has been obtained. The condition that unstable plastic flow (necking) occurs before the heterogeneous Luders strain is complete has been derived in terms of the strain-hardening exponent (n) and the yield parameters (k_y and σ_i). The effects of metallurgical variables such as grain size, substructure and strain-aging on the plastic-instability transition temperature for impure tantalum have been assessed quantitatively. Down to at least 77°K, no cleavage fracture has been found in polycrystalline tantalum; however, {100} cleavage occurs in suitably oriented single crystals at 195°K.

Cambridge has found that the activation energy for the annealing-out of dislocation loops in columbium and tantalum, as observed by transmission electron microscopy of thin films, corresponds to 3.0 ±0.5 e.v. This relatively low value suggests that the recovery process may involve pipe-diffusion instead of volume-diffusion as generally assumed for the process of dislocation climb.

This technical documentary has been reviewed and is approved.

I. Perlmutter
Chief, Physical Metallurgy Branch
Metals and Ceramics Laboratory
Directorate of Materials and Processes

TABLE OF CONTENTS

TABLE OF CONTENTS (Cont.)

TABLE OF CONTENTS (Cont.)

LIST OF FIGURES

LIST OF FIGURES (Cont.)

LIST OF FIGURES (Cont.)

LIST OF FIGURES (Cont.)

LIST OF FIGURES (Cont.)

LIST OF FIGURES (Cont.)

LIST OF FIGURES (Cont.)

LIST OF FIGURES (Cont.)

LIST OF FIGURES (Cont.)

LIST OF FIGURES (Cont.)

LIST OF FIGURES (Cont.)

LIST OF TABLES

LIST OF TABLES (Cont.)

I. SUMMARY OF RESULTS

The main results of the five research participants are summarized below. These results as well as supporting information are discussed in detail in parts III to VII of this report. Definitions of metallurgical terms as used for describing substructure in this report are given in Appendix B. A list of publications that have resulted thus far from the work accomplished on this program is given in Appendix A.

A. Manufacturing Laboratories, Inc.- Ductile-Brittle Transition in Refractory Metals

1. Light microscopic examination revealed that the structure of the as-drawn tungsten (W-P4) wire consists of heavily deformed fibrous grains containing relatively few etch-pit subboundaries. Annealing at temperatures up to 800°C results in the appearance of subboundaries, consisting of clearly delineated etch pits; the number of these subboundaries per unit length measured transverse to the wire axis also increases to a maximum. This increase in subboundaries may be associated with segregation of interstitial elements to dislocations.

2. The microstructural changes during recovery-annealing above 800°C consist of a progressive widening of the fibers, polygonization, and subgrain growth. The resultant structure at 1400°C consists of irregular fibrous grains, composed of slightly elongated subgrains with sharply defined boundaries. In the range of 1500 to 1800°C, rapid, preferential grain growth occurs at the expense of the fibrous structures.

3. The hardness was found to increase slightly during isothermal recovery-annealing and then go through a maximum. The temperature dependence of the maximum corresponds to an activation energy of approximately 35 kcal/mol. Above about 800°C, the hardness and strength properties decrease rapidly.

4. The ductile-brittle transition temperature (T_d) increases linearly from about -10°C after annealing at 800°(10-minute time) to +50° after annealing at 1400°C. There is a sharp decrease in room temperature ductility that correlates with the rise of T_d above room temperature. The ductility measured above T_d, however, continues to increase with increasing annealing temperature and goes through a maximum at about 1200°C.

5. Using the Cottrell-Petch equation, the calculated value of the crack propagation energy (γ') for tungsten (W-P4) wire in the as-drawn condition is 1.1×10^4 ergs/cm^2 and does not change appreciably on annealing up to 1400°C even though extensive polygonization and subgrain growth occur.

6. It appears likely that the increase in T_d with increasing annealing temperature from 800° to 1400°C is mainly due to the increase in fiber width.

7. Based on the Griffith-Orowan equation, the calculated critical crack length for test temperatures in the vicinity of T_d was found to be the same order of magnitude as the fiber width.

Manuscript released by the authors April 1962 for publication as a WADD Technical Report.

8. A slight broadening of the (400) diffraction lines of tungsten (W-P2) strip, which reaches a maximum at about 700°C (1-hour time), has been found by statistical analysis. This broadening effect is believed to be associated with the formation of twin faults (micro-twins) reported by Rutgers to occur during the annealing of tungsten (W-P5) foil.

9. As determined by x-ray diffraction line shape analysis, the particle size terms of Ta-P2, Mo-P2 and Cb-P2 strip were found to increase slightly with time during isothermal recovery-annealing in the range of 600 to 850°C.

10. The particle size terms of Mo-E1, Mo-E2 and Mo-E3 strip in the most severely deformed state are between 1100 and 1200A in the [100]. Faulting appears to play only a minor role in the deformation of Mo-E2, and appears to be absent in Mo-E1 and E3.

11. The particle size terms of Cb-E1 and E4 strip after 80% R.A. are approximately 750 and 500A. The difference is attributed to the 500 ppm higher oxygen content of Cb-E4. Faulting appears to have no effect in the deformation of either material.

12. The [100] particle size terms of Ta-E1, E2, E3 and E4 strip after 80% R.A. range from approximately 800 to 450A in the order listed, which correlates with the order of increasing hardness. Faulting appears to have an appreciable effect in the deformation of these materials.

13. The substructure in as-rolled molybdenum (Mo-E1, E2 and E3) strip was found to be well-developed and to change only slightly during subsequent recovery-annealing.

14. The tensile transition temperature of molybdenum (Mo-E1) strip was found to decrease from -50°C in the recrystallized condition to -125°C after 40% reduction at 900°C plus 80% reduction at 400°C.

15. The substructure found by light microscopy in Ta-E1, E2, E3, and E4 wires (both recrystallized and cold worked) consists of randomly distributed etch pits. No well-defined subgrains were observed. In Cb-E1 and E4 wires, no etch pits or other substructure was found.

B. Massachusetts Institute of Technology - Fibering in Refractory Metals

1. The transition temperature of 30 mil tungsten (W-P4) wire is reduced about 100°C by drawing at 150°C to 20 mils. Room-temperature tensile tests show that increased annealing temperature first reduces and then increases ductility up to about 1100°C, above which there is a sharp drop as the transition temperature increases to room temperature and above.

2. Transmission electron microscopy of longitudinal sections of 30-mil W-P4 wire has revealed many important details of the substructure of worked and annealed tungsten. Results to date indicate that the competing processes of polygonization and strain-induced boundary migration of fiber boundaries dominate the annealing up to 1400°C.

3. The texture of tungsten sheet (W-P3 and W-P5) is predominantly (100) [011] . Annealing to 1300°C produces a slight sharpening of the texture, which is attributed to subgrain growth without a textural change.

4. Texture and microstructure changes during drawing of columbium (Cb-E4) wire partially confirm the suggestions in previous reports concerning the origin of ribbon-like grains as a result of heavy drawing of b.c.c. metals. The microstructure changes proceed as observed before, but the concurrent texture changes are in need of continued study.

5. Mechanical property determinations of drawn and annealed Fe-3.19% Si show that most of the return of strength and ductility to the annealed values occurs prior to recrystallization. This behavior in many ways parallels that of the refractory metals. A growing body of data suggests that extensive softening by recovery prior to recrystallization is common in many metals and alloys.

C. Rutgers, The State University — Study of Superjogs, Dislocation Tangles and Cell Structure of Refractory Metals

1. Tantalum (Ta-E1) foil subjected to progressive amounts of tensile elongation up to 3% at room temperature following a 1500°C recrystallization-anneal was found by transmission electron microscopic observation of thin-film specimens to display the following dislocation features:

a) superjogs — enlarged dislocation jogs arising from cross-slip of screw dislocations;

b) edge dislocation dipoles — edge dislocation segments associated with bowed-out screw dislocations;

c) isolated dislocation loops — pinched-off dislocation dipoles, probably arising from considerable cross-slip;

d) dislocation tangles.

2. The dislocation tangles appear to be formed by the interaction of dislocations moving on different slip systems.

3. In the as-recrystallized condition (1000°C), hexagonal dislocation networks were observed, which are the result of the following reaction:

$$\frac{a}{2}[111] + \frac{a}{2}[1\bar{1}\bar{1}] = a[100]$$

4. In order to elucidate the mechanism of the formation of dislocation tangles, quantitative analyses of the strain distribution in tantalum single crystals (Ta-E5) deformed in compression up to 1.44% were carried out. These analyses are based on precision measurements of d-spacing using the x-ray back-reflection divergent beam method. The following evidence was obtained:

4.1 Slip activity occurs on different slip systems for deformation below the upper yield point corresponding to 0.077% and 0.097% compression. The formation of dislocation tangles is attributed to this slip activity.

4.2 The maximum principal strain for the deformation below the upper yield point exhibits positive values, indicating lattice expansion in the direction of the maximum principal strain; whereas for deformation above the upper yield point (1.44% compression), a negative value was obtained, indicating lattice contraction.

4.3 Extensive slip on many slip systems must have occurred after 1.44% compression in order to account for the shift in direction of the maximum principal strain. This is in agreement with the increased complexity of dislocation tangles as observed by transmission electron microscopy.

5. Based on a preliminary study involving the x-ray back-reflection divergent beam method applied to Mo-E5 single crystals pulled in tension at room temperature, the relatively low ductility of molybdenum compared to tantalum appears to be associated with the observed restriction of plastic deformation in molybdenum to fewer active slip planes.

D. University of Liverpool — Yield Phenomena in Refractory Metals

1. Annealed polycrystalline tantalum with greater than 40 ppm of interstitial solute exhibits all the general features of discontinuous yielding.

2. The flow stress at zero strain (σ_f^0) and the corresponding Petch frictional stress (σ_i) are unaffected by variations in dislocation density between 5×10^9 and 5×10^{10} dislocations/cm^2. The non-thermally activated component of the flow stress is greater in tantalum containing 150 ppm of oxygen than in the two alloys containing less than 75 ppm total interstitial solute.

3. When the interstitial solute content is less than 75 ppm, the Petch locking parameter (k_y) increases with decreasing dislocation density. With more than 150 ppm of oxygen there is no significant variation of k_y. In annealed tantalum containing oxygen or nitrogen as the major interstitial solute, k_y increases with decreasing testing temperature but when the major solute is carbon there is no variation.

4. Measurement of σ_i by extrapolation of the plot of yield stress versus $d^{-1/2}$ to infinite d and by extrapolation of the homogeneous strain-hardening curve to its intersection with the elastic line give the same value of σ_i which is a work-hardening parameter that is unconnected with dislocation unlocking.

5. On annealing cold worked tantalum at successively higher temperatures, dislocation rearrangements occur in the following sequence: a) rearrangement and annihilation without the formation of subboundaries, b) formation of subboundary networks, c) coarsening of the networks, and d) removal of the networks accompanied by a marked decrease in dislocation density. Most of the networks are of the <111>/<100> type.

6. On quenching annealed tantalum (Ta-E2) from successively higher temperatures the room-temperature values of σ_i and n do not vary with quenching temperature between 293° and 1200°K, but k_y decreases with increasing

quenching temperature and approaches zero at 950°K. At 1200°K the discontinuous yield point reappears and k_y has a positive value. Assuming that the decrease in k_y with increasing quenching temperature is due to evaporation of interstitial solute atoms from the dislocations, the binding energy of solute to a dislocation is about 0.53 e.v.

7. The presence of a very early stage in the strain-hardening process, as suggested by Stein and Low, has been confirmed. This stage in tantalum is characterized by an increase in σ_i; and a corresponding decrease in n with increased aging time, and is probably due to Snoek ordering of interstitials in the dislocation strain fields.

8. The second stage of aging in tantalum (corresponding to the Wilson-Russell first stage) is characterized by an increase in k_y with aging time, σ_i and n remaining unchanged. This effect is produced by long-range diffusion of interstitials to dislocations.

9. The variation of flow stress with dislocation density of tantalum can be represented by:

$$\sigma_f = \sigma_o + \alpha \mu b \sqrt{N}$$

The value of σ_o is affected markedly by the initial dislocation density.

10. The extent of the yield drop in tantalum single crystals is independent of crystal orientation.

11. The cleavage plane in tantalum single crystals is $\{001\}$.

12. In terms of the usual yield and strain-hardening parameters, the condition that necking should occur before the heterogeneous deformation (Luders strain) is complete is

$$k_y d^{-1/2} = \left[\frac{(En)^n}{\sigma_i^{n-1}} - \sigma_i \right]$$

The highest plastic instability temperature (T_{PI}) occurs in fine-grained tantalum with a high oxygen content. The increase of the plastic instability temperature with decreasing grain size is small between $d^{-1/2} = 1.0$ to $10.0\ mm^{-1/2}$ and, consequently, the use of coarse-grained tantalum to reduce the instability temperature is not justified in practice.

E. University of Cambridge — A Transmission Electron Microscope Study of Defects in Columbium and Tantalum

1. Based on transmission electron microscopic observations of the annealing-out of dislocation loops in thin-film specimens of cold rolled and annealed single crystals, the activation energy for self-diffusion in columbium and in tantalum as calculated by the Silcox-Whelan formula were both found to be 3.0 ± 0.5 e.v.

2. This value is significantly lower than that reported by Resnick (4.33 e.v.) for columbium, which suggests that the recovery process may involve "conservative climb" controlled by dislocation pipe diffusion instead of regular climb, by volume diffusion.

3. As distinct from columbium, marked precipitation was observed in the tantalum thin films recovery-annealed above about 600°C. This results in "punched-out" dislocation loops and helices due to differential thermal contraction stresses on cooling.

II. INTRODUCTION

A. Scope

This progress report covers the period of 1 April 1961 to 31 March 1962 on Contract No. AF33(616)-6838 which has expired. The program is being continued on Contract No. AF33(616)-8424. The status of fabrication and distribution of experimental materials is given in this part of the report. Parts III, IV, V, VI, and VII contains the individual reports of the five research participants. A list of reports and papers that have resulted at least partly from the work accomplished so far on the current program is given in Appendix A.

B. Status of Experimental Materials

1. Interstitial Contents - The results of interstitial analyses performed by National Research Corp. on starting and fabricated materials are summarized in Tables 1, 2, and 3. Table 3 shows that contamination of Ta-E1 occurred by both vacuum annealing and wire drawing operations. By chemical milling, it was possible to remove the carbon contamination; however, the oxygen contamination due to process annealing exists throughout the wire section.

2. Ingots - Because of excessive difficulty encountered by the General Electric Co. in meeting the chemical and surface requirements, the W-E3 and W-E4 ingots have been dropped from the program. The Mo-E4, W-E1, and W-E2 ingots made recently were hot extruded and submitted to Westinghouse (Blairsville). Some question exists as to their suitability for subsequent fabrication.

3. Fabrication - The status of fabrication of the experimental Ta, Cb, W and Mo materials to wire and strip is given in Tables 4 and 5 respectively. The details of fabrication schedules for Ta and Cb wire and strip are given in Tables 6 and 7 , for Mo wire bar and strip bar in Table 8, and for Mo strip in Table 9.

4. Distribution - The distribution of experimental materials in crystal, wire and strip form is given in Tables 10, 11, and 12 respectively.

Table 1

Interstitial Contents of Experimental Materials in Ingot, Extruded Billet or Crystal Form

Item	Other Identification	Form	Interstitial Contents in ppm. C	N	O	H
W-E1-1	S-152	billet	10	10	3	-
W-E1-2	S-158	billet	9	7	12	-
W-E1-3	S-167	billet	5	10	3	-
W-E2-1	S-154	billet	5-39	9	2	-
W-E2-2	S-168	billet	63-241	14	5	-
W-E5-1	-	crystal	9	4	2	-
W-E5-12	-	crystal	10	21	2	-
Mo-E1	S-119	billet	12	3	5	-
Mo-E2*	S-141	billet	80	< 2	2	-
Mo-E3-1*	S-128	billet	8	8	3	-
Mo-E3-2*	S-129	billet	12	2	8	-
Mo-E4	S-169	billet	12	3	35-80	-
Mo-E5-17	-	crystal	8	2	< 1	-
Mo-E5-18	-	crystal	4	3	13	3
Mo-E7	S-107	billet	204	4	3	-
Ta-E1	-	ingot	<10	18	7	-
Ta-E2	-	ingot	35	12	12	-
Ta-E3	-	ingot	8	100	14	-
Ta-E4	-	ingot	3	12	94	-
Ta-E5	-	crystal	8	20	40	-
Cb-E1	-	ingot	15	80	96	-
Cb-E4	-	ingot	16	76	625	-
Cb-E5	-	crystal	25	50	53	-

*Intended as Mo-E3 compositions, but correspond to Mo-E1.

Table 2

Interstitial Contents of Fabricated Experimental Materials

Item	Form.	Thickness or Diameter mils	Interstitial Content in ppm. C	N	O	H
Mo-E1-E-1	strip	30	32	-	22	-
Mo-E1-E-2	strip	30	34	-	20	-
Mo-E1-F-1	strip	30	13	4	23	0.8
Mo-E1-H-7	strip	30	42	-	31	-
Mo-E1-H-1	strip	30	53	-	17	-
Mo-E1-TA	rod	230	33	15	5.5	-
Mo-E1-T_1B	rod	230	27	10	6	-
Mo-E2-C-1	strip	30	44	-	15	-
Mo-E2-E-1	strip	30	75	3	46	-
Mo-E2-H-1	strip	30	40	-	13	-
Mo-E2-H-8	strip	30	36	-	65	-
Mo-E2-1*	rod	230	38	5	381	1.0
Mo-E2-1	rod	230	49	-	2.5	-
Mo-E2-1	rod	230	56	-	2.1	-
Mo-E2-2	rod	230	54	-	3.3	-
Mo-E2-2	rod	230	59	-	17	-
Mo-E3-E-1	strip	30	-	7	18	-
Mo-E3-E-1	strip	30	-	8	26	-
Mo-E3-F-2	strip	30	12	7	29	0.1
Mo-E3-H-4	strip	30	-	14	12	-
Mo-E3-H-8	strip	30	-	15	13	-
Mo-E3-T_2A	rod	230	15	17	8.3	-
Mo-E3-T_2C	rod	230	24	8	5.0	-

*Specimen probably not representative.

Table 2 (Cont'd.)

Item	Form	Thickness or Diameter mils	Interstitial Content in ppm. C	N	O	H
Ta-E1-W2-.067	wire	30	6	-	24	5
Ta-E2-W0-.030	wire	30	63	-	50	27
Ta-E2-W1-.030	wire	30	62	-	96	-
Ta-E2-W1-.072	wire	30	67	-	48	-
Ta-E3-W0-.030	wire	30	-	19	220	21
Ta-E3-W1-.030	wire	30	-	26	240	-
Ta-E3-W1-.072	wire	30	-	20	70	-
Ta-E4-W0-.030	wire	30	-	-	65	25
Ta-E4-W1-.030	wire	30	-	-	50	-
Ta-E4-W1-.072	wire	30	-	-	52	-
Ta-E5-W0-.030	wire	30	29	9	41	6
Ta-E5-W1-.030	wire	30	28	6	167	3
Ta-E1-S1-.030	strip	30	10	18	46	2
Ta-E1-S1-.150	strip	30	8	17	40	125
Ta-E2-S1-.030	strip	30	70	-	72	-
Ta-E2-S1-.150	strip	30	67	-	-	-
Ta-E3-S1-.030	strip	30	-	103	39	-
Ta-E3-S1-.150	strip	30	-	65	-	-
Ta-E4-S1-.030	strip	30	-	-	132	-
Ta-E4-S1-.150	strip	30	-	-	150	-
Ta-E6-Q	rod	125	3	15	2	-
Cb-E1-W0-.030	wire	30	15	79	128	8
Cb-E1-W1-.030	wire	30	27	50	140	4
Cb-E1-W1-.072	wire	30	12	80	161	9
Cb-E4-W0-.030	wire	30	-	-	687	17
Cb-E4-W1-.030	wire	30	-	-	767	-
Cb-E4-W1-.072	wire	30	-	-	628	-
Cb-E5-W0-.030	wire	30	90	35	91	5
Cb-E5-W1-.030	wire	30	45	50	550	9
Cb-E1-S1-.030	strip	30	23	46	130	2
Cb-E1-S1-.150	strip	30	20	90	184	65
Cb-E4-S1-.030	strip	30	-	-	626	-
Cb-E4-S1-.150	strip	30	-	-	694	-
Cb-E6-L	rod	125	3	27	25	.3

Table 3

Variation in Interstitial Content of Ta-E1

Due to Both Vacuum Annealing and Wire Drawing

Condition	Interstitial Content in ppm. C	N	O	H
Ingot top	<10	20	9	-
Ingot bottom	<10	15	5	-
0.125 wire as drawn	-	-	5	-
0.125 wire recrystallized by Vac-Hyd	13	-	62	-
0.0303 wire as drawn	27	-	103	-
Etched to 0.027	9	11	58	9
After vacuum heat treating 1 hour each at 925°C and 950°C at Kinetics	6	25	77	3
After additional 1 hour at 975°C	10	14	86	0.7
After additional 1 hour at 1010°C*	13	11	90	0.5

*Final item designation is Ta-E1-W2-.0303.

Table 4

Status of Fabrication of Experimental Materials to Wire

Item	Now at*	Present Status
Mo-E1	M. L.	1/4 - inch rod
Mo-E2	M. L.	1/4 - inch rod
Mo-E3	M. L.	1/4 - inch rod
Mo-E5	West. (Bloom.)	Being fabricated
Ta-E1-W0	M. L.	Completed
Ta-E1-W1-.030 to 0.67	M. L.	Completed
Ta-E1-W2-.030	M. L.	Completed
Ta-E1-W2-.0303 to .067	In transit	Completed
Ta-E2-W0	M. L.	Completed
Ta-E2-W1-.030	M. L.	Completed
Ta-E2-W1-.0339 to .072	In transit	Completed
Ta-E3-W0	M. L.	Completed
Ta-E3-W1-.030	M. L.	Completed
Ta-E3-W1-.0339 to .072	In transit	Completed
Ta-E4-W0	M. L.	Completed
Ta-E4-W1-.030	M. L.	Completed
Ta-E4-W1-.0339 to .072	In transit	Completed
Ta-E5-W0	M. L.	Completed
Ta-E5-W1	M. L.	Completed
Cb-E1-W0	M. L.	Completed
Cb-E1-W1-.030	M. L.	Completed
Cb-E1-W1-.0339 to .072	In transit	Completed
Cb-E4-W0	M. L.	Completed
Cb-E4-W1-.030	M. L.	Completed
Cb-E4-W1-.0339 to .072	In transit	Completed
Cb-E5-W0	M. L.	Completed
Cb-E5-W1	M. L.	Completed

*Company names

G. E. ..... General Electric
West. (Bloom.) .... Westinghouse at Bloomfield
West. (Blairs.) .... Westinghouse at Blairsville
W. C. ..... Wah Chang
M. L. ..... ManLabs

Table 5

Status of Fabrication of Experimental Materials to Strip

Item	Now at *	Status
W-E1	West. (Blairs.)	Being fabricated
W-E2	West. (Blairs.)	Being fabricated
W-E5	West. (Bloom.)	Being rolled
Mo-E1	M. L.	Completed
Mo-E2	M. L.	Completed
Mo-E3	M. L.	Completed
Mo-E4	West. (Blairs.)	Being fabricated
Mo-E5	West. (Bloom.)	Being fabricated
Ta-E1-S0	M. L.	Completed
Ta-E1-S1-.030 to .150	M. L.	Completed
Ta-E2-S0	M. L.	Completed
Ta-E2-S1-.005	M. L.	Completed
Ta-E2-S1-.030 to .150	M. L.	Completed
Ta-E3-S0	M. L.	Completed
Ta-E3-S1-.005	M. L.	Completed
Ta-E3-S1-.030 to .150	M. L.	Completed
Ta-E4-S0	M. L.	Completed
Ta-E4-S1-.005	M. L.	Completed
Ta-E4-S1-.030 to .150	M. L.	Completed
Ta-E5-S0	M. L.	Completed
Ta-E5-S1	M. L.	Completed
Cb-E1-S0	M. L.	Completed
Cb-E1-S1-.005	M. L.	Completed
Cb-E1-S1-.030 to .150	M. L.	Completed
Cb-E4-S0	M. L.	Completed
Cb-E4-S1-.005	M. L.	Completed
Cb-E4-S1-.030 to .150	M. L.	Completed
Cb-E5-S0	M. L.	Completed
Cb-E5-S1	M. L.	Completed

*Company names

G. E.	General Electric
West. (Bloom.) .	Westinghouse at Bloomfield
West. (Blairs.) .	Westinghouse at Blairsville
W. C.	Wah Chang
M. L.	ManLabs

Table 6a

Fabrication Schedule for Ta and Cb Wire and Strip

Ingot	Ta-E1	Ta-E2 Ta-E3 Ta-E4	Cb-E1	Cb-E4	Cb-E5 Ta-E5
1. Common fabrication from	3 - 7/8 d	3 - 1/4 d	3 - 1/2 d	3 - 1/4 d	0.20 d
a. Breakdown to:	3 - 1/4 d	-	2 sq.	2 sq.	-
by	Cold forge	-	Cold press	Cold press	
b. Cold swaged to:	1 - 1/8 in. diam. then wire and strip bars separated.				
2. Wire production					
a. Cold swaged to:	5/8 d	3/4 d	3/4 d	3/4 d	0.088 d
b. Cold drawn to:	1/8 d	-	1/8 d	1/8 d	0.033 d
c. Chemically milled to:	-	-	0.10 d*	0.11 d*	0.030 d
d. Process annealed (recrystallized)	1165°C 1/2 hr	-	825°C 1 hr*	1 hr. each 825, 850 & 875°C*	-
e. Cold drawn to	graded sizes to yield 80-0% R.A., (Table 6b).				
f. Chemically milled** by 0.003 in diameter, and vacuum annealed to recrystallize, (Table 7).					
g. Cold drawn*** to final dimension, (Table 6b), and chemically milled by 0.003 in diameter.					
3. Strip production					
a. Cold forged to	5/8 x 1 - 1/8	7/16 x 1 - 1/2	3/8 x 1 - 1/2	3/8 x 2	-
b. Process annealed (recrystallized)	1165°C 1/2 hr	-	1 hr each 825, 850 & 875°C*	1 hr each 825, 850, 875 & 915°C*	-
c. Cold rolled to:	graded sizes to yield 80-0% R.A., (Table 6b)				0.005
d. Chemically milled to clean surfaces, and vacuum annealed to recrystallize (Table 7).					
e. Cold rolled to final size of 0.030 and chemical milled to clean surfaces.					-

Notes:

a. All dimensions in inches.
b. In all fabrication operations the material was reversed between passes.
c. W0 and S0 material removed before annealing of steps 2f and 3d respectively.
d. Foil production: S0 and S1 to final dimension in step 3c, S2 in step 3e.
* Omitted in fabricating W0X and S0X materials.
** Except Ta-E1-W1 which was not milled prior to annealing.
*** At room temperature, except Ta-E1-W1-DI which were at -80°C.

Table 6b

Nominal Reductions in Area and Sizes of Ta and Cb Wire and Strip

	Ta-E1-W1		Ta-E1-W2		Ta-E2, Ta-E3, Ta-E4, Cb-E1, Cb-E4 wire			All strip	
R.A.	graded drawn diam.	final drawn diam.	graded drawn diam.	final drawn diam.	graded drawn diam.	chemically milled diam.	final drawn diam.	inter-mediate thickness	final thick-ness
corresponding step of Table 6a	2e* in.	2g in.	2e* in.	2g in.	2e in.	2f* in.	2g in.	3c* in.	3e in.
80%	0.0671	0.0300	0.0671	0.030	0.0750	0.072	0.033	0.150	0.030
40%	0.0388	0.0300	0.0388	0.027	0.0440	0.041	0.033	0.050	0.030
20%	0.0336	0.0300	0.0336	0.027	0.0410	0.038	0.033	0.0375	0.030
10%	0.0316	0.0300	0.0316	0.0265	0.0380	0.035	0.033	0.0333	0.030
5%	0.0308	0.0300	0.0308	0.027	0.0369	0.0339	0.033	0.0316	0.030
2%	0.0303	0.0300	0.0303	0.0265	0.0369	0.0333	0.033	0.0306	0.030
0%	0.0300	-	0.0300	-	0.0330	0.030	-	0.0300	-

All wires, except some pilot lots, were chemically milled to 0.003 smaller diameter from the final drawn diameter.

*Nominal sizes for designation of material.

Table 7

Recrystallization Annealing Schedule of Ta and Cb Wire and Strip

Materials were subjected to 1 hr. vacuum anneals at approximately:

A	850°C	D	945°C	G	1030°C	J	1150°C
B	885°C	E	970°C	H	1060°C		
C	930°C	F	1005°C	I	1095°C		

After each run material was cooled to room temperature, and specimens metallographically examined for recrystallization.

Nominal R.A., %	Wire Ta-E1-W2*	Ta-E2	Ta-E3	Ta-E4	Ta-E5	Cb-E1	Cb-E4	Cb-E5
80	CDEFG	GGIJ	CDFH	GGIJ	-	AC	AC	-
40	CDEF	GGIJ	CDF	GG	-	AC	AC	-
20	CDEF	GGIJ	CDF	GGI	-	AB	AC	-
10	CDEF	GGIJ	CDFH	GGHI	-	**	AC	-
5	CDEF	GGIJ	CDFH	GG	-	AB	AC	-
2	CDEF	-	-	-	-	AB	AC	-
0	CDE	GGI	CDF	GG	DEFIJ	AB	AC	***
	Strip							
	Ta-E1	Ta-E2	Ta-E3	Ta-E4	Ta-E5	Cb-E1	Cb-E4	Cb-E5
80	CDEFGHI	GIJJ	GG	CDE	-	ACEF	ACEF	-
40	CDEFGHI	GIJJ	GG	CDE	-	AB	ACE	-
20	CDEFGH	GIJ	GGH	CDE	-	AC	ABD	-
10	CDEFGH	GIJ	GG	CDE	-	AB	ABD	-
5	CDEFGH	GIJ	GG	CDE	-	AC	AC	-
2	CDEFGH	-	-	-	-	-	-	-
0	CDEFGH	GIJ	GG	CDE	-	AB	AC	-
Foil (S1 only)	-	G	G	D	DEF	AC	AC	ACFI

*All Ta-E1-W1 annealed 1/2 hr. at 1180°C.
**Two sublots: CB-E1-W1-.035-C = AC, Cb-E1-W1-.035 D = AB.
***Cb-E5-W10, 15 = ACF Cb-E5-W17 = AC Cb-E5-W24 = ACEF
Cb-E5-W13 = AB Cb-E5-W22 = ACFF

Example: Ta-E3-W1-.038 - This is wire of nominally 20% R.A. (from Table 6b) and had annealing treatments CDF (from above) which were: 1 hour at 930°C and cooling to room temperature, then 1 hour at 945°C and cooling to room temperature, and then 1 hour at 1005°C.

Table 8

Fabrication Schedule for Mo Wire and Strip Bars

A. Mo-E1 Billet

1. Cut off nose and tail ends, macroetched and photographed.
2. Cut billet into 5 sections as shown below:

	T4	T3	T2	T1	T	
Nose End	3-1/4"	4-3/4"	4-3/4"	5-1/4"	5-1/4"	Tail End

T, T1 - 45% of billet weight for wire rod.
T2 - for strip item H.
T3 - for strip items A, B, C, E, and G.
T4 - for strip items D and F.

3. Section lathe conditioned to 1-3/4" diameter and spot ground where necessary.
4. FORGING IN ARGON ATMOSPHERE

4.1 Wire Bar - after a 50% reduction each of the bars was cut in two and further forged to 3/4" diameter.

Item	Forge Temp. °C	Forged Size	Conditioned Size
T-a	1250	3/4" dia. x 14-1/8"	.700" dia. x 13-7/16"
T-b	1250	3/4" dia. x 12-1/8"	.700" dia. x 11-7/16"
T1-a	1250	3/4" dia. x 13-3/4"	.700" dia. x 11-7/8"
T1-b	1250	3/4" dia. x 12-1/4"	.700" dia. x 11-5/8"

4.2 Strip Bar

Item	Forge Temp. °C	Forged Size	Conditioned Size
T2	1150	5/8" x 1-5/8" x 11"	.597" x 1-5/8" x 9-7/8"
T3	1250	5/8" x 1-9/16" x 12"	.562" x 1-5/8" x 10-15/16"
T4	1250	5/8" x 1-1/2" x 8-5/16"	.570" x 1-1/2" x 7-1/4"

B. Mo-E2 Billet

1. Received billet Mo-E2 - 1-7/8" diameter by length - 19.9 lbs.
2. Billet cut into four pieces as shown below and lathe conditioned to 1-3/4" diameter by length.

T4	T3	T2	T1
4-1/2"	3-1/4"	3"	5"

T1 - for wire rod
T2 - for strip item H
T3 - for strip items A, B, C, E, F
T4 - for strip items G and D.

Table 8 (Continued)

Fabrication Schedule for Mo Wire and Strip Bars

3. FORGING IN ARGON ATMOSPHERE

3.1 Wire Bar - after a 50% reduction the bar was cut in two and further forged to 3/4" diameter.

Item	Forge Temp. °C	Forged Size	Conditioned Size
T1	1275-1285	3/4" x 26"	.725 x 12 - 2 pcs.

3.2 Strip Bar

Item	Forge Temp. °C	Forged Size Inches	Conditioned Thickness
T2	1200	1-5/16 x 5/8 x 9-1/6	.600
T3	1275	1-5/16 x 5/8 x 12-3/4	.604
T4	1275	1-7/16 x 5/8 x 9-5/8	.594

4. Swaging of Section T1 (.725 x 12" long - 2 pcs.)

Piece Number	Die Size	Total Length	Temp. °C Inlet
Pc. 1	.710	13"	950
	.639	15"	950
	.546	21"	950
	.467	28"	950
	.421	34"	950
	.360	45"	950
	.325	56"	900
	.279	76"	900
	.250	---	900
Pc. 2	.710	13"	950
	.639	15"	950
	.546	21"	950
	.467	28"	950
	.421	34"	950
	.360	45"	950
	.325	56"	900
	.279	76"	900
	.250	---	900

C. Mo-E3 Billet

1. Cut off nose and tail ends, and macroetched. No time to photograph billet.
2. Cut billet into 4 sections as shown below.

Table 8 (Continued)

Fabrication Schedule for Mo Wire and Strip Bars

Nose End	T3	T2	T1	T	Tail End
	3-5/8"	8-1/8"	3-5/8"	3-5/8"	

T2 - 45% of billet weight for wire rod.
T - for strip item H
T1 - for strip items A, B, C, E and G.
T3 - for strip items D and F.

3. Sections lathe conditioned to 1-3/4" diameter and spot ground where necessary.

4. FORGING IN ARGON ATMOSPHERE

4.1 Wire Bar - after a 50% reduction the bar was cut into 3 pieces and further forged to 3/4" diameter.

Item	Forge Temp. °C	Forged Size	Conditioned Size
T2-a	1250	3/4" dia. x 14-1/4"	3/4" dia. x 13-3/8"
T2-b	1250	3/4" dia. x 12-5/8"	3/4" dia. x 11-1/8"
T2-c	1250	3/4" dia. x 13-5/8"	3/4" dia. x 12-15/16"

4.2 Strip Bar

Item	Forge Temp. °C	Forged Size	Conditioned Size
T	1150	5/8" x 1-5/8" x 8-5/8"	.596" x 5/8" x 7-1/8"
T1	1250	5/8" x 1-5/8" x 8-3/4"	.577 x 1-5/8" x 6-7/8"
T3	1250	5/8" x 1-5/8" x 9"	.582" x 1-5/8" x 4-9/16"

Table 9a

Fabrication Schedule for Mo-El Strip

Item*	Temp. °C	Initial Thickness Inches	No. of Passes	Initial Heat Time Min.	Reheat Times Min.	Final Thickness Inches	Approximate Reduction %
T2-H	1000	.579	5	5	2-3	.280	53.1
"	900	.275	3	4	2	.163	40.7
"	400	.159/.160	9	5	2-3	.031/.032	80
T3-G	1250	.562	4	5	2-3	.346	38.4
			Cut off piece for items A, B, C, and E				
"	1000	.346	4	4	2-3	.105	70
"	900	.099	3	3	2	.060	40
"	400	.054/.055	4	5	2	.032/.033	40/40.7
T3-E	1250	.562	6	5&4	2-3	.257	54.3
			Cut off piece for items A, B, and C				
"	1000	.257	3	3	2	.078	70
"	900	.066	3	3	2	.040	40
"	400	.038/.039	1	3	---	.034/.035	10/10.5
T3-C	1250	.562	9	5,4,3	2-3	.153	73
"	1000	.153	3	3	2	.044	71.2
			Piece was cut for Item B - however it was inadvertently conditioned as Item C.				
T4-F	1250	.570	4	5	2-3	.268	53
			Cut off piece for Item D				
"	1000	.268	3	4	2	.081	70
"	900	.074	3	3	1-2	.044	40
"	400	.039/.040	2	3	1	.031/.032	20/20.5
T4-D	1250	.570	5	3,5	2-3	.235	58.8
"	1000	.235	3	3	2	.069	70
"	900	.066	3	2	1-2	.039	40
			Cut into 3 pcs. and conditioned by belt sanding.				

*All material was heat-treated 1 hr. at 1200°C and conditioned before rolling at 900°C. The strip was again conditioned by belt sanding and pickling in hot potash before cold rolling at 400°C.

Table 9b

Fabrication Schedule for Mo-E2 Strip

Item	Temp. °C	Initial Thickness Inches	No. of Passes	Initial Heat Time (Min.)	Re-heat Time Min.	Final Thickness	Remarks
T3	1250	.604	6	5	3	.283	
	1000	.283	3	5	3-2	.068	Recrystallize
	900	.065	2	6	3	.043	
F1	400	.040	4	10	5-2	.031	
F2	400	.040	2	10	5	.032	
F3	400	.040	2	10	5-2	.032	
E	1250	.280	1	4	-	.257	
E	1000	.255	3	5	3-2	.078	Recrystallize
E1	900	.067	3	5	3	.041	
E2	900	.067	3	5	3	.042	
E3	900	.067	3	5	3	.041	
E1	400	.036	4	10	6-5-3	.031	
E2	400	.036	4	10	6-3	.031	
E3	400	.036	3	10	6-3	.032	
ABC	1250	.257					Cut in half
AB	1250	.257	4	5	2	.157	
C	1250	.257	2	5	3	.151	
AB	1000	.157	3	4	3/4-1	.046	Cut in half
C	1000	.151	4	4	1-3/4	.048	Recrystallize
A	900	.037	7	3	2-1	.022	
B	900	.037	8	4	2-1	.022	Recrystallize before run
C	Conditioned to .030						
A	400	.020	9	1 hr.	5 min.	.019	Cracked & split not recrystallized.
B	400	.020	14	1 hr.	5 min.	.007	
T4	1250	.594	5	5	1-5	.358	
	Cut off 85% of length identify as item G remainder item D.						
D	1250	.358	2	4	1	.239	
G	1000	.358	4	5	3-1	.099	Recrystallized & cut into 3 pieces.

Table 9b (Continued)

Fabrication Schedule for Mo-E2 Strip

Item	Temp. °C	Initial Thickness Inches	No. of Passes	Initial Heat Time (Min.)	Re-heat Time Min.	Final Thickness	Remarks
D	1000	.239	4	5	3-1	.070	Recrystallized
D	900	.062	4	5	2-3	.035	
D	Conditioned to					.030	
G1	900	.094	4	5	2-3	.057	
G2	900	.094	4	5	2-3	.057	
G3	900	.094	4	5	2-3	.057	
G1	400	.054	6	15	5	.032	
G2	400	.054	5	15	5	.032	
G3	400	.053	6	15	5	.032	
T2							
H	1000	.600	11	5	3-2	.286	Recrystallized & cut
H1	900	.275	4	5	3	.163	
H2	900	.275	4	5	3	.158	
H1	400	.160	7	15	10-5	.032	Cut in half H1a & H1b
H2	400	.154	7	15	10-5	.032	

H1a and H1b, were cut into three pieces each. E1, E2, E3, F1, F2, F3, G1, G2, G3, and H2 were each cut in half.

All pieces except C & D were roller straightened, conditioned and then all pieces were pickled for two minutes in hot caustic potash.

Table 9c

Fabrication Schedule for Mo-E3 Strip

Item *	Temp. °C	Initial Thickness Inches	No. of Passes	Initial Heat Time Min.	Reheat Times Min.	Final Thickness Inches	Approximate Reduction %
T-H	1000	.596	5	5	2-3	.284	52.3
"	900	.275	3	4	2-3	.163/.164	40
"	400	.159/.160	10	5	2-3	.031/.032	80
T1-G	1250	.577	4	5	2-3	.357	38
			Cut off piece for Items A, B, C and E				
"	1000	.357	4	4	2-3	.104	70.9
"	900	.097	3	3	2	.059	40
"	400	.055/.056	5	3	2	.033/.034	40
T1-E	1250	.577	7	5	2-4	.254	56
			Cut off piece for Items A, B, and C				
"	1000	.254	4	3	2	.076	70
"	900	.070	3	2	2	.042	40
"	400	.038/.039	1	2	---	.034/.035	10.2/10.5
T1-C	1250	.577	10	5	2-4	.157	72.9
"	1000	.157	4	2	2	.046	71
			Cut off piece for Item B. Lost Item C during pickling.				
T1-B	1250	.577	10	5	2-4	.157	72.9
"	1000	.157	4	2	2	.046	71
"	900	.037	5	2	1-2	.022	40
"	400	.021	4	2	1	.009	57
T3-F	1250	.582	4	5	2-3	.268	55
			Cut off piece for Item D				
"	1000	.268	3	4	2	.086	68
"	900	.083	3	3	2	.048	42
"	400	.039/.040	3	2	1	.031/.032	20
T3-D	1250	.582	5	5	2-3	.237	60
"	1000	.237	4	4	2	.072	71.3
"	900	.065	2	3	2	.038	41
			Conditioned to .032/.033				

*All material was heat-treated 1 hr. at 1200°C and conditioned before rolling at 900°C. The strip was again conditioned by belt sanding and pickling in hot potash before cold rolling at 400°C.

Table 10

Status of Distribution of Experimental Materials in Zone Refined Crystal Form

Item	Form	Length in Feet				
		ManLabs	MIT	Rutgers	Liverpool	Cambridge
W-E5	0.2 in. rod	-	-	2.5	-	3.5
Mo-E5	0.2 in. rod	-	-	0.6	-	-
Ta-E5	0.2 in. rod	0.3	-	0.3	1.5	0.3
Ta-E6	0.2 in. rod	-	-	2.5	-	2.7
Cb-E5	0.2 in. rod	-	-	0.3	12	0.3
Cb-E6	0.2 in. rod	-	-	1.5	-	1.3

Table 11

Status of Distribution of Experimental Materials in Wire Form

Item	Length in Feet				
	Man-Labs	MIT	Rutgers	Liver-pool	Cam-bridge
Ta-E1-W0-.030	25	25	-	8	-
Ta-E1-W0-.067	-	1.0	-	-	-
Ta-E1-W1	350	-	-	40	-
Ta-E1-W2-.030	0.2	-	-	-	-
Ta-E1-W2-.0308	0.2	-	-	-	-
Ta-E1-W2-.067	1.2	-	-	-	-
Ta-E2-W0-.030	1	100	-	42	-
Ta-E2-W0-.041	.25	1.0	-	-	-
Ta-E2-W0-.072	.25	1.0	-	-	-
Ta-E2-W1-.030	6	-	-	-	-
Ta-E2-W1-.0339	0.2	-	-	-	-
Ta-E2-W1-.072	1.2	-	-	-	-
Ta-E3-W0-.030	1	100	-	36	-
Ta-E3-W0-.041	-	1.0	-	-	-
Ta-E3-W0-.072	2	1.0	-	-	-
Ta-E3-W1-.030	6	-	-	-	-
Ta-E3-W1-.0339	0.2	-	-	-	-
Ta-E3-W1-.072	1.2	-	-	-	-
Ta-E4-W0-.030	1	100	-	36	-
Ta-E4-W0-.041	-	1.0	-	-	-
Ta-E4-W0-.072	-	1.0	-	-	-
Ta-E4-W1-.030	6	-	-	-	-
Ta-E4-W1-.0339	0.2	-	-	-	-
Ta-E4-W1-.072	1.2	-	-	-	-
Ta-E5-W0	1	11	-	27	-
Ta-E5-W1	11	-	-	-	-
Cb-E1-W0X-.030	6	-	-	6	-
Cb-E1-W0-.030	-	100	-	30	-
Cb-E1-W0-.041	.25	1.1	-	-	
Cb-E1-W0-.072	.25	1.1	-	-	
Cb-E1-W1-.030	11.20	-	-	-	
Cb-E1-W1-.0339	.20	-	-	-	-
Cb-E1-W1-.072	1	-	-	-	-
Cb-E4-W0X-.030	-	-	-	10	-
Cb-E4-W0-.030	-	110	-	30	-
Cb-E4-W0-.041	.25	1.1	-	-	-
Cb-E4-W0-.072	.25	1.1	-	-	-
Cb-E4-W1-.030	11.20	-	-	-	-
Cb-E4-W1-.0339	.20	-	-	-	-
Cb-E4-W1-.072	1.20	-	-	-	-
Cb-E5-W0	1	11	-	23	-
Cb-E5-W1	11	-	-	-	-

Table 12

Status of Distribution of Experimental Materials in Strip Form

Item	Length in Feet				
	Man-Labs	MIT	Rutgers	Liver-pool	Cam-bridge
Mo-E1-	2.5	-	-	-	-
Mo-E2-	0.1	-	-	-	-
Mo-E3-	1.0	-	-	-	-
Ta-E1-S0-.005	-	-	1.0	1.0	1.0
Ta-E1-S0-.010	-	-	0.5	0.5	0.5
Ta-E1-S0-.030	0.5	0.1	-	-	-
Ta-E1-S1-.030	0.3	-	-	-	-
Ta-E1-S1-.150	0.2	-	-	-	-
Ta-E1-S2-.005	-	-	-	2	-
Ta-E2-S0-.005	-	-	2	2.5	1.4
Ta-E2-S0-.030	0.5	-	-	-	-
Ta-E2-S1-.005	-	-	-	-	1.25
Ta-E2-S1-.030	0.3	-	-	-	-
Ta-E2-S1-.150	0.2	-	-	-	-
Ta-E2-S2-.005	-	-	-	2	-
Ta-E3-S0-.005	-	-	2	3.3	1.8
Ta-E3-S0-.030	0.5	-	-	-	-
Ta-E3-S1-.005	-	-	-	-	1.5
Ta-E3-S1-.030	0.3	-	-	-	-
Ta-E3-S1-.150	0.2	-	-	-	-
Ta-E3-S2-.005	-	-	-	2	-
Ta-E4-S0-.005	-	-	2	4.5	1.17
Ta-E4-S0-.030	0.5	-	-	-	-
Ta-E4-S1-.005	-	-	-	-	1.25
Ta-E4-S1-.030	0.3	-	-	-	-
Ta-E4-S1-.150	0.2	-	-	-	-
Ta-E4-S2-.005	-	-	-	2	-
Ta-E5-S0	-	-	2	3.2	0.67
Ta-E5-S1	-	-	-	-	3.75
Cb-E1-S0-.005	-	-	-	2.5	1.25
Cb-E1-S0X-.030	0.5	0.5	-	-	-
Cb-E1-S1-.005	-	-	-	-	1.25
Cb-E1-S1-.030	0.4	-	-	-	-
Cb-E1-S1-.150	0.2	-	-	-	-
Cb-E1-S2-.005	-	-	-	2	-
Cb-E4-S0-.005	-	-	-	1.3	0.6
Cb-E4-S0X-.030	0.5	0.5	-	-	-
Cb-E4-S1-.005	-	-	-	-	0.6
Cb-E4-S1-.030	0.4	-	-	-	-
Cb-E4-S1-.150	0.2	-	-	-	-
Cb-E4-S2-.005	-	-	-	2	-
Cb-E5-S0	-	-	2	3.2	3

III. DUCTILE-BRITTLE TRANSITION IN REFRACTORY METALS - Work carried out at Manufacturing Laboratories, Inc. by B. S. Lement, E. M. Passmore, Steven Allen, J. E. Boyd, C. Andersson and I. Vilks.

A. Scope

This report covers research on recovery, recrystallization, tensile ductile-brittle transition and mode of fracture of tungsten (W-P4) wire and molybdenum (Mo-E1) strip. Microstructural studies were also made of substructure in tantalum (Ta-E1, E2, E3 and E4) wire and molybdenum (Mo-E1, E2 and E3) strip in the worked, recovered, and recrystallized states. In addition, both isochronal and isothermal annealing series of tungsten (W-P2), molybdenum (Mo-P2), tantalum (Ta-P2) and columbium (Cb-P2) strip were subjected to x-ray diffraction determinations of the variation in particle size and strain terms. Molybdenum (Mo-E1, E2 and E3) tantalum (Ta-E1, E2, E3 and E4) and columbium (Cb-E1, E4) strip were examined by the same method.

B. Experimental Procedure

1. Annealing

1.1 Vacuum Muffle Furnace - Prior to annealing, both wire and strip specimens were degreased in organic solvents (alcohol, acetone, and xylene) and wrapped in degreased tantalum foil. Annealing treatments at temperatures up to 1150°C were carried out in a continuously evacuated quartz tube heated in a cylindrical muffle furnace. The vacuum pressure was maintained at 10^{-5} mm. Hg or less, and a liquid nitrogen cold trap was used to minimize oil vapor contamination from the diffusion pump. Heating times from room temperature to the annealing temperatures were kept at about 5 minutes by first preheating the muffle furnace and then quickly placing it around the quartz tube. Following withdrawal of the furnace, specimens cooled to below 400°C in less than two minutes. Temperatures were controlled to ± 5°C and were measured to ± 2°C by means of a Pt/Pt-13% Rh thermocouple placed adjacent to the specimen.

1.2 Inert Atmosphere Furnace - Annealing treatments above 1150°C were carried out on wire and strip specimens in a flowing tank argon atmosphere in a Kanthal-Super element furnace. Heating and cooling times of about two minutes were achieved by drawing the wires from the cold zone into the hot zone and then out again after annealing. Temperatures were held to $\pm$ 10°C and measured by means of a Pt/Pt-13% Rh thermocouple placed adjacent to the specimens.

The annealing procedure used for some of the isochronal series of x-ray diffraction strip specimens was described previously[1]. Tank argon flowing through a nichrome-wound muffle furnace was utilized. The tantalum foil protective wrapping showed evidence of pin point penetrations after long runs. To avoid this, it was decided to interrupt long annealing treatments by rapidly cooling the specimens to room temperature and replacing the tantalum foil wrappings before continuing the anneal.

2. Metallography

2.1 Tungsten - Tungsten wire specimens were electropolished for microscopic examination in 2% NaOH and then etched in 3% H_2O_2, using the procedures described previously[1]. These procedures are listed in Table 13.

The microstructural aspects of fracture were determined by the examination of the fracture paths in wires that were bent to fracture at room temperature. Longitudinal sections of the wires were first electropolished and etched. Then the microstructures of selected areas were photographed either by taking overlapping light micrographs directly of the specimen or indirectly of cellulose acetate replicas that were stripped from the specimen and shadowed with chromium. The wire was then clamped securely and bent with the polished area on the tension side until fracture occurred. The polished surface adjacent to the fracture was then photographed and the fracture path carefully plotted on the photomicrographs of the original structure.

2.2 Molybdenum - Specimens of molybdenum strip were mounted and then polished electrolytically in a solution consisting of 75 cc methyl alcohol and 25 cc H_2SO_4 at a current density of about 1 amp/cm^2. The samples were then etched using one of the etchants listed in Table 14.

2.3 Tantalum - Tantalum specimens were mechanically polished and then chemically polished using the procedures described previously[1]. The samples were etched using one of the etchants listed in Table 15.

2.4 Columbium - Columbium specimens were either prepared the same way as tantalum or electropolished using a solution consisting of: 170 ml HNO_3, 50 ml HF, 5 grams citric acid and 510 ml of methyl alcohol[6] at a current density of 5 amps/cm^2. The specimens were then etched using one of the etchants listed in Table 15.

3. Microhardness Testing

Microhardness was measured on polished longitudinal sections of both wire and strip specimens using a 500-gram load and a diamond pyramid (Vickers) indentor. Tungsten and molybdenum specimens were electropolished before testing, whereas tantalum and columbium were mechanically and then chemically polished. The indentations were oriented with one diagonal parallel to the wire axis or strip rolling direction. Ten hardness readings were made on each specimen, and the average values were corrected in accordance with tests made on a calibrated standard of approximately the same hardness as the material being tested.

4. Tensile Testing

4.1 Preparation of Test Specimens - Tungsten wire specimens were prepared for tensile testing by first electropolishing 0.5 mil off the surface of the entire 1 3/8-inch length in an aqueous solution of 2% NaOH using a current density of 0.7 amp/cm^2. A 1-liter stainless steel beaker was used to contain the

Table 13

Metallographic Polishing Procedures

Metal	Method	Polishing Medium
Tungsten	Electrolytic dc, 1 amp/cm^2	2% NaOH 98% H_2O
Tantalum	Mechanical and Chemical	Linde "B" Alumina with 5% Chromic acid in H_2O 30 cc Lactic Acid 10 cc HNO_3 5 cc HF
Molybdenum	Mechanical	Linde "B" with 5% chromic acid in H_2O
	Electrolytic dc, 2 amp/cm^2	25 cc H_2SO_4 75 cc Methyl Alcohol
Columbium	Mechanical and Chemical	Same as Ta
	Electrolytic d-c, 5 amp/cm^2	170 cc HNO_3 50 cc HF 5 grams citric acid 510 cc methyl alcohol[6]

Table 14

Etching Procedures for Molybdenum

Etchant	Method of Application	Etching Time	Reference
3 vol. % H_2O_2	Immersion in boiling solution.	20 seconds	(1)
1 part 25 $^{w}/_{o}$ $CuSO_4$ 1 part NH_4OH (conc.)	Immersion, slight agitation.	30 seconds	(2)
1 part 10 $^{w}/_{o}$ NaOH 1 part 30 $^{w}/_{o}$ $K_3Fe(CN)_6$	Immersion, slight agitation	20 seconds	(3)
0.5 $^{w}/_{o}$ Oxalic acid	Electrolytic, 6 volts D.C. with stainless steel cathode.	40 seconds	(4)
Cathodic Etching	Argon at a partial pressure of 40 microns, 3500 volts/10 M.A. per cm^2.	15 minutes	(5)
3 gms $FeCl_3$ 50 gms $CuSO_4$ 75 cc NH_4OH 225 cc H_2O	Immersion, slight agitation.	10 seconds	
1 part HF 2 parts HNO_3 3 parts H_2O	Immersion, slight agitation.	30 seconds	

Table 15

Etching Procedures for Tantalum and Columbium

Etchant	Temp. °C	Etching Time	Reference
5 parts 95% H_2SO_4 2 parts 70% HNO_3 2 parts 48% HF	25-40	1/2-1 min.	(7,8)
3 parts conc. lactic acid 1 part conc. HCl (or HNO_3) 1 part 48% HF	20-25	1/2-3 min.	(8)
1 part 20% NH_4F 1 part 30% HF	50-60	3-5 min.	(7,8)
1 part conc. H_2SO_4 1 part 48% HF 1 part H_2O few drops H_2O_2	20-25	1/2-3 min.	(9)

solution and also acted as the cathode. The ends were then coated with lacquer, and the diameter of the 0.5-inch gage length was further reduced 2.5 to 3.0 mils by electropolishing. The surfaces were uniform and no pits, undulations, or undercutting at the intersection with the shoulders occurred. In over 90% of the measurements, the smallest diameter occurred within the middle 0.3 inch of the gage section.

Molybdenum sheet specimens were prepared by first surface grinding the sheet from 30 to 20 mils thick and then engraving the specimens to the dimensions shown in Fig. 1. Close tolerances were achieved by using a pantograph guided by an oversized template. The ends were then coated with lacquer and 2 mils were electropolished off the thickness of the gage length. Electropolishing of the molybdenum specimens was also done in a stainless steel beaker, using a 25% H_2SO_4 plus alcohol solution at a current density of 2 amps/cm^2.

4.2 Measurement of Test Specimen Dimensions - Diameters of wire specimens and widths of sheet tensile specimens were measured before testing at 0.1 inch intervals to $\pm$ 0.2 mil using a micrometer stage microscope. Sheet specimen thicknesses were measured to $\pm$ 0.2 mil using a micrometer.

The variation in the diameter between the maximum and minimum measured for each specimen varied from 0.1 mil to 2.4 mils, with about three-fourths of the specimens having a variation of one mil or less. The range of Mo sheet tensile specimen gage widths varied from 0.2 to 1.8 mils, with about 95% having a variation of one mil or less. Since the locations of the minimum diameters of the wire specimens and the locations of the minimum widths of the sheet specimens were found to coincide with the fracture locations in several specimens, these dimensions were used in the calculations of the initial areas. The minimum thicknesses, which varied less than the widths, were also used.

Gage lengths of both wire and sheet were measured to $\pm$ 2 mils using the micrometer stage microscope. Wire specimen gage lengths were measured as the distances between the shoulders and sheet specimen gage lengths were measured as the distances between the points where the shoulder radii were tangent to the parallel reduced sections.

Specimen dimensions after fracture were measured at the points of minimum areas using the same techniques, except that the micrometer stage microscope was also used to measure sheet thicknesses. Reductions in area of wire and sheet specimens were calculated using both the minimum initial and final areas.

Elongations of wire specimens were calculated at first from both microscopic measurements of gage lengths before and after fracture and from the recorded load-extension curves. As shown by the corresponding values as listed in Table 16, there was good correlation between the two techniques. Since the elongations also showed less scatter when taken from the recorded curves and the values were easier to obtain, the latter technique was adopted for all subsequent tests.

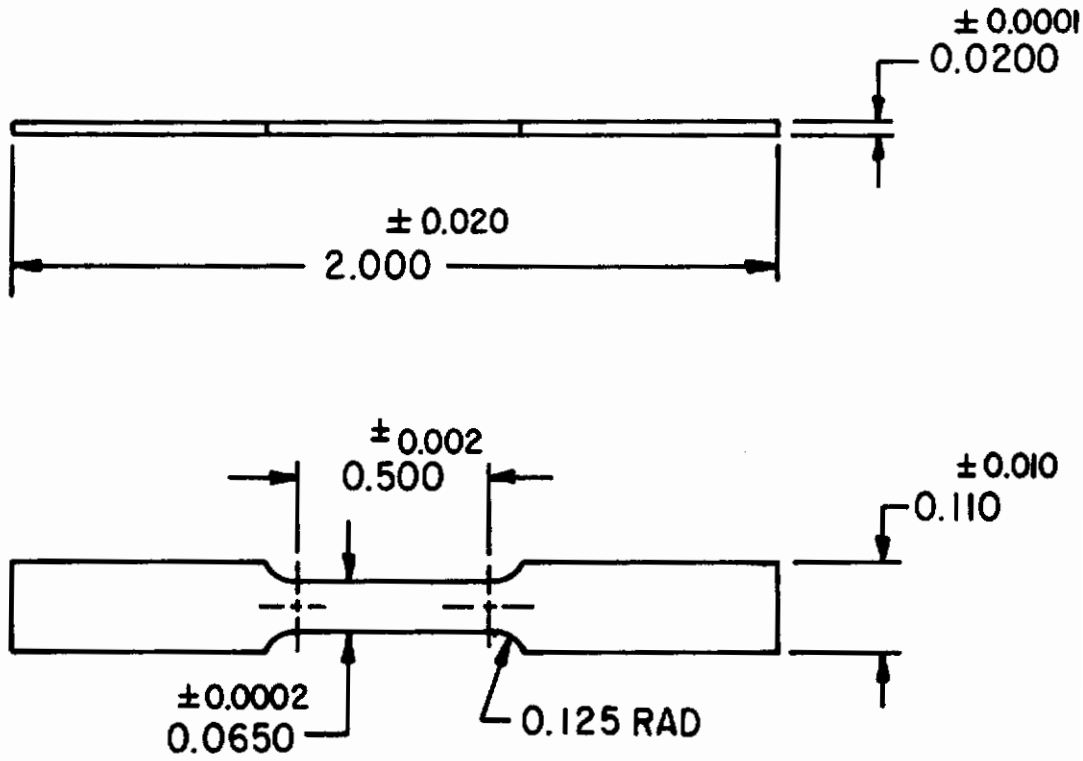

Fig.1- Molybdenum sheet tensile specimen

Table 16

Comparison of Elongation Measurement Techniques

Specimen Number	Direct Elongation Measurement, %	Chart Elongation %
TW-1050-63	6.18	6.07
TW-1050-64	4.28	5.17
TW-1200-54	0	0.64
TW-1200-55	4.78	4.53
TW-AR-78	0	0.82
TW-AR-79	0.61	0.71

4.3 Tensile Apparatus - A modified Polanyi tensile tester of a design similar to that described by Adams[10] and shown in Fig. 2 was used for measurement of tensile properties of W wire and Mo sheet. Load was applied to the specimens by movement of the lower grips which were connected to a movable frame cross-head by means of a tie rod. The cross-head was driven by a translating screw through reduction gears by a constant speed synchronous motor. The upper grips were connected by means of a tie rod to a load measuring dynamometer, which was connected to the stationary part of the frame. Axiality of loading was facilitated by means of universal joints at the upper and lower ends of the tie rod and at the lower grips. Modified commercial pin chucks, Eclipse No. 160 (James Neill and Co., Ltd., Sheffield, England), were used for wire testing. Wedge grips of ManLabs design were used for sheet testing.

Two interchangeable resistance strain gage dynamometers (J. Langham Thompson, Ltd., Bushey Heath, Hertshire, England) of the proving ring type, with load ranges of 0 to 200 pounds and 0 to 500 pounds, respectively, were used for load measurement. Constant voltages of 12 or 18 volts were supplied to these by lead storage batteries. Controlled variations in input voltage were provided by decade resistors in series between the batteries and the dynamometer. Dynamometer output voltage was recorded on a Honeywell Brown Electronik potentiometer recorder. Autographic recording of specimen extension, as well as load, was made possible by determination of the proportionality between the constant movable frame cross-head speed and the constant chart speed.

Tensile test temperatures below room temperature were obtained by using a Wessel-type liquid nitrogen evaporator, in which the specimen-grip assembly and the movable frame were contained. Liquid nitrogen introduced into the boiler evaporated and entered the interior of the vessel through a number of pin holes. Baffles prevented the nitrogen gas from impinging on the specimen and thermopile, improving the circulation and temperature uniformity in the cooling chamber. Temperature control of $\pm$ 2°C was obtained with a copper-constantan thermopile in conjunction with a controller, which activated a solenoid valve. The valve regulated the flow of liquid nitrogen from a pressurized tank. Temperatures were measured by means of a copper-constantan thermocouple and a potentiometer.

Agitated silicone oil heated in an insulated tank by an immersion type electric resistance heater was used for testing above room temperature. A thermoswitch was used for controlling the temperature to within $\pm$ 1.5°C and a mercury thermometer was used for temperature measurement.

4.4 Tensile Test Procedure - The tensile testing of tungsten wire was carried out using the 0 to 200-pound dynamometer. The specimens were gripped with pin chucks and pre-loaded approximately 20 pounds at room temperature. After the test temperature was obtained, 10 to 15 minutes were allowed for the establishment of temperature equilibrium. Then the specimens were loaded to fracture at a strain rate of 2.8×10^{-4} sec^{-1}, controlled by the selection of the constant cross-head speed.

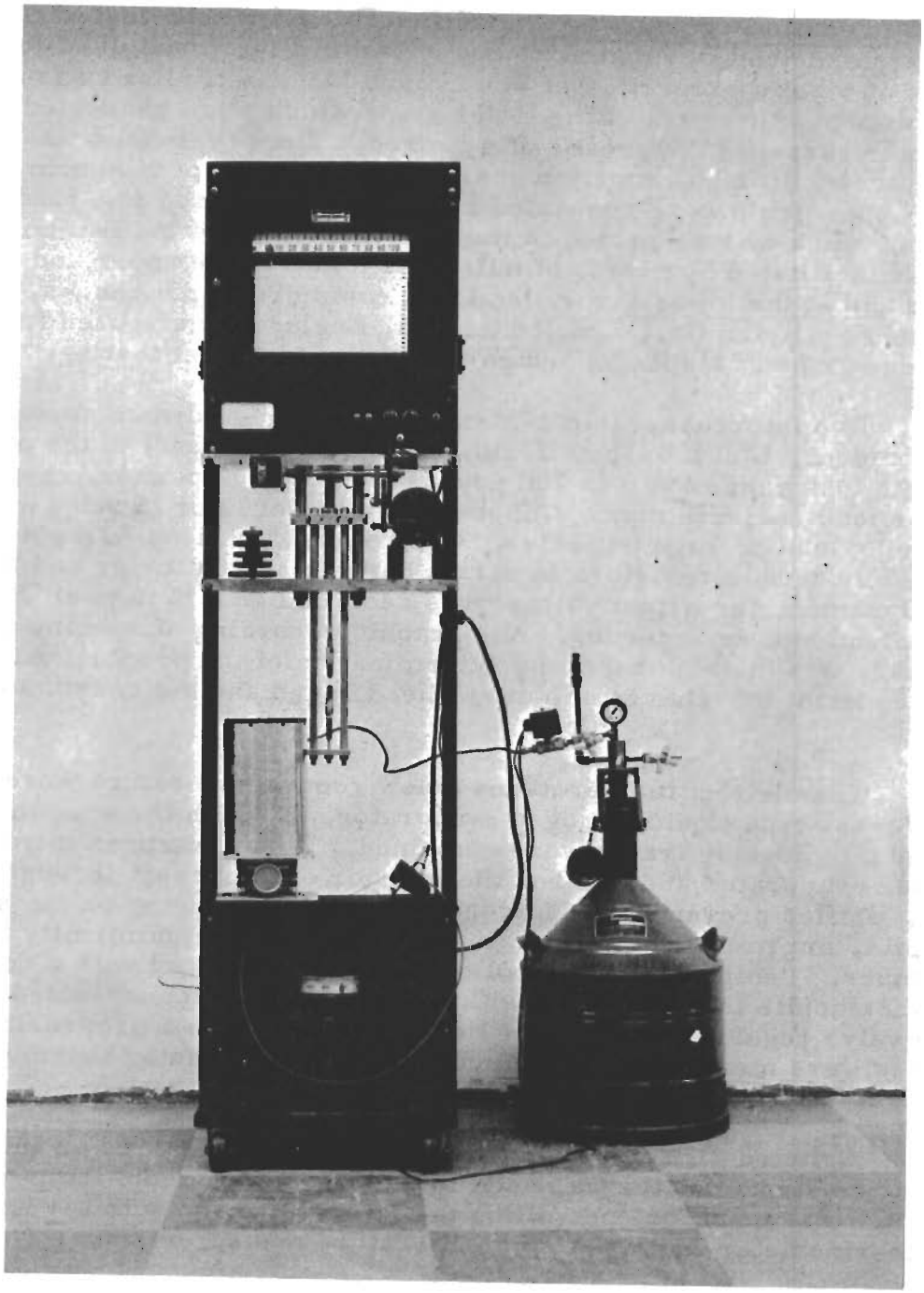

Fig. 2 - Tensile tester and cryostat.

The tensile testing of molybdenum strip was carried out using the 0 to 500-pound dynamometer with the input voltage and potentiometer range adjusted to give a full scale load of 225 pounds. The specimens were held with wedge grips, preloaded within the elastic range to 40 or 50 pounds at room temperature to align tensile machine prior to cooling and then uloaded to 10 pounds. After the test temperature was obtained and 10 to 15 minutes allowed for the establishment of equilibrium, the specimens were loaded to fracture at a strain rate of 2.8×10^{-4} sec^{-1}.

5. X-Ray Diffraction

5.1 Specimen Preparation - For the x-ray diffraction measurements, surfaces representative of the strip interior were prepared by following the procedures given previously[1]. This results in a section parallel to the rolling plane. Because of the texture of the specimens, the (200) (400) series can readily be measured from this orientation. For measurements of other series, it was often necessary to use other sections, which were obtained by appropriately stacking a number of layers of the strip material to give sufficient area of a selected orientation chosen on the basis of the texture. These specimens were held together either by cementing with an epoxy resin or by mounting in a pressure molded metallographic mount.

5.2 Line Profile Measurements - The theoretical considerations, diffractometer measurements and data reduction were those discussed previously[1].

5.3 Experimental Scatter - In view of the scatter found in the particle size and strain data, especially in the isothermal series, some of the possible causes were investigated in order to ameliorate this. Based on the smoothness of both the particle size coefficient and displacement vs. lattice distance plots and on the magnitude of the "hook effect"[1], the data for Ta-P2 and for Cb-P2 appear to be the most and the least reliable respectively. Since better accuracy is highly desirable and relatively poor correlations between small variations of the measured half-widths and the variations in particle size and strain terms were found[1], an effort was made to check the reproducibility of these terms. This was an extension of the work which involved measurement and improvement of the reproducibility in terms of the much more readily measured half-widths.

Basically, the investigation was carried out by attempting to vary only a single parameter at one time. The first variable studied was repeatability of the measurement on a given specimen. The use of the same specimen reduces the possibly large specimen-to-specimen variation to a smaller variation[1] within a single specimen. The specimens were subjected to either a) a repeat of the final polishing stages, or b) a repeat from 320 grit silicon carbide paper, followed by all the other grinding and polishing stages. This resulted in a number of different surfaces for measurement on any one specimen.

The results of this study are given in Table 17. The reproducibility of the Ta-P2 data is excellent; whereas that of W-P2 strip (for example) is considerably poorer even though the scatter in the half-widths is not larger. There also appear to be no correlations with the integral breadths of these peaks or the area under the peaks.

Upon further examination for correlations, it was found that the primary cause of scatter is associated with the measurement of the (200)

Table 17

Repeat Runs of the Same Specimens of P2 Strip

Material Specimen No. and Condition	Particle Size, A	Strain $\times 10^4$	Half-width (200), $^\circ\theta$	Half-width (400), $^\circ 2\theta$
W-P2 (No. WX32) 500°, 1 hr.	924	9.45	0.265	1.77
Repolished	638	8.43	0.275	1.81
Reground and polished	830	9.05	0.263	1.76
Mo-P2 (No. MoX27) 300°, 1 hr.	1230	7.62	0.250	1.96
Reground and polished	1105	7.48	0.263	1.99
Ta-P2 (No. TaX26) 400°, 1 hr.	498	15.0	0.325	1.49
Repolished	490	15.2	0.338	1.54
Reground and polished	480	15.9	0.343	1.55
Cb-P2 (No. CbX17) 500°, 1 hr.	744	12.4	0.275	1.28
Repolished	667	11.6	0.280	1.30
Reground and polished	624	12.2	0.290	1.29

diffraction profile, not the (400). This was apparent when "cross-matches" of the diffraction profiles were made. Instead of using the (200) and (400) of the same specimen preparation (see Table 17) as should be done for the line profile analysis, this involved using the repolished (200) with (for example) the original (400). It was found that when any (400) of the specimen, or similar specimens, was used with a given (200) in the calculations, essentially the same particle size and strain terms resulted.

This finding was somewhat unexpected since it had been thought that the lower intensity and resulting poorer statistics would make the (400) much more susceptible to fluctuations. This conclusion considerably narrowed the field of causes to be investigated.

As run in this investigation, using a 30 in/hour chart speed and a 1/8 degree 2θ/min diffractometer speed, the chart recordings of the (200) peak have a large slope. The amount of error that could be introduced in converting the analog data (chart recording of the diffraction line profile) to digital (numbers for input to the 704 computer program[1]), was checked first. In doing this the same recording was used. Operator parameter was obtained by having different workers read the charts, whereas an estimate of the maximum likely error was obtained by consciously reading charts to give a maximum possible intensity at each point of the profile and then a minimum. This and the error introduced by different operators, can account only for an 1 to 2% variation in the particle size term and was found to have no appreciable effect on the details (smoothness) of the particle size coefficient plot[1].

In addition the error introduced by estimating the background, which is subtracted from the gross profile intensity by the computer to give a net profile intensity, was evaluated by comparing computations using respectively the high and low limits of background of the same chart recording.

The result of varying the background correction was also found to have only a minor effect on the corrected particle size term or detail of the coefficient plot although the expected variations in the hook-effect were observed[1], the hook becoming more pronounced as more intensity was subtracted as background.

Whereas the two-pulse resolving time of the electronics had been given as 5 microseconds[1] the manufacturer of the pulse height analyzer-(Baird-Atomic) states that, depending on the pulse shaping, 1 to 10 microsecond resolving times are obtained.

A correction for loss of counts is made during the 704 computation. This correction is only appreciable in the computations of the (200) data, not the (400), and because the intensity of repeat runs varies considerably, could affect the repeatability.

This parameter was varied by changing the resolving time used in the computer correction. The degree of effect that a change of resolving time from one to ten microseconds has on the particle size term was evaluated. It was found to give approximately 10% change, without appreciable change in detail of the coefficient plot, and so would not serve to explain the scatter.

As a result of these experiments and the lack of correlation that was found in comparing the particle sizes with intensity, it is believed that the scatter is a cumulative effect of a number of causes. In measuring particle sizes of the 500A and larger in polycrystalline specimens of the type used, it is unlikely that the scatter can be appreciably reduced.

C. Results and Discussion

1. Recovery-Annealing of Tungsten (W-P4) Wire

1.1 Changes in Microstructure - Light microscopic examination showed the structure of the as drawn wire to consist of heavily deformed, fibered grains, approximately 2 microns in width containing relatively few etch-pit subboundaries (Fig. 3). Annealing at 500° for 8 hours or at 800° for 10 minutes results in the appearance of longitudinally oriented subboundaries consisting of clearly delineated etch pits (Fig. 4). Continued annealing at 800° results in the formation of subgrains surrounded by etch-pit subboundaries (Fig. 5) which may be considered a type of polygonization. These qualitative observations of additional etch-pit subboundaries in the annealed wire were confirmed by quantitative measurements of the number of longitudinal subboundaries per unit length measured in the transverse direction (subboundary density, N_s/L), which also shows an increase after recovery-annealing (Fig. 7). These etch-pit subboundaries are probably a manifestation of low-angle boundaries formed by dislocation interaction and rearrangement during recovery-annealing. The sharp, well-defined appearance of the etch-pits may result from diffusion of impurity atoms to the dislocations.

The microstructural changes above 800° consist of a progressive widening of the fibers, polygonization, and subgrain growth. Two types of polygonization were observed. One type is analogous to that observed at 800° after annealing for 8 hours (Fig. 5) and results in the formation of similar subgrains, within the fibered grains, and predominantly surrounded by etch-pit subboundaries. It first becomes evident at about 1050° after 10 minutes (Fig. 6) and becomes more fully developed at higher annealing temperatures (Fig. 8). Another type of polygonization begins to become evident at about 1050° by the presence of clearly defined transverse boundaries dividing the fibers into segments. The boundaries are more prevalent at 1100° and do not appear to be made up of separate etch-pits (Fig. 8). They may arise from the division of the twisted fibers into relatively strain-free segments, separated by low-angle twist boundaries. At 1200° some of these polygonized segments appear to have grown preferentially by lateral movement of their longitudinal boundaries (Fig. 9). The sharply defined subgrains resulting from growth of these polygonized segments are not easily distinguished from the subgrains delineated by etch-pit subboundaries because of the similarity in shape and the difficulty of resolving the etch pits.

Above 1200°, more extensive preferential subgrain growth occurs, especially of the polygonized segments. The resultant structure at 1400° consists of irregular fibrous grains, approximately 4 microns in width, compared to 2 microns in the as-drawn wire. The fibrous grains are composed of slightly elongated subgrains with sharply defined boundaries (Fig. 10). They do not appear to consist of etch pits, although pits are still evident within some of

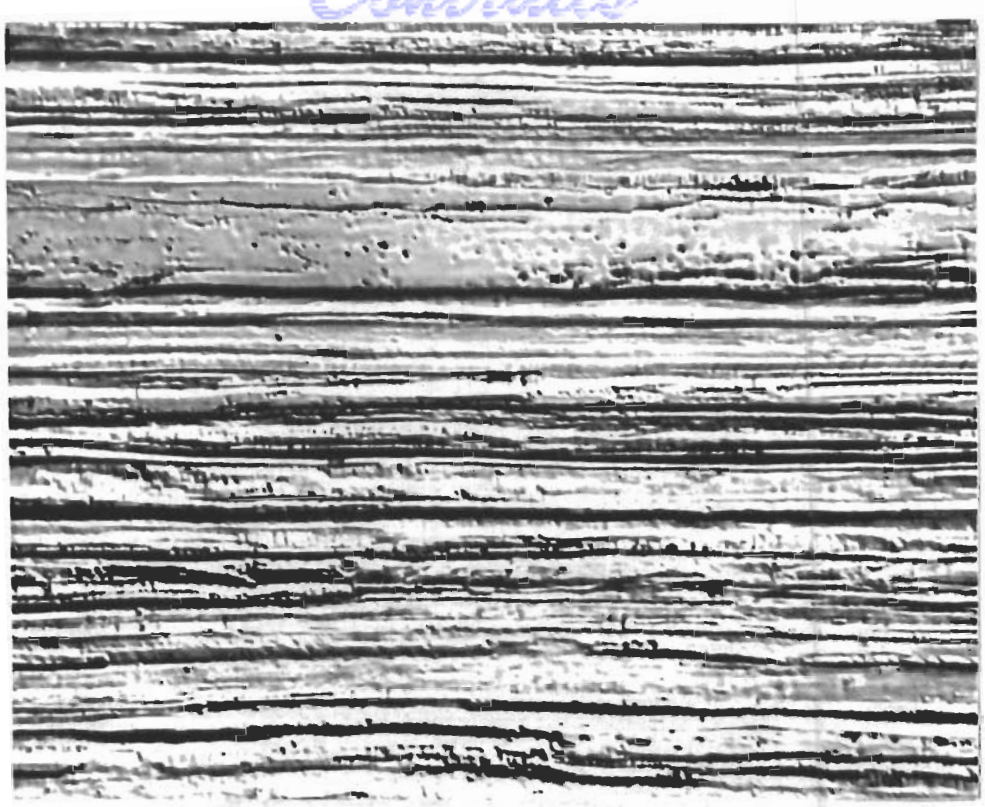

H_2O_2 etch 3330 2000X

Fig. 3 - Microstructure of as-drawn tungsten (W-P4) wire.

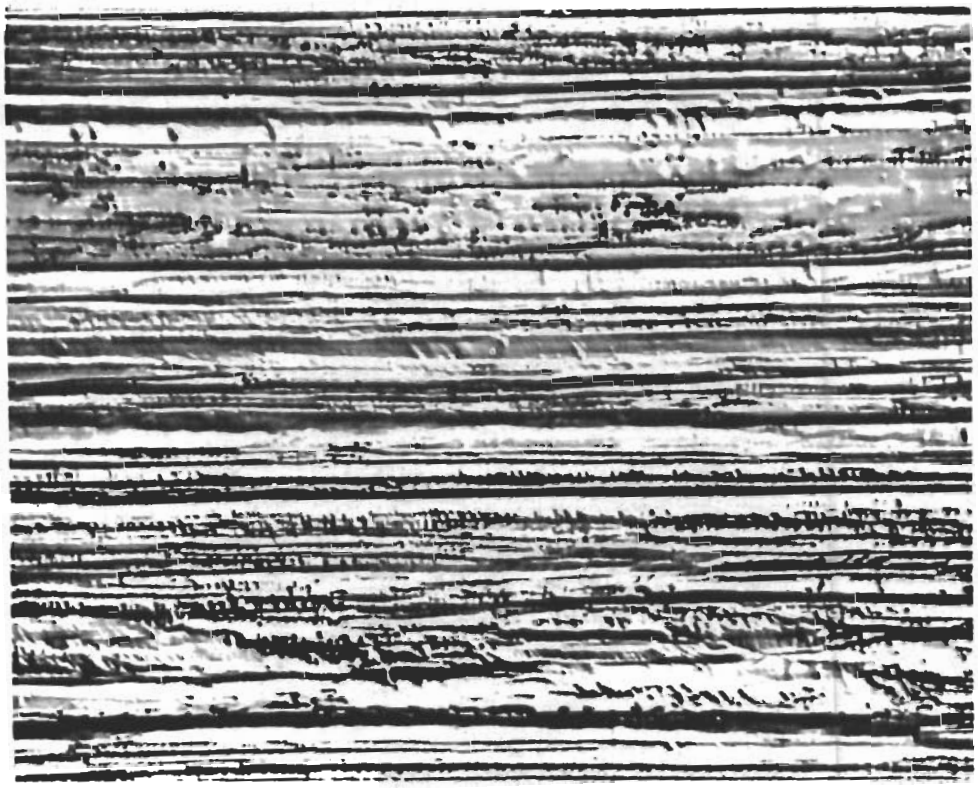

H_2O_2 etch 3331 2000X

Fig. 4 - Substructure developed in tungsten (W-P4) wire by annealing for 10 minutes at 800°C.

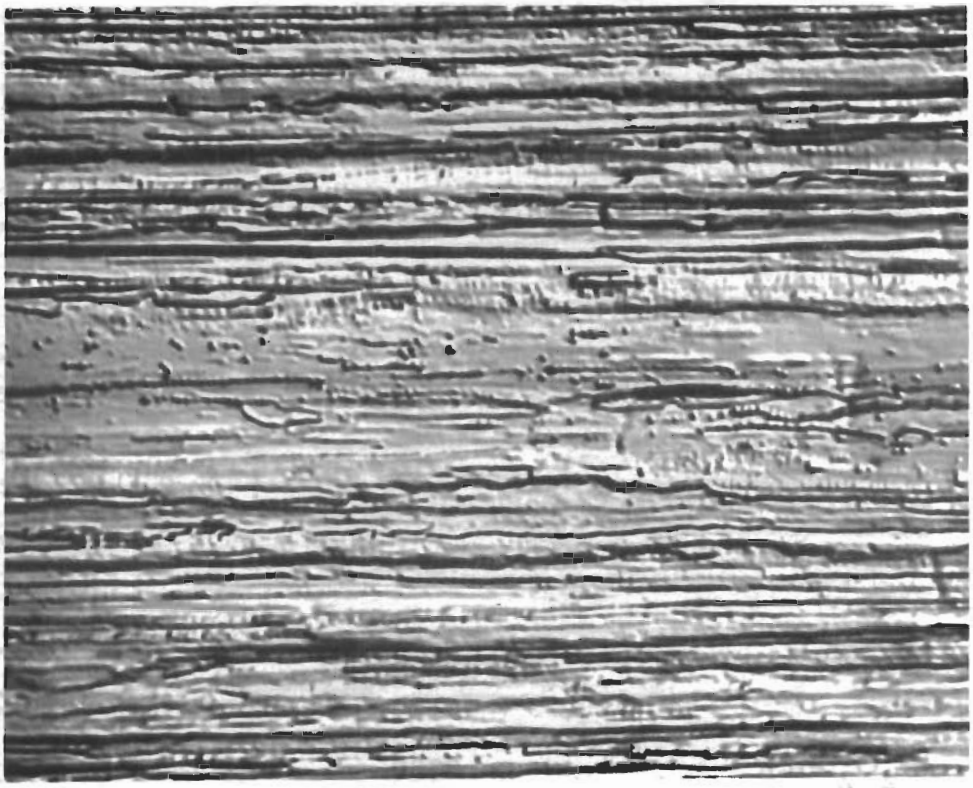

H_2O_2 etch 3712 2000X

Fig. 5 - Substructure developed in tungsten (W-P4) wire by annealing for 8 hours at 800°C. Note subgrains surrounded by etch pit subboundaries.

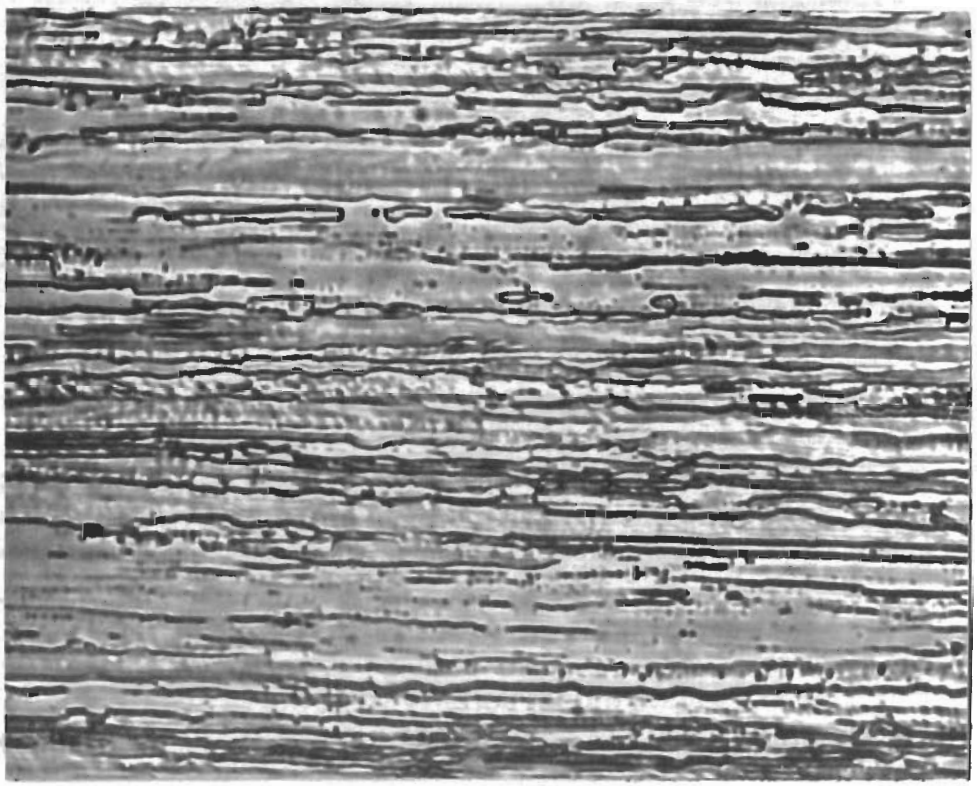

H_2O_2 etch 3868 2000X

Fig. 6 - Microstructural changes in tungsten (W-P4) wire after annealing for 10 minutes at 1050°C. Note subgrains surrounded by etch pit subboundaries.

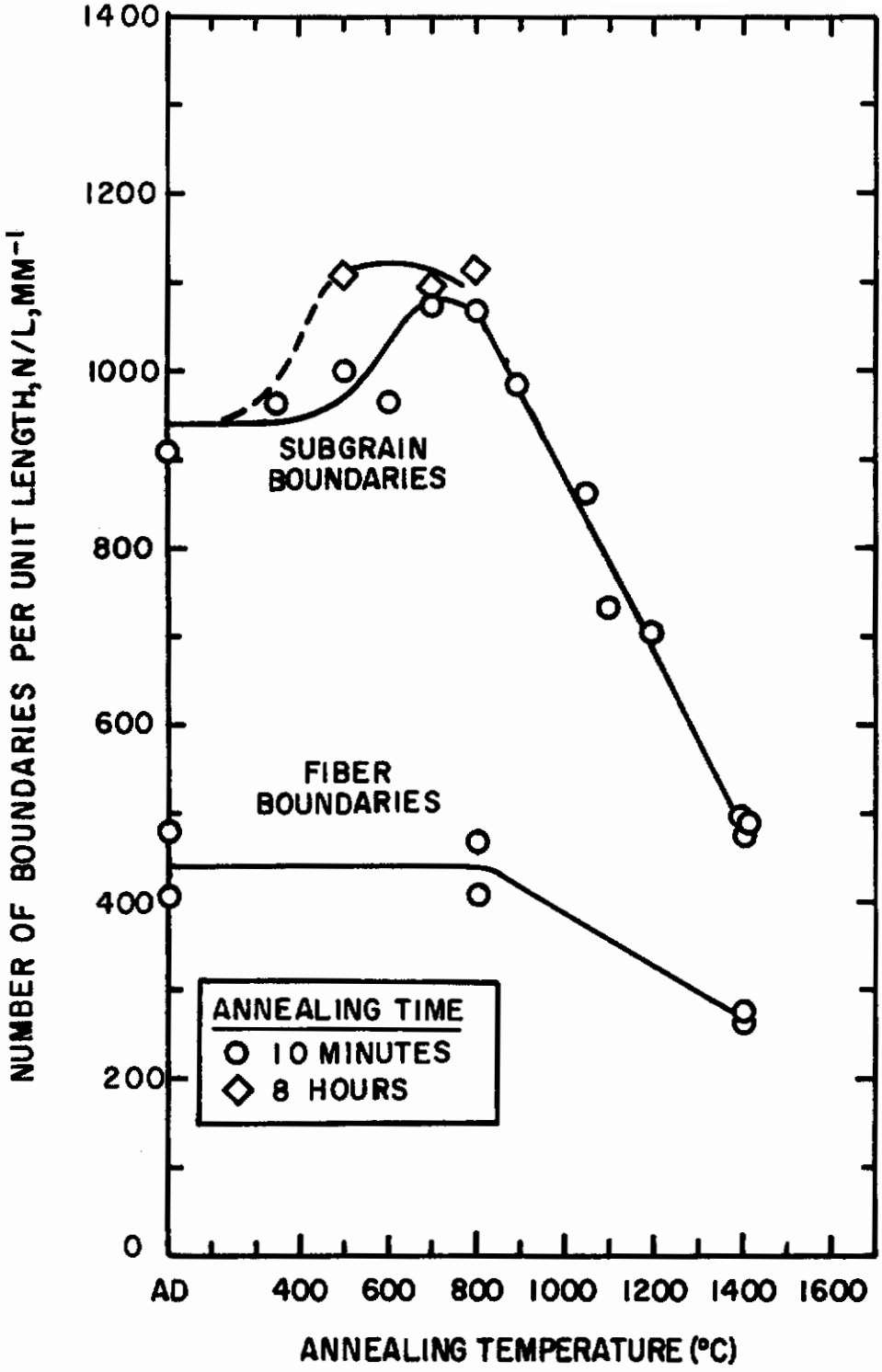

Fig.7- Effect of annealing on density of longitudinal boundaries in tungsten wire (W-P4)

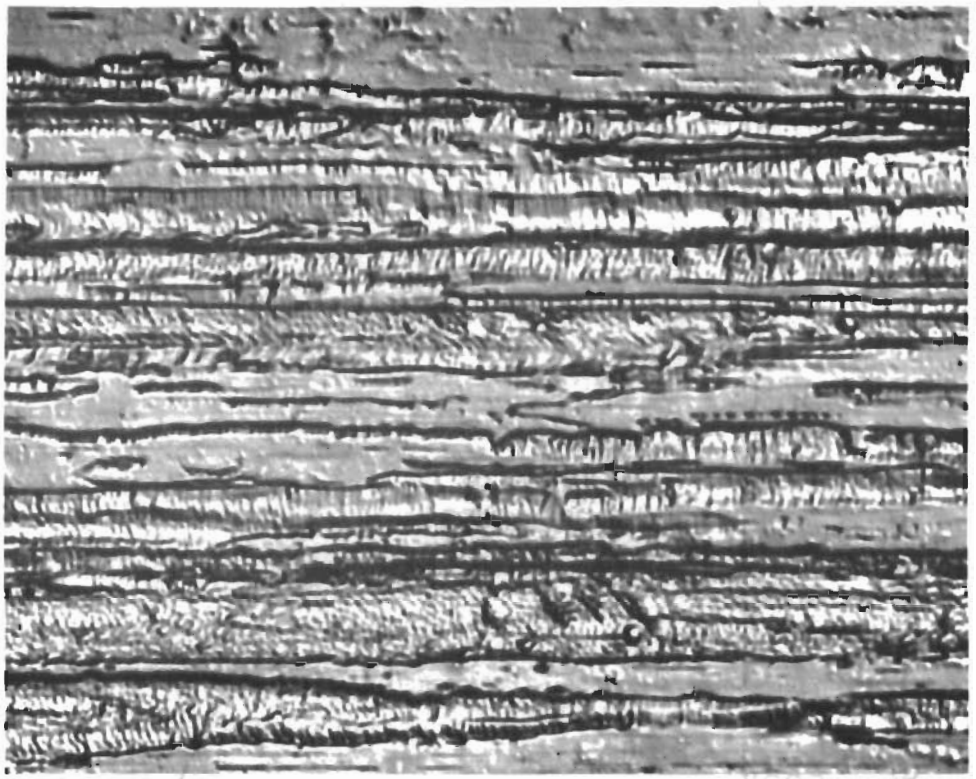

H_2O_2 etch 3865 2000X

Fig. 8 - Microstructural changes in tungsten (W-P4) wire after annealing for 10 minutes at 1100°C. Note the transverse boundaries.

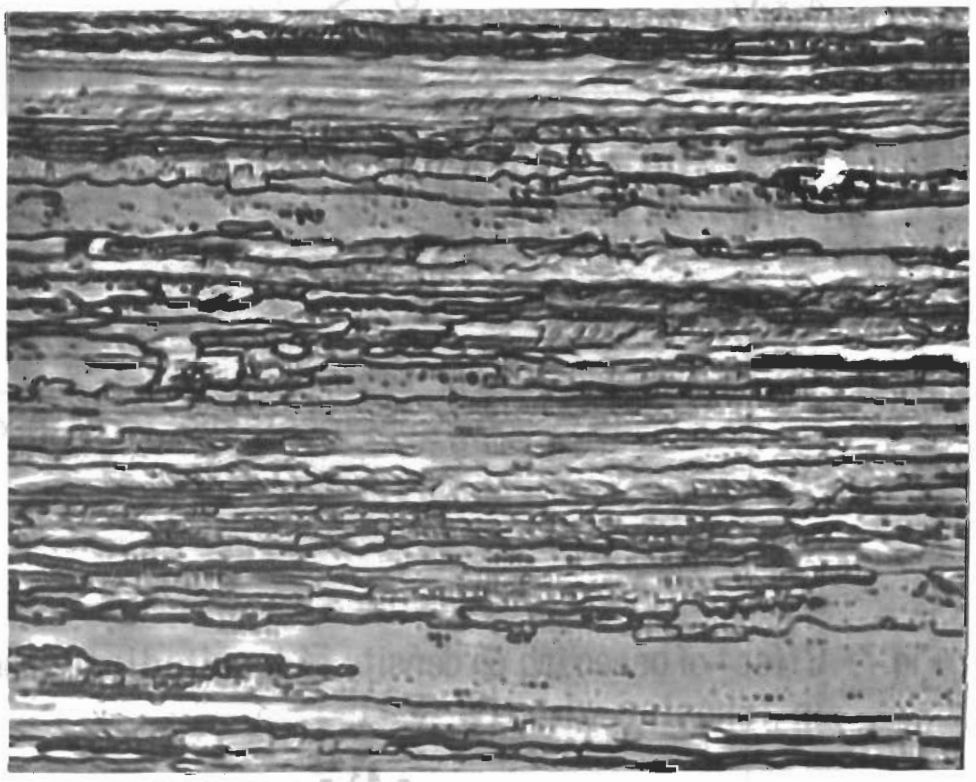

H_2O_2 etch 3869 2000X

Fig. 9 - Subgrain growth in tungsten (W-P4) wire after annealing for 10 minutes at 1200°C.

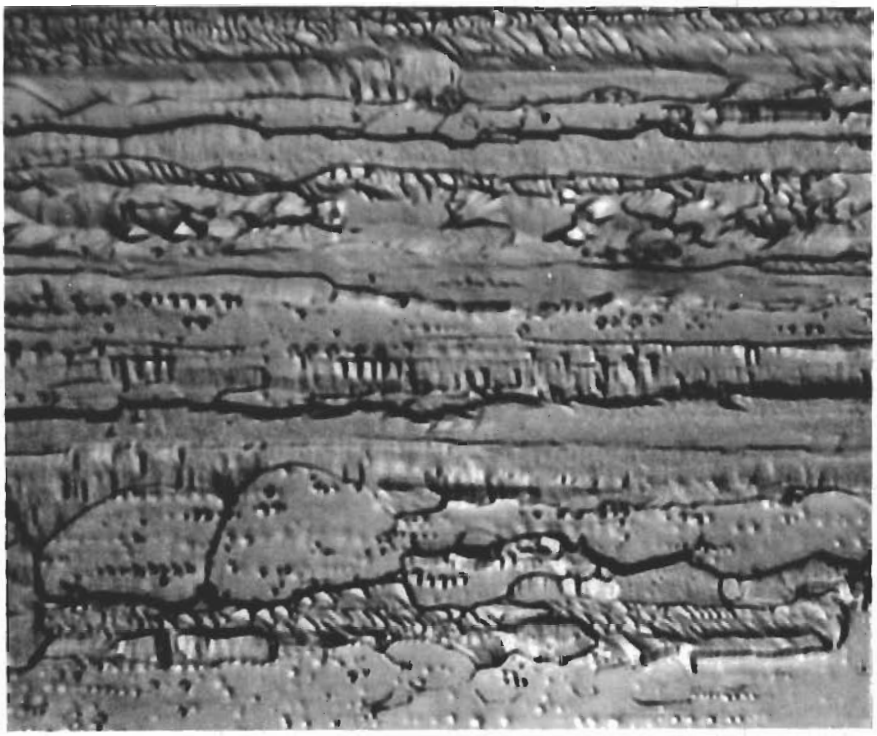

H_2O_2 etch 3892 2000X

Fig. 10 - Microstructure of tungsten (W-P4) wire after annealing for 10 minutes at 1400°C.

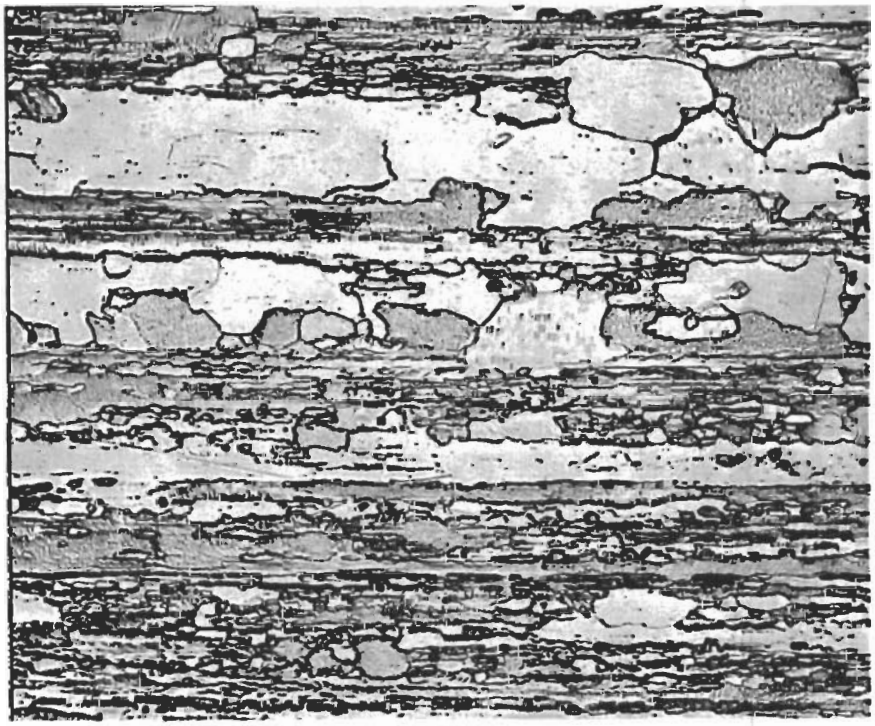

$NaOH + K_3Fe(CN)_6$ etch 3377 500X

Fig. 11 - Microstructure of tungsten (W-P4) wire after annealing for 10 minutes at 1580°C.

the subgrains. There are no further marked changes until the annealing temperature exceeds 1500°, where rapid preferential growth of a few large grains occurs at the expense of the coexisting fibrous structure (Fig. 11).

1.2 Changes in Microhardness - On annealing at 500°, a maximum occurs after 8 hours (Fig. 12) as well as after 10 minutes at 800°, as previously found[1]. Using these data, an approximate calculation of the activation energy (Q_H) associated with the initial hardening process was made. It was assumed that the logarithm of the time to attain maximum hardness is proportional to the reciprocal of the absolute temperature and that the slope equals Q_H/R where R is the gas constant. On this basis, Q_H was found to be approximately 33 kcal/mol.

As shown in Table 18, the calculated value of Q_H is within about ±15,000 cal/mol of the reported values of the activation energy for diffusion of oxygen and carbon (one value) in tungsten. Since the activation energy for diffusion of nitrogen in tungsten has apparently not been determined as yet, no comparison could be made with this element. However, considering the approximate value of the calculation of Q_H and the relative closeness of its value to at least the activation energy for diffusion of oxygen in tungsten, it seems likely that the hardening process is controlled by the diffusion of interstitials.

1.3 Effect of Recovery-Annealing on the Ductile-Brittle Transition Behavior - The effects of test temperature on the yield and fracture stress, elongation, and reduction of area of the as-drawn wire show behavior typical of b.c.c. metals (Fig. 13). With increasing test temperature starting at -195°, yield stress decreases continuously and ductility remains at a low level up to about -20°, at which an abrupt increase occurs. Fracture stress remains slightly above the yield stress up to about -20°, and then also increases abruptly. The temperature at which these abrupt changes occur is called the ductility transition temperature, T_d[12]. Above T_d, reduction of area increases gradually with increasing test temperature; whereas elongation remains constant and fracture stress decreases.

The transition behavior of the annealed wire is similar to that of the as-drawn wire, except for differences in the values of the various parameters (Figs. 14, 15, 16, 17, 18, 19). Yield and fracture stress levels at equivalent test temperatures decrease with increasing annealing temperatures up to 1400° (10 minutes at temperature). Reductions of area and elongations above T_d first decrease at 800° (Figs. 20 and 21) and then increase at higher test temperatures. Only slight changes occur in elongation values, but reductions of area at 80° test temperature increase appreciably above 800° and then go through a maximum at 1200° (Fig. 21).

The transition temperature, T_d, increases with increasing annealing temperature over the entire range studied (Fig. 22). Above 800°, the slope of the curve of T_d versus annealing temperature is steeper than below 800°. At the highest annealing temperature studied (1400°) T_d attains a value of +52°.

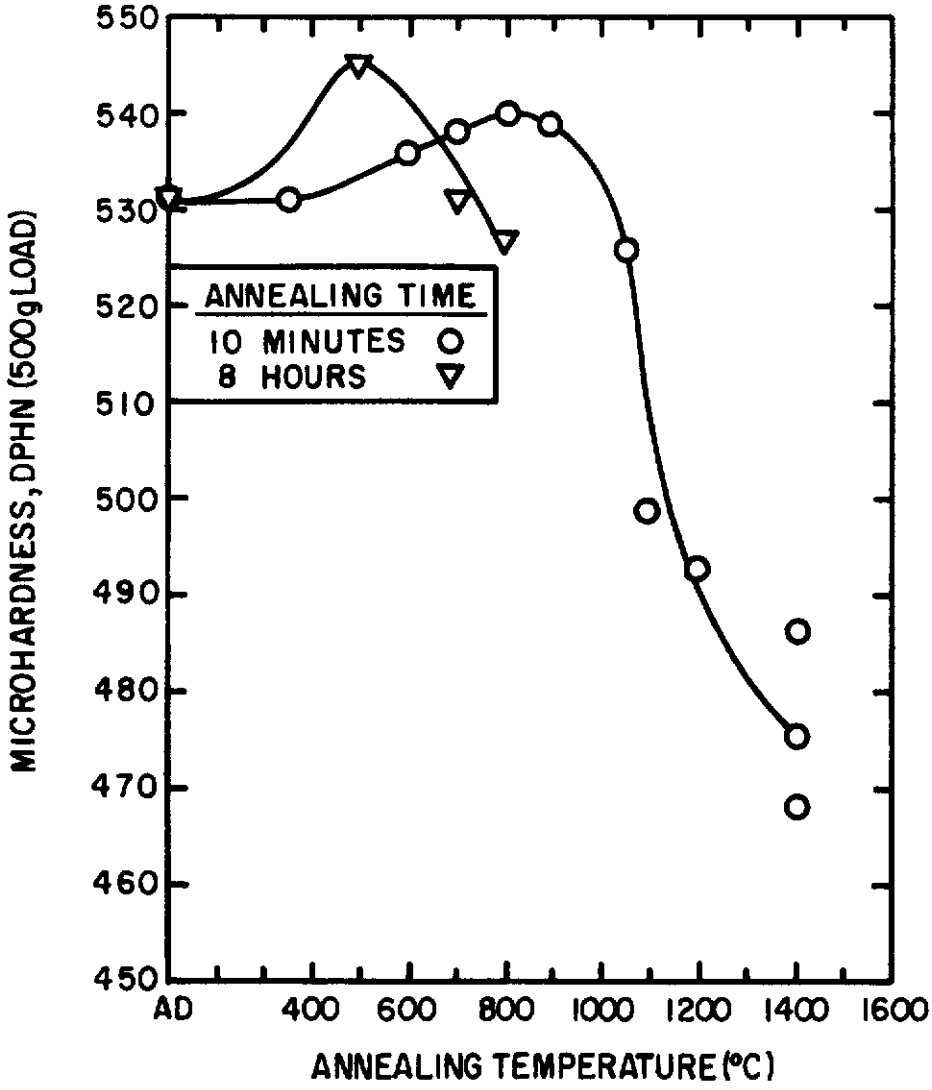

Fig.12- Effect of recovery-annealing on the micro-hardness of 0.030 inch tungsten wire (W-P4)

Table 18

Activation Energies for Diffusion in Tungsten (11)

Diffusing Element	Activation Energy kcal/mol	Investigators
O	16	Muller
O	19	Wortman, Gomer, and Lundy
O	30	Wortman, Gomer, and Lundy
C	39.5	Samsonov and Latysheva
C	112	Kreimer, Efron, and Voranova
C	59	Pirani and Sandor
C	125	Zwickker
C	100	Klein
W	135	Vasiler and Chernomorchenko
W	106.5	Muller
W	73.2	Sokolovskaia
W	72.0	Barbour, et al.

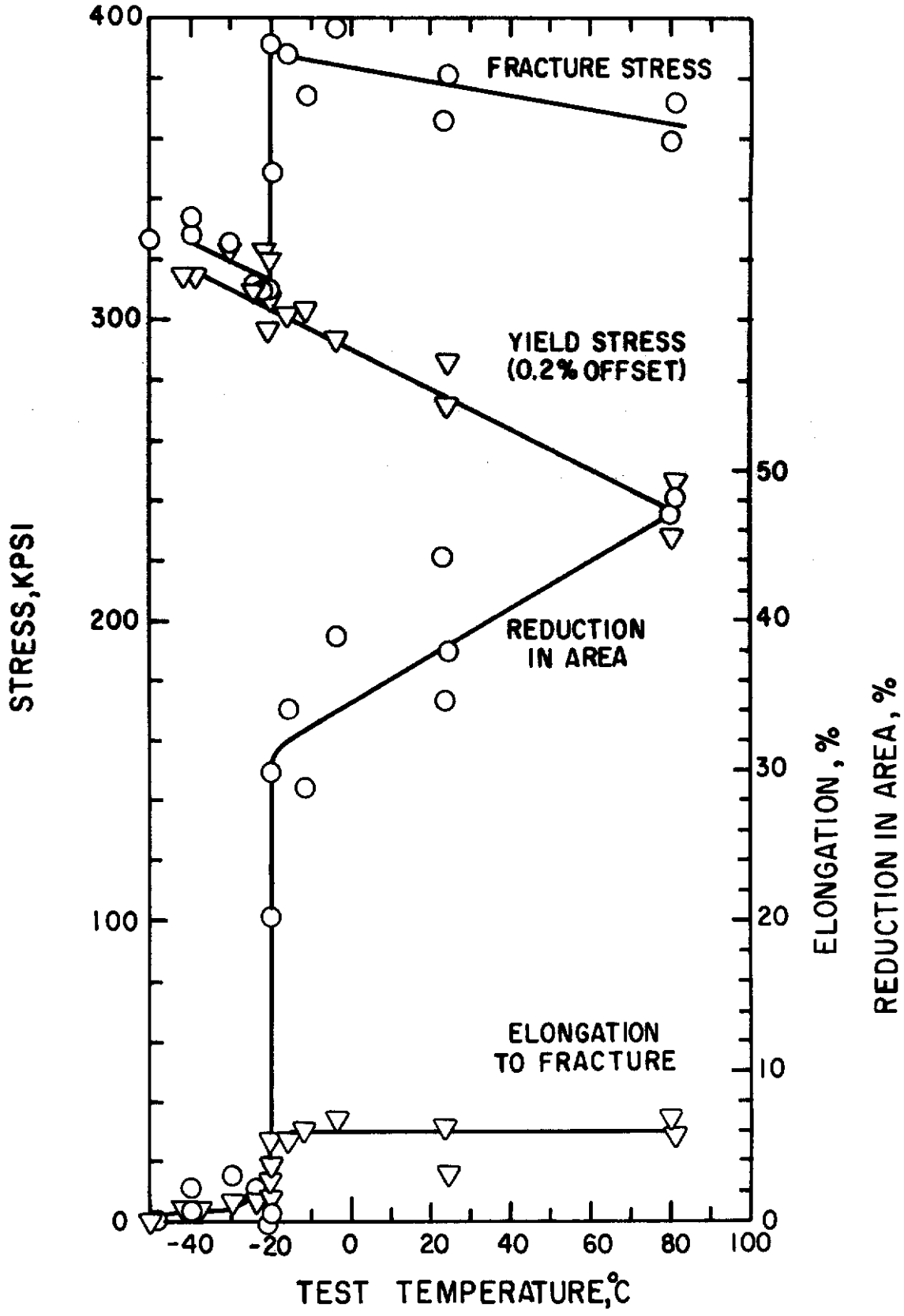

Fig.13- Effect of test temperature on the tensile properties of 0.030 inch as-drawn tungsten wire (W - P4)

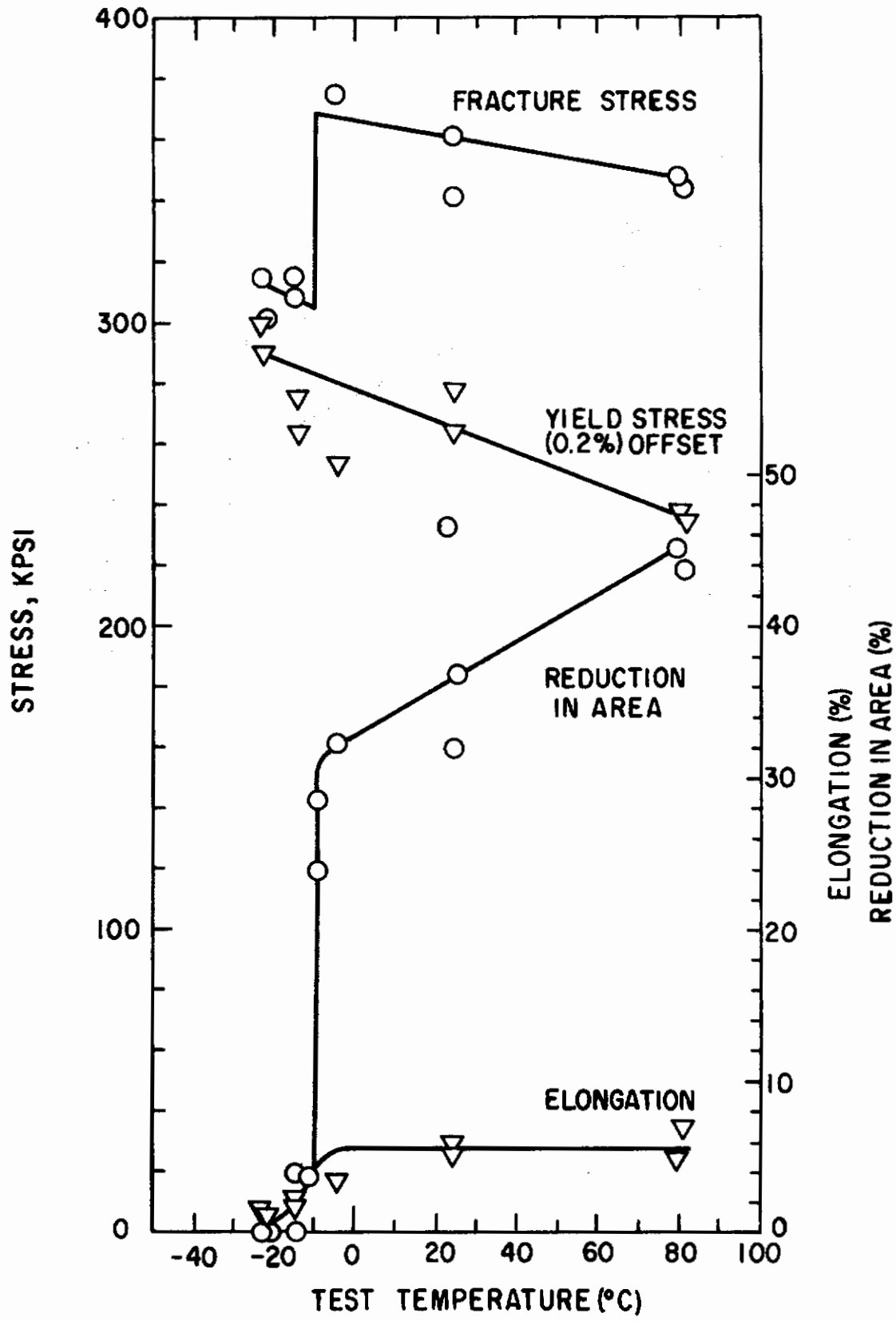

Fig.14- Effect of test temperature on the tensile properties of 0.030 inch tungsten wire (W-P4) annealed for 10 minutes at 800°C

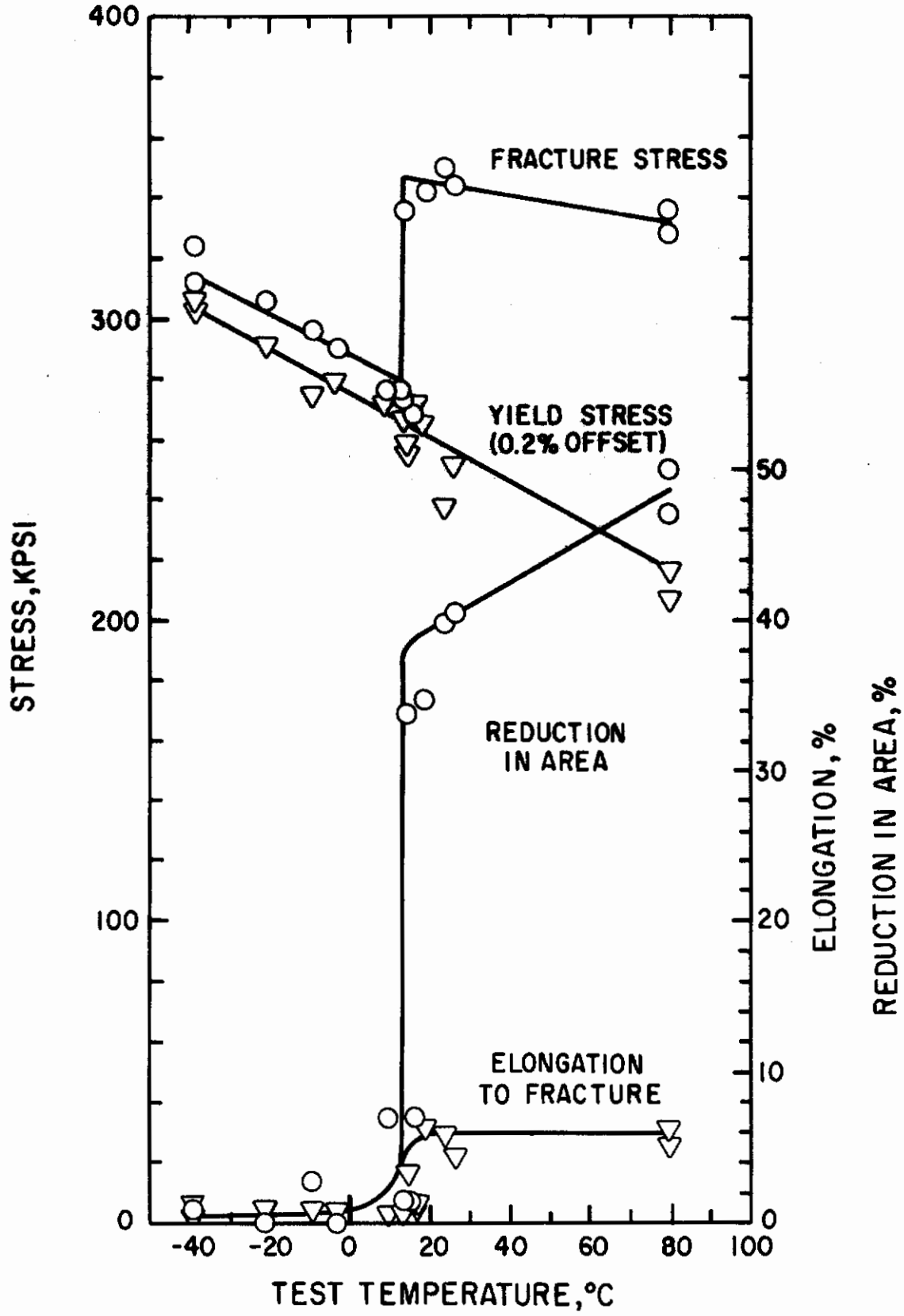

Fig. 15 Effect of test temperature on the tensile properties of 0.030 inch tungsten wire (W-P4) annealed for 10 minutes at 1050°C

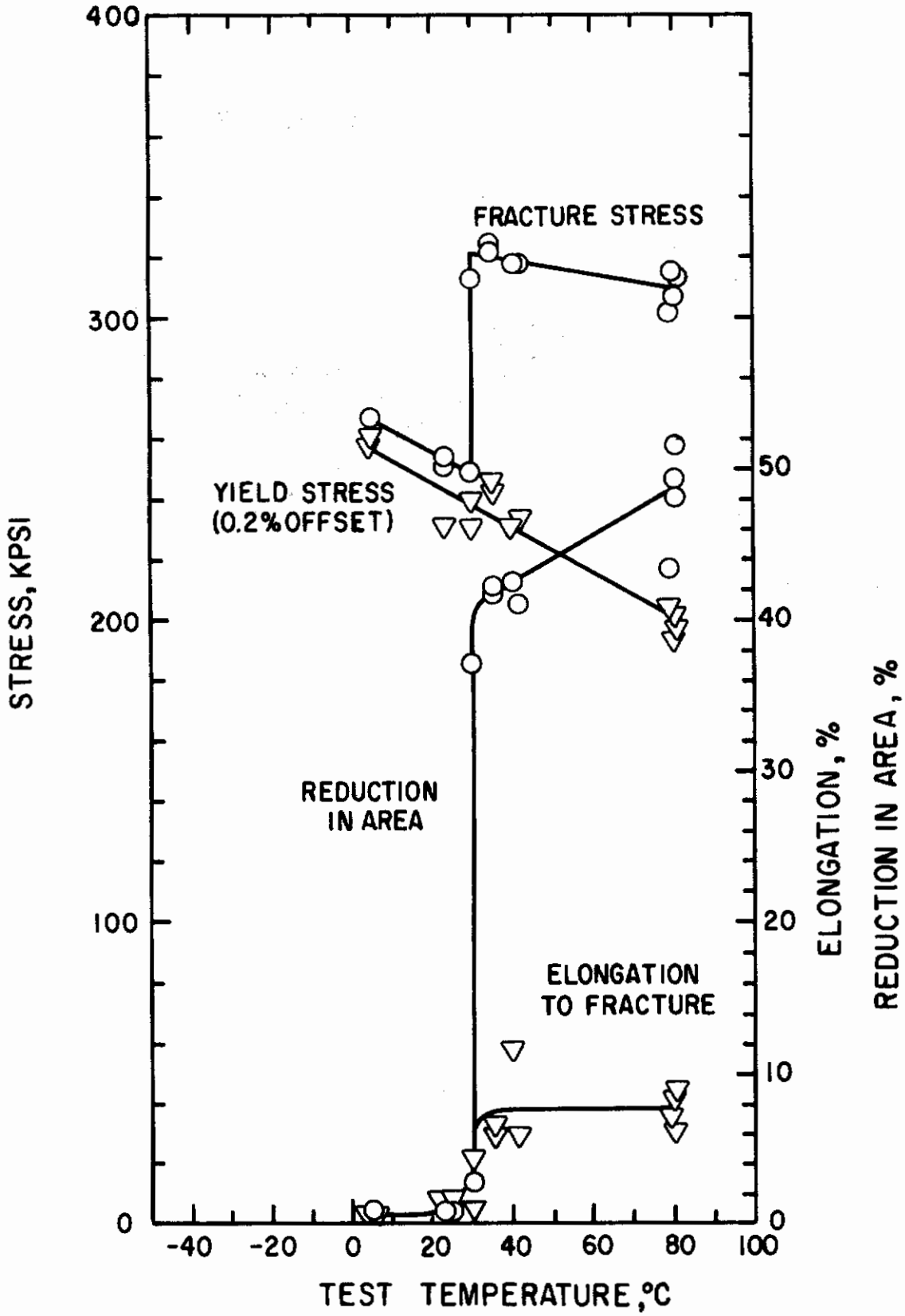

Fig.16- Effect of test temperature on the tensile properties of 0.030 inch tungsten wire (W-P4) annealed for 10 minutes at 1200°C

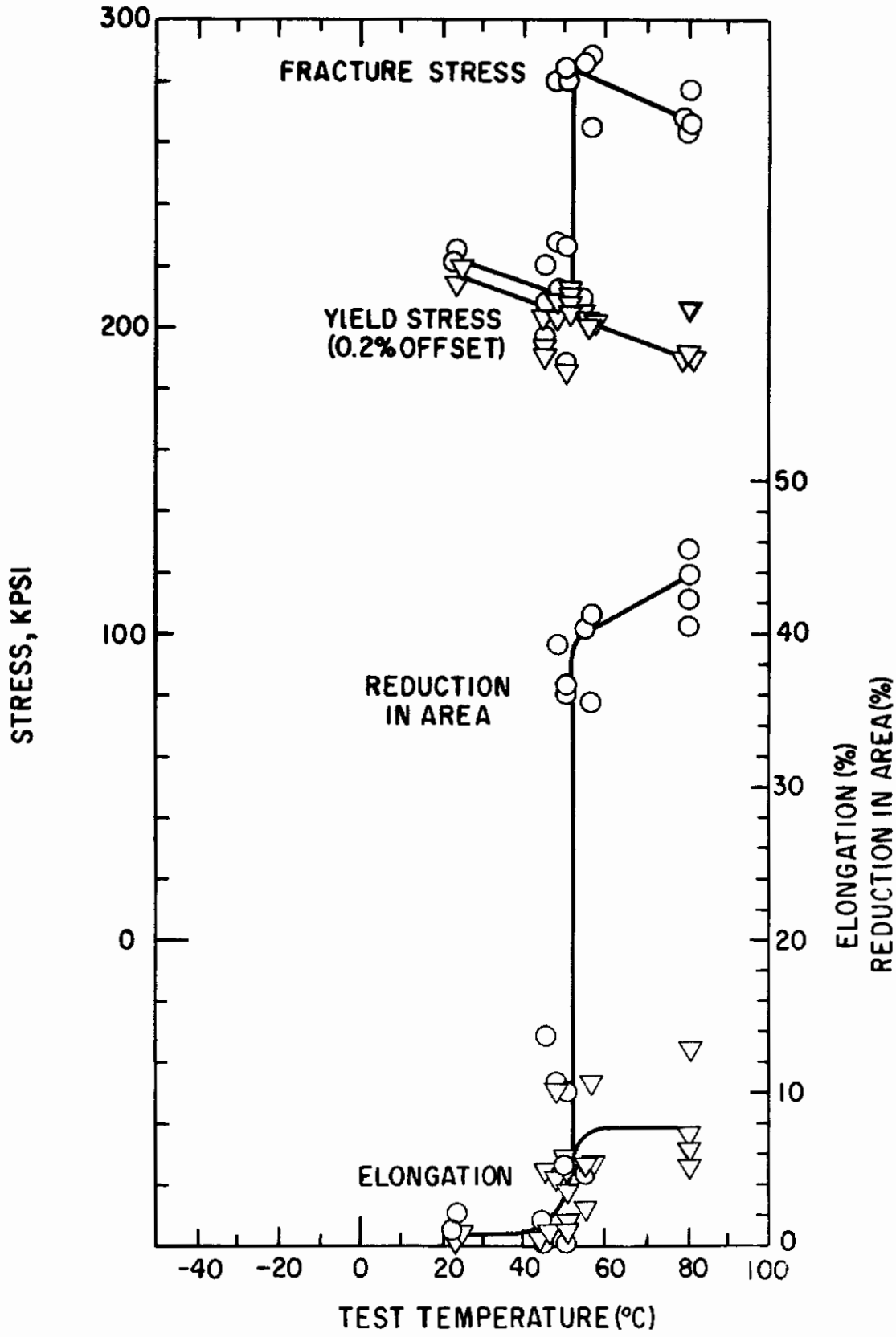

Fig.17-Effect of test temperature on the tensile properties of 0.030 inch tungsten wire (W-P4) annealed for 10 minutes at 1400°C

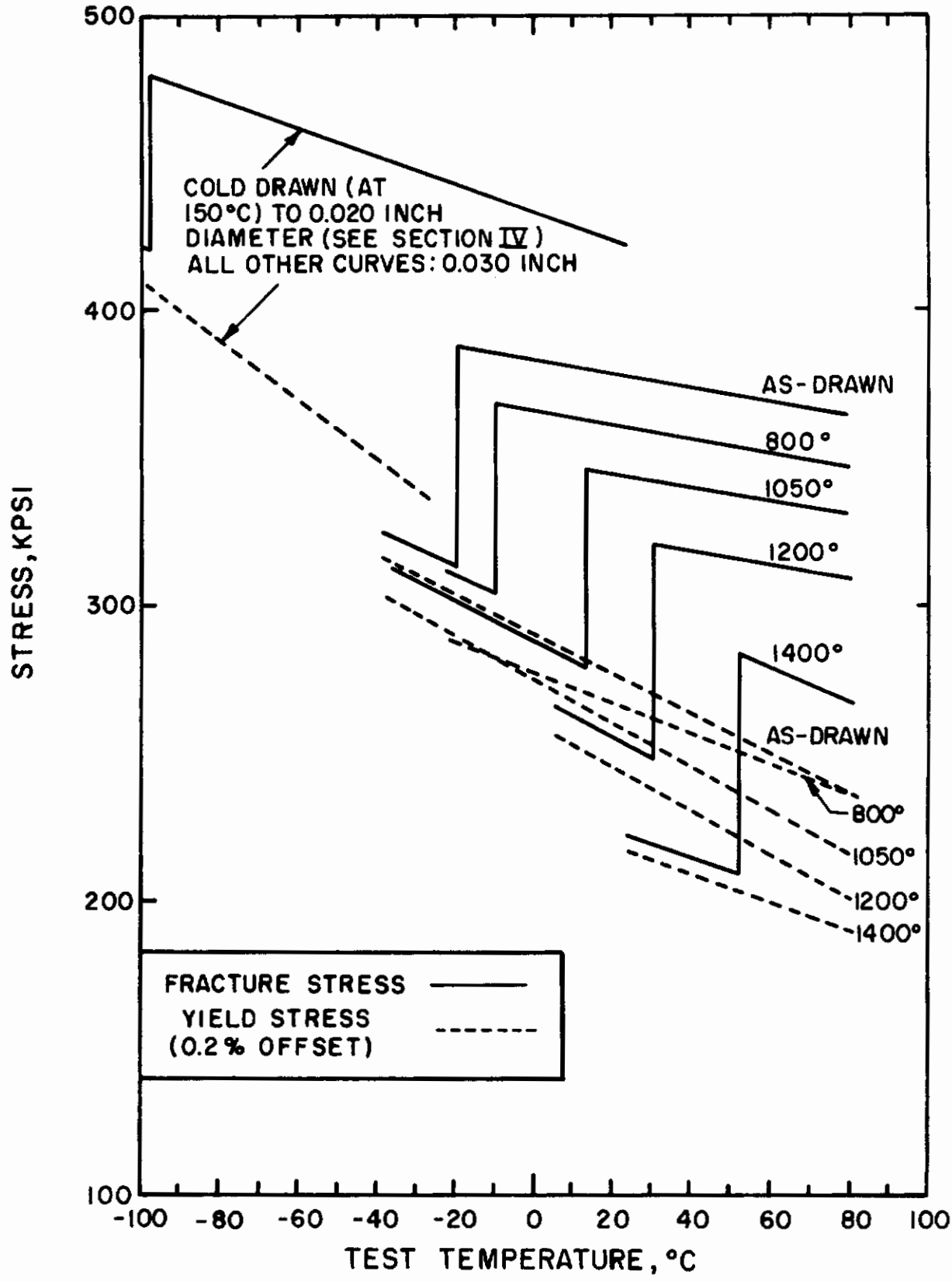

Fig. 18 - Effect of recovery-annealing (10 minute time) on the ductile-brittle transition behavior of tungsten wire (W-P4)

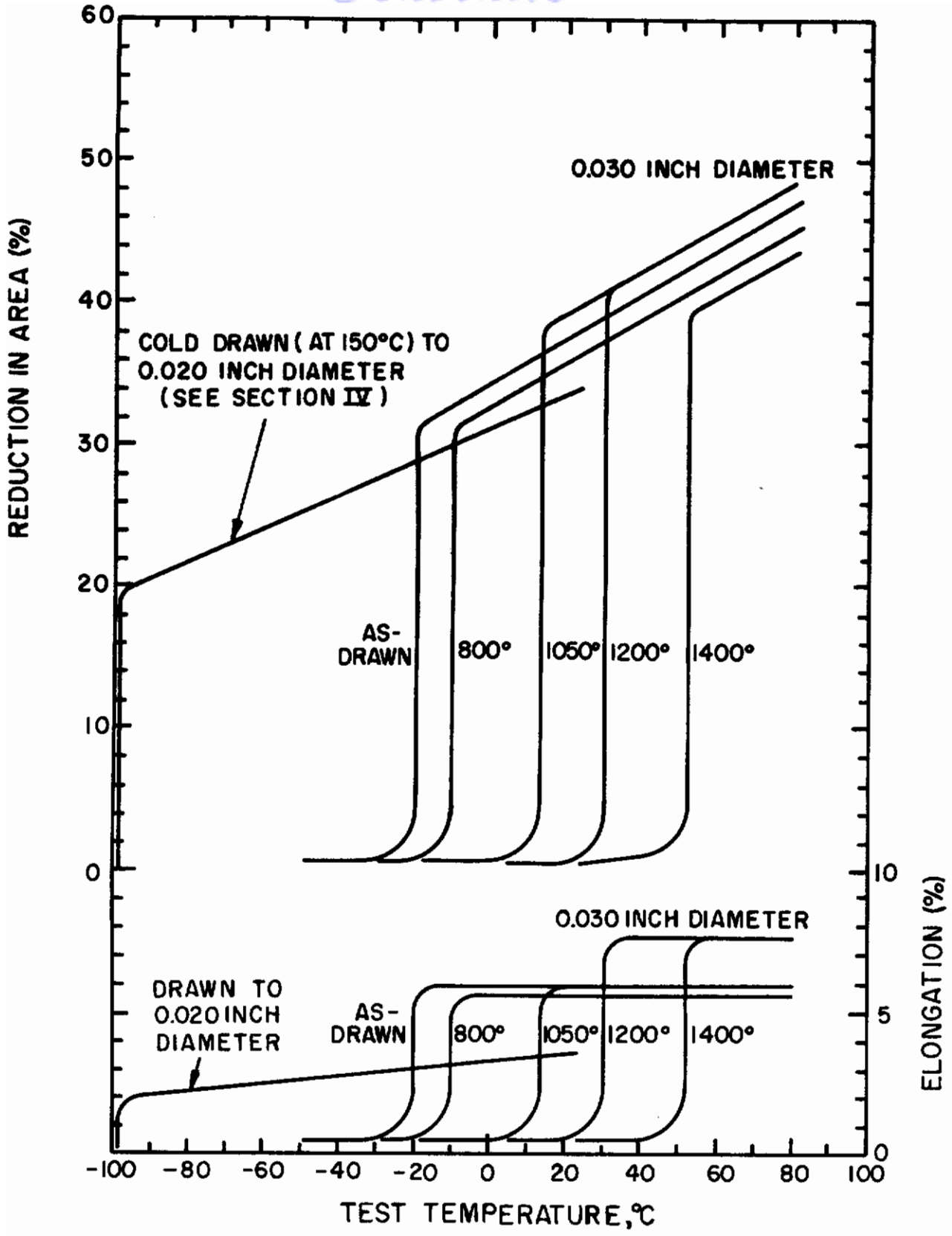

Fig.19- Effect of recovery-annealing (10 minute time) on the ductile-brittle transition behavior of tungsten wire (W-P4)

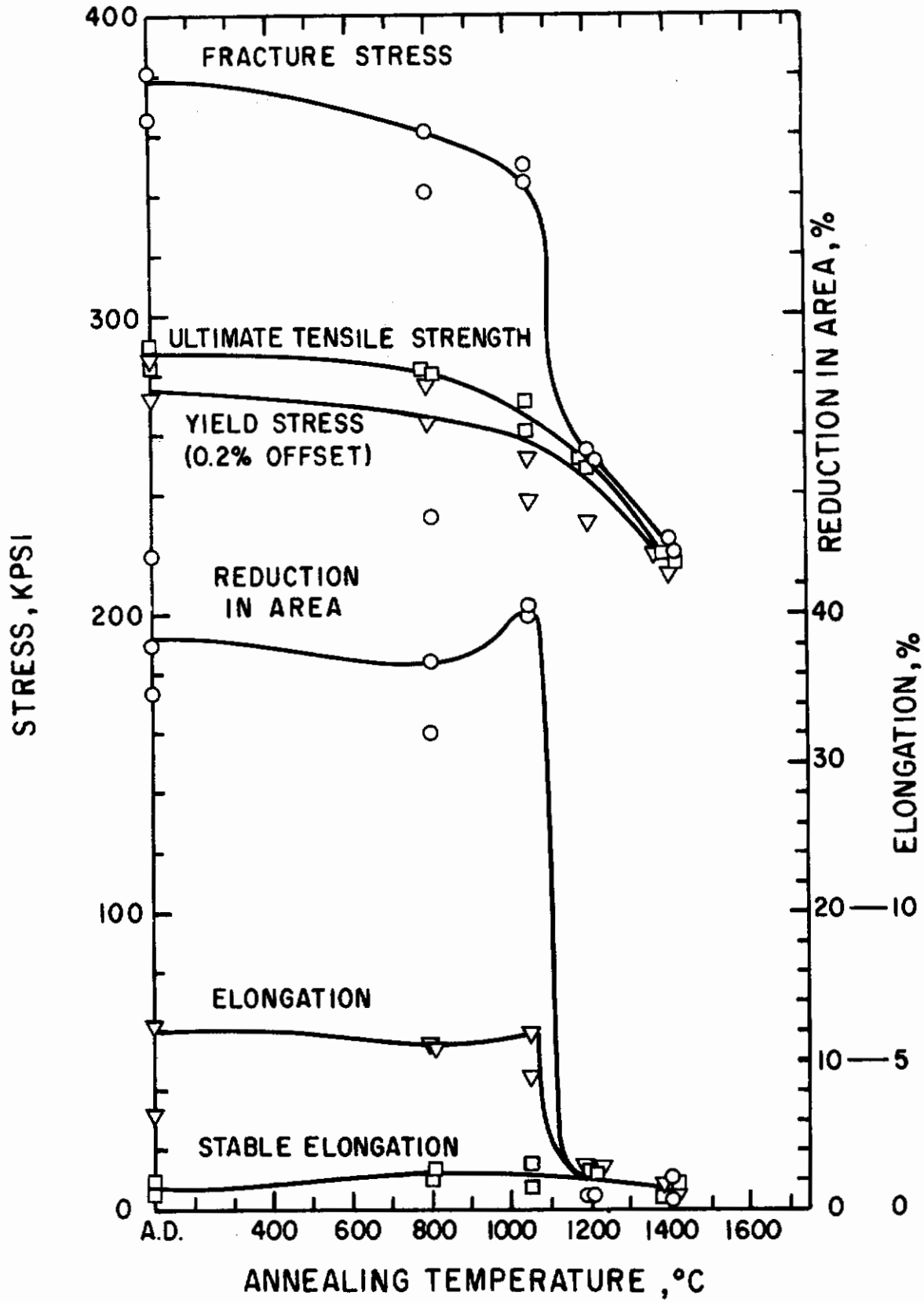

Fig.20-Effect of annealing temperature on the tensile properties of 0.030 inch tungsten wire (W-P4) tested at room temperature

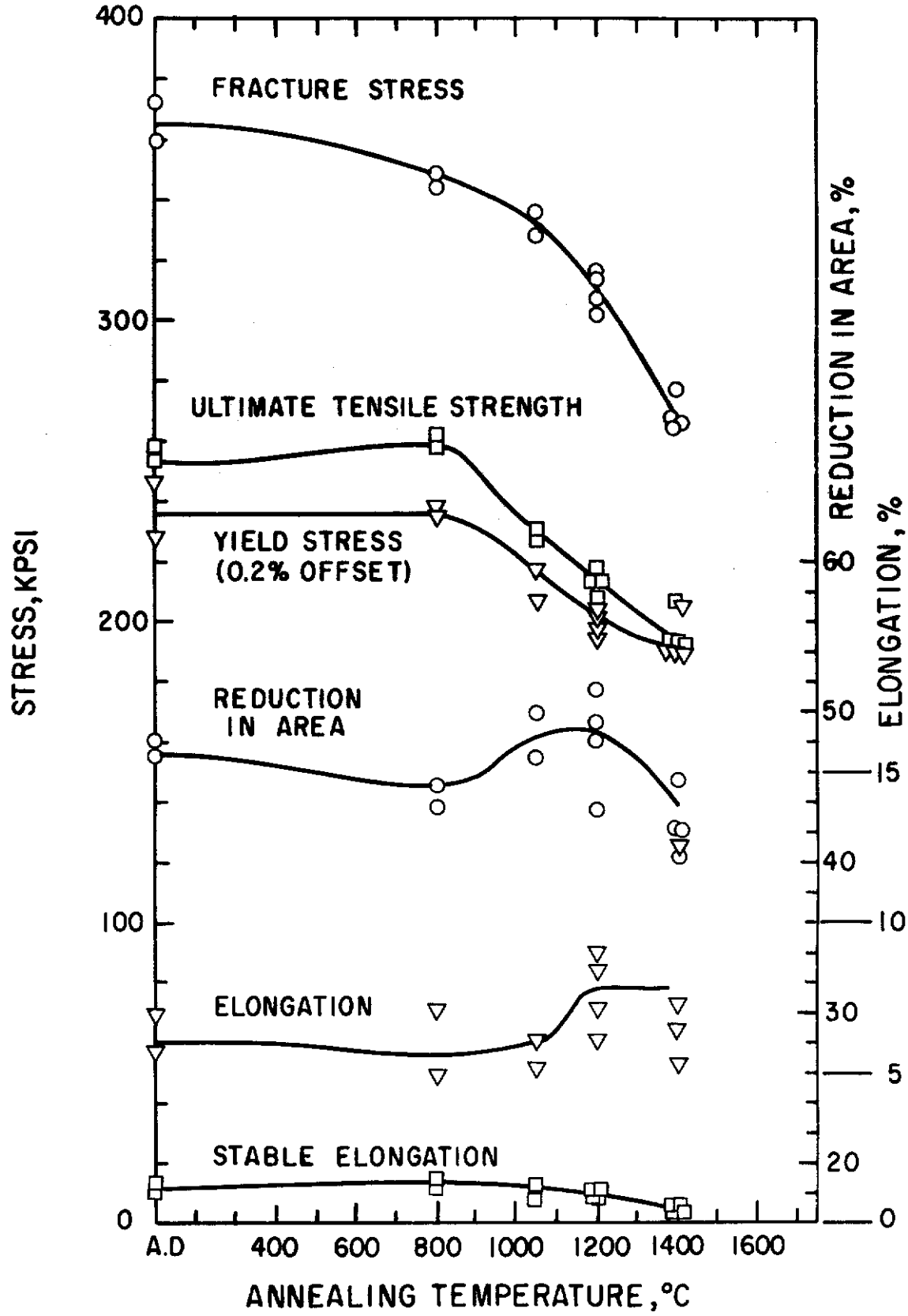

Fig.21 - Effect of annealing temperature on the tensile properties of 0.030 inch tungsten wire (W-P4) tested at 80°C.

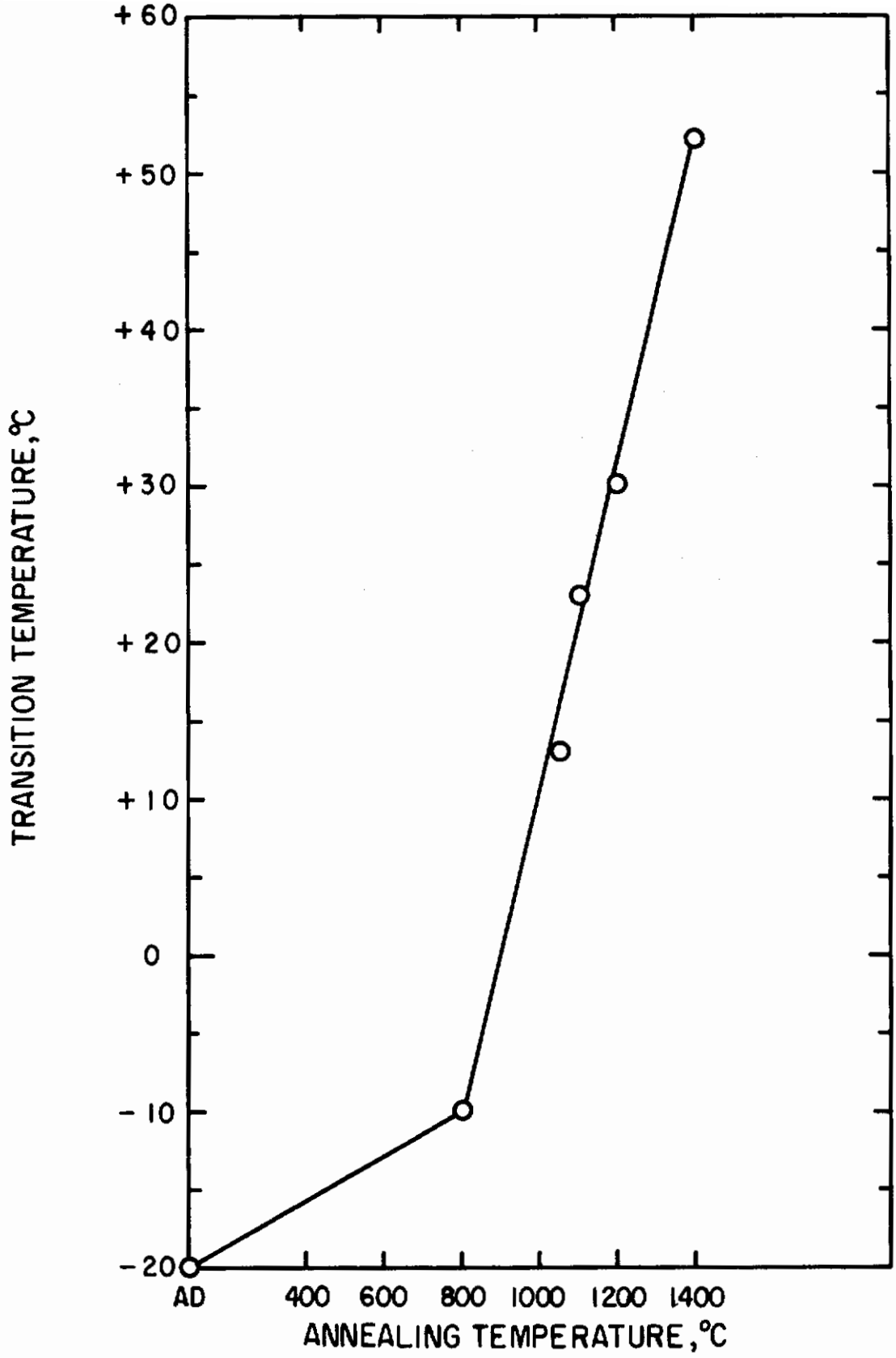

Fig.22-Effect of recovery-annealing temperature (10 minute hold) on the ductile-brittle transition temperature of 0.030 inch tungsten wire (W-P4)

1.4 Effect of Recovery-Annealing on the Load-Elongation Behavior - Typical load-elongation curves are shown in Figs. 23, 24, 25, 26, 27 and 28 for wires tested either below or above their transition temperature both in the as-drawn and in the recovery-annealed condition. Some plastic deformation is evident in all cases, even below T_d. The sharpness of the ductile-brittle transition is clearly illustrated by the large differences in elongation at similar flow stress levels for test temperatures just below and just above T_d. The occurrence of some ductility below T_d is consistent with current theories of brittle fracture[13, 14] which ascribe the nucleation of cracks to the deformation process itself.

Some evidence of discontinuous yielding is found after annealing at 1050°, 1200°, and 1400°. An annealing temperature of 800° results in more extensive strain hardening (Fig. 28), and consequently higher values of stable elongation and ultimate tensile strength (Fig. 20, 21) than for the as-drawn wire or for annealing temperatures above 800°.

2. Microstructures of Deformed and Fractured Tungsten (W-P4)

Tensile fractures exhibiting ductile behavior were found to occur either adjacent to the necked region, in the shoulder of the neck, or at the point of minimum diameter of the neck, Figs. 29 and 30. The fracture locations seem to be more or less random and not related in any discernible way to either metallurgical condition or test temperature. Transverse microcracks and longitudinal intergranular cracks both within and adjacent to the necked region are much more prevalent in the room temperature than in the 80° fractures.

The fibrous grains in the shoulder of the neck appear to be twisted and shortened, especially in the specimens tested at 80°. At the minimum diameter location, however, the fibers appear relatively long and straight, much like those in the uniformly strained regions outside the necked region, Figs. 29 and 30. The apparent shortening of the fibers in the shoulders of the neck can be attributed to bending and twisting during deformation, which probably occur in order that adjacent fibers can conform to each other under conditions of limited available slip systems. As a result, the fibers become initially oriented at an angle to the planar metallographic section. As deformation proceeds further, the twisted and bent fibers may tend to straighten out again, approaching an orientation parallel to the wire axis. Thus, the fibers appear longest at the location of the minimum diameter, where the deformation is highest.

It seems likely that the observed increase in ductile-brittle transition temperature (T_d) in the annealing range above 800° is associated with the possible role of the transverse subboundaries formed during polygonization in promoting fracture by aiding either crack nucleation or propagation. To determine if such transverse subboundaries constitute preferential fracture paths and thus aid crack propagation, a study was made of the fracture paths in bending and the micro-structures of several polygonized specimens. A definite correlation between the fracture paths and the longitudinal fiber boundaries was found in wires annealed for 10 minutes at 1050° and 1400°, Figs. 33 to 36; however, no clear correlation was found with transverse subboundaries. Thus, at present it seems more likely that the transverse subboundaries contribute to fracture by facilitating crack nucleation rather than propagation.

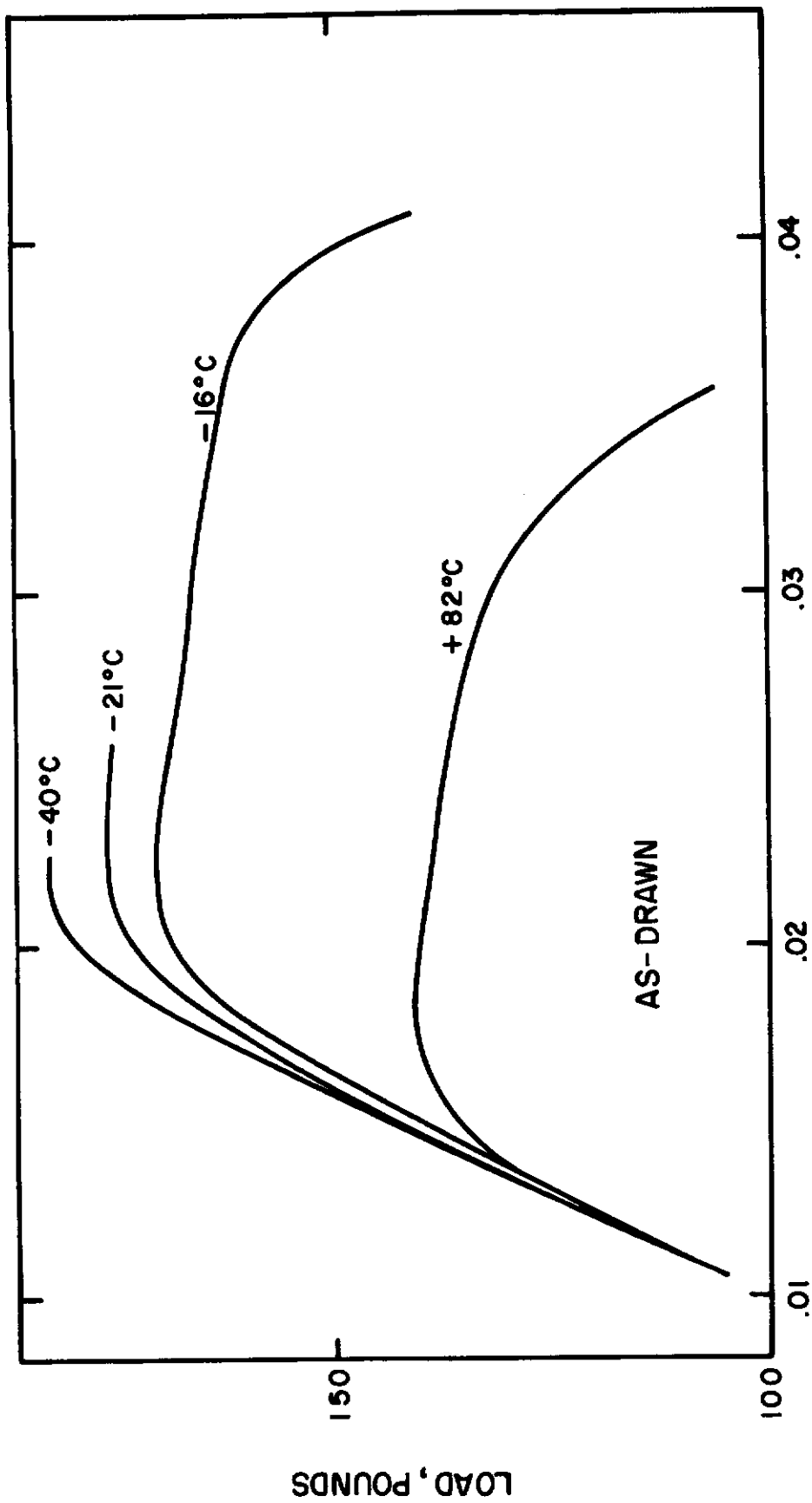

Fig.23- Load-elongation behavior of tungsten wires (W-P4) tested at various temperatures in the as-drawn condition.

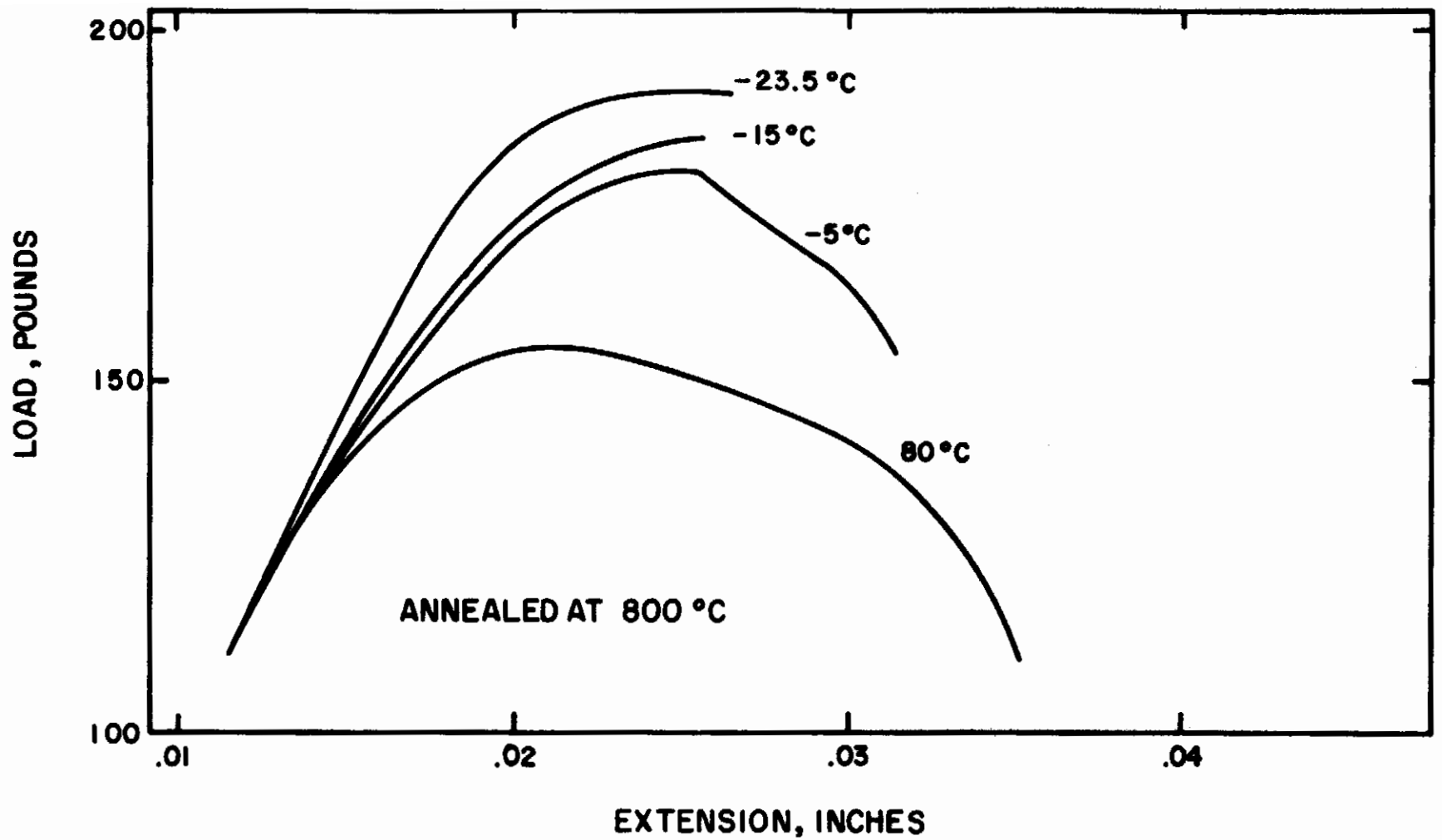

Fig.24-Load-elongation behavior of tungsten wires (W-P4) tested at various temperatures after annealing for 10 minutes at 800°C

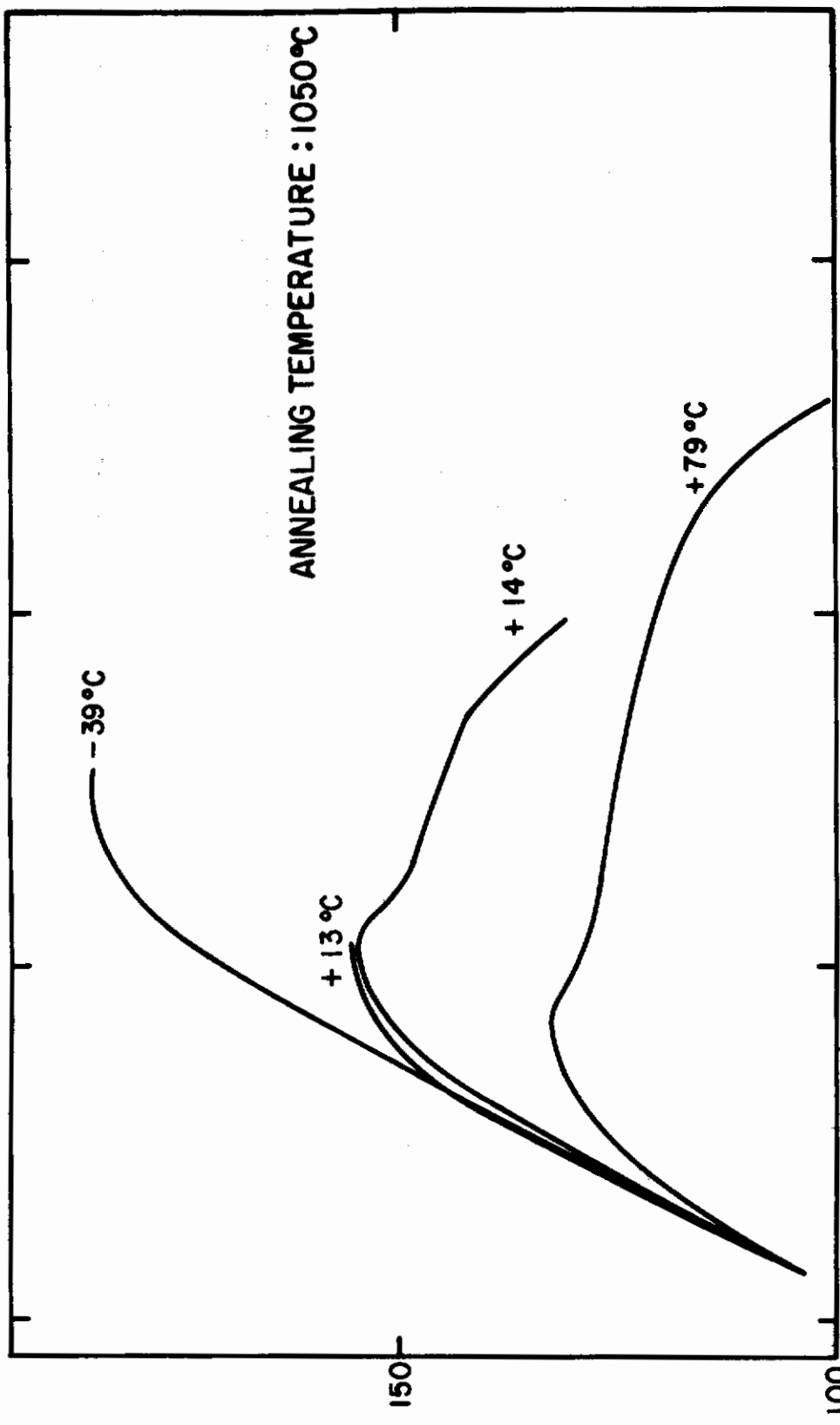

Fig.25- Load - elongation behavior of tungsten wires (W-P4) tested at various temperatures after annealing for 10 minutes at 1050°C

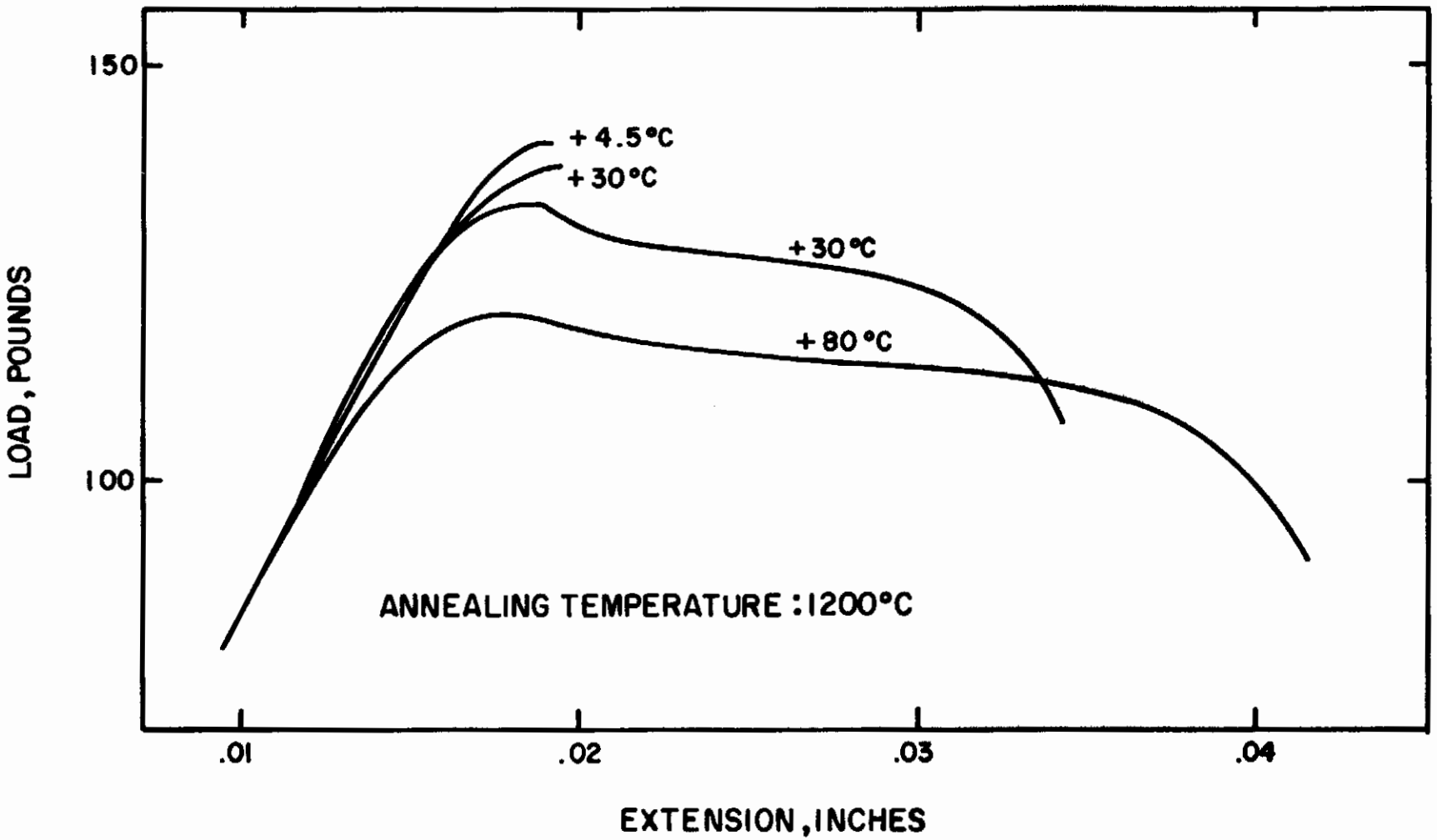

Fig.26- Load-elongation behavior of tungsten wires (W-P4) tested at various temperatures after annealing for 10 minutes at 1200°C

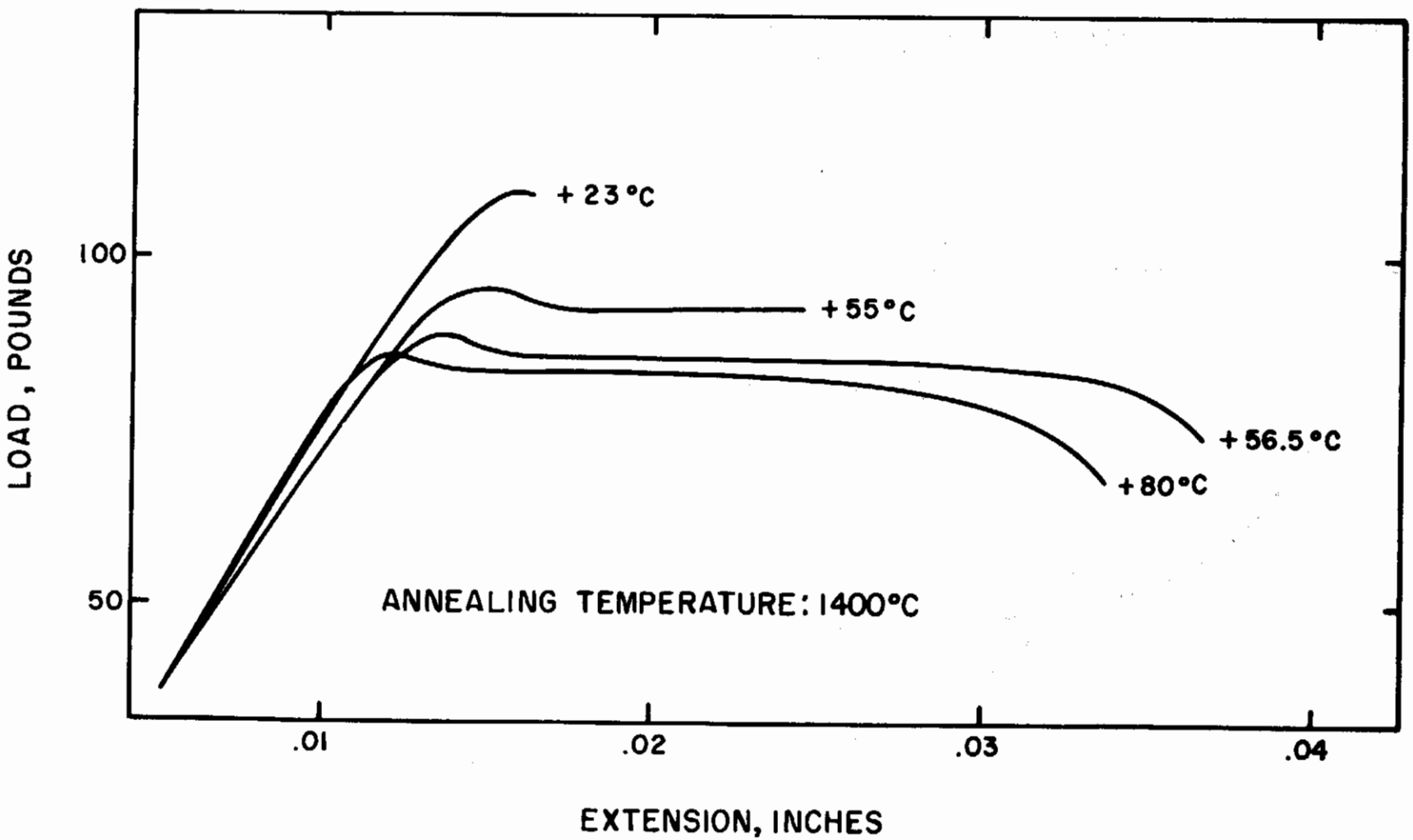

Fig.27- Load-elongation behavior of tungsten wires (W-P4) tested at various temperatures after annealing for 10 minutes at 1400°C

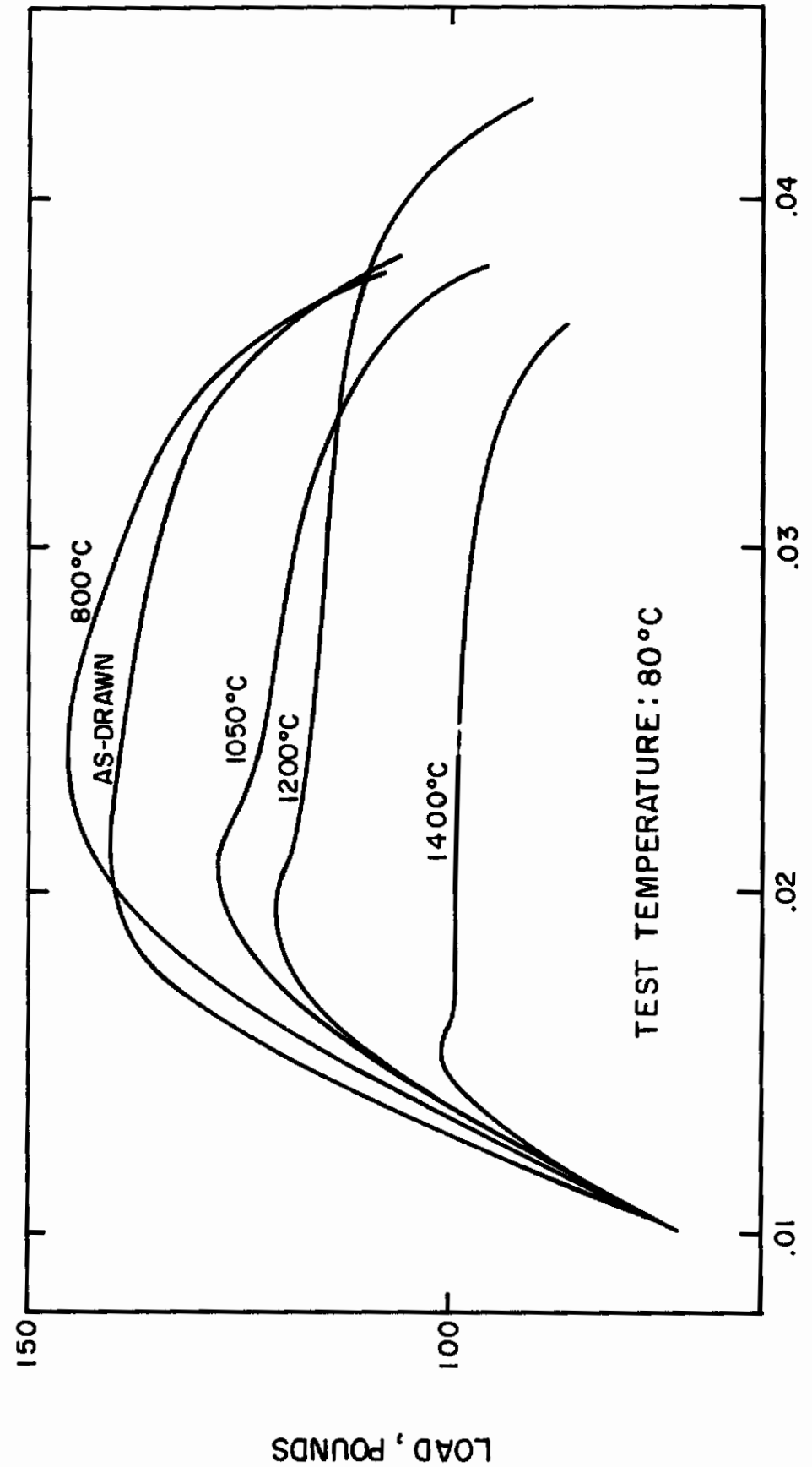

Fig.28-Load-elongation behavior of tungsten wires (W-P4) tested at 80°C after annealing for 10 minutes at various temperatures

3832 3833

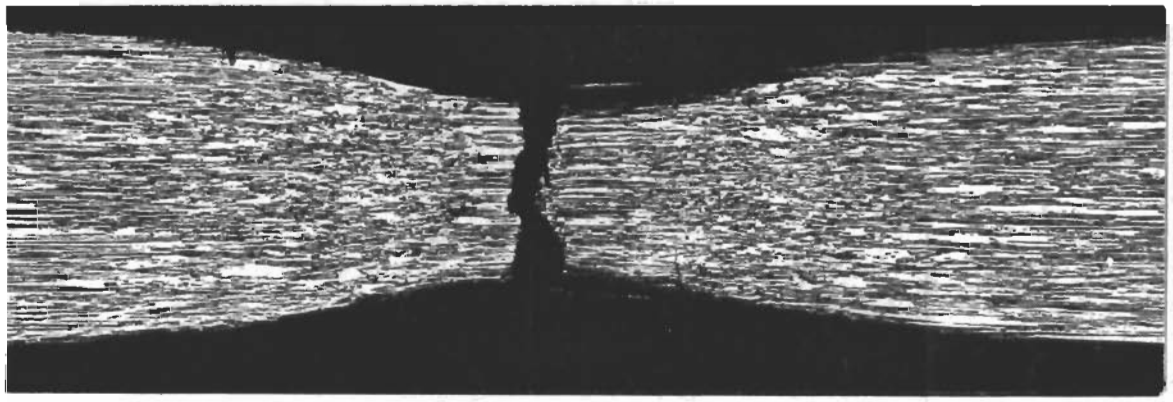

3835 .3735

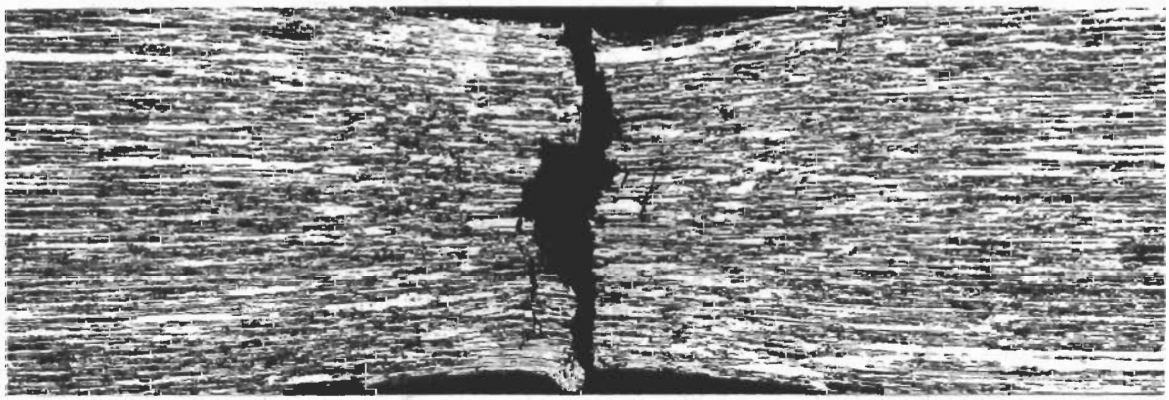

NaOH + $K_3Fe(CN)_6$ etch 3834 3724 100X

Fig. 29 - Necked regions of tungsten (W-P4) wire tensile specimens tested at room temperature. From top to bottom: as-drawn, annealed 10 minutes at 800°C, annealed 10 minutes at 1050°C.

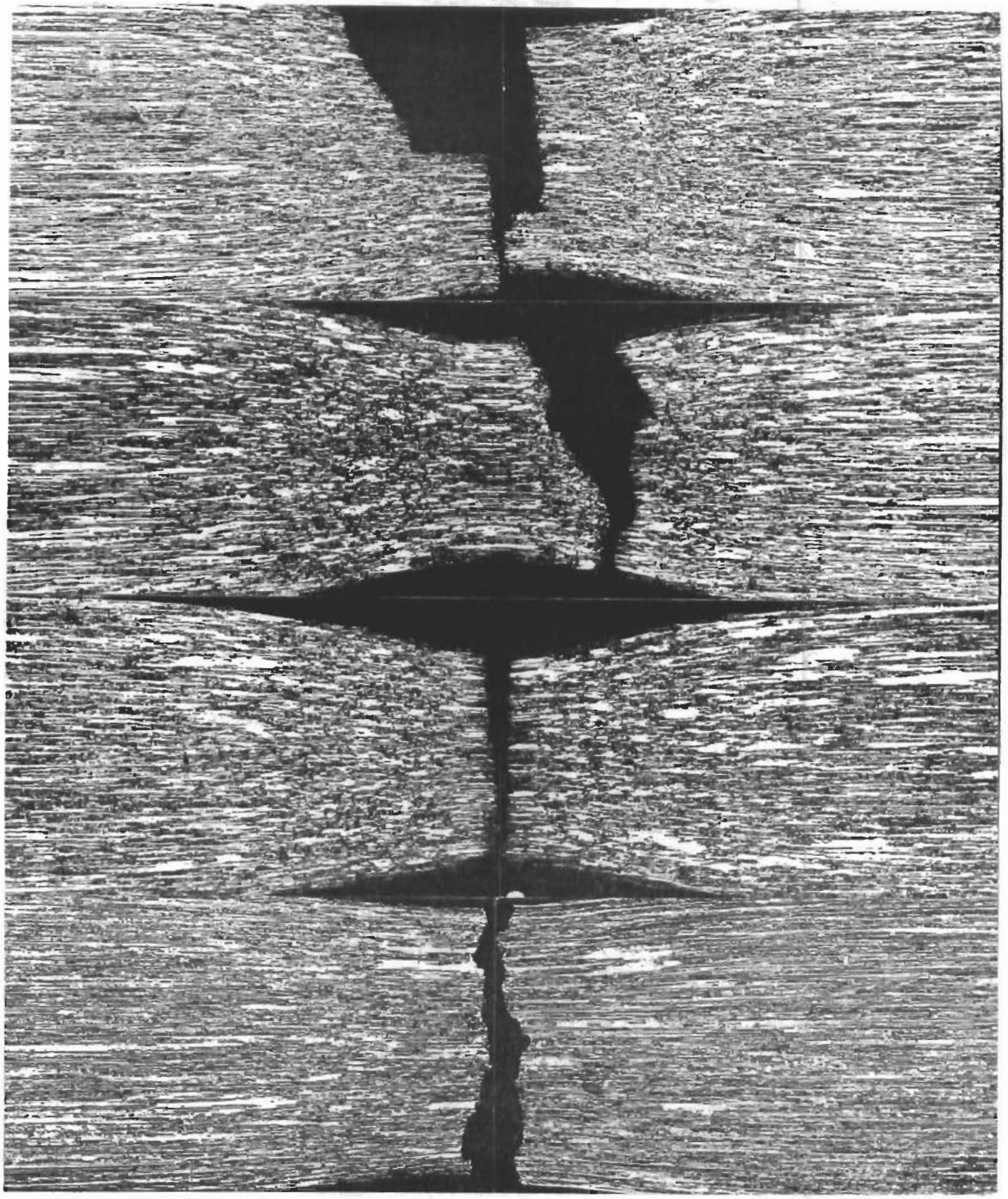

$NaOH + K_3Fe(CN)_6$ etch 100X

Fig. 30 - Necked regions of tungsten (W-P4) wire tensile specimens tested at 80°C. From top to bottom: as-drawn, annealed 10 minutes at 800°C, annealed 10 minutes at 1200°C, annealed 10 minutes at 1400°C.

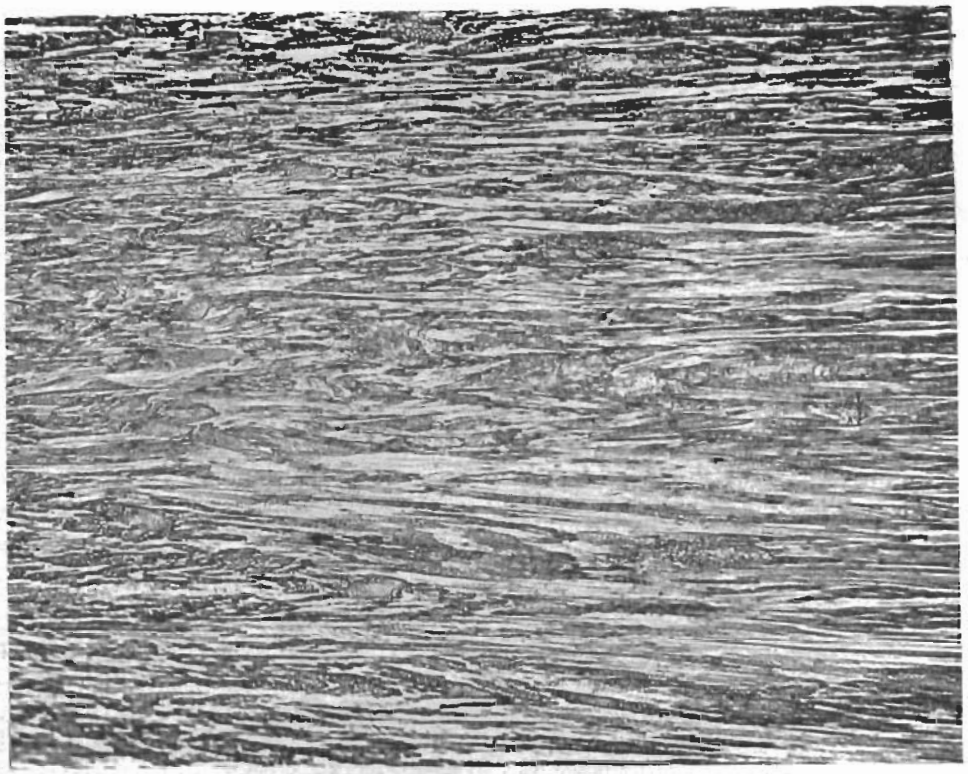

H_2O_2 etch 3728 500X

Fig. 31 Microstructure in the necked region of a tungsten (W-P4) wire tensile specimen tested at 80° in the as-drawn condition.

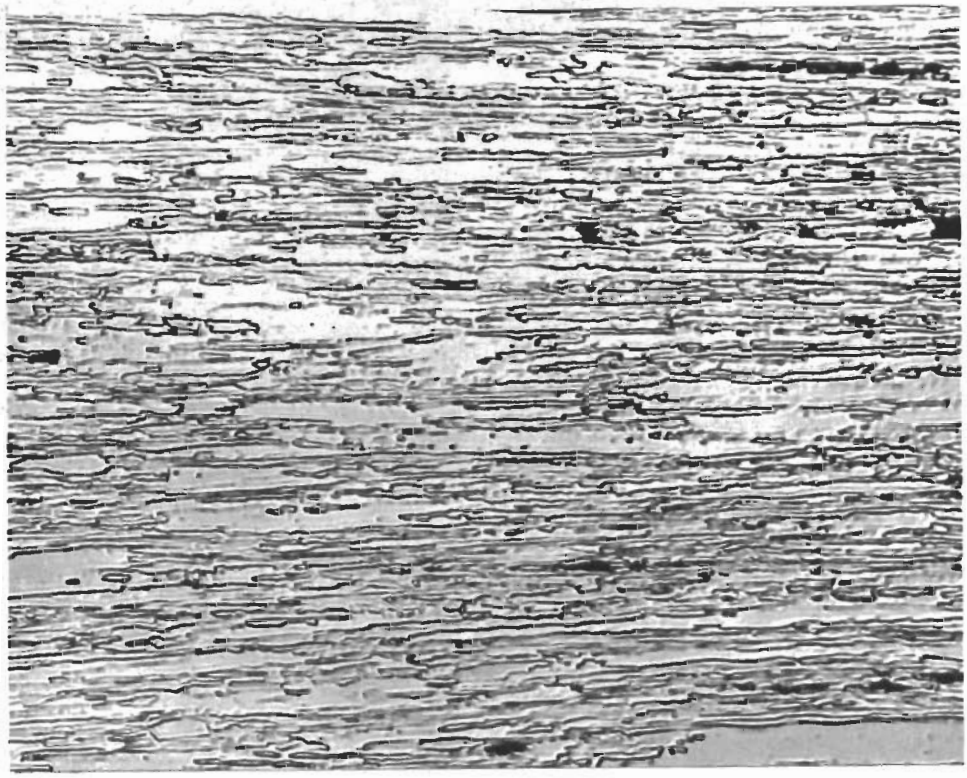

H_2O_2 etch 5008 500X

Fig. 32 - Microstructure in the necked region of a tungsten (W-P4) wire tensile specimen tested at 80° after annealing for 10 minutes at 1400°C.

H_2O_2 etch 2000X

Fig. 33 - Longitudinal section showing fracture path on tension side of bent tungsten (W-P4) wire specimen, annealed 10 minutes at 1050°C, then polished and etched before fracture. Note relationship of fracture path to longitudinal boundaries.

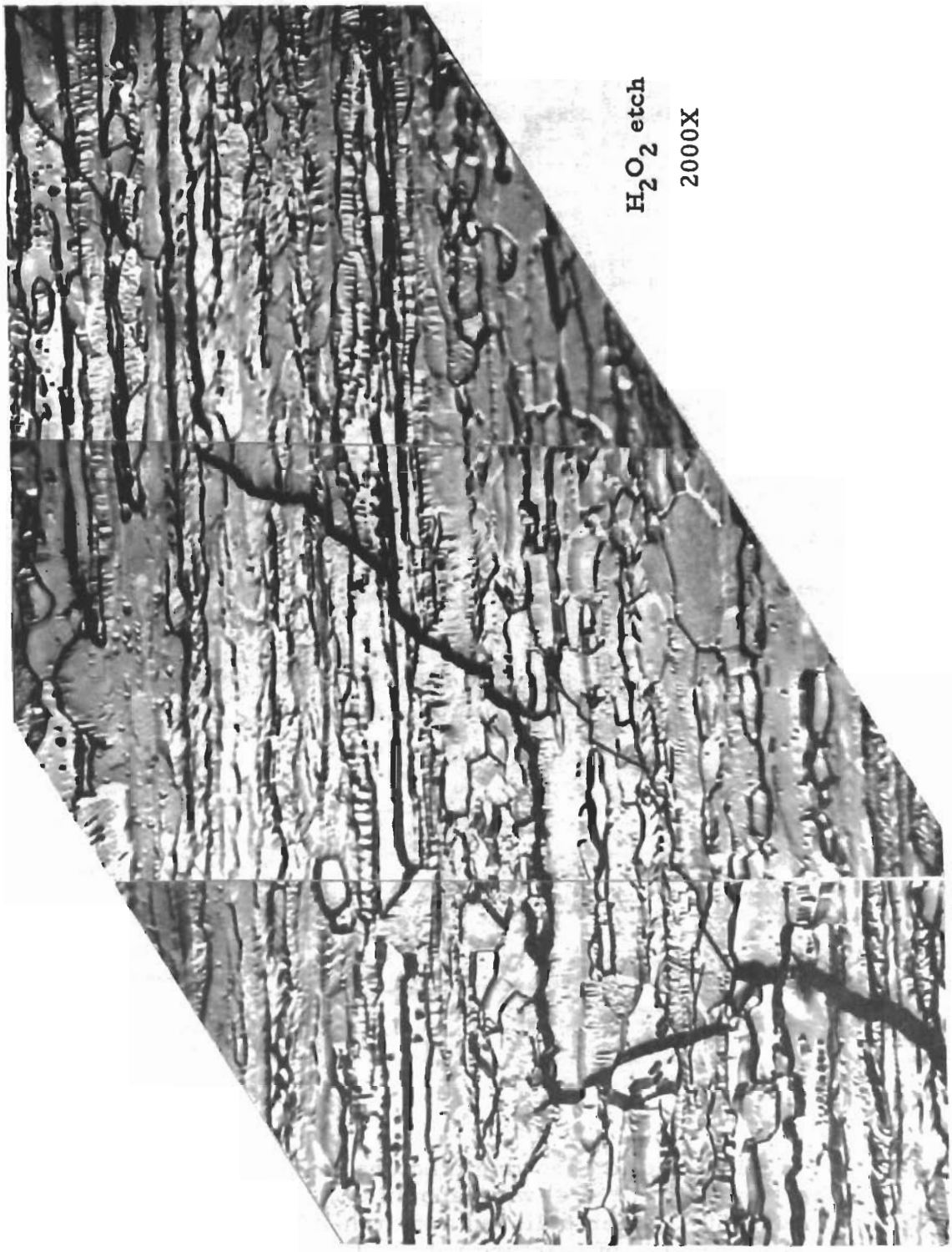

Fig. 34 - Longitudinal section showing fracture path on tension side of bent tungsten (W-P4) wire specimen, annealed 10 minutes at 1400°C, then polished and etched before fracture. Note relationship of fracture path to longitudinal boundaries.

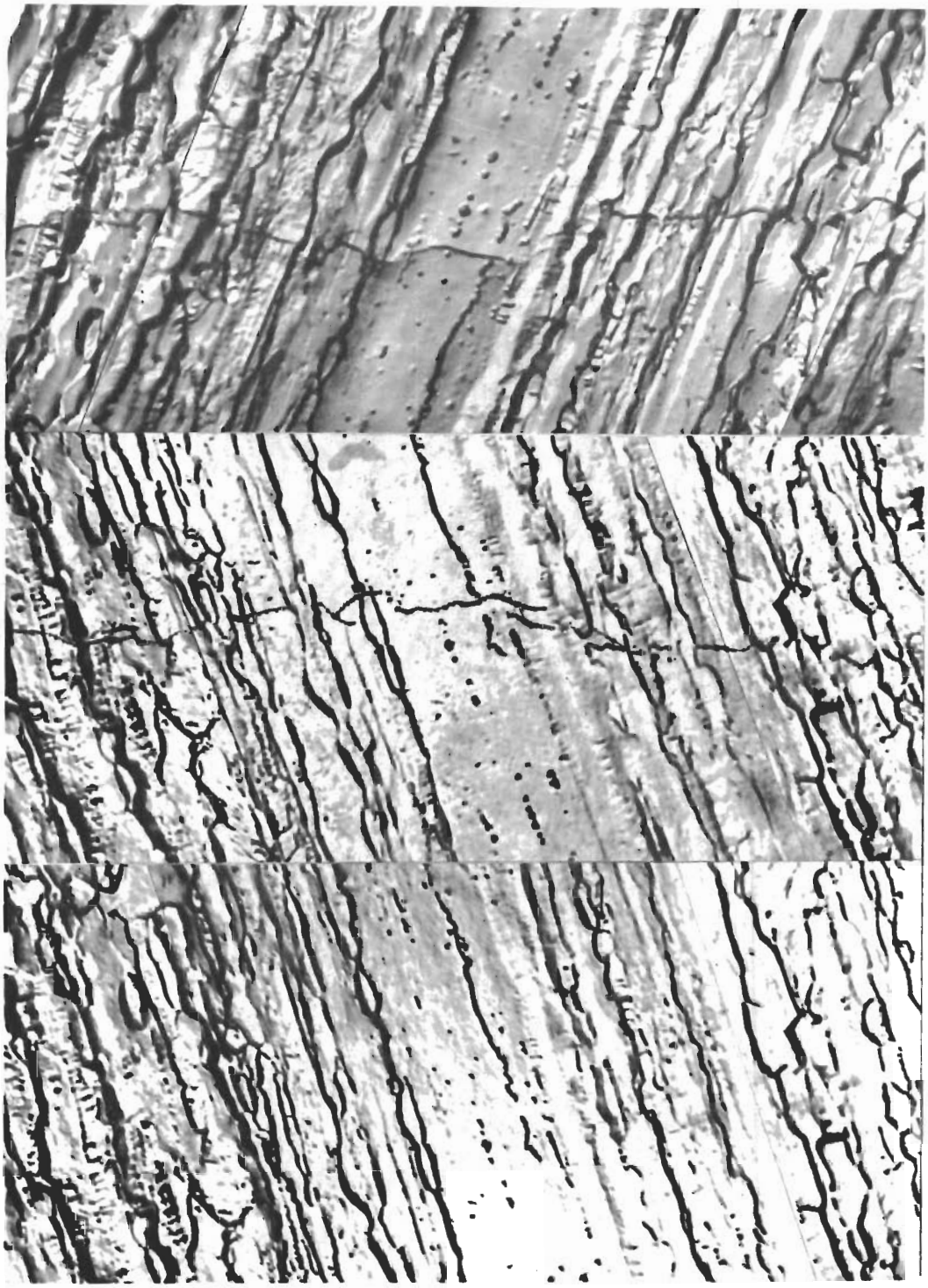

H_2O_2 etch 2000X

Fig. 35 - Longitudinal sections showing fracture path on tension side of bent tungsten (W-P4) wire specimen, annealed 10 minutes at 1400°C, then polished and etched before fracture. From top to bottom: Specimen after fracture. Fracture path plotted on replica of original microstructure. Replica of original microstructure.

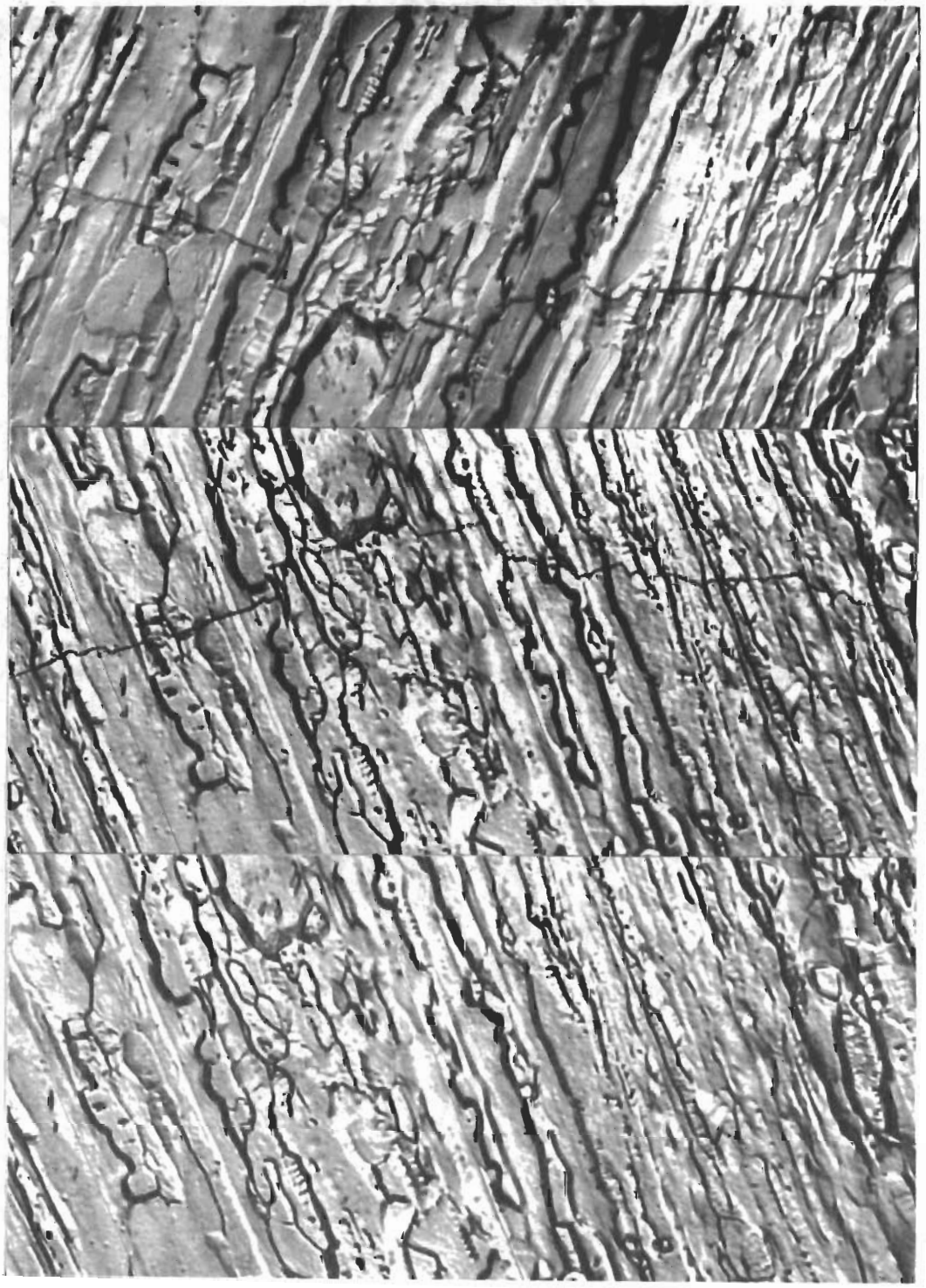

H_2O_2 etch 2000X

Fig. 36 - Longitudinal sections showing fracture path on tension side of bent tungsten (W-P4) wire specimen, annealed 10 minutes at 1400°C, then polished and etched before fracture. From top to bottom: Specimen after fracture. Fracture path plotted on replica of original microstructure. Replica of original microstructure.

3. Discussion of the Transition Behavior of Tungsten (W-P4) Wire

The ductile-brittle transition behavior of recrystallization-annealed tungsten rods has been studied previously by Bechtold and Shewmon[15] and by Pugh[16], who also studied worked tungsten. The effect of recovery-annealing on the room temperature tensile properties of heavily worked tungsten wires has been studied by Davis[17] and by Pugh[18]. More recently, Koo[19] has correlated changes in room temperature tensile properties of worked tungsten rods due to recovery-annealing with changes in substructure. However, no results have so far been found to be reported on the changes in ductile-brittle transition behavior during recovery.

The previously reported effects of recovery-annealing on the room temperature tensile properties can now be interpreted in terms of the effects observed on the transition behavior. The increase in room temperature reduction of area between annealing temperatures of 800 and 1050° and the corresponding increases at 80° are typical of the changes in ductility of b.c.c. metals occurring during annealing for test temperatures above T_d. The sharp drop in room temperature ductility after annealing at 1100° (Fig. 20) corresponds to an increase in T_d above the test temperature (23°), which is consistent with the other measurements of T_d (Fig. 22).

Although the sharp drop in room temperature ductility may seem to indicate the onset of a new process above 1050°, the continuous increase in ductility above T_d up to 1200° indicates that there is nothing unique about annealing at temperatures in the vicinity of 1100°. The phenomena responsible for the sharp drop in room temperature ductility are apparently occurring during the entire range from 800 to 1200°, as is indicated by the continuous increase in T_d over this range.

The results of Davis[17] and of Pugh[18] on the effect of annealing on the tensile properties of tungsten can be interpreted in a similar way. Pugh found a rise in room temperature elongation to a maximum at an annealing temperature of 600°, followed by a sharp drop at higher annealing temperatures. He attributed the embrittlement to polygonization and strain aging, but noted the perplexing observation of both a rise and then a decrease in ductility. However, the present results show that the abrupt decrease in room temperature ductility probably reflects the combined effects of a gradual increase in T_d and the discontinuous nature of the ductile-brittle transition itself. It does not necessarily imply a process peculiar to the particular annealing temperature range which results in the ductility decrease. If a higher test temperature than room temperature were used, the ductility would probably have been observed to increase continuously with increasing annealing temperature. It is, therefore, the increase in ductility as a result of annealing, as well as the implied increase in T_d, that is significant in Pugh's results. The increase in ductility is probably less characteristic of strain aging than of polygonization.

Davis reported that the tensile elongation of tungsten wires tested at 200° increases with increasing annealing temperatures up to 1900°, where T_d presumably passes above 200°. He attributed the sharp drop in ductility to the onset of recrystallization. This interpretation may be misleading, since it is based on the circumstance that the annealing temperature for embrittlement is approximately the same as that for recrystallization. Whereas the recrystallization temperature is relatively independent of the conditions used to detect

it (test temperature, metallographic preparation, etc.), the apparent embrittlement temperature depends to a great extent on the relationship of the test conditions (temperature, strain rate, etc.) to T_d. The embrittlement itself, in fact, is more a characteristic of the ductile-brittle transition than of recrystallization. Rather than the reported embrittlement due to recrystallization, the significant effects observed by Davis seem to be the continuous rise of ductility over a wide range of ductilities and annealing temperatures, together with the implied rise in T_d. Work conducted by Shine at M. I. T. on 20-mil tungsten wire (see Section IV) has shown behavior similar to that found by Pugh, by Davis, and the present work.

The increase in transition temperature on annealing above 800°C may be tentatively attributed both to the increase in fiber width and to substructural changes such as polygonization and subgrain growth. The magnitude of the substructural contribution to the change in T_d remains to be determined.

4. Calculation of the Crack Propagation Energy for Tungsten(W-P4) Wire

According to Cottrell and Petch[13, 14], brittle fracture occurs in tension just below the transition temperature (T_d) provided that the following condition is satisfied:

$$\sigma_c = \frac{2 G \gamma'}{k_y d^{1/2}} \qquad (1)$$

where σ_c = fracture stress (tension)

G = shear modulus

γ' = crack propagation energy(or effective surface energy)

k_y = yield locking parameter

d = semi-grain size (effective slip distance is more correct)

According to Rosenfield[20], the ratio of yield locking parameter to the shear modulus is constant:

$$\frac{k_y}{G} \cong 5 \times 10^{-5} \qquad (2)$$

Using a factor of 2 to take into account the larger effective slip distance due to preferred fiber orientation:

$$\gamma' = 5 \times 10^{-5} \sigma_c d^{1/2} \qquad (3)$$

Using values of fracture stress (σ_c) as determined from Figs. 13 to 17 and values of semi-fiber width (d) as determined metallographically (based on average values measured by ManLabs and M. I. T.), the magnitude of γ' for W-P4 wire in the as-drawn condition was found to be about 1.1×10^4 ergs/cm^2. As shown in Table 19, this does not vary appreciably with annealing temperature up to at least 1400°.

Table 19

Calculated Crack Propagation Energy (γ') of W-P4 Wire at Transition Temperature

Condition	T_d °C	σ_c dynes/cm^2	d cm	γ' * ergs/cm^2
As-drawn	-20	2.1×10^{10}	1.0×10^{-4}	1.1×10^{4}
800°C Anneal	-10	2.1×10^{10}	0.9×10^{-4}	1.0×10^{4}
1050°C Anneal	+13	1.9×10^{10}	1.3×10^{-4}	1.1×10^{4}
1200°C Anneal	+30	1.7×10^{10}	2.0×10^{-4}	1.2×10^{4}
1400°C Anneal	+52	1.4×10^{10}	2.5×10^{-4}	1.2×10^{4}

* $\gamma' = 5\times10^{-5}\ \sigma_c\ d^{1/2}$ ergs/cm^2

The insensitivity of γ' to annealing temperature in the range where extensive polygonization and subgrain growth occur is an indication that these changes in substructure have little effect on γ'. This is consistent with the results of experiments on fracture paths (described in III. C. 2.), which showed no correlation with transverse subboundaries. It appears likely, then, that substructural changes play a minor role in the increase of T_d during recovery-annealing. The predominant factor affecting T_d in the range of annealing temperature from 800° to 1400°C is probably the increase in fiber width (Fig. 7).

Using the Griffith-Orowan[21] equation, the critical crack length was calculated using values of γ' given in Table 19:

$$c = \frac{2 E \gamma'}{\Pi \sigma_c^2} \qquad (4)$$

where c = semi crack length
E = Young's modulus (4.0×10^{12} dynes/cm^2 for tungsten)

As shown in Table 20, the ratio of the critical crack length to fiber width (c/d) for a given condition decreases with decreasing test temperature, and there is a discontinuous decrease in this ratio of about one order of magnitude in going from just above to just below T_d. The magnitude of c/d is about 5 above T_d and 0.5 below T_d. Thus, the critical crack length appears to be of the order of the fiber width both above and below T_d.

Annealing results in an initial increase in c/d, a maximum at about 800°C and a decrease up to at least 1400°C as calculated for temperatures both above and below T_d. However, this could be partly due to a variation of k_y which was assumed constant in the calculations ($k_y = 7.9 \times 10^7$).

In order to be used above T_d where considerable necking occurs, it is believed necessary to modify the Cottrell-Petch equation (1) by substituting the flow locking parameter (k_f) for the yield locking parameter (k_y), as follows:

$$\sigma_c = \frac{\beta G \gamma'}{k_f d^{1/2}}$$

where β = 2 times the ratio of maximum shear stress to maximum normal stress
G = shear modulus (1.6×10^{12} dynes/cm^2 for tungsten).

For severe necking, a state of hydrostatic tension occurs and β is generally considered equal to 1/3. From the experimental values of fracture stress (σ_c) and semi-fiber width (d) corrected for the reduction of area in the neck, it is possible to calculate k_f using equation (5). As shown in Table 21, k_f is approximately equal to 2.4×10^7 cgs and does not vary appreciably with test temperature or annealing condition. Thus, the ratio k_f/k_y is approximately equal to 0.3, which agrees with results for tantalum (about 0.2) as determined by Owen in part VI of this report. Likewise, the ratio k_f/G is approximately equal to 1.5×10^{-5} which is 0.3 times the ratio of k_y/G (5×10^{-5}) according to Rosenfield[20].

Table 20

Calculated Critical Crack Length (c) of W-P4 Wire

Condition	Test Temp. °C	R.A. %	σ_c ksi	c^* cm	d^{**} cm	c/d
As-drawn	+82	48	372	4.4×10^{-4}	7.6×10^{-5}	5.8
	-20	22	390	4.0×10^{-4}	9.1×10^{-5}	4.4
	-20	1	315	6.4×10^{-5}	1.0×10^{-4}	0.64
	-40	1	324	5.8×10^{-5}	1.0×10^{-4}	0.58
800°C Anneal	+80	44	348	4.4×10^{-4}	7.1×10^{-5}	6.2
	-10	39	370	4.4×10^{-4}	7.3×10^{-5}	6.0
	-10	1	305	5.8×10^{-5}	9.1×10^{-5}	0.64
	-25	1	315	5.2×10^{-5}	9.1×10^{-5}	0.57
1050°C Anneal	+80	48	333	4.8×10^{-4}	9.1×10^{-5}	5.3
	+13	35	345	4.4×10^{-4}	1.0×10^{-4}	4.4
	+13	2	275	7.8×10^{-5}	1.3×10^{-4}	0.60
	-40	1	324	5.8×10^{-5}	1.3×10^{-4}	0.45
1200°C Anneal	+80	48	310	6.6×10^{-4}	1.5×10^{-4}	4.4
	+30	37	320	6.2×10^{-4}	1.6×10^{-4}	3.9
	+30	3	250	1.0×10^{-4}	2.0×10^{-4}	0.50
	+ 5	1	265	9.4×10^{-5}	2.0×10^{-4}	0.47
1400°C Anneal	+80	44	268	9.2×10^{-4}	2.0×10^{-4}	4.6
	+52	39	264	8.0×10^{-4}	2.0×10^{-4}	4.0
	+52	4	210	1.5×10^{-4}	2.5×10^{-4}	0.60
	+20	1	220	1.3×10^{-4}	2.5×10^{-4}	0.52

$^*c = 2.6 \times 10^{12} \frac{\gamma E}{\sigma_c^2}$ cm

**Corrected for the decrease in d due to reduction in area.

Table 21

Calculated Locking Parameter for Flow (k_f) above T_d for W-P4 Wire

Condition	Test Temp.	R.A. %	d* cm	σ_c ksi	k_f** cgs	k_f/G cgs
As-drawn	+82	48	7.6×10^{-5}	372	2.5×10^{7}	1.6×10^{-5}
	-20	22	9.1×10^{-5}	390	2.2×10^{7}	1.4×10^{-5}
800°C Anneal	+80	44	7.1×10^{-5}	348	2.6×10^{7}	1.7×10^{-5}
	-10	39	7.3×10^{-5}	370	2.4×10^{7}	1.5×10^{-5}
1050°C Anneal	+80	48	9.1×10^{-5}	335	2.6×10^{7}	1.7×10^{-5}
	+13	35	10.4×10^{-5}	345	2.4×10^{7}	1.5×10^{-5}
1200°C Anneal	+80	48	15×10^{-5}	310	2.5×10^{7}	1.6×10^{-5}
	+30	37	16×10^{-5}	320	2.2×10^{7}	1.4×10^{-5}
1400°C Anneal	+80	44	19.8×10^{-5}	265	2.5×10^{7}	1.6×10^{-5}
	+52	39	20.3×10^{-5}	285	2.2×10^{7}	1.4×10^{-5}

* Corrected for decrease in d due to reduction in area

** $k_f = \dfrac{G\gamma'}{3\sigma_c d^{1/2}}$

5. Recovery-Annealing of Molybdenum (Mo-E1 Strip)

5.1 Microstructural Observations - The seven etchants listed in Tables 14 and 22 were evaluated by comparing their effects on Mo-E1 strip of two deformation extremes (identified as no. SM1E and SM1H). As in the case of tungsten, H_2O_2 proved to be the best over-all substructure etchant. The $CuSO_4$ + NH_4OH and the NaOH + $K_3Fe(CN)_6$ etchants develop substructure fairly well for the as-rolled but not the recovery-annealed condition. Oxalic acid reveals substructure well, but also stains extensively. Cathodic etching brings out deformation markings and recrystallized areas better than any of the other etchants, but does not develop etch pits. The other two etchants evaluated bring out little or no structure.

A well-developed substructure is evident in the relatively lightly deformed (40% reduction at 900°C, no. SM1E) Mo-E1 strip (Fig. 38). After recovery-annealing, little obvious change in the substructure is evident (Fig. 39). Similar substructure was found present in the similarly treated Mo-E2 and Mo-E3 strips. In the heavily deformed Mo-E1 strip (40% reduction at 900°C plus 80% at 400°C, no. SM1H), substructure of a finer scale is present (Fig. 40).

5.2 Tensile Transition Behavior - The dependence of fracture stress, yield stress, reduction of area, and elongation on test temperature is shown in Figs. 41 and 42 for recrystallized (SM1C) and for heavily deformed (SM1H) Mo-E1 strip of the same initial grain size. The effect of 40% reduction at 900° plus 80% reduction at 400° after recrystallization is to lower the ductility transition temperature (T_d) from -50°C in the recrystallized condition to -125°C. The decrease in T_d brought about by the deformation may be associated with the decrease in effective grain size due to fibering. Substantial increases in the yield and fracture stresses along with a decrease in ductility (at test temperatures above T_d) were found to result from the deformation of the strip. The transition behavior is substantially similar to that of the W-P4 wire already described, except that the ductility of the Mo-E1 strip just below T_d is substantially higher than that of the W-P4 wire at equivalent test temperatures.

6. Substructural Examination of Experimental Tantalum and Columbium Wire

The four etchants listed in Tables 15 and 23 were evaluated by comparing their effects on Ta-E1, E2, E3, and E4 wires in both the recrystallized and cold-worked (5% and 80% R.A.) conditions. It was found that H_2SO_4 + HF + H_2O_2 gave the best delineation of substructure.

As summarized in Table 24 and illustrated in the Figures 43 to 50, wide variations in grain size were found, from 0.011 mm average diameter in the Ta-E2 wire to 0.030 mm in the Ta-E1 and Ta-E4 wires. Relatively dense, random etch pits were found in 1/3 to 1/2 of the grains in both the recrystallized and deformed conditions. No well defined subgrains could be discerned in any of the compositions studied. In addition to the random etch pits, larger pits aligned parallel to the wire axes were found in the Ta-E2 wires.

Although grain boundaries were delineated in Cb-E1 and E4 wires by all of the etchants listed in Table 15, no etch pits or other substructural entities were developed within the grains.

H_2O_2 etch 3893 1250X

Fig. 37 - Recrystallized Mo-El strip (no. SMIC, longitudinal section).

H_2O_2 etch 3677 1250X

Fig. 38 - Substructure developed in recrystallized Mo-El strip by 40% reduction at 900°C plus 10% reduction at 400°C (no. SMIE-AR, longitudinal section).

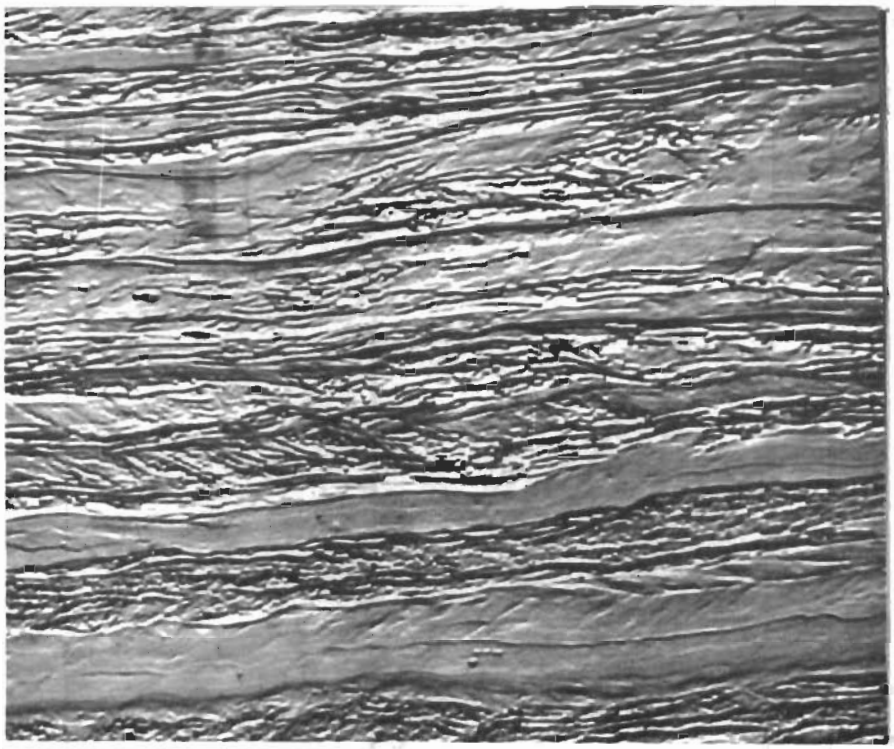

H_2O_2 etch 3705 1250X

Fig. 39 - Substructure in Mo-E1 strip after recovery-annealing at 910°C for 1 hour following 40% plus 10% reduction (no. SMIE-AR, longitudinal section).

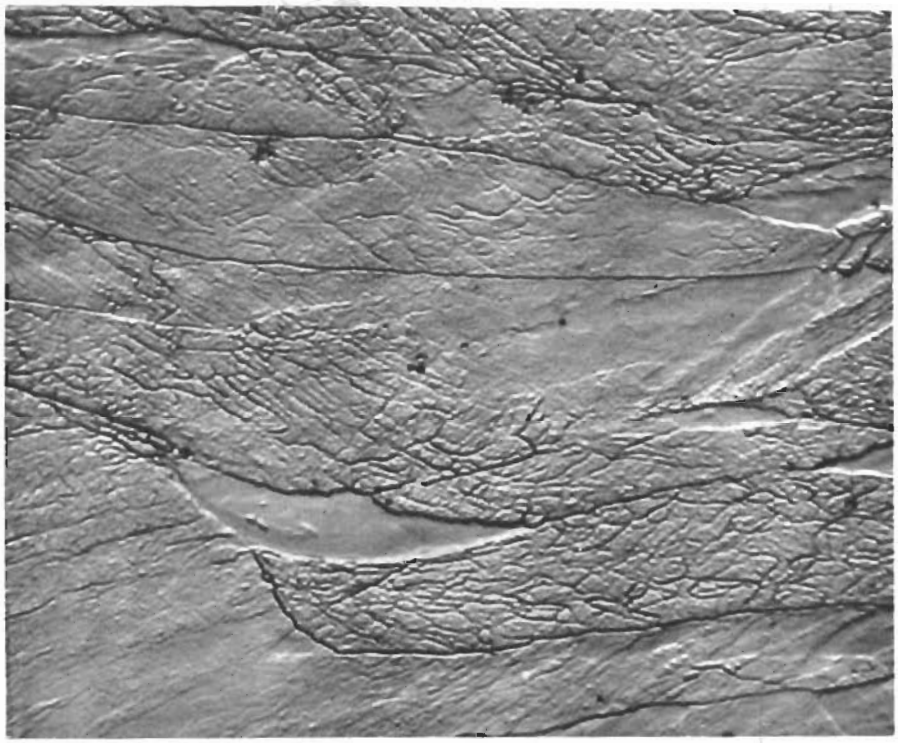

H_2O_2 etch 3675 1250X

Fig. 40 - Substructure developed in recrystallized (see Fig. 32) Mo-E1 strip by 40% reduction at 900°C plus 80% reduction at 400°C (no. SMIH-AR, longitudinal section).

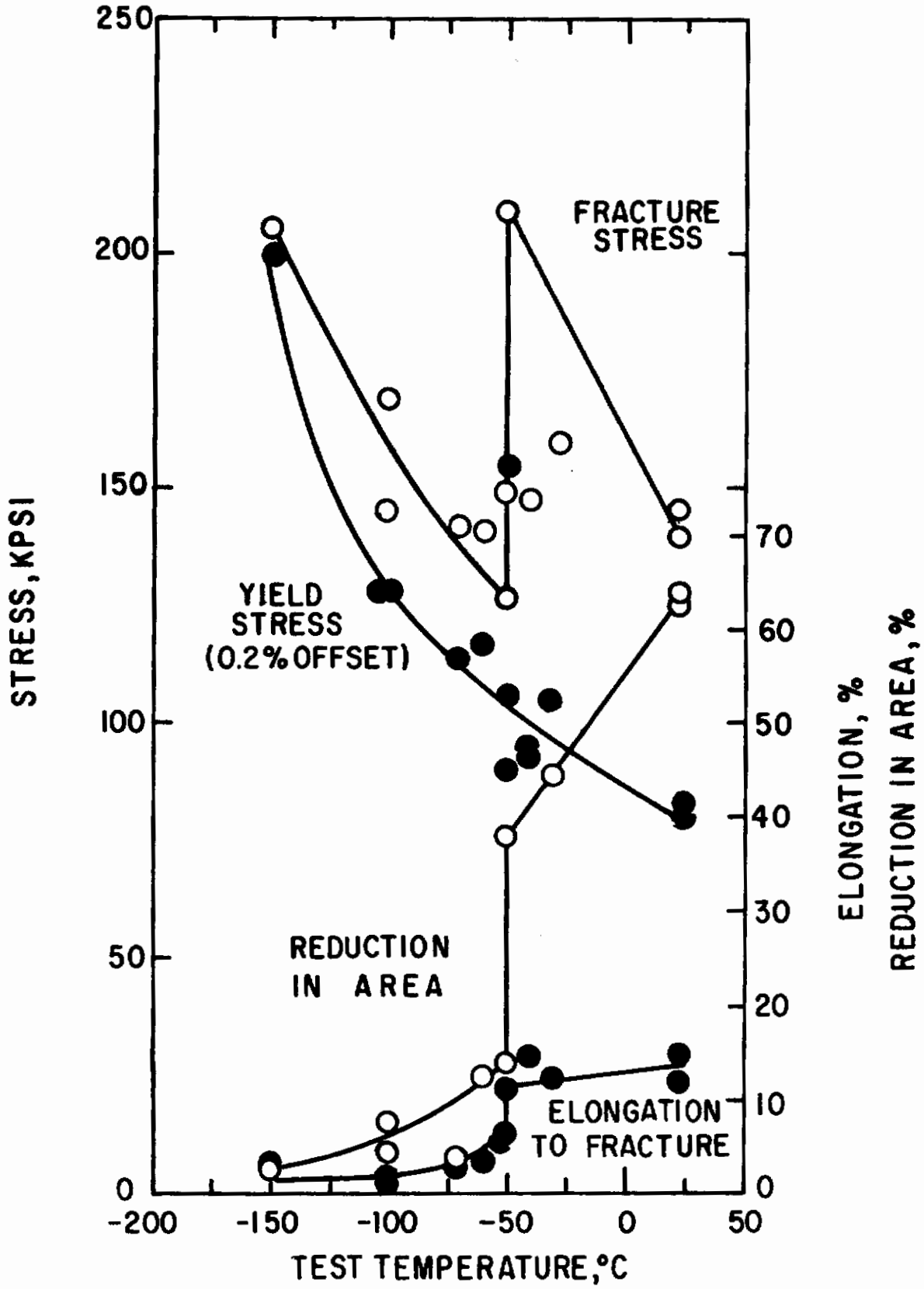

Fig.41- Effect of test temperature on the tensile properties of high purity molybdenum (Mo-El) strip in the as-recrystallized condition (no. SMIC).

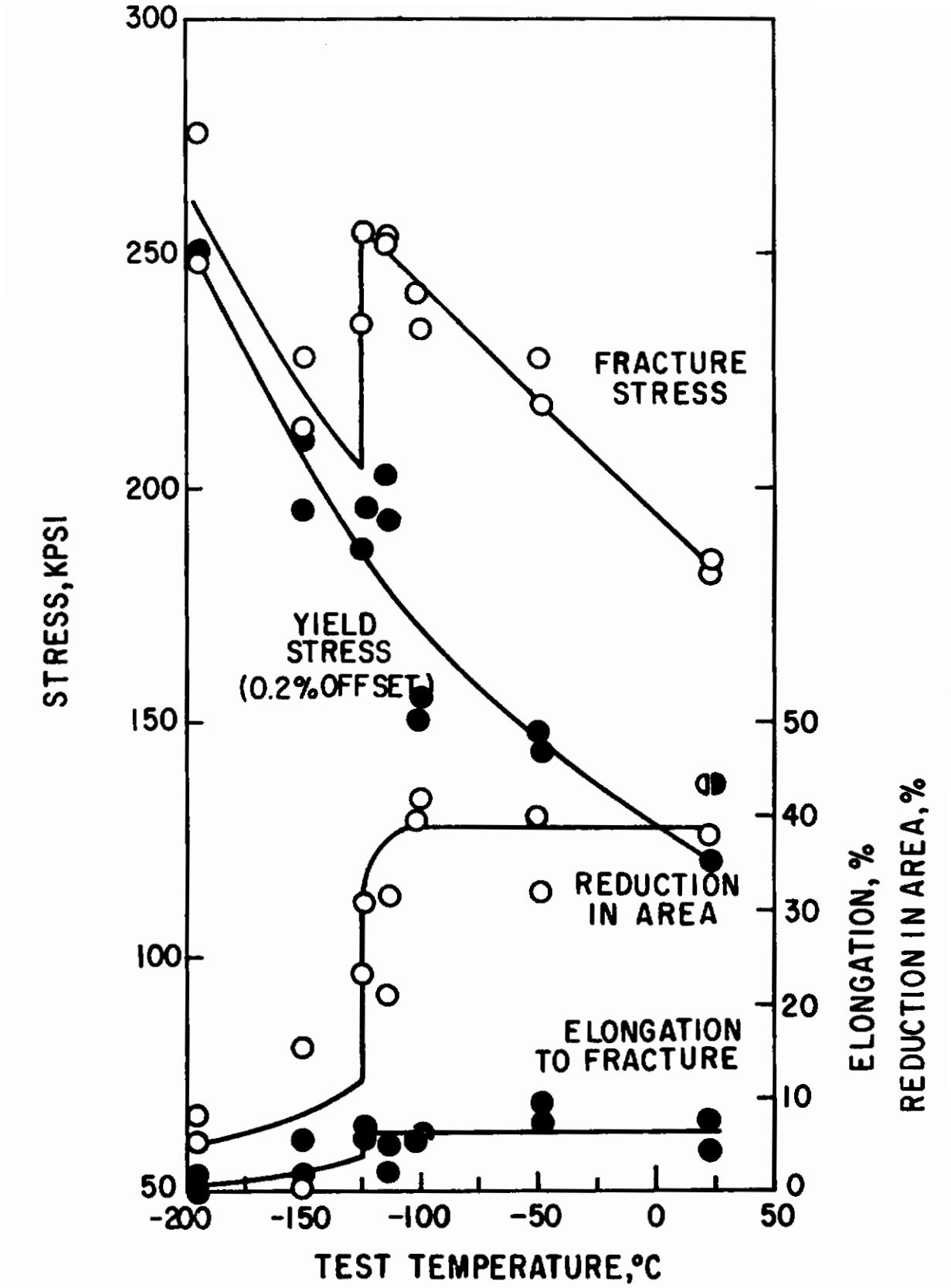

Fig.42- Effect of test temperature on the tensile properties of high purity molybdenum strip in the heavily cold worked condition (80% reduction at 400°, no. SM1H).

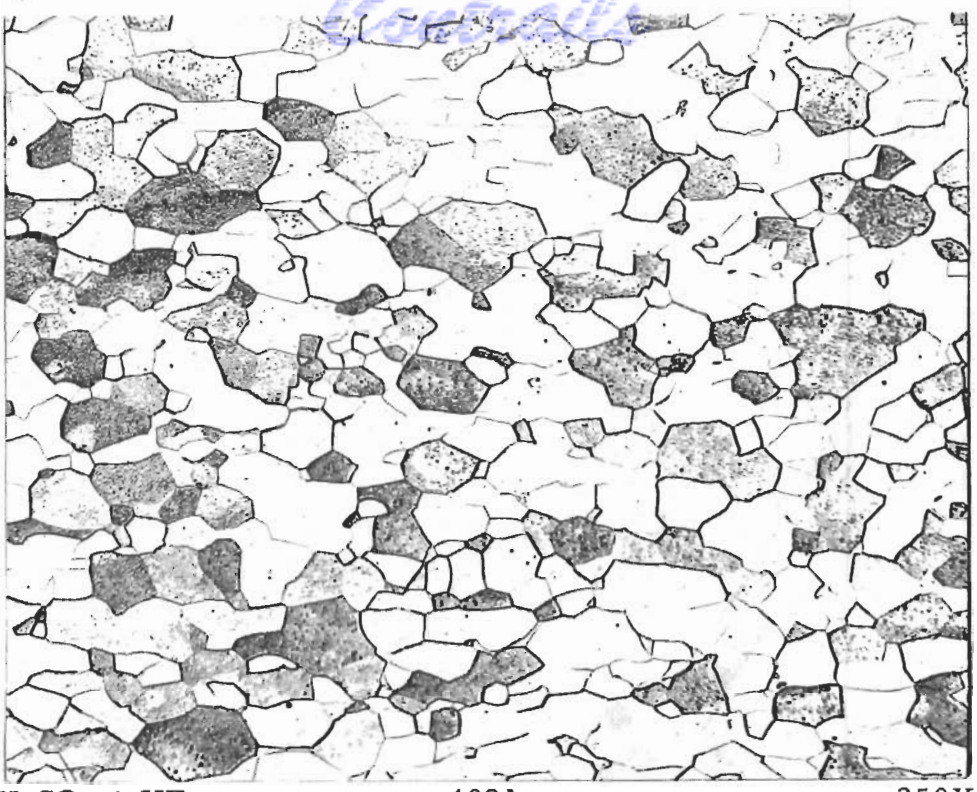

H_2SO_4 + HF + H_2O_2 etch 4091 250X

Fig. 43 - Substructure in recrystallized Ta-El wire.

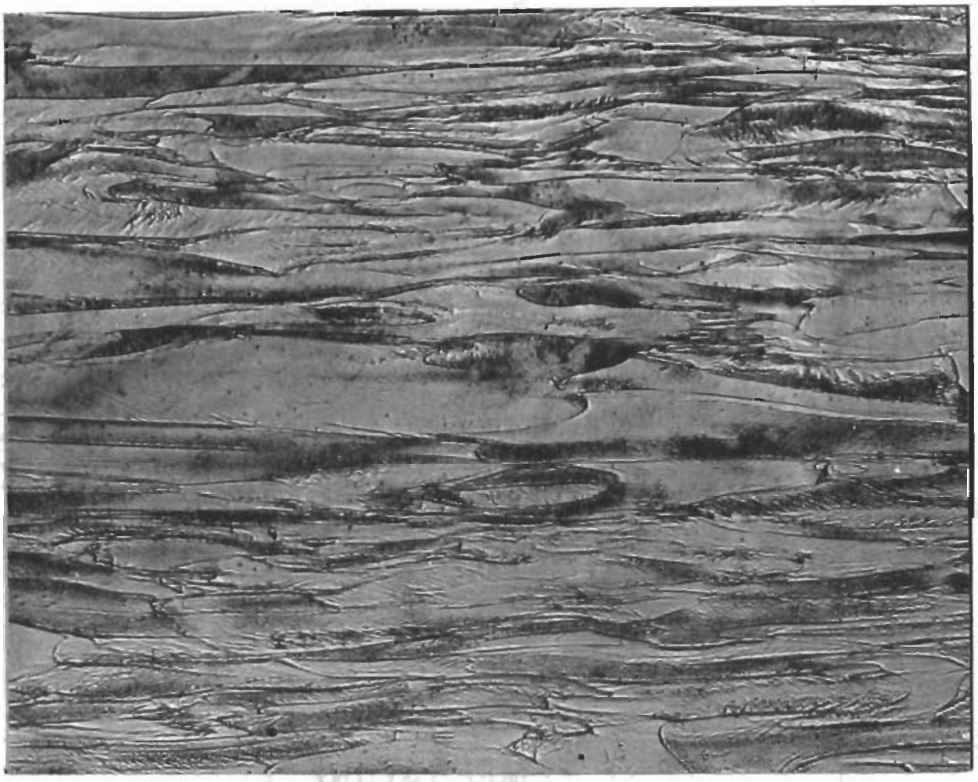

H_2SO_4 + HF + H_2O_2 etch 4092 250X

Fig. 44 - Substructure in Ta-El wire after 80% cold work.

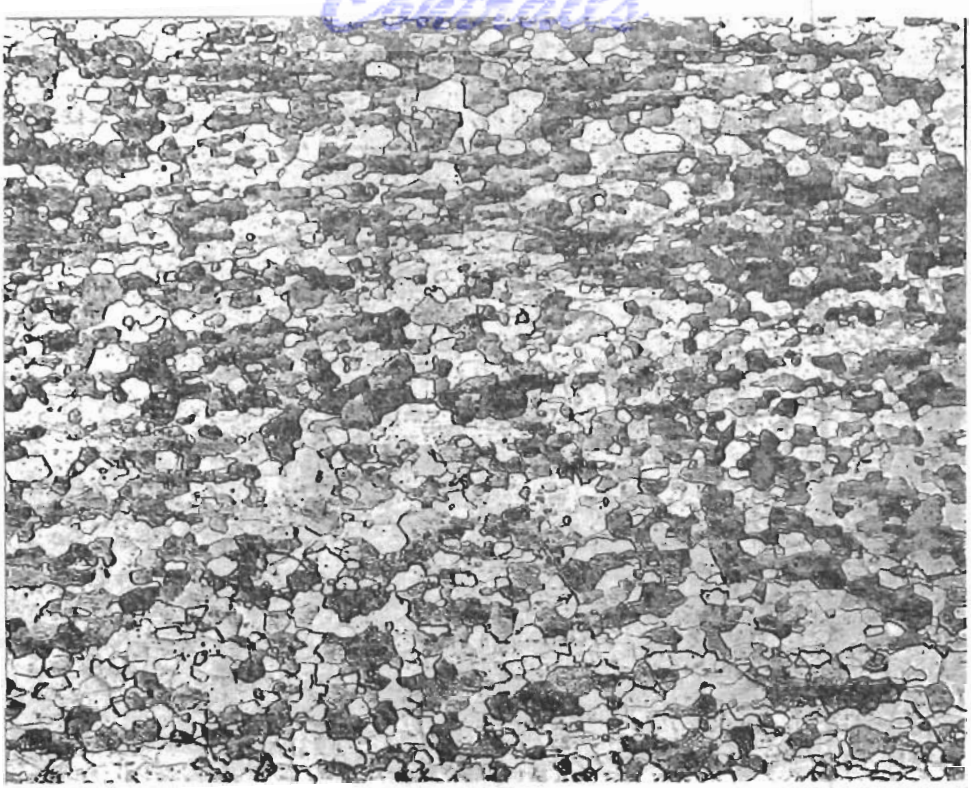

H_2SO_4 + HF + H_2O_2 etch 4093 250X

Fig. 45 - Substructure in recrystallized Ta-E2 wire.

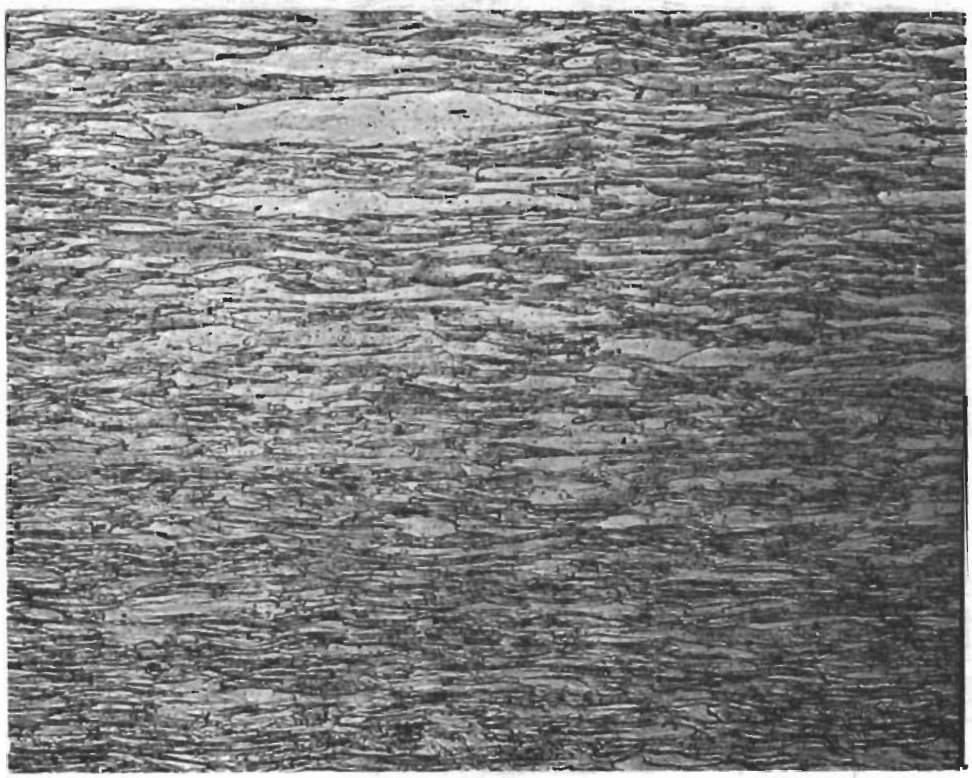

H_2SO_4 + HF + H_2O_2 etch 4094 250X

Fig. 46 - Substructure in Ta-E2 wire after 80% cold work.

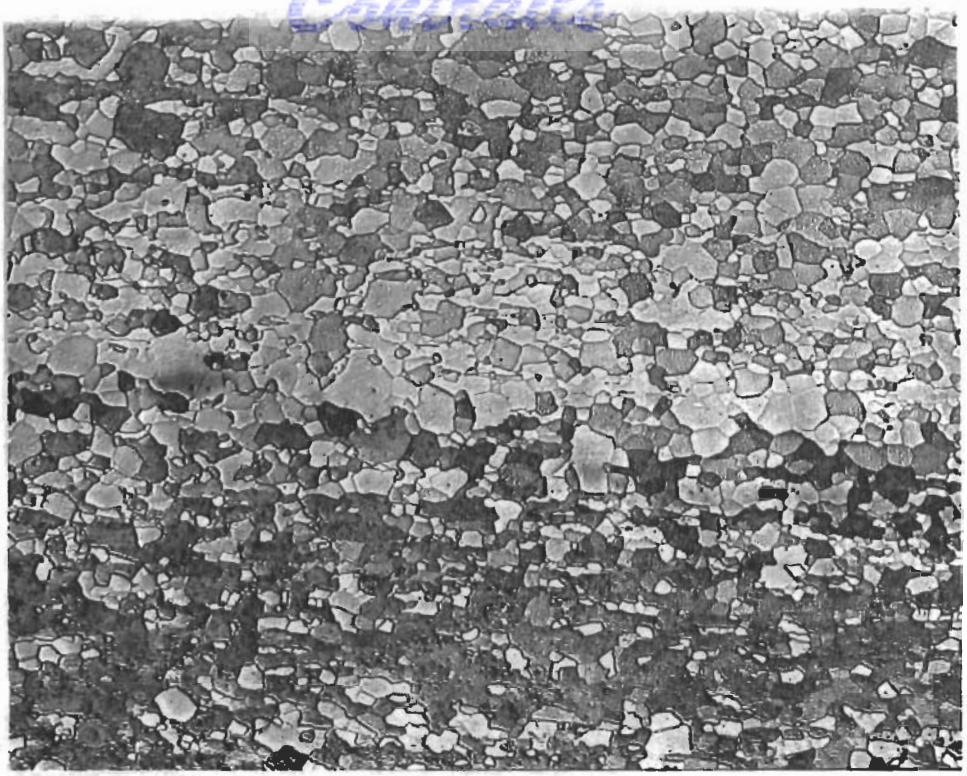

H_2SO_4 + HF + H_2O_2 etch 4095 250X

Fig. 47 - Substructure in recrystallized Ta-E3 wire.

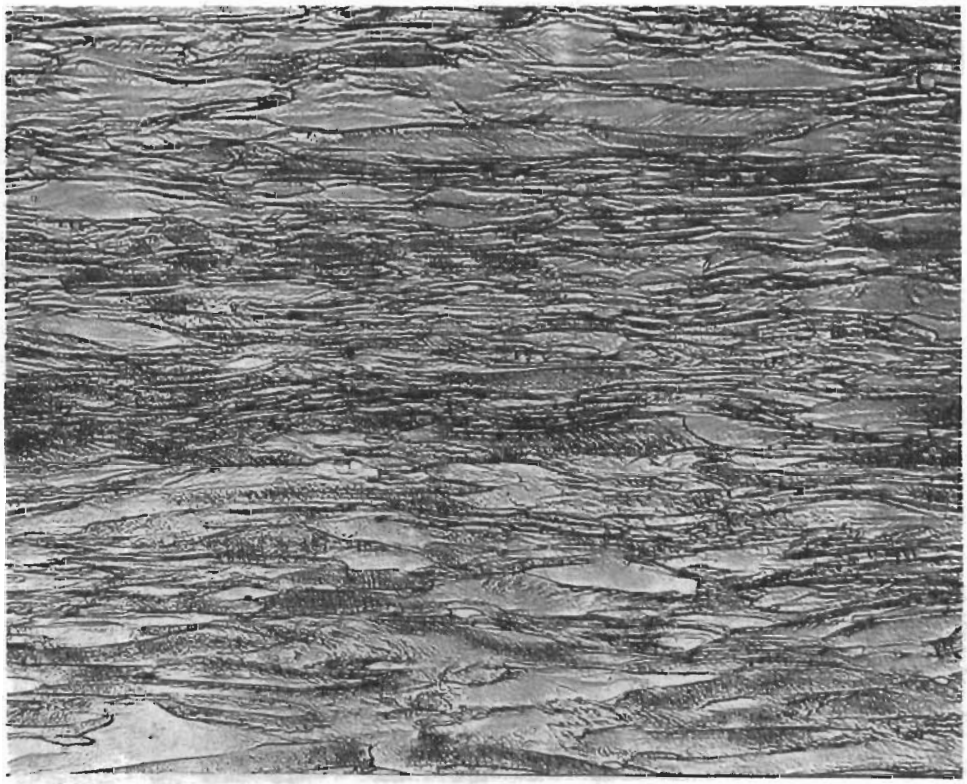

H_2SO_4 + HF + H_2O_2 etch 4096 250X

Fig. 48 - Substructure in Ta-E3 wire after 80% cold work.

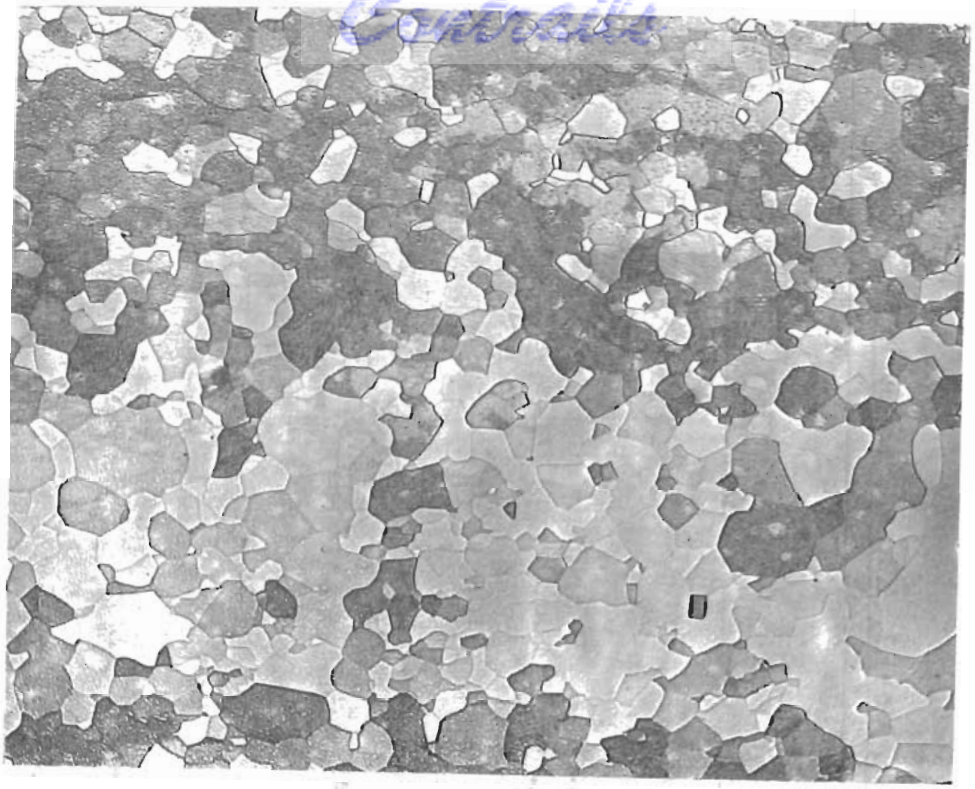

H_2SO_4 + HF + H_2O_2 etch 4097 250X

Fig. 49 - Substructure in recrystallized Ta-E4 wire.

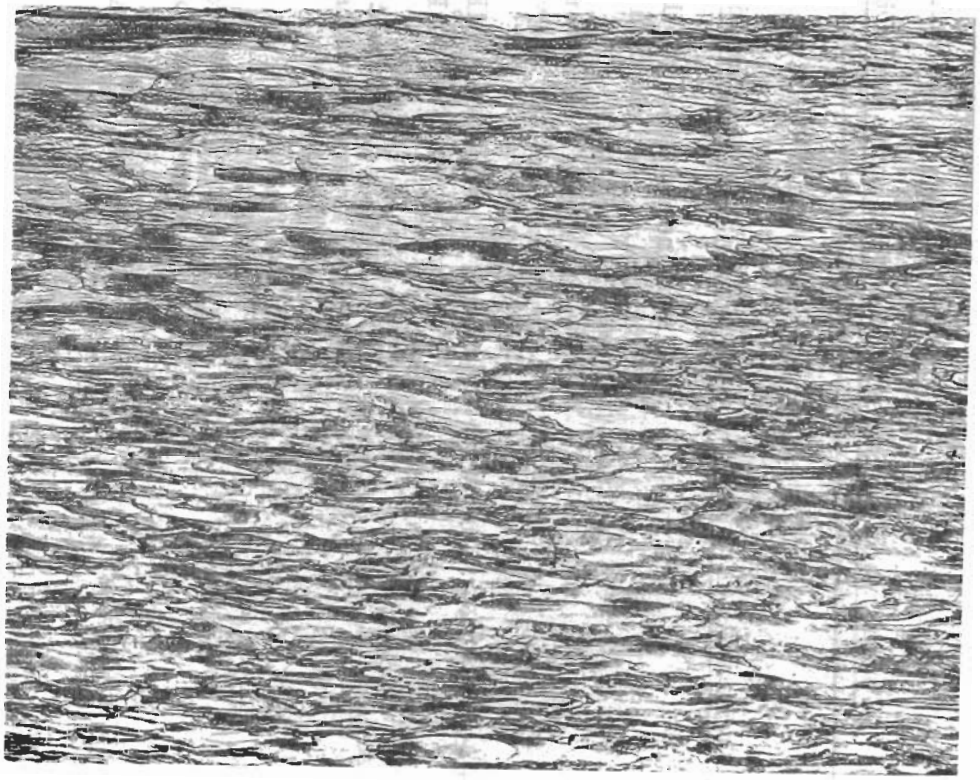

H_2SO_4 + HF + H_2O_2 etch 4098 250X

Fig. 50 - Substructure in Ta-E4 wire after 80% cold work.

Table 22

Comparison of Substructure Etchants and Observations on Mo-E1, E2, and E3 Strip

Etchant	As-Rolled	Recovery-Annealed
H_2O_2	Grain boundaries well etched, substructure clearly defined.	Same as rolled.
$CuSO_4 + NH_4OH$	Reveals grain boundaries and substructure but not as well as H_2O_2.	Poor delineation of grain boundaries and substructure.
$NaOH + K_3Fe(CN)_6$	Grain boundaries well defined, substructure defined poorly.	Same as rolled.
Oxalic Acid	Orientation dependent stain; unstained areas reveal substructure clearly.	Same as rolled.
Cathodic Etching	Grain boundaries and deformation markings clearly developed, no other substructure observed.	Same as rolled.
$FeCl_3 + CuSO_4 + NH_4OH$	Not selective; specimens roughened.	Same as rolled.
$HF + HNO_3$	Not selective; specimens roughened.	Same as rolled.

Table 23

Comparison of Etchants Used for Examination of Substructure in Ta-E1, E2, E3, and E4 Wires, in both the Cold-Worked and Recrystallized Conditions

Etchant	Observations
5 parts 95% H_2SO_4 2 parts 70% HNO_3 2 parts 48% HF	Poor delineation of substructure, specimen chemically polished.
3 parts conc. Lactic acid 1 part conc. HCL (or HNO_3) 1 part 48% HF	Grain boundaries well defined, substructure poorly defined.
1 part 20% NH_4F 1 part 30% HF	Good substructure and grain boundary etch, but not so good as HF, H_2SO_4, H_2O_2 etchant.
1 part conc. H_2SO_4 1 part 48% HF few drops H_2O_2 1 part H_2O	Best etchant clearly reveals substructure and grain boundaries.

Table 24

Observations on Experimental Tantalum Wire

Material	Metallurgical Condition	Average Grain dia., mm	Observations
Ta-E1	Recrystallized	.030	Random etch pitting in about 1/3 of the grains
Ta-E1	5% R.A.		
Ta-E1	80% R.A.		
Ta-E2	Recrystallized	.011	Dense, random etch pit distribution in about 1/2 of the grains and larger etch pits aligned parallel to the wire axis.
Ta-E2	5% R.A.		
Ta-E2	80% R.A.		
Ta-E3	Recrystallized	.016	Dense, random etch pits in about 1/2 of the grains.
Ta-E3	5% R.A.		
Ta-E3	80% R.A.		
Ta-E4	Recrystallized	.030	Similar to Ta-E3.
Ta-E4	5% R.A.		
Ta-E4	80% R.A.		

7. X-Ray Diffraction Line Profile Measurements

7.1 General - The x-ray line profile and associated measurements cover three series: a) an isochronal series of one-hour anneals on W-P2, Mo-P2, Ta-P2 and Cb-P2 strip; b) an isothermal series on the above materials at 600, 700, 800 and 850°; and c) a deformation series showing the effects of increasing reduction of area on the as-worked condition on experimental materials. These series are interrelated and can be visualized as lines or plane sections of a three-dimensional network with annealing temperature, annealing time, and degree of deformation as axes. Because of the very large number of combinations such a three-dimensional network represents even for one material, it was not feasible to measure each state. Therefore, the use of a more limited range was dictated. In addition, because of the scatter obtained in the data, it became necessary to investigate possible causes in order to ameliorate this error. Based on the results obtained on the isochronal and isothermal series of the practice materials and on the information obtained from investigation of possible causes of scatter, decisions were reached as to which measurements should be made on the various experimental materials. Because a controlled range of initial reductions was not available in the practice materials, the effect of this parameter could not be studied until the experimental materials became available.

7.2 Isothermal Series - The data from the (200)-(400) diffraction lines representing isochronal series for the P2 strip materials were used to determine particle size and strain terms as previously reported[1]. Data representing isothermal series were reported as half-width values. Since then, particle size and strain terms for the (200)-(400) lines representing isothermal series have been determined and are given in Figs. 51 to 54.

Time intervals used for the isothermal series were approximately factors of four, ranging from 15 minutes to 256 hours at temperature. For the 600, 700, and 800° series, these times are not long enough to allow the onset of recrystallization. At 850°, Mo-P2 shows no evidence of appreciable recrystallization* after 18 hours; but approximately 25% recrystallization after 70 hours. Ta-P2 is approximately 5% recrystallized after 4 hours and approximately 50% recrystallized after 18 hours at 850°. W-P2 and Cb-P2 show no recrystallization even after 70 hours at 850°.

Ta-P2 and Cb-P2 strip were found to be composed of recognizably different sub-lots. Because of the limited quantity involved, a number of sub-lots had to be used for the isothermal series. Internal consistency of the isothermal data was obtained by using only one sub-lot at a single temperature. The various sub-lots used are indicated in the legends of Figs. 53 and 54.

* As indicated by a microstructural change in the primary grain structure.

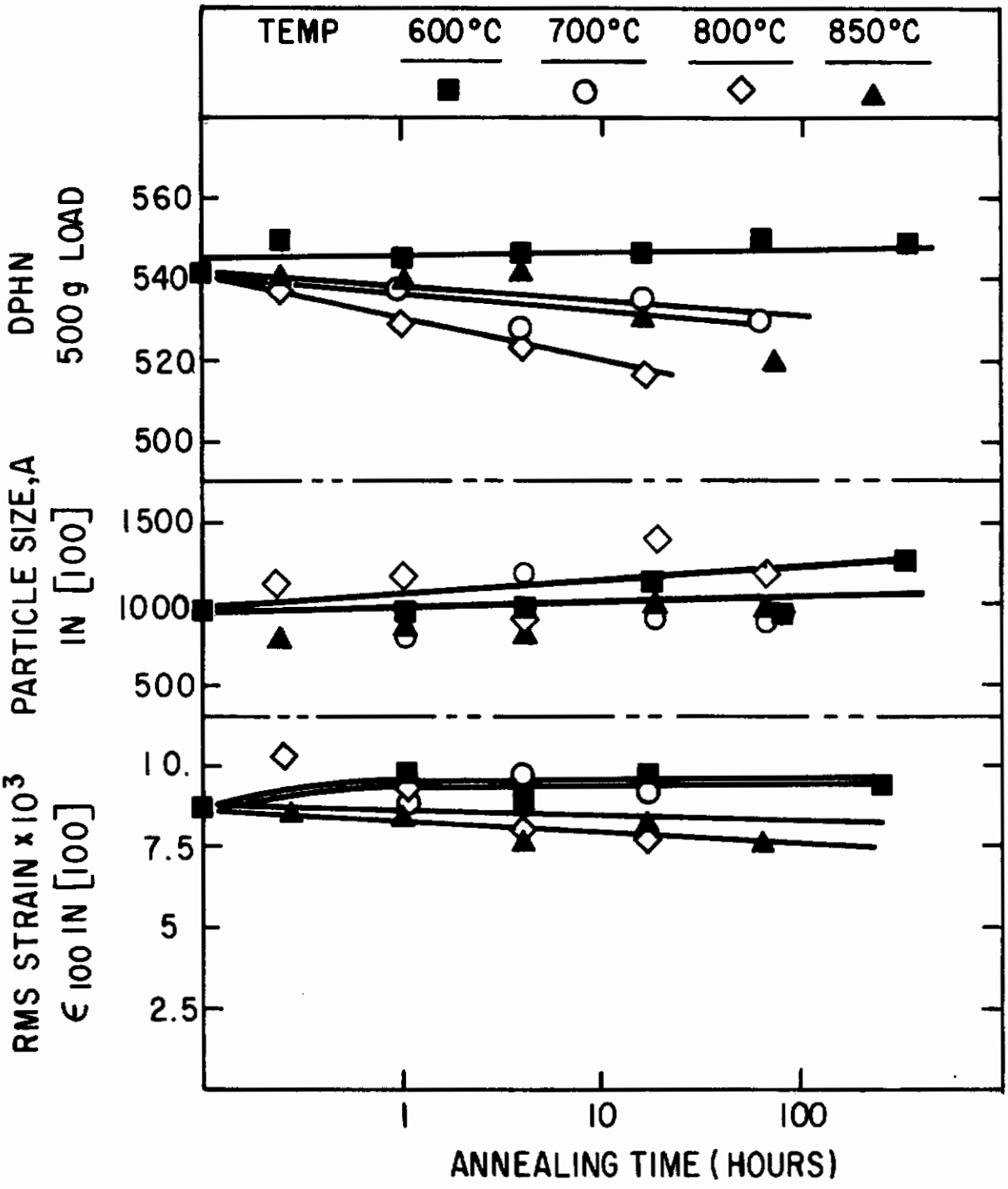

Fig.51-Effect of annealing at 600, 700, 800 and 850°C on the hardness, particle size and strain of tungsten strip (W-P2)

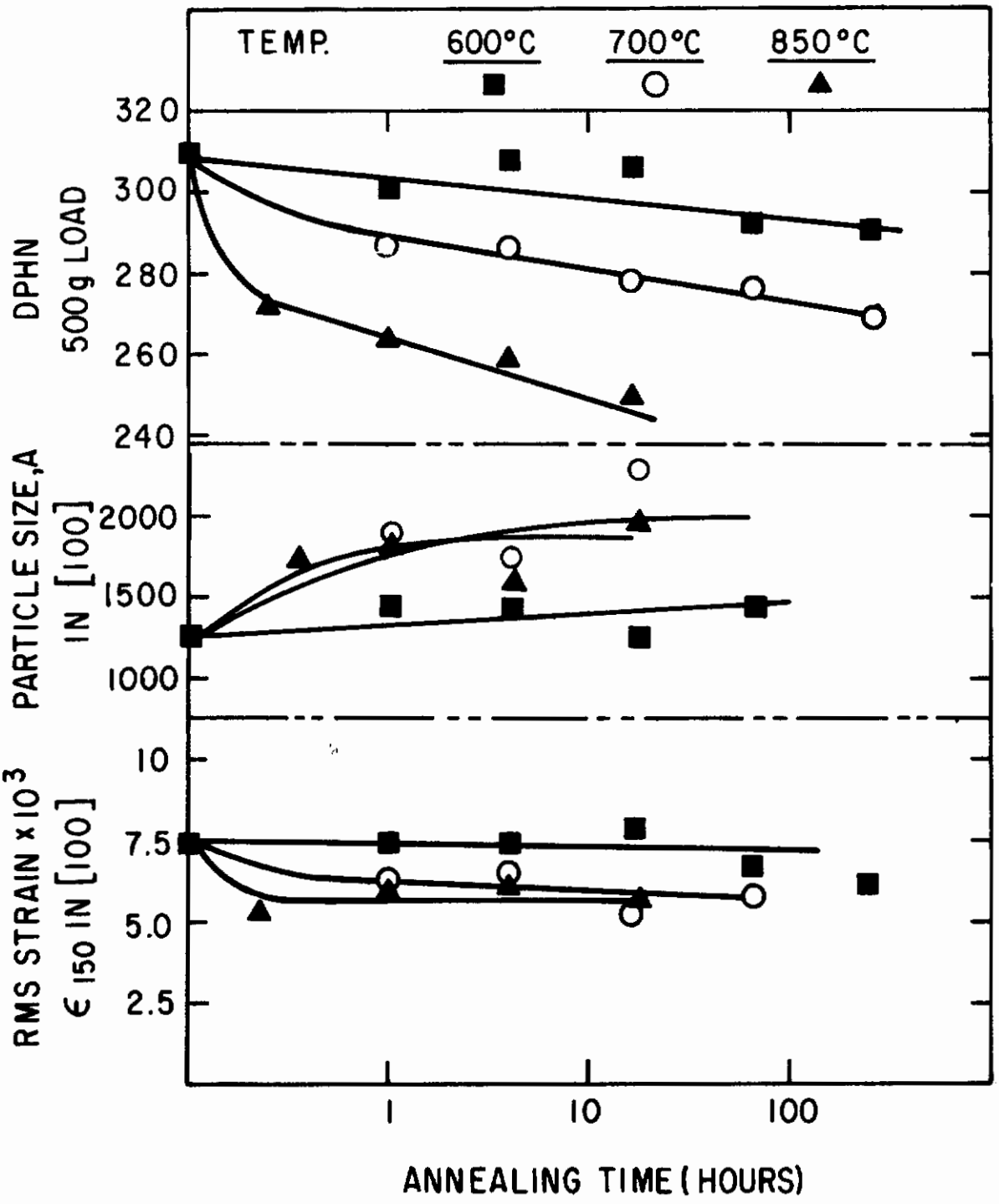

Fig.52-Effect of annealing at 600, 700 and 850°C on the hardness, particle size and strain of molybdenum strip (Mo-P2)

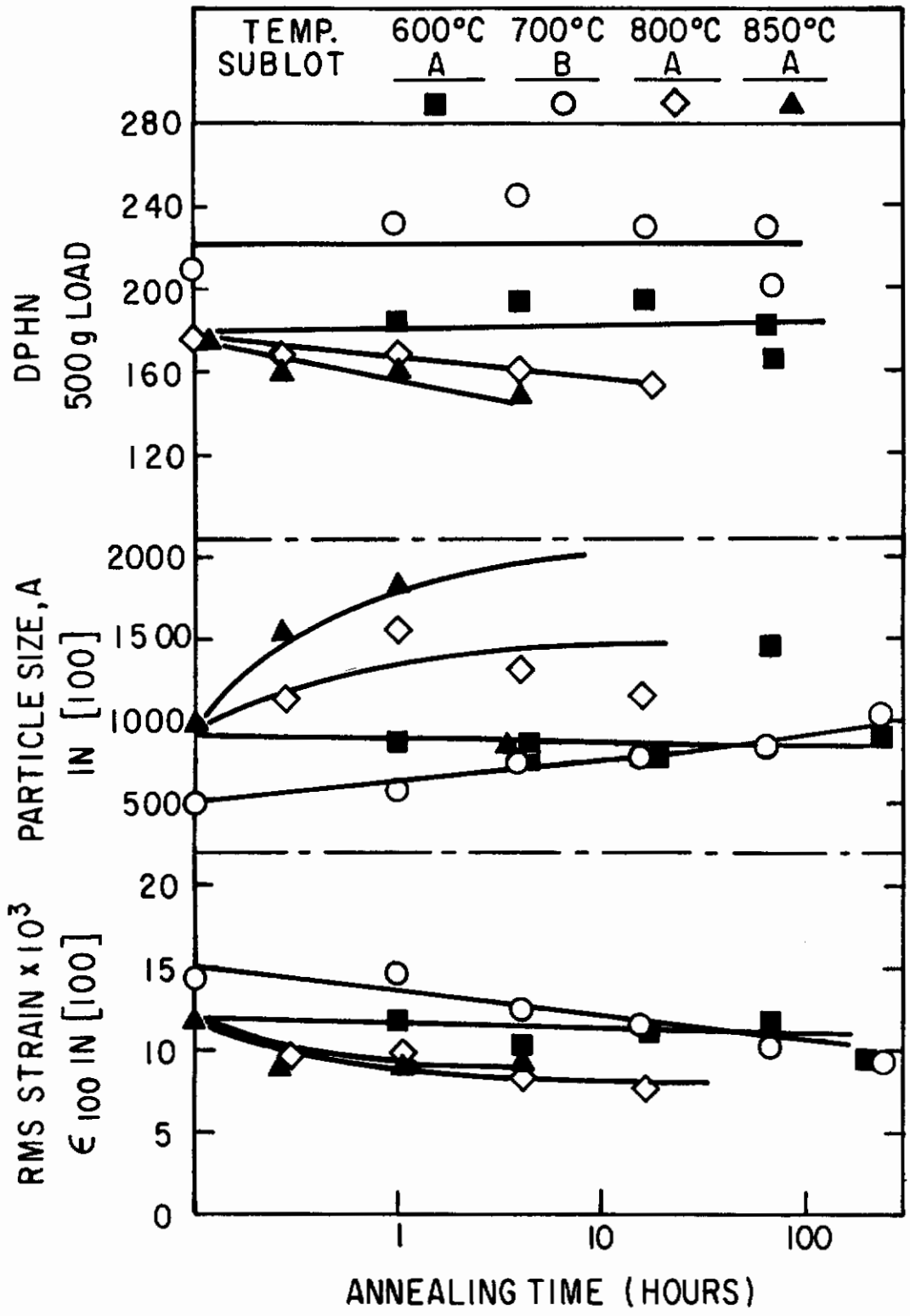

Fig.53-Effect of annealing at 600, 700, 800 and 850°C on the hardness, particle size and strain of tantalum strip (Ta-P2)

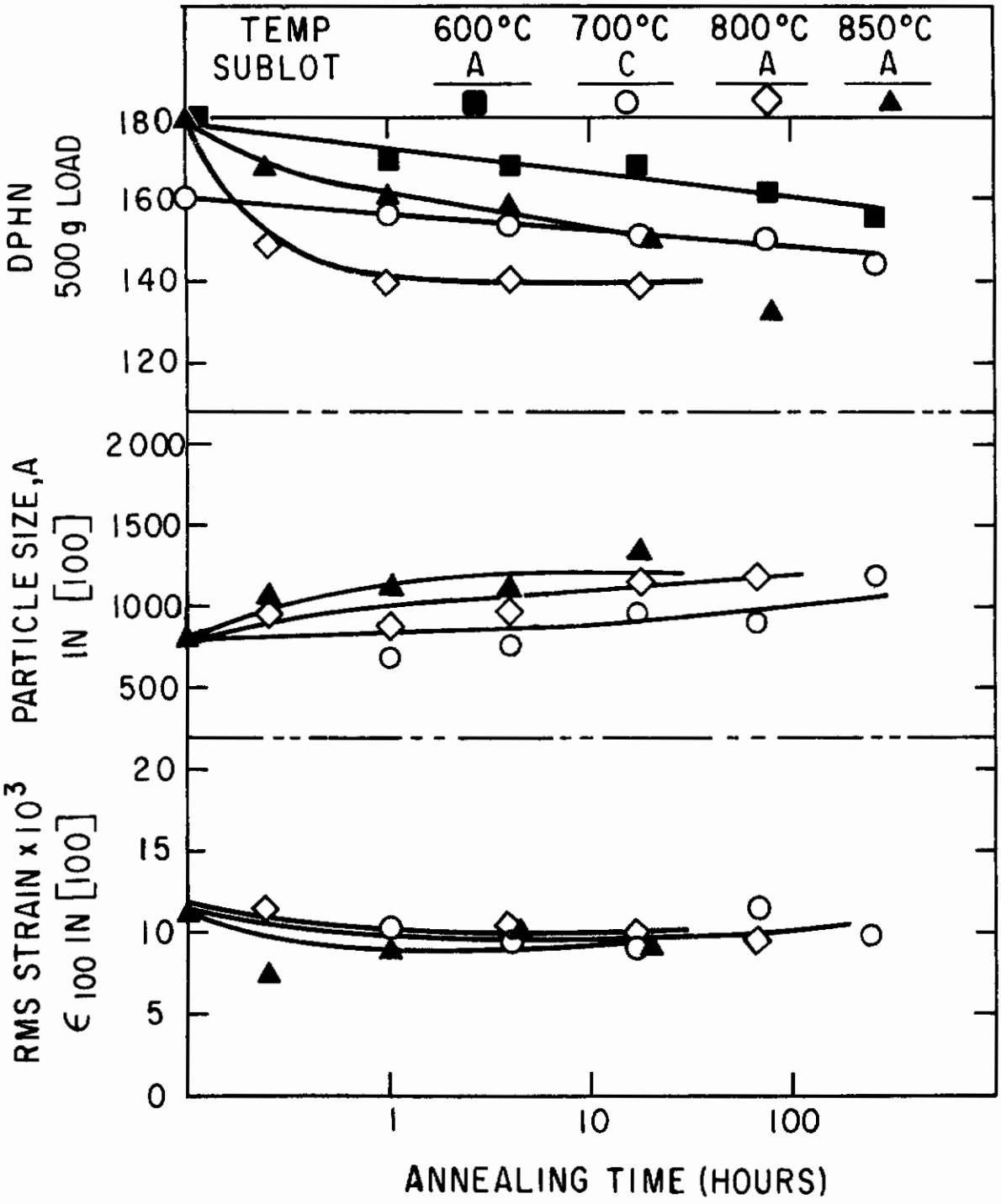

Fig.54-Effect of annealing at 600, 700, 800 and 850°C on the hardness, particle size, and strain of columbium strip (Cb-F2)

It was anticipated that the changes found in the strain and particle size terms would undergo recovery kinetics similar to those previously reported[1] for the changes of half-widths. In typical recovery kinetics, the highest rate at a given temperature occurs initially and the process terminates at levels characteristic of the temperature[22]. Since most of the observed changes in half-widths are relatively small, it was anticipated that the corresponding changes in particle size and strain would likewise be small. The occurrence of relatively small changes in half-widths is attributed to the limited amount of deformation given to the P2 materials. The only exception is Ta-P2 which, in the as-worked condition, shows the effects of appreciably greater deformation[1].

The variations of particle size and strain on isothermal annealing show considerable scatter, but in general are consistent with the kinetics expected for recovery. The isothermal series represent a relatively low annealing temperature for W-P2, and the changes are masked by the experimental scatter. Due to the scatter, the 800 and 850° series at first appeared to show some appreciable changes in particle size. Re-runs of the (200), using repolished specimens, indicate that this is not correct, at least within the limits that can be detected.

7.3 Isochronal Series on Broadening of W-P2 - Rutgers has reported observing substructural changes by transmission electron microscopy on annealing W-P5 tungsten in the range of 400 to 600°[1]. Previously, some changes in this range appear to have been observed in the half-widths of line profile measurements conducted on the W-P2 isochronal series[1]. Because of the small differences involved, a closer correlation was attempted by heat treating specimens of W-P5 foil and examining them at both facilities. The line profile measurements proved to be unsuccessful because the reproducibility of the half-widths on the foil was quite poor. Furthermore, because of scatter in the particle size and strain terms, no significant changes in the W-P2 isochronal series were seen in this temperature range. Because of the importance of a correlation with both the electron microscopic observations and the mechanical property changes[1], the apparent changes in half-widths were studied further. A number of repeat measurements were made, some on the original specimens of W-P2 and some on new specimens. Since the effort involved in converting data to particle size and strain terms is large, it was decided to obtain the data in the form of widths of the (400) diffraction peaks at 1/5, 1/3, 1/2 and 3/4 of the maximum of height of α_1 above background. Any measurement of these widths is affected by the statistical fluctuations of the intensity measurements. Because the intensities were actually measured several time constants apart, largely independent pieces of data were obtained. Using these data separately is considered essentially equivalent to re-measuring the line shape.

The results of width determinations corresponding to the selected fractional heights are shown in Fig. 55. Values for 1/5 height are not included because of the considerably greater scatter. A trend indicating an increase of line width on annealing up to 700° had previously been detected. In order to confirm this, least squares analyses were made on the assumption that no change occurred between the as-received condition and 300°. The least square slopes calculated on this basis are shown in Fig. 55. It is evident that

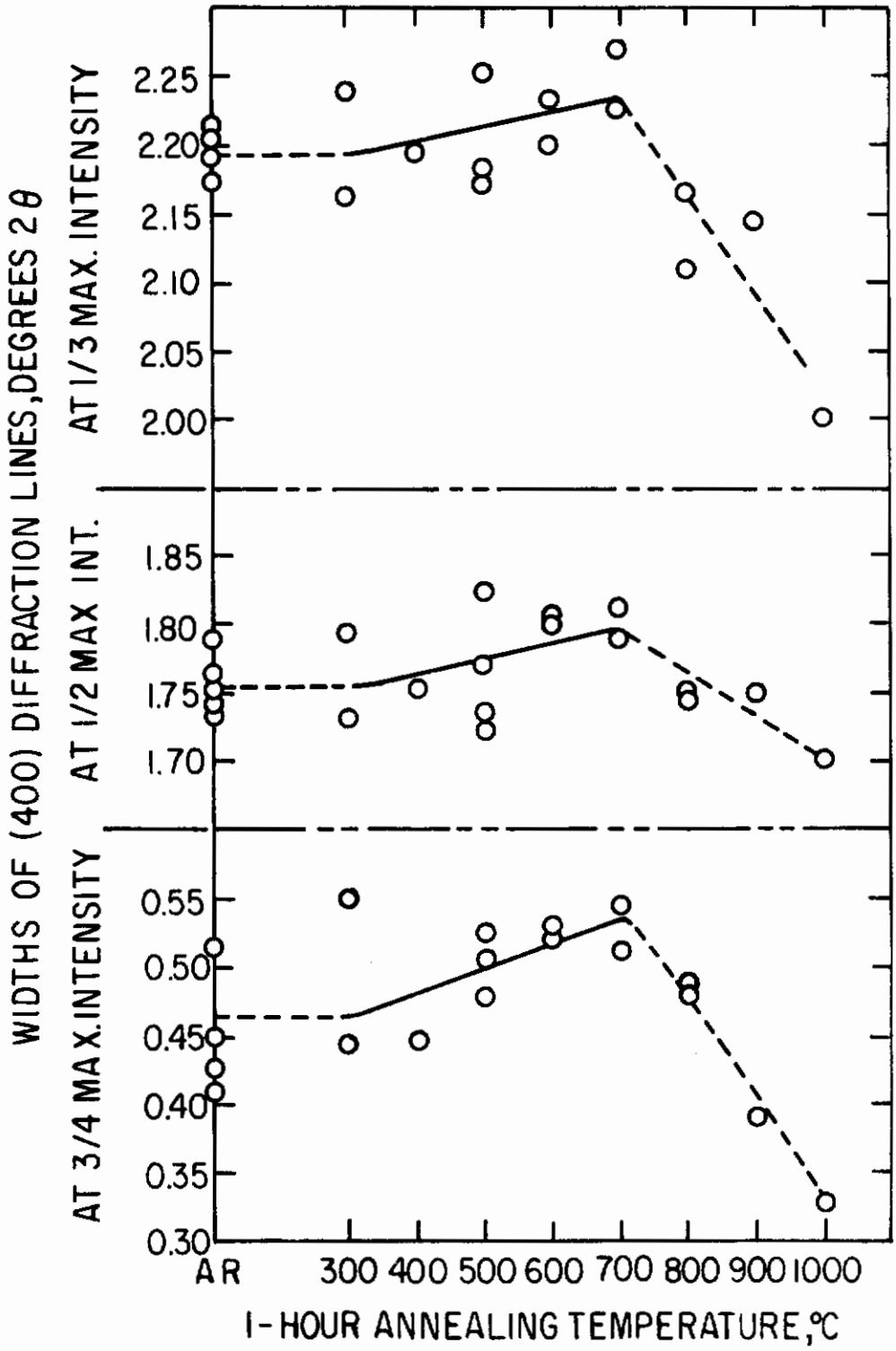

Fig.55- Effect of annealing on the (400) diffraction line widths of tungsten strip (W-P2)

broadening occurs up to about 700° and is followed by some degree of sharpening. Probable errors calculated for the slopes are given in Table 25. From the probable errors, it is believed that the occurrence of broadening on isochronal annealing of W-P2 is a reasonable conclusion.

The observed increase in diffraction line width may mean that an unusual dislocation reaction takes place in tungsten. Diffraction lines of the (100) series are particularly sensitive to the effects of faulting on random (211) planes[23]. The increase would be caused by a decrease of the effective particle size term (D_{eff}). This term is related to the true domain size (D) and the faulting effect (D_F) by[23]:

$$\frac{1}{D_{eff}} = \frac{1}{D} + \frac{1}{D_F}$$

A given spacing of twin faults has 2/3 the effect of the same spacing of stacking faults with respect to decreasing D_F, and thereby causing broadening. There are no means of separating these effects by x-ray diffraction, since the line shape assymmetry caused by twin faults is much too small to allow direct determination[23].

The postulate of increasing faulting probability in the isochronal annealing series can not be confirmed by line profile analysis because of the scatter that the analysis introduces. An approximation for fault spacing can be made by using the increase in line breadth and assuming a linear addition of broadenings. If all of the broadening were caused by stacking faults, the average spacing would be roughly 5,000A; if all by twin faults, 3,300A. Rutgers observed only twins[1] (microtwins) and an approximate spacing of 6,700A[24] was reported. This is believed to be in fairly good agreement with the ManLabs approximate calculation. Because of the approximations involved in both types of measurements, closer agreement would not be expected.

Upon annealing above 700°, either D, D_F or both may increase. This would give an increased D_{eff} and result in a decrease in line width as observed.

7.4 Deformation Series - The scatter of particle size terms that is obtained in measurements of these polycrystalline specimens limits the minimum size of changes that can reasonably be detected. In order to determine the maximum extent of these changes, it was decided to check the extremes of the deformation series (80% R.A. and 0% R.A.). In addition to providing a comparison with the P2 strip materials, this yielded information as to the influence of interstitial content on the severity of straining produced by the deformation. Since the degree of preferred orientation allowed measurement of (110) (220) series for some of the experimental materials, information on the particle sizes in the [110] directions were obtained; this enabled an estimate to be made of the degree of faulting that accompanies the deformation.

The results for Mo-E1-H, Mo-E2-H and Mo-E3-H are given in Table 26, for the [100] was well as for the [110] direction. In order to make the instrumental correction for the (110) series, the line profiles of Mo-E2-C (0% R.A.) were used. The justification of this is based on a comparison of the

Table 25

Calculated Broadening of the (400) Diffraction Line of W-P2 Strip on Isochronal (1 Hour) Annealing

Width at	Rate of Increase 10^{-5} $^{o}2\theta/^{o}C$	Probable Error in Rate 10^{-5} $^{o}2\theta/^{o}C$
1/3 maximum	9.95	3.42
1/2 maximum	10.2	3.30
3/4 maximum	15.2	4.80

Table 26

Particle Size Terms of Experimental Molybdenum Strip

Material	Condition	Particle Size terms, A. [100]	[110]
Mo-E1 strip	40% R. A. at 900° + 80% R. A. at 400°	1110	1110
Mo-E2 strip	" "	1170	1320
Mo-E3 strip	" "	1140	1170

Table 27

Particle Size Terms of Experimental Columbium Strip

Material	Condition	Orientation	Particle Size Terms, A. [100]	[110]
Cb-E1 strip	80% R.A.	rolling plane	750	
		transverse	740	750
Cb-E4 strip	80% R.A.	rolling plane	520	520

results obtained by using the Mo-E2-C specimen as a standard for the (200) series with those obtained using the Mo-P2 in recrystallized condition. The data for these materials show that there is no effect on the [100] particle size due to varying the compositions. Mo-E1 and Mo-E3 strip are nearly alike in composition, whereas Mo-E2 differs because of its higher carbon content as shown in Table 2. The data for the [110] indicate that this higher carbon content increases the faulting and also results in a larger domain size for 80% R.A. The ratio ($D_{[110]eff}/D_{[100]eff}$) is 1.1, which by comparison with the theoretical range of 1.0 (for no faulting) to 2.8 (for faulting only) and the reported measured ranges of 1.0 to 2.3[23], indicates that faulting has a very minor influence. This is in agreement with results in which no faulting was detected for filings (25). A comparison of the particle size terms of the experimental strip with the as received practice (Mo-P2) strip ($D_{eff(100)}$ of 1250A) indicates that the latter underwent only slightly less severe deformation.

The results of particle size measurements for Cb-E1 and Cb-E4 strip are given in Table 27. In the case of Cb-E1, sufficient intensity was not obtained to allow measurement of the (110)(220) on the rolling plane. Specimens were obtained by cutting the strip and mounting it to expose a number of transverse sections. A transverse orientation was chosen because the preferred orientation gives a strong (110)(220) intensity. In the case of Cb-E1 strip (80% R.A.), this allows a measurement of the (200)(400) series on the transverse plane for comparison with the rolling plane. Such a comparison gives a check on the implicit assumption[1] that the D_{eff} is isotropic. Surprisingly, the two measurements were found to be in good agreement; therefore, at least for this case, the isotropic assumption seems reasonable. The degree of faulting appears negligible. The approximately 500 ppm higher oxygen content of Cb-E4 (see Table 2) was found to increase the severity of the 80% R.A., yielding a particle size considerably smaller than in Cb-E1 for the same amount of deformation. This effect is much stronger than that observed by Schoening[26] who in filings found only a minor decrease when the hydrogen content of Ta was increased from a minimum to 6.5 at. %. It is believed that the present findings are more reliable since the amounts of deformation of Cb-E1 and E4 were the same. When filings are made, the following occurs: a) much more extreme deformation results, and b) the amounts of deformation involved in filing two different materials to the same mesh size is unlikely to be the same particularly if one is much more brittle than the other. If the material is ductile, the predominant effects in filing are cutting and bending whereas if the material is brittle, fracture instead of bending will occur.

Although the 500 weight ppm oxygen increase represents a difference of only 0.003 atomic percent, it is the general metallurgical experience[27,28] that this can contribute to hardening. This can be seen in Fig. 56 for Cb-E1 and Cb-E4. Therefore, the present results are more reasonable than those of Schoening[26].

Comparing the particle size data for Cb-E1 and Cb-E4 with those of as-received Cb-P2[1] and allowing for the higher interstitial content of Cb-P2[1], it appears that the latter received less than the 80% R.A. given the experimental materials. This confirms the conclusion based on half-width data which was previously reported[1].

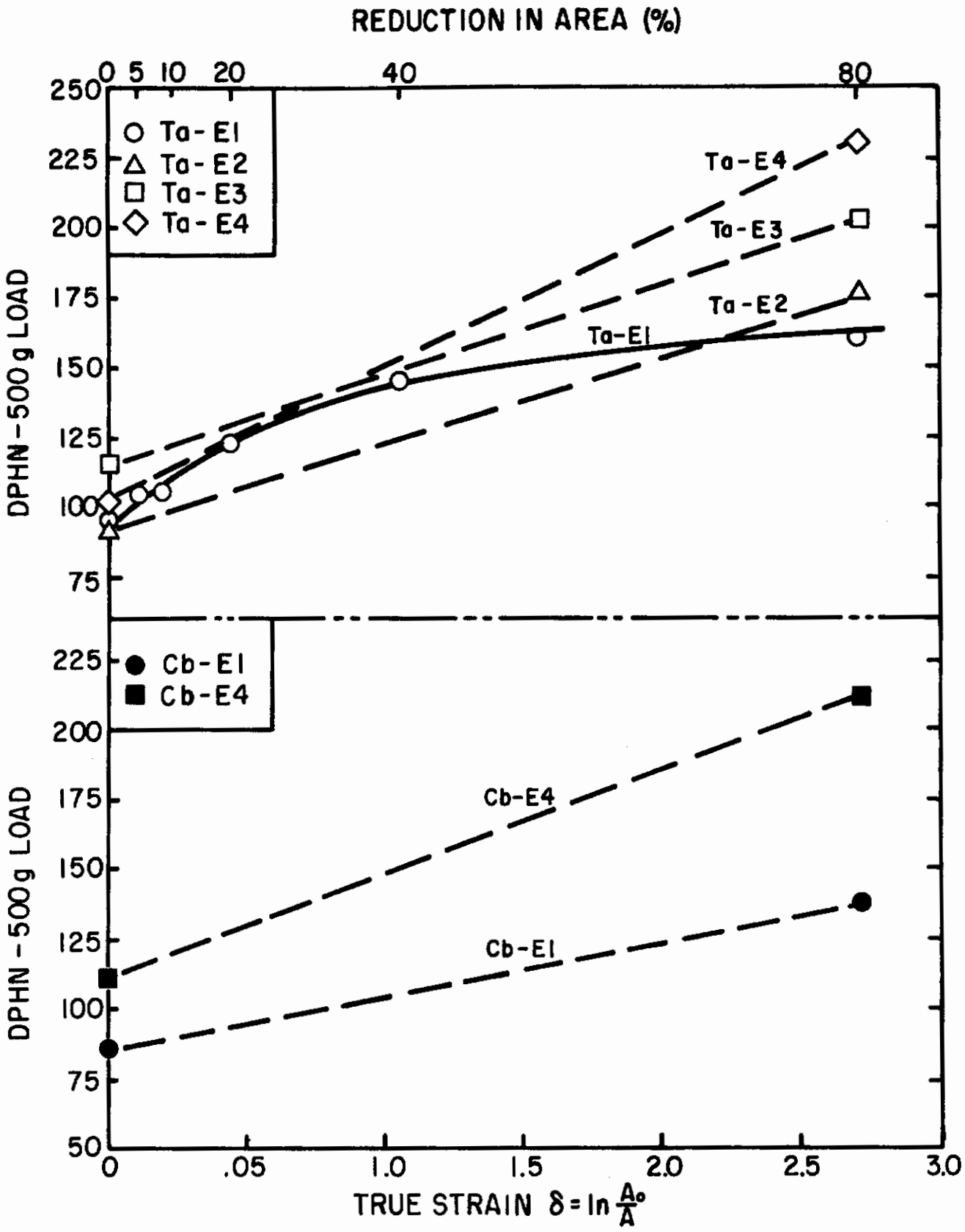

Fig.56 - Effect of deformation on the hardness of tantalum and columbium strip

The variation in hardness of the Ta-E1 strip as a function of increasing deformation is shown in Fig. 56. Hardness values for the 0% R.A. and 80% R.A. conditions of the Ta-E2, Ta-E3 and Ta-E4 strip are included. As expected, the hardness of Ta-E1 increases with increasing degree of deformation (Fig. 56.) For 80% R.A., the order of increasing hardness is Ta-E1, Ta-E2, Ta-E3 and Ta-E4.

The results of the particle size measurements for Ta-E1, Ta-E2, Ta-E3 and Ta-E4 strip of 80% R.A. are given in Table 28. Ranking these strip materials in the order of decreasing $D_{[100]\ eff}$, gives the same order as for increasing hardness. The differences in the interstitial contents of these strip materials are relatively small (see Table 2), especially compared to the difference between Cb-E1 and Cb-E4 materials. Furthermore, the differences cannot be simply expressed in terms of only one interstitial element except perhaps for the Ta-E4 strip materials which are definitely highest in oxygen. Therefore, whereas only a rough correlation was found between decreasing particle size and increasing interstitial content for the Ta-E series at 80% R.A., a more definite relationship exists between $D_{[100]\ eff}$ and the 80% R.A. hardness resulting from deformation.

The line profiles of the 0% R.A. Ta-E1, Ta-E2, Ta-E3 and Ta-E4 were so nearly alike, and similar to that of Ta-P2, that a Fourier analysis was deemed inapplicable. For 0% R.A., the ranking based on half-widths seems to be the same as the ranking based on hardness. However, this may not be significant because the measured differences are too small to be considered reliable.

The intensity of the (110)(220) series diffracting from rolling-plane specimens was found to be insufficient for line profile measurements. Instead, specimens of transverse sections were employed for these measurements, using a transverse specimen of Ta-E2 strip of 0% R.A. as the instrumental standard. Since the preferred orientation of this standard also allowed measurement of the (200)(400), this was compared with the line profile of the Ta-P2 standard used for the (200)(400). If a material is completely recrystallized, the diffraction line profiles should be independent of the orientation in which they are measured. This was confirmed for Ta-E2.

The data of Schoening[26] on Ta filings referred to above also yields information of the influence of faulting. These data indicate a ratio $D_{[110]\ eff}/D_{[100]\ eff}$ of about 1.7. The data of Table 28 show a variation of the ratios from about 1.2 to 1.7. Because of the scatter in the data, especially that of the (110)(220), the differences cannot be readily interpreted. However, it is believed that they show that faulting does have an effect; although in these rolled specimens the effect is probably less than that found by Schoening in filings.

Table 28

Particle Size Terms of Experimental Tantalum Strip

Material	Condition	Particle size terms, A. [100]	Particle size terms, A. [110]	$D_{[110]}/D_{[100]}$
Ta-E1 Strip	80% R.A.	850	1030	1.2
Ta-E2 Strip	80% R.A.	800	1330	1.7
Ta-E3 Strip	80% R.A.	630	850	1.3
Ta-E4 Strip	80% R.A.	460	720	1.6

REFERENCES

(1) B. S. Lement, et al, "Substructure and Mechanical Properties of Refractory Metals," Section III, WADD Technical Report 61-181, (1961).

(2) U. E. Wolff, "Dislocation Etch Pits in Tungsten," Acta Met. 6 (1958) 559.

(3) A. Iannucci, J. Intrater, G. Murray and S. Weinig, "The Investigation of the Mechanism of Substructural Formation in Refractory Metals and the Relation to the Observed Mechanical Properties," Materials Research Corporation, WADC TR 59-441 (1959).

(4) The Metal Molybdenum, American Society for Metals, (1958) 405.

(5) T. K. Bierlein, H. W. Newkirk, Jr. and B. Mastel, "Etching of Refractories and Cermets by Ion Bombardment," Journal of the American Ceramic Society, 41, No. 6 (1958) 196-200.

(6) O. J. Krudtaa and K. Stokland, "Electropolishing of Columbium and Tantalum," Metal Progress 77 (1960) 101.

(7) G. A. Miller, Tantalum and Niobium, Butterworth Scientific Publications, London (1959) 726.

(8) R. Bakish, "Dislocation Configurations and Densities in Tantalum Crystals," Acta Met. 6 (1958) 120.

(9) A. B. Michael and F. J. Huegel, "Observations on Etch Pits and Sub-boundaries in Columbium," Acta Met. 5 (1957) 339.

(10) M. A. Adams, "Design for an Autographically Recording Tensile Machine," AERE M/R 2604, United Kingdom Atomic Energy Authority, Harwell (1958).

(11) N. L. Peterson, "Diffusion in Refractory Metals," WADD Technical Report 60-793 (1960).

(12) G. T. Hahn, B. L. Averbach, W. S. Owen, M. Cohen, "Initiation of Cleavage Microcracks in Polycrystalline Iron and Steel," Chap. 5, Fracture, John Wiley and Sons (1959) 91-116.

(13) A. H. Cottrell, "Theory of Brittle Fracture in Steel and Similar Metals," Trans. AIME, 212 (1958) 192-202.

(14) N. J. Petch, "The Ductile-Brittle Transition in the Fracture of α-Iron:I", Phil. Mag. 3 (1958) 1089-1097.

(15) J. H. Bechtold and P. G. Shewmon, "Flow and Fracture Characteristics of Annealed Tungsten," Trans. ASM, 46 (1954) 397-408.

(16) J. W. Pugh, "Tensile and Creep Properties of Tungsten at Elevated Temperatures," Proc. ASTM, 57 (1957) 1-10.

(17) G. L. Davis, "Recrystallization of Tungsten Wires," Metallurgia, 58 (1958) 177-184, 228-232.

(18) J. W. Pugh, "On the Recovery and Recrystallization of Tungsten," Plansee Proceedings 1958, Reutte/Tyrol (1959) 97-107.

(19) R. C. Koo, "Recovery in Cold-Worked Tungsten," Jour. Less-Common Metals, 3 (1961) 412-428.

(20) W. S. Owen, AIME Meeting (April 1962), Chicago.

(21) E. Orowan, "Classical and Dislocation Theories of Brittle Fracture," Chap. 7, Fracture, John Wiley and Sons (1959) 147-160.

(22) M. B. Bever, "On the Thermodynamics and Kinetics of Recovery," Creep and Recovery, ASM, 1957.

(23) B. E. Warren, "X-Ray Study of Deformed Metals," Progress in Metal Physics, 8 (1959) 147.

(24) S. Weissmann, Private Communication.

(25) J. Despujols and B. E. Warren, "X-ray Study of Cold Work in Molybdenum," J. Appl. Phys. 29, (1958) 195.

(26) F. R. L. Schoening, "Fourier Analysis of X-Ray Diffraction Profiles obtained from Tantalum Filings," Acta Met., 4, (1956) 510.

(27) B. S. Lement and I. Perlmutter, "Mechanical Properties Attainable by Alloying of Refractory Metals," J. Less-Common Metals, 2, (1960) 253.

(28) R. T. Begley, "Development of Niobium-Base Alloys," WADC TR57-344.

IV. FIBERING IN REFRACTORY METALS - Work carried out at Massachusetts Institute of Technology by D. A. Thomas, M. F. Comerford, E. S. Meieran, J. F. Peck, and M. C. Shine, Jr.

A. Introduction

This work is concerned with the microstructure, substructure, and mechanical properties of heavily worked refractory metals. The information obtained on the mechanical properties of W-P4 tungsten wire has now been augmented by extensive transmission electron microscopy on the same wires as used for tensile tests. Preliminary progress is reported on an intensive study of the simultaneous development of microstructures and textures in drawn high-purity (Cb-E1) and controlled-purity (Cb-E4) columbium wire. The mechanical property work on drawn iron-silicon alloy is largely completed, and attention is now being devoted to microstructure and substructure studies for correlation with the mechanical properties. Preferred orientation determinations in sheet tungsten are now completed.

The following sections will describe the results in each of the above areas of investigation.

B. Mechanical Properties of Tungsten Wire

1. Experimental Methods

Tensile tests have been carried out on W-P4 wire and on wire drawn from W-P4 in the laboratory. As-received 30-mil W-P4 wire was reduced to 20-mil diameter by drawing through tungsten carbide dies in the steps: 28.0, 26.5, 22.9, 21.2, and 20.0 mils. The temperature at the die was approximately 150°C and the drawing speed was about 0.5 inch per minute. The effects of recovery-annealing temperature and, to some extent, testing temperatures have been investigated.

Wires for tensile specimens were sealed in evacuated vycor or fused quartz tubes and annealed for 30 min. at temperatures as high as 1500°C. One-inch gage sections were electropolished on specimens for room-temperature testing and 0.5-inch gage sections on specimens for transition-temperature determination. The diameter was reduced approximately 2 to 3 mils.

Specimens for room-temperature testing were pulled in a Tinius Olsen machine at a crosshead speed of 0.02 inch per minute. Data were recorded autographically on a load-time basis, with time as a measure of extension. Tests below room temperature were conducted on a modified Polanyi tensile machine at ManLabs.

2. Experimental Results

Room-Temperature Tests

The results of the tensile tests on the 30-mil and 20-mil wires are shown in Figs. 57 to 60.

From room temperature to the vicinity of 700°C, increasing annealing temperature results in decreasing total elongation, decreasing reduction in area, and increasing strength, Figs. 57 to 60. The stable elongation, which is total plastic elongation until the load drops off, was practically constant at 2% for the 30-mil specimens and 1% for the 20-mil specimens.

Above about 700°C, increasing annealing temperature results in decreasing yield strength and ultimate strength and increasing elongation and reduction in area. As indicated by curves B-1, B-2 and B-3 in Fig. 57, considerable irregularity of behavior was exhibited by 30-mil wire annealed in the neighborhood of 1000°C. Specimens on the lower curves broke prematurely with low elongation and it must be supposed that the behavior in this range is very sensitive to small variations in test condition or in the condition of the specimen.

Above annealing temperatures of about 1100° and 1250°C the 30-mil and 20-mil wires respectively showed brittle behavior. The fracture surfaces of specimens that did not neck were shiny in comparison with those that showed necking, but the fineness of the microstructure made detailed fracture observations difficult.

Transition-Temperature Tests

Figure 61 shows the transition temperature of the 30-mil as-received wire to be approximately -20°C. Figure 62 shows the transition temperature of the 20-mil as-drawn wire to be approximately -100°C. The transition temperature was sharply pinpointed because the fracture stress and the ductility change sharply through the transition region.

3. Discussion

A complete phenomenological description of the room-temperature tensile properties is possible only if the effect of recovery annealing on tensile test parameters and on transition temperature is taken into account. Similarly, interpretation of the results requires knowledge of the effect of recovery annealing on substructure and of the relation of substructure to tensile properties.

The transition temperatures of the 30-mil and 20-mil wire in the as-drawn condition are -20 and -100°C, respectively (Figs. 61 and 62). Tests at ManLabs show a generally increasing transition temperature with increasing annealing temperature for 30-mil wire, and similar behavior is expected for the 20-mil wire, on which tests are in progress. Thus the room-temperature brittleness after annealing at 1200 to 1300°C indicates simply that the transition temperature has been raised to room temperature or above.

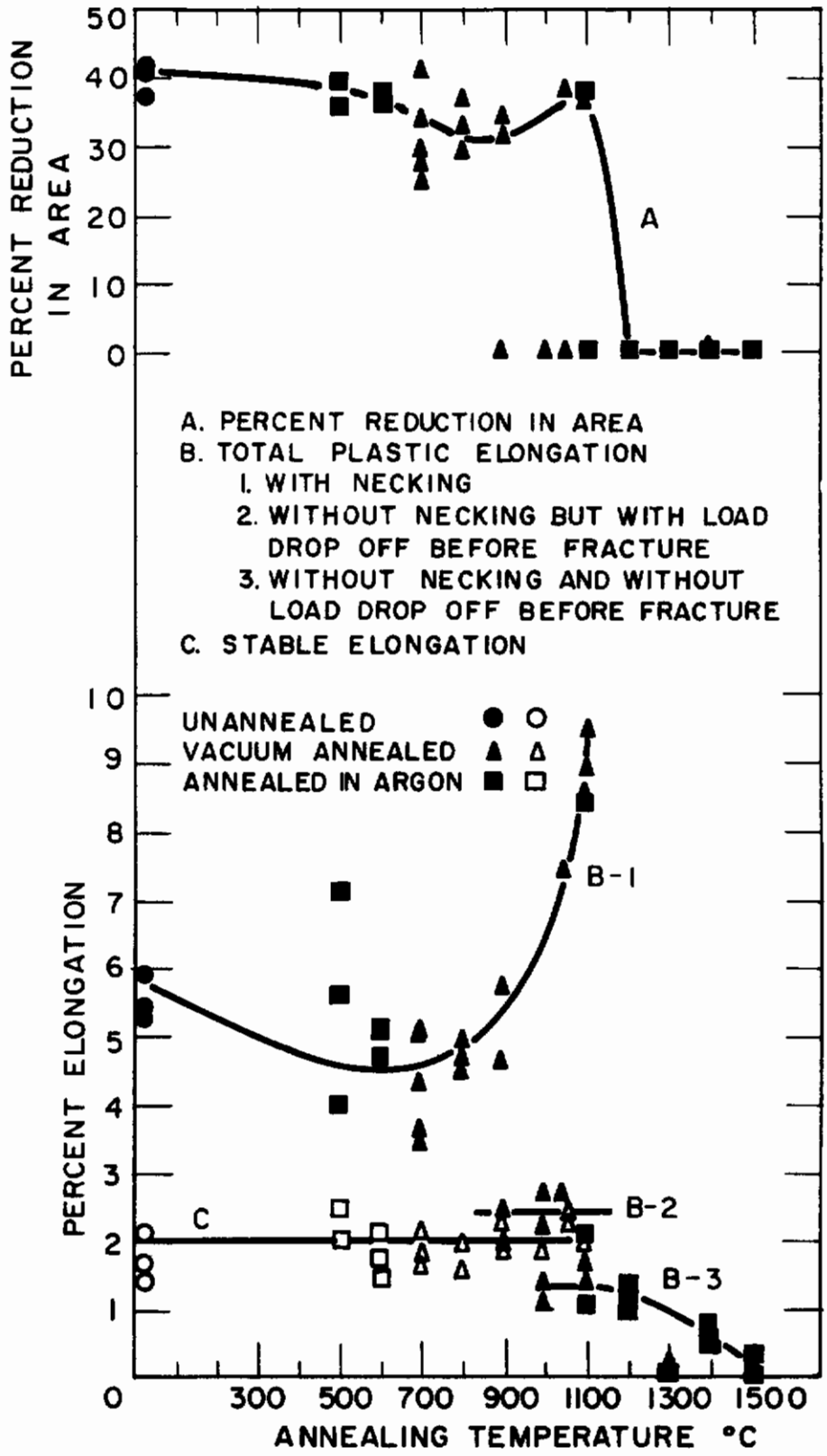

Fig. 57 - Effect of annealing for 30 min. on room-temperature tensile properties of 30-mil W-P4 tungsten wire.

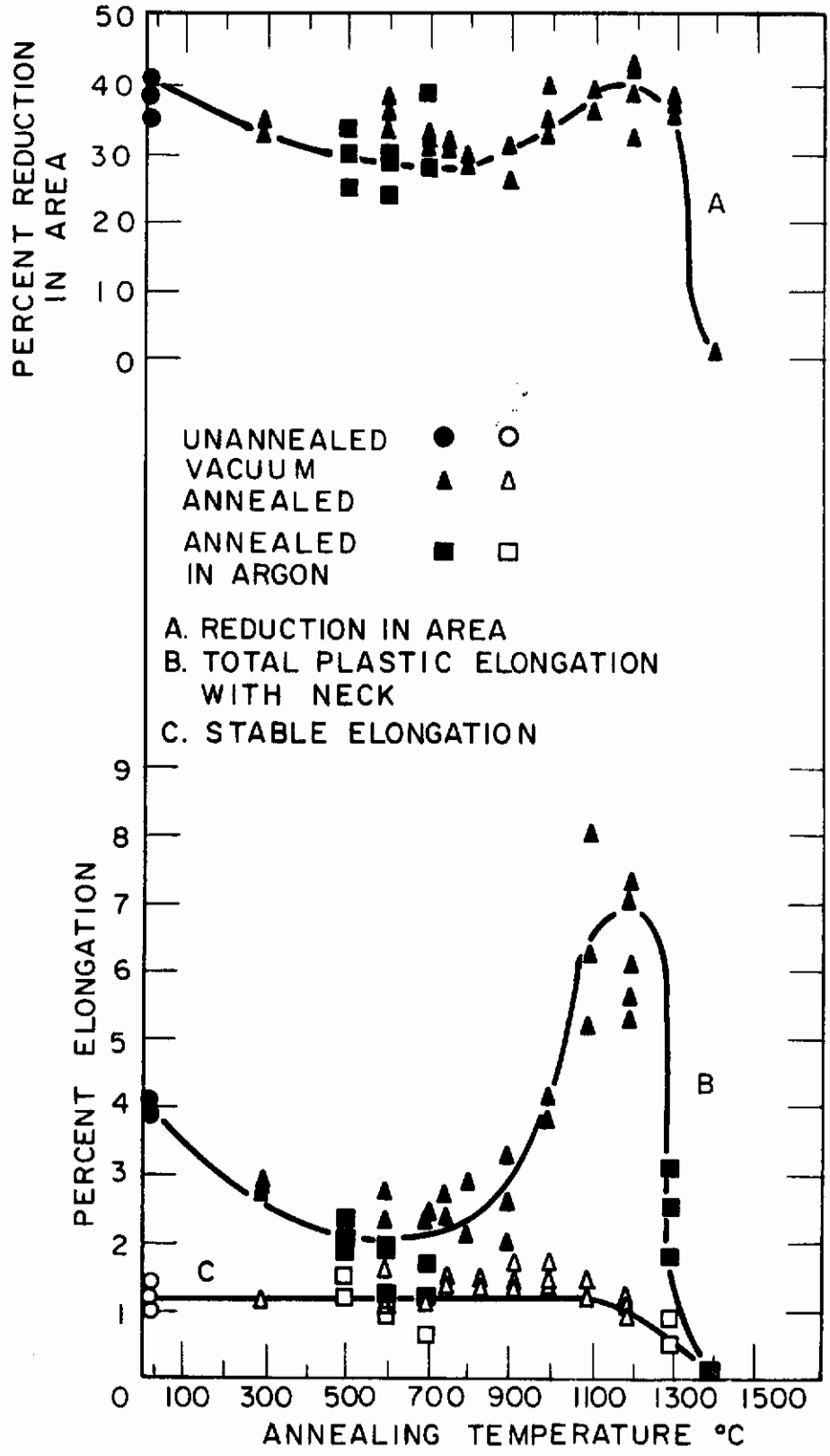

Fig. 58 - Effect of annealing for 30 min. on room-temperature tensile properties of 20-mil tungsten wire.

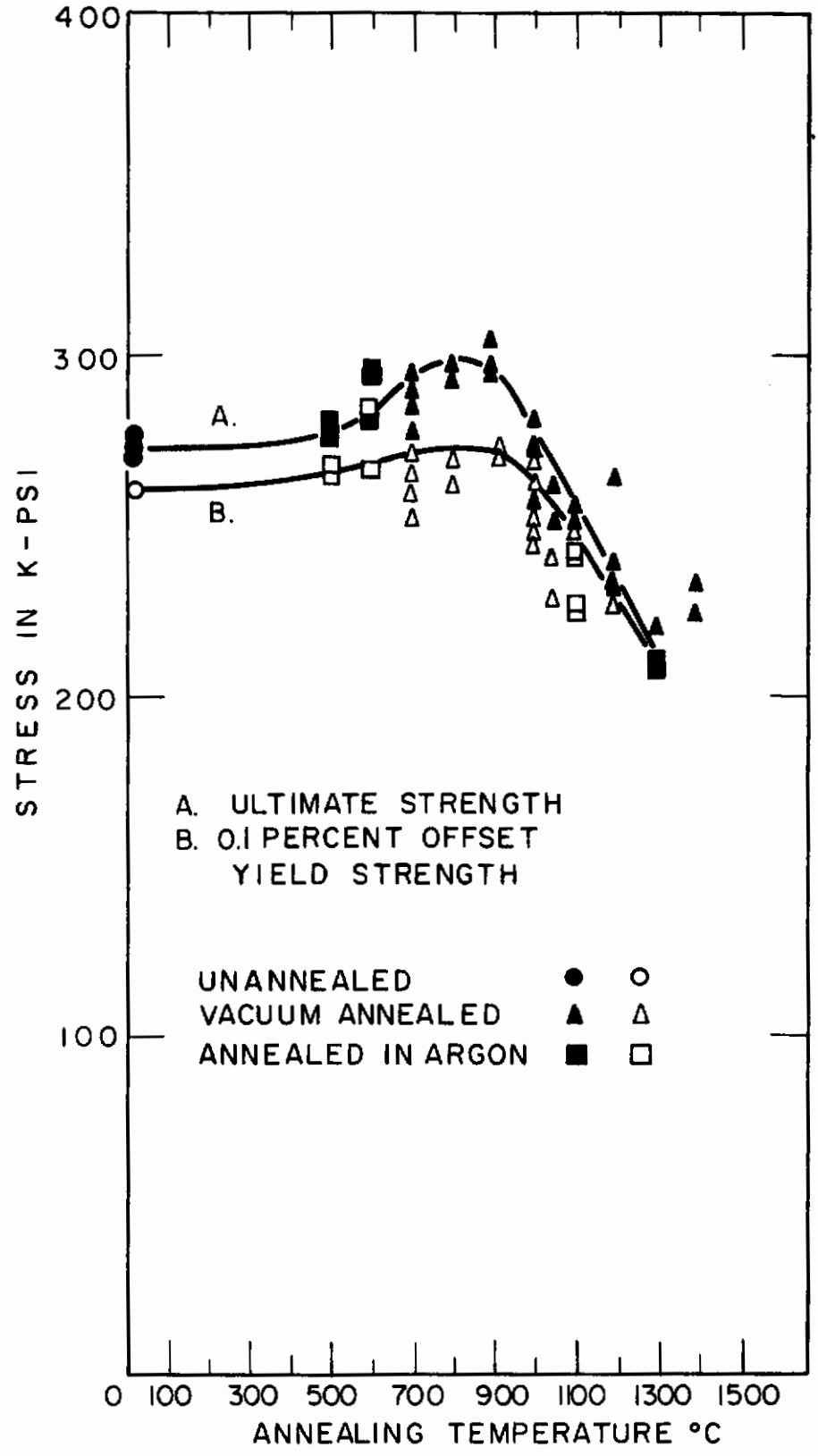

Fig. 59 - Effect of annealing for 30 min. on room-temperature tensile properties of 30-mil W-P4 tungsten wire.

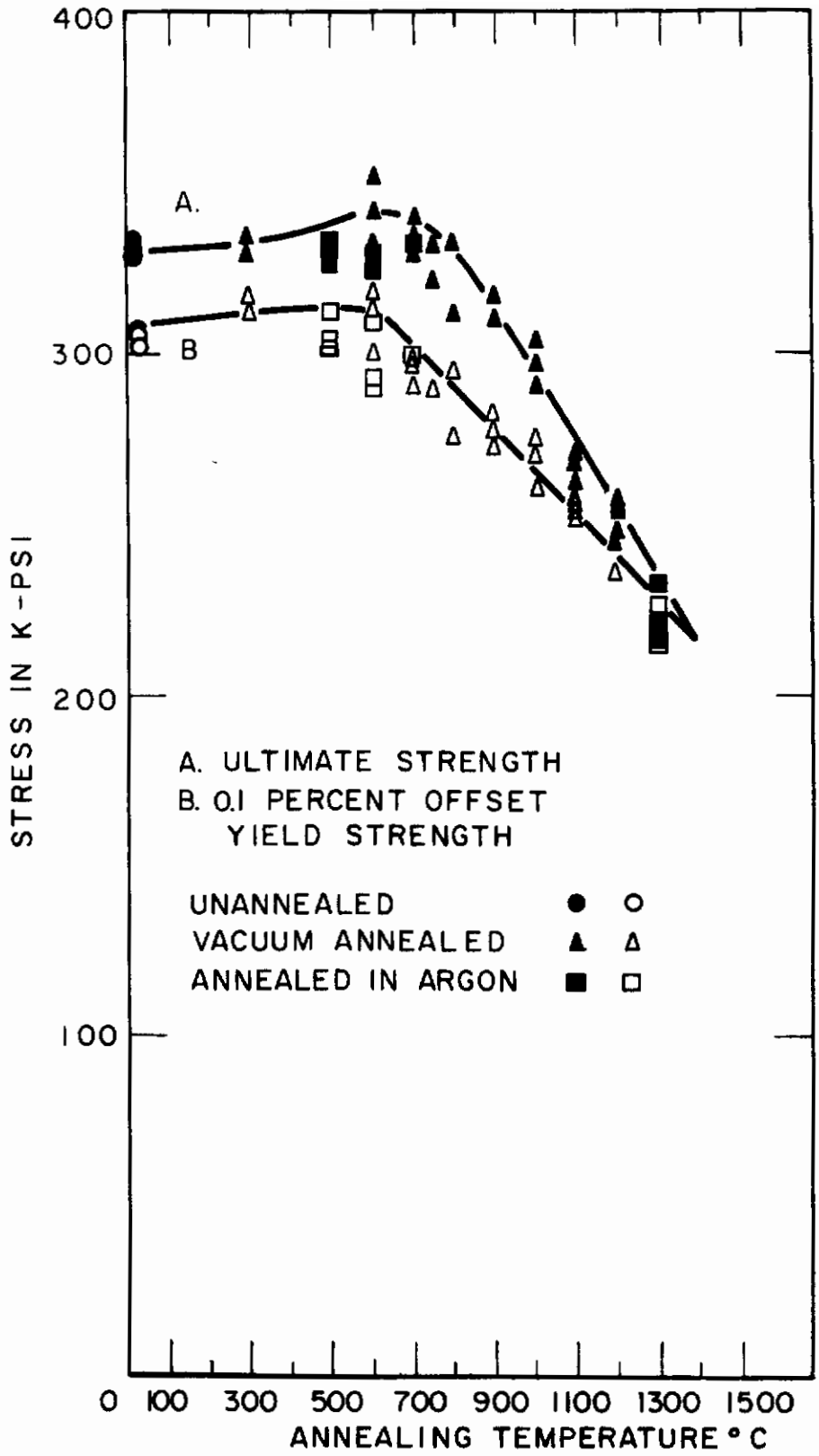

Fig. 60 - Effect of annealing for 30 min. on room-temperature tensile properties of 20-mil tungsten wire.

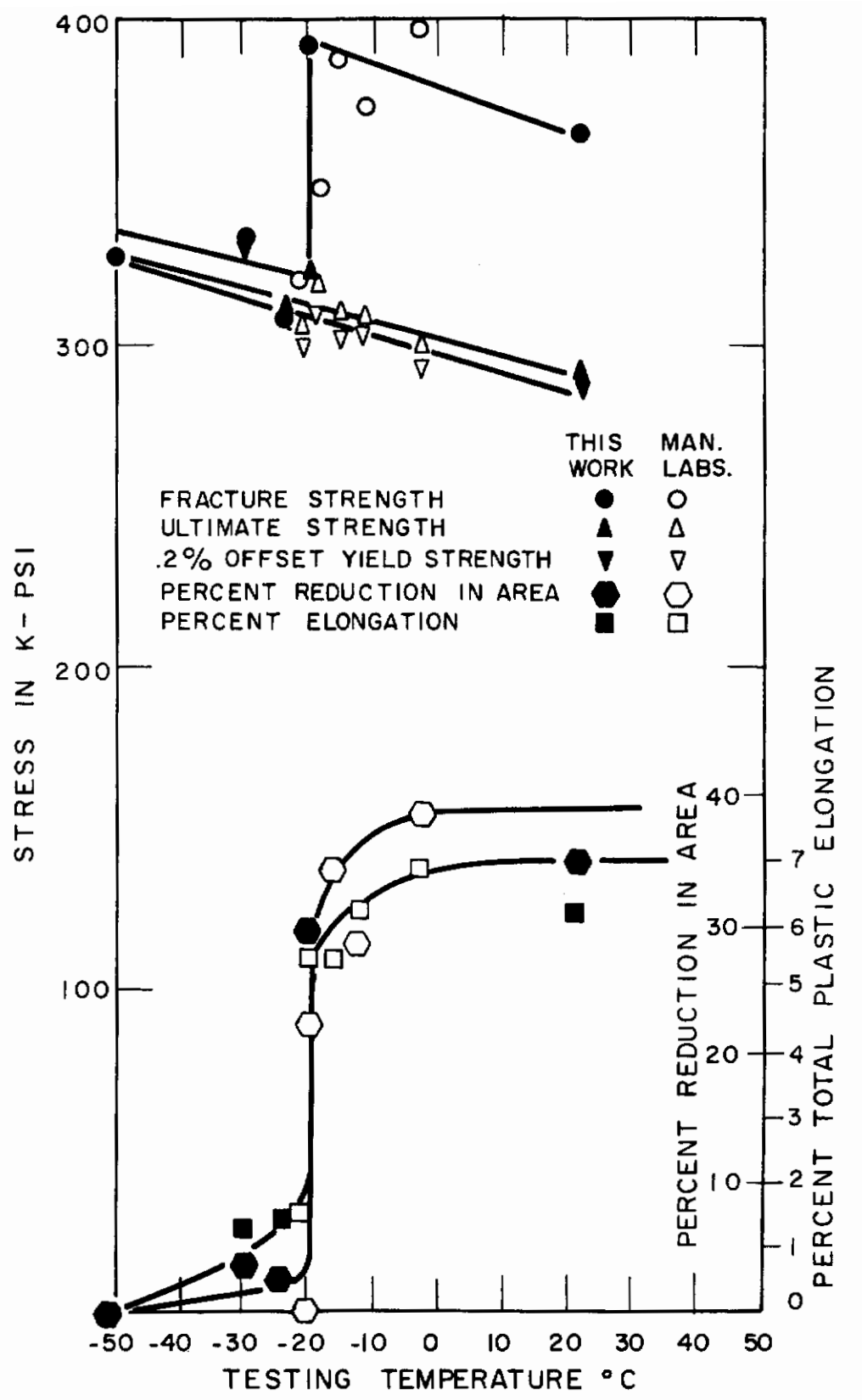

Fig. 61 - Transition behavior of 30-mil W-P4 tungsten wire.

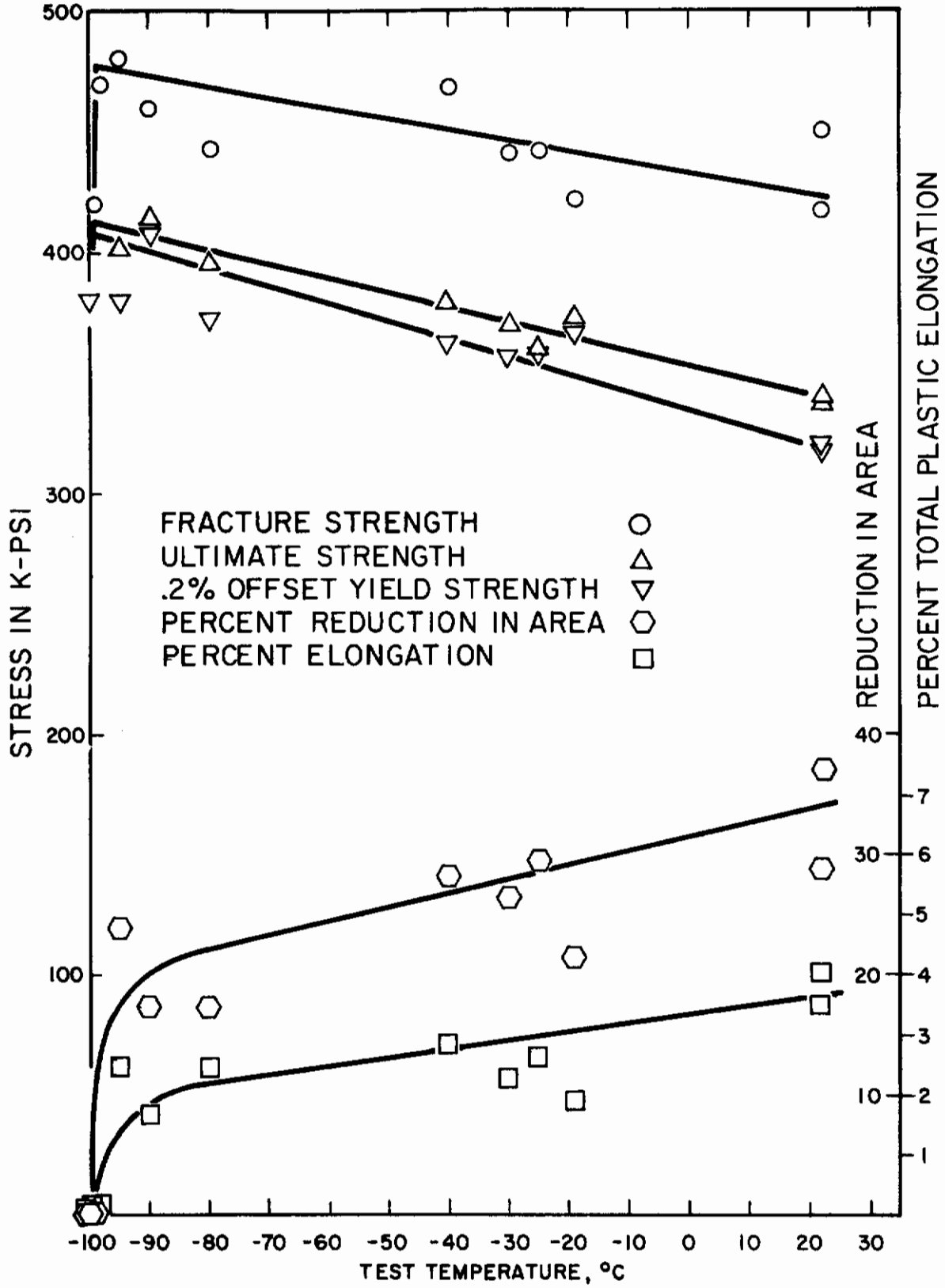

Fig. 62 - Transition behavior of 20-mil tungsten wire.

The ductility above the transition temperature will be called the "intrinsic ductility" because it is a measure of the ductility of the metal when it shows normal behavior. Although this intrinsic ductility varies somewhat with testing temperature above the transition temperature it is a simple parameter that indicates the extent that ductility has been altered by annealing. For example, fully annealed, recrystallized tungsten has an intrinsic ductility (that is, ductility above its transition temperature of about 250°C) of approximately 60% elongation (1) compared with 3% elongation for the as-drawn 20-mil wire.

The reduced room-temperature ductility resulting from annealing up to 700°C probably involves a reduced intrinsic ductility. Possible structural changes that could lead to reduced intrinsic ductility are dislocation rearrangements and strain aging. The ductility loss is greater for the 20-mil wire, which received more cold work and therefore should have a larger driving force for any structural change. Pugh (2) observed total loss of room-temperature ductility after 700°C annealing of still more severely worked wire, drawn from 30 to 10 mils at room temperature, but the detailed behavior upon annealing was different from that observed here, and it is not clear whether or not similar mechanisms are operating.

Annealing above 700°C results in increasing ductility for both 30- and 20-mil wire, which almost certainly indicates that annealing increases the intrinsic ductility. This is normal behavior for the annealing of cold-worked metals, but no reports of such behavior during the recovery-annealing of tungsten have been found in the literature. Cold-worked iron recovers in a similar way (3), however, and b.c.c. metals generally seem to show pronounced recovery of mechanical properties (4). The ductility of the 30- and 20-mil tungsten wires reaches a maximum at 1100 or 1200°C, where the values are about 9 and 7% elongation respectively, well above the initial values of 6 and 4%.

The increasing intrinsic ductility presumably arises from structural changes taking place during recovery annealing. Light metallography readily reveals substructure changes at 1000°C and above, and transmission electron microscopy reveals the existence and alteration of distinct subgrains at lower temperatures. Hardness, yield strength, and tensile strength also decrease above 900°C. Softening and increasing ductility thus go hand-in-hand with the substructure changes, although no detailed correlations are possible at present.

At the same time that strength and ductility properties are changing, the transition temperature also changes. Drawing to 20-mil wire substantially lowers the transition temperature, but increases the strength and reduces the intrinsic ductility. The presumed increase in transition temperature brought on by recovery annealing is not understood. In fact, it is hoped that work of the present sort will eventually provide a basis for better understanding of the ductile-to-brittle transition.

C. Transmission Electron Microscopy of Tungsten Wire

1. Experimental Method

A technique has been devised for preparation of thin-foil specimens of 0.030 inch diameter tungsten wire (W-P4), suitable for metallographic investigation by transmission electron microscopy. Electron microscopy is essential to reveal the substructure in W-P4 because the fibrous grains are narrower than 1μ. Furthermore, transmission electron microscopy allows dislocations and other substructure features to be observed directly, and it is now realistic to look toward direct correlation of substructure and mechanical properties in heavily worked refractory metals.

Because most techniques of specimen preparation apply to sheet material rather than wire, the present technique is described here. The technique or modifications of it should be quite useful when wires are either convenient or necessary as experimental materials.

The first step in the preparation of thin-foil specimens from wire is to grind opposite parallel faces on the wire, reducing the thickness to about 0.010 inch. These wafers are then cut into 1/8 inch lengths, to fit in the specimen holder of the electron microscope. The next step is to grip the ground wire in platinum-tipped tweezers which are connected to the anode of a DC source. The cathode is a copper tube, 0.010 inch I.D. at the tip, through which 10% NaOH passes by gravity feed. The tip of the electrode is placed 2-4 mm above the specimen. An impression is electrolytically polished in each surface of the specimen, thinning the specimen locally to a few thousandths of an inch.

The third step is the polishing of the entire specimen in 2% NaOH, using a stainless steel cathode. A light source is placed under the specimen, which is viewed during polishing through a binocular microscope. Since the region between the two impressions is thinner than anywhere else, a hole will appear there first. As soon as light is seen in the microscope through the specimen, polishing is stopped and the specimen is washed in water, alcohol, and ether.

The finished specimen can be photographed optically, as in Fig. 63a, and with the electron microscope, as in Fig. 63b. The exact area that is examined by transmission microscopy can be located on the optical photomicrograph. Thus, direct correlation between optical and electron microscopy can be obtained.

2. Results

As-drawn wire and wires annealed for both 10 and 30 min. at 800, 900, 1000, 1100, 1200, 1300, and 1400°C have been examined. The specimens are the same ones for which mechanical properties and microstructures have been reported. Only the as-drawn samples, those annealed 10 min. at all temperatures, and those annealed 30 min. at 1000°C have been examined sufficiently for presentation at this time.

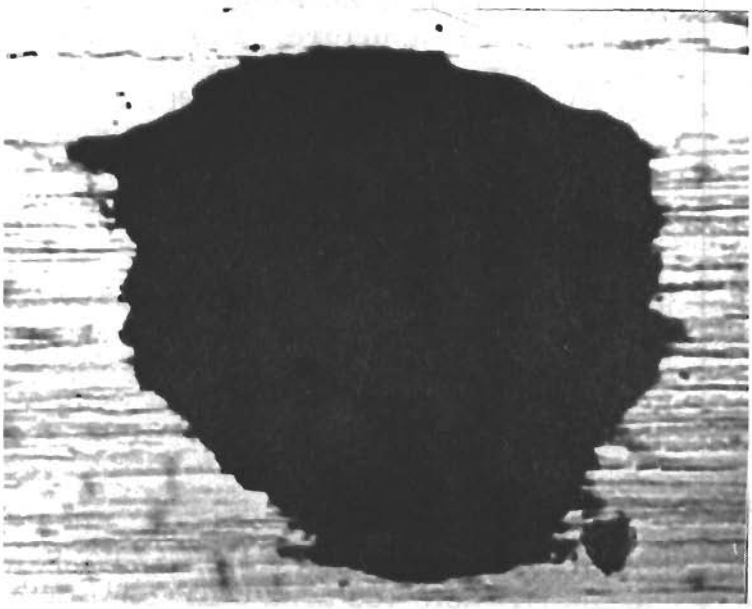

a. - Optical micrograph, reflected light, approximately 4000X. Electropolishing has resulted in sufficient etching to reveal the fiber structure clearly.

b. - Same area by transmission electron microscopy, approximately 6000X. Electron transmission is apparent through the fibers at the edge of the hole.

Fig. 63 - Hole in transmission electron microscopy specimen. W-P4 tungsten wire, annealed 10 minutes at 1000°C.

It must be remembered when viewing the electron micrographs that only a very tiny region of the material is observed. Thus, no one photograph is representative of the entire microstructure. Furthermore, since individual fibers, or grains, are being examined, and they are in reality ribbon-like rather than fiber-like in shape (4,5), the apparent fiber width depends on the orientation of the fiber with respect to the foil surface. Hence, individual fiber sizes cannot be compared directly.

As-drawn W-P4

The two major characteristics of as-drawn wire are the fairly straight fiber boundaries and the tendency toward a cell structure within individual fibers. Almost all of the fibers have a substructure of cells, such as in Figs. 64a and 64b. The cells are relatively free of dislocations, but the material as a whole has a high dislocation density.

The nonuniform apparent fiber width and the fiber boundaries are shown in Figs. 65a and 65b. It is often difficult to determine whether a given boundary is actually a grain boundary (dividing two fibers) or a subboundary (dividing two cells of one fiber). Selected area diffraction is expected to resolve this difficulty.

900°C - 10 minutes

After annealing the wire in vacuo for 10 min. at 900°C, the structure appears as in Figs. 66a and 66b. The cell structure is less prominent than in as-drawn specimens, and transverse subboundaries have appeared across some fibers. Occasional examples are found in which one fiber appears to grow into an adjacent one. Thus at 900°C (not apparent at 800°C), strain-induced boundary migration apparently begins to occur.

1000°C - 10 minutes

There is little difference between the microstructure of this sample and that of the previous one, except for an apparent decrease in average fiber size, Fig. 67a. Another slight change between the two treatments is the ordering of some dislocations into nets, as seen in Fig. 67b. Striations normal to the fiber axis in Fig. 67b were observed in all specimens, regardless of annealing treatment, and will be discussed in a later section.

1100°C - 10 minutes

There is still little change in microstructure after annealing at 1100°C, as seen in Fig. 68a. However, there are few wide grains, and the average grain width is a minimum.

Fig. 64a - As-received. 40,000X.

Fig. 64b - As-received. 56,000X.

Fig. 65a - As-received. 40,000X.

Fig. 65b - As-received. 20,000X.

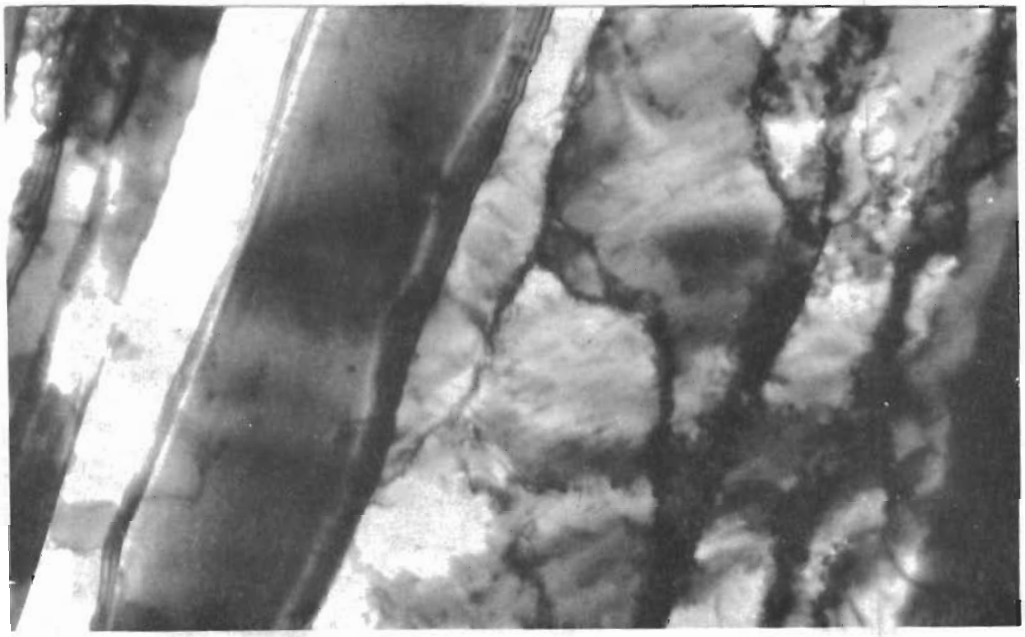

Fig. 66a - Annealed 10 minutes at 900°C. 40,000X.

Fig. 66b - Annealed 10 minutes at 900°C. 40,000X.

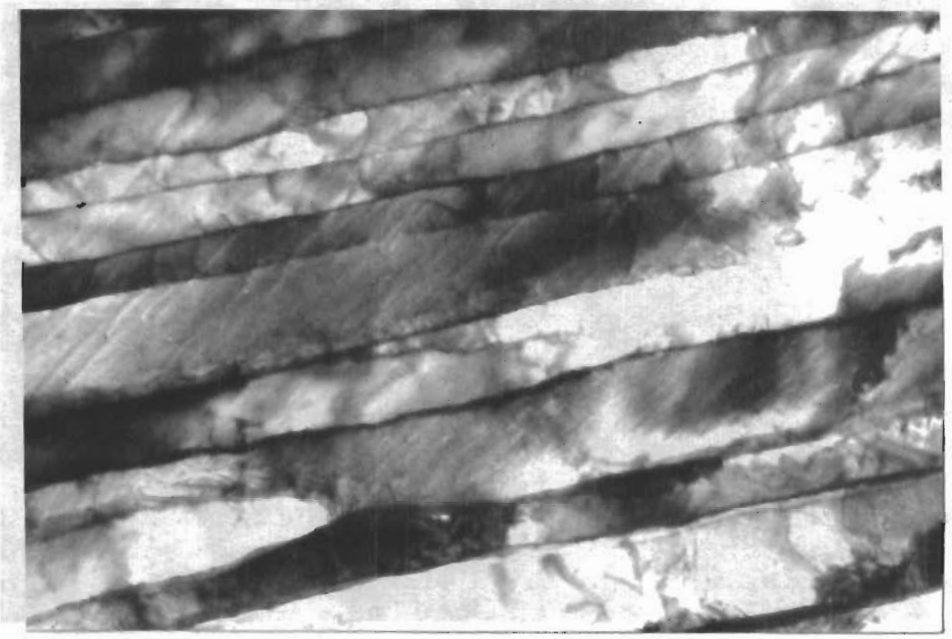

Fig. 67a - Annealed 10 minutes at 1000°C. 40,000X.

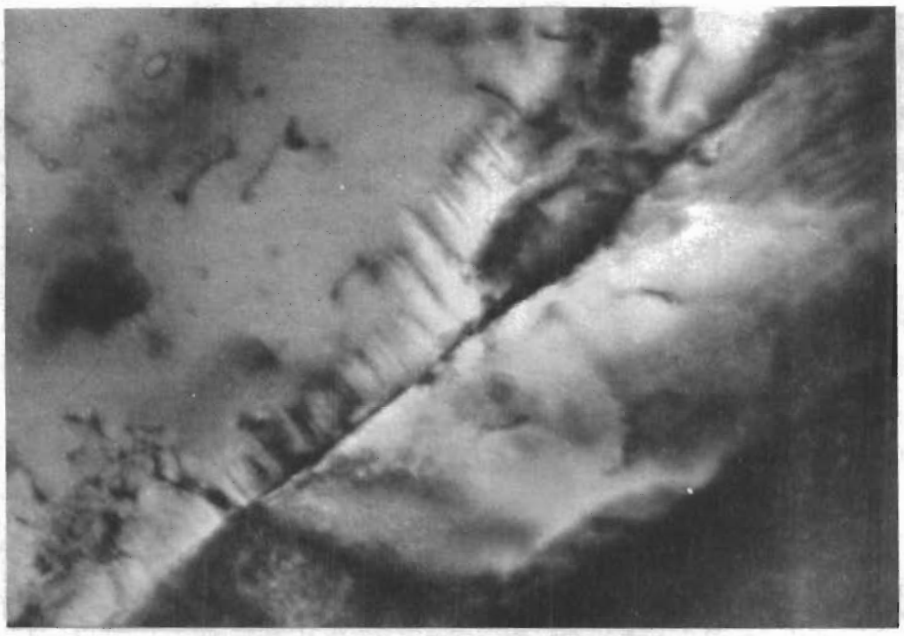

Fig. 67b - Annealed 10 minutes at 1000°C. 96,000X.

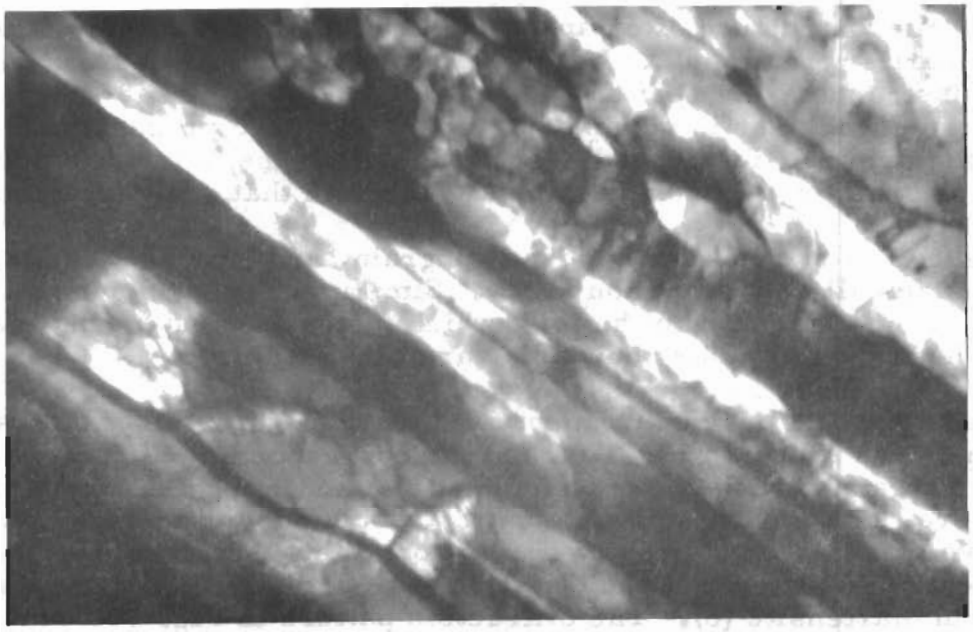

Fig. 68a - Annealed 10 minutes at 1100°C. 20,000X.

Fig. 68b - Annealed 10 minutes at 1200°C. 20,000X.

1200°C - 10 minutes

The microstructure after annealing at 1200°C is markedly different from those of earlier treatments. Larger grains have appeared and have a polygonized substructure, as seen in Fig. 68b. Most of the large subgrains meet transverse boundaries in neighboring fibers and have probably arisen by migration of the original fiber boundaries. Almost all the fibers are polygonized, and the average grain size is considerably larger than that of the previous case.

Figure 69a shows a polygonized subgrain, and it is seen that the subboundary is actually a dislocation array. Similarly Fig. 69b shows a dislocation array almost parallel to the foil, which forms a boundary between two subgrains. The irregular fiber boundaries are also evident.

The striations previously mentioned that appear in all samples at all annealing stages are shown in Fig. 70a and the corresponding diffraction pattern in Fig. 70b. The striations appear on both optical and replica electron micrographs, so there is an etching characteristic associated with them. However, Fig. 70a shows that the boundaries of grains containing the striations are corrugated, which indicates that the striations are actually thin plates, similar to those seen in martensite (6). The diffraction pattern in Fig. 70b shows reciprocal lattice points elongated in a direction perpendicular to the striations, which is characteristic of thin crystals. Furthermore, in many cases the fibers containing these striations are completely etched away during the polishing process, and all that remains are small traces of the edges of the fibers. These edges show the striations, which indicates that the etched away-grains were actually striated. Conclusive evidence as to whether the striations are twins or not awaits further analysis of diffraction patterns such as Fig. 70b.

1300°C - 10 minutes

Many dislocation nets are visible after annealing at 1300°C for 10 min., as seen in Fig. 71a. Most of the subgrains are well polygonized, and some seem to be almost dislocation free. Some sort of grain boundary migration process is occurring, as is subgrain growth. These two are apparently competing processes.

1400°C - 10 minutes

Figure 71b shows a typical microstructure after annealing at 1400°C. There is little difference between this and the previous microstructure, except that polygonization is just about complete. However, it must be noticed that the grains still are elongated in the direction of the wire axis. Also, there are still many dislocations present inside the fibers.

1000°C - 30 minutes

The microstructure of wire annealed for 30 minutes at 1000°C appears in Figs. 72a and 72b. More dislocation nets are visible inside the fibers than in the samples annealed 10 minutes at 1000°C. There is no evidence of the large

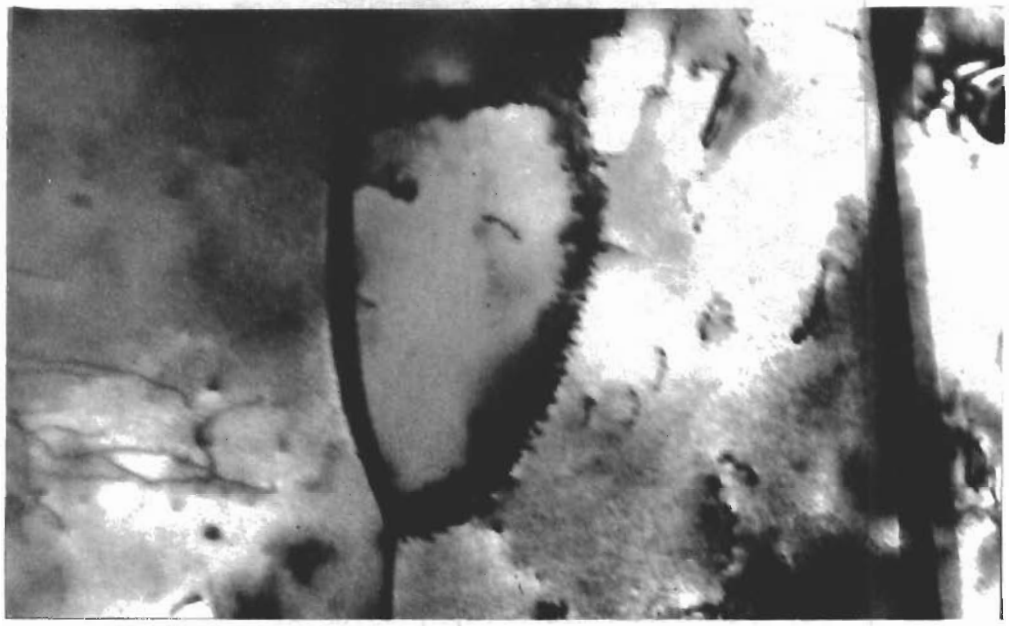

Fig. 69a - Annealed 10 minutes at 1200°C.

Fig. 69b - Annealed 10 minutes at 1200°C. 40,000X

a. - Electron micrograph, 40,000X.

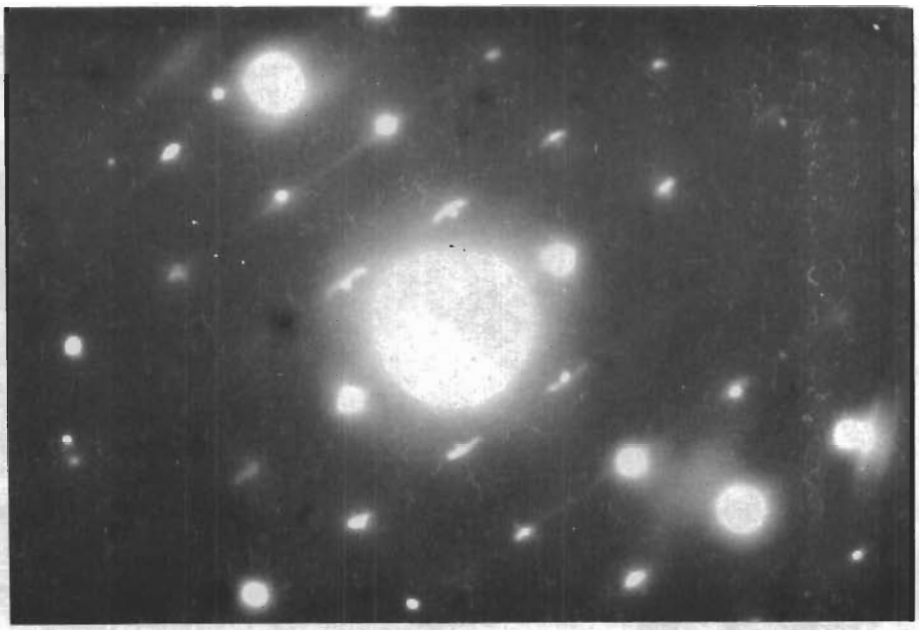

b. - Electron diffraction pattern.

Fig. 70 - Annealed 10 minutes at 1200°C.

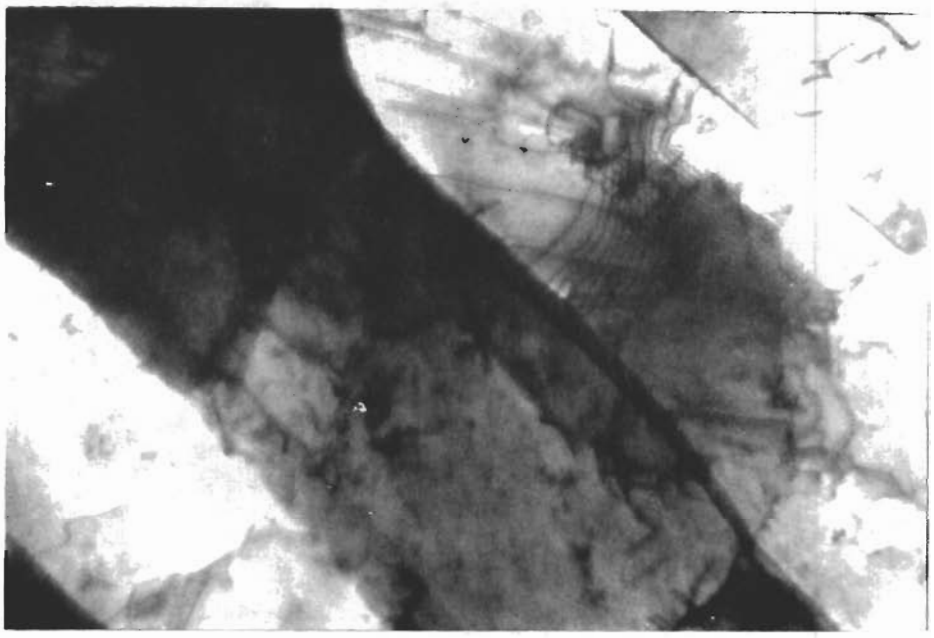

Fig. 71a - Annealed 10 minutes at 1300°C. 40,000X.

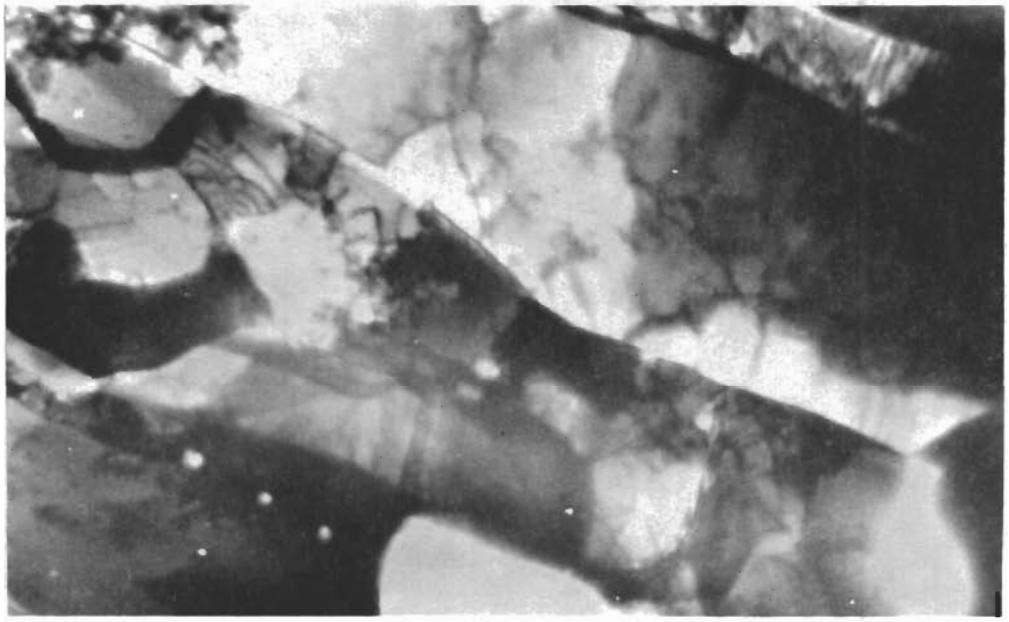

Fig. 71b - Annealed 10 minutes at 1400°C. 20,000X.

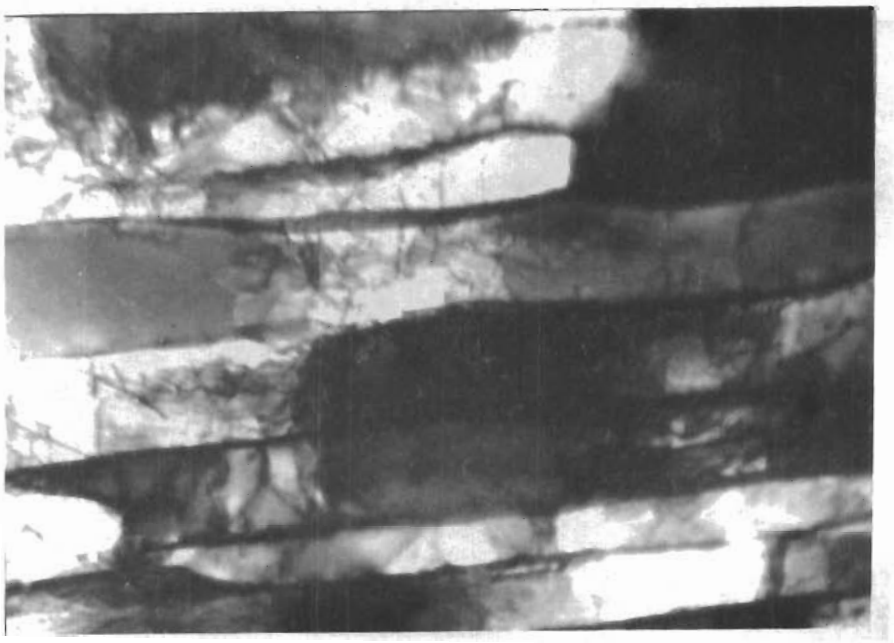

Fig. 72a - Annealed 30 minutes at 1000°C. 40,000X.

Fig. 72b - Annealed 30 minutes at 1000°C. 40,000X.

subgrain growth at 1200°C, but the general appearance of the structure is closer to that annealed at 1100°C for 10 minutes than that of the 1000°C annealed for 10 minutes.

3. Discussion

The annealing of the drawn W-P4 wire is obviously complex, with many overlapping stages. At present, only a preliminary qualitative understanding is possible, and more work will have to be undertaken before the picture becomes clear. In view of the known effects of additions (impurities, doping, thoria) on the annealing of tungsten (7), the details of the structural changes may be expected to vary considerably in different tungstens.

The as-drawn wire is characterized by straight fiber boundaries and a cell structure within the fibers. Both these features tend to disappear after annealing at 800 to 900°C for 10 minutes. The cell boundaries tend to align normal to the fiber axis, leading to the transverse boundaries seen in both optical and electron micrographs.

The as-drawn fibers are ribbon-like in shape, with (001) in the plane of the ribbon and the length of the ribbon parallel to [110]. The ribbon-like fibers are several μ wide, 0.2 to 0.6 μ thick, and very long. Optical microscopy of transverse sections of wire has shown that the fibers are curved to maintain continuity with neighboring fibers (5). Thus, after annealing, these bent fibers would polygonize, giving longitudinal polygon boundaries, parallel to [110], in addition to the transverse boundaries observed. This leads to more fiber boundaries (or subboundaries) in longitudinal section.

The next stage of the annealing process occurs about 1200°C, where either strain-induced boundary migration or grain growth occurs. Many dislocation nets are formed during this stage, and are seen inside the fibers. Competing with this process is the growth of some subgrains into neighboring fibers. This is readily visible in the optical photographs.

The prominent role that the original fiber boundaries apparently have, through strain-induced boundary migration, is observed here because the small fiber widths result in numerous fiber boundaries in each field of view. Thin foil specimens prepared from rolled sheets, on the other hand, rarely have grain boundaries visible because the specimen is thin compared with the thickness of the rolled grains. Accordingly, it seems possible that strain-induced boundary migration is important in the annealing of sheets, but that transmission electron microscopy normally reveals only the changes within the grains. This possibility will be pursued by examination of edge sections of rolled sheets, in which grain boundaries will be numerous, as in drawn wires. Specimen preparation techniques for wires should be readily applicable to edge sections of rolled sheets, at least for sheet thicknesses of 0.020 to 0.030 inch or greater.

The next stage in the process of annealing is the ordering of dislocation arrays into well defined nets, while polygonization and grain growth continue. The microstructure of this material shows many dislocation-free subgrains, which might act as recrystallization nuclei. Jones (8) and Koo (9) have made similar observations.

Annealing has not been carried to the point at which recrystallization in the usual sense occurs. In fact, it is more likely, as Davis (10) and others have suggested, that the enlarged grains observed to form here undergo secondary recrystallization at higher temperatures. Ordinary recrystallization thus may not occur in tungsten, at least with the usual purity and processing history.

D. Microstructures and Textures in Wire Drawing

In prior reports (4,5), the curved shape of the grains in transverse sections of drawn b.c.c. W or Fe wires has been described, and a hypothesis was proposed to explain this phenomenon. Only two <111> slip directions are active in the elongation of a b.c.c. wire with a perfect <110> wire texture. This means that only one dimension of a transverse section of a grain will change, thus producing an elliptical grain shape. Since contiguous grain boundaries and elliptical grains are not compatible, the grains curve.

An intensive investigation of b.c.c. Cb is now being undertaken to study both microstructure and texture changes during drawing. The preliminary results reported here indicate that further study is indeed required in order to obtain a more complete understanding of the phenomena.

Cb-E4 wire of initial diameter 0.108 inch has been drawn in true strain increments of about 0.15. The material was received in the cold-worked condition and was then annealed at 1200°C to obtain a fine, uniform grain size. A pinhole x-ray technique described by Leber (11) is being used for texture determination. It has the advantage of revealing not only the fiber texture in wires but the "cylindrical" texture as well. All the x-ray patterns reported here are taken from wires that have been etched to 5/8 of their diameter after drawing.

Figure 73 shows the microstructure and a diffraction pattern of the as-annealed starting material. An initial texture is evidently present, as is common in b.c.c. metals (12). The texture is similar to a <110> fiber texture, except that one of the peaks in the second set of rings (200) is displaced from its expected 45° position.

At a true strain of 0.10, there is a well defined <110> fiber texture, as shown in Fig. 74. The corresponding photomicrograph of a transverse section shows little indication of being deformed, however.

At a true strain of 0.46 the texture has become much less distinct, as shown by the diffraction pattern in Fig. 75. The corresponding photomicrograph of a transverse section is easily recognizable as a deformed structure. The etch used

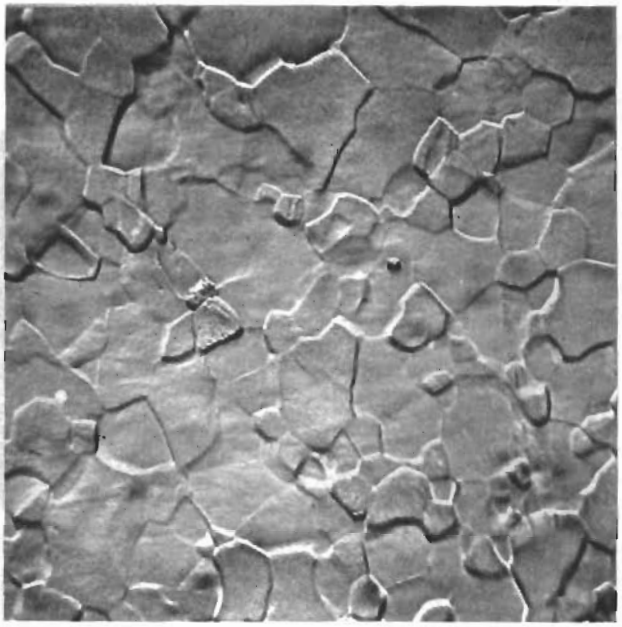

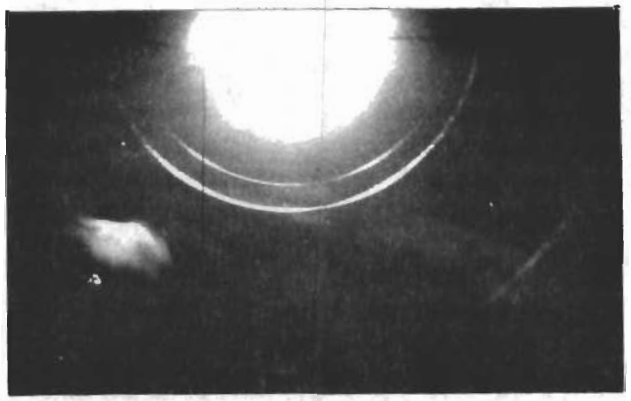

a. - Photomicrograph, 500X. b. - X-ray pattern.

Fig. 73 - Cb-E4 wire, annealed, 0.108 inch diameter.

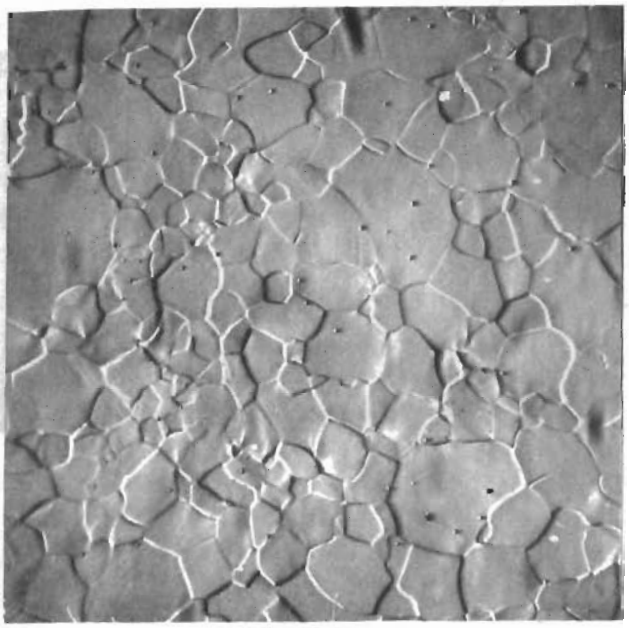

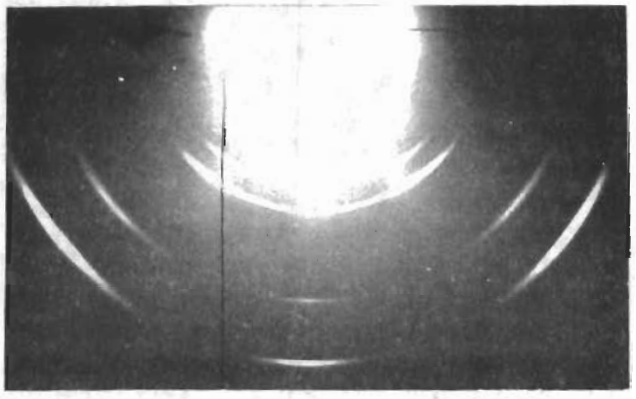

a. - Photomicrograph of transverse section, 500X. b. - X-ray pattern.

Fig. 74 - Drawn, true strain 0.10.

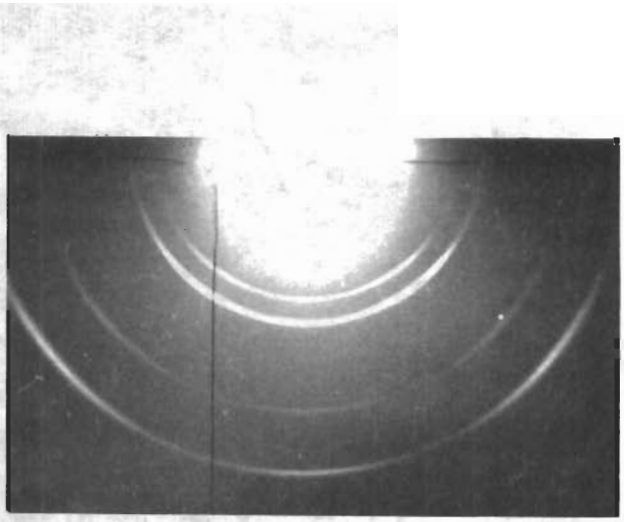

a. - Photomicrograph of transverse section, 500X.

b. - X-ray pattern.

Fig. 75 - Drawn, true strain 0.46.

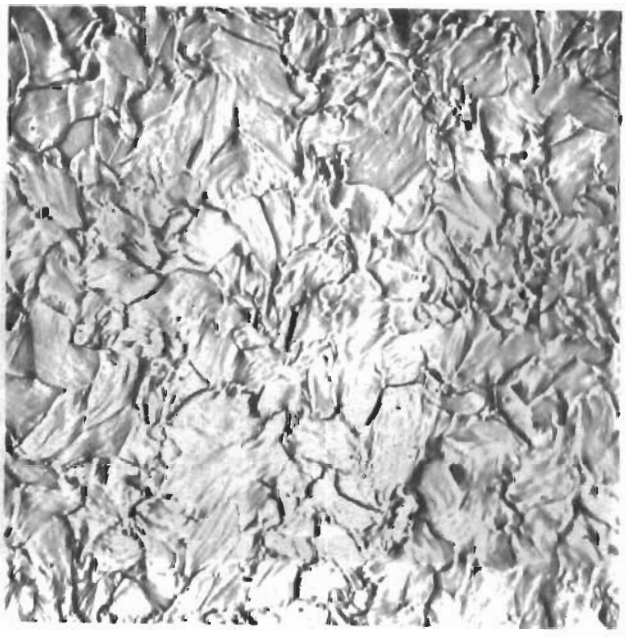

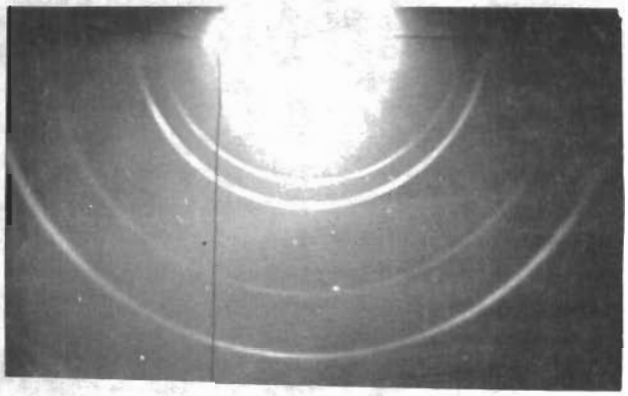

a. - Photomicrograph of transverse section, 500X.

b. - X-ray pattern.

Fig. 76 - Drawn, true strain 0.81.

is orientation sensitive, thus the markings in the individual grains may very well be deformation bands, or at least denote a lattice rotation of some kind within the individual grains. This could be the cause of the apparent destruction of the texture.

At a true strain of 0.81, the texture is even less distinct, but the change is not so marked as the one occurring between a true strain of 0.10 and 0.46. The diffraction pattern and photomicrograph of transverse section are shown in Fig. 76. The photomicrograph is the first one showing a definite thinned and curved grain shape.

The present case is simpler in one respect than the case considered earlier (5), in which the <110> texture was assumed to develop during drawing. With the <110> texture present initially, as found in Cb-E4, only changes in grain shape need be considered in the development of the thinned, curved grains. Assuming that the grains have an ideal <110> wire texture and that they are cube-shaped, we can approximate the effect of drawing on the grain shape by deforming a cube along one edge of a transverse section only. If the length of the cube is doubled by drawing, the transverse section is half as thick but remains the same width. This corresponds to 50% reduction in area, or a true strain of 0.69. This agrees with the appearance of the thinned, curved grains at a true strain between 0.63 and 0.81 in the experimental Cb, which had a well defined <110> texture at a true strain of 0.10. On the other hand, subtle texture changes are occurring throughout the drawing, and these must be understood before an adequate picture is developed of texture and microstructure changes during drawing.

E. Mechanical Properties of Fe-Si Alloy

An Fe-3.19 wt. % Si alloy, containing about 0.019 wt. % carbon, is being studied in the cold-worked state and after annealing, with a view to interpreting the mechanical behavior in terms of the corresponding microstructures and substructures.

Bars one-inch square were cut longitudinally from the center of a slab, forged to three-eighth inch rounds, centerless ground to 0.250 inch diameter and swaged to 0.108 inch diameter. From this material three batches of drawn and annealed wire were prepared with diameters of 0.0423 inch, 0.0604 inch and 0.098 inch. Each was drawn to 0.035 inch diameter without intermediate anneals. This produced three lots of wire with 31, 66, and 87% reductions of area, respectively. Specimens of each were annealed for thirty minutes at a series of temperatures up to 1000°C, electropolished over a one inch gauge length, and tested in tension. All testing was done at room temperature at a crosshead speed of 0.02 inch per minute.

The test results are shown in Figs. 77, 78, and 79 where engineering values of yield stress and ultimate tensile strength, uniform elongation, and reduction of area at fracture are plotted against annealing temperature.

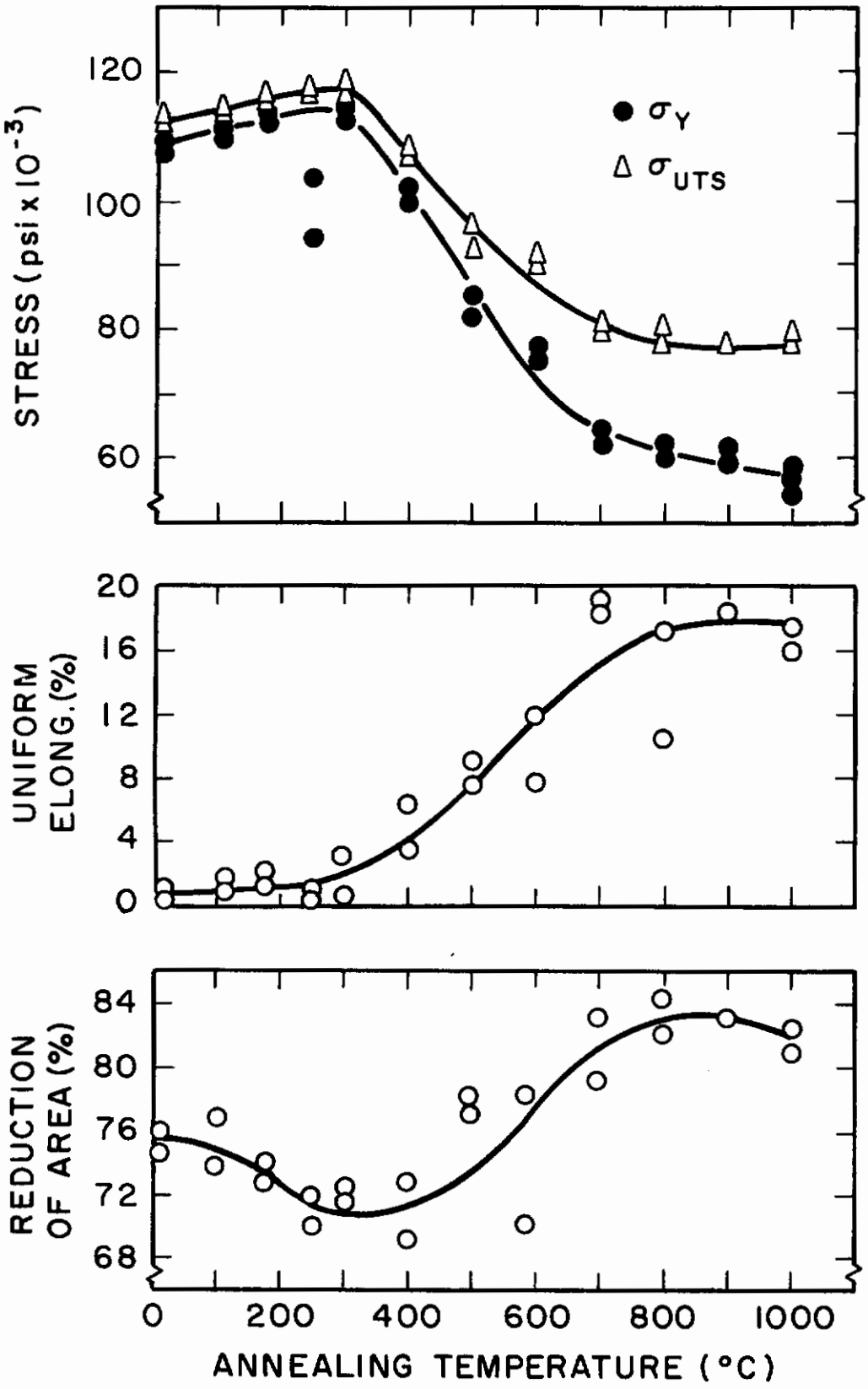

Fig. 77 - Effect of annealing on the mechanical properties of Fe-3.19 Si cold drawn 31%.

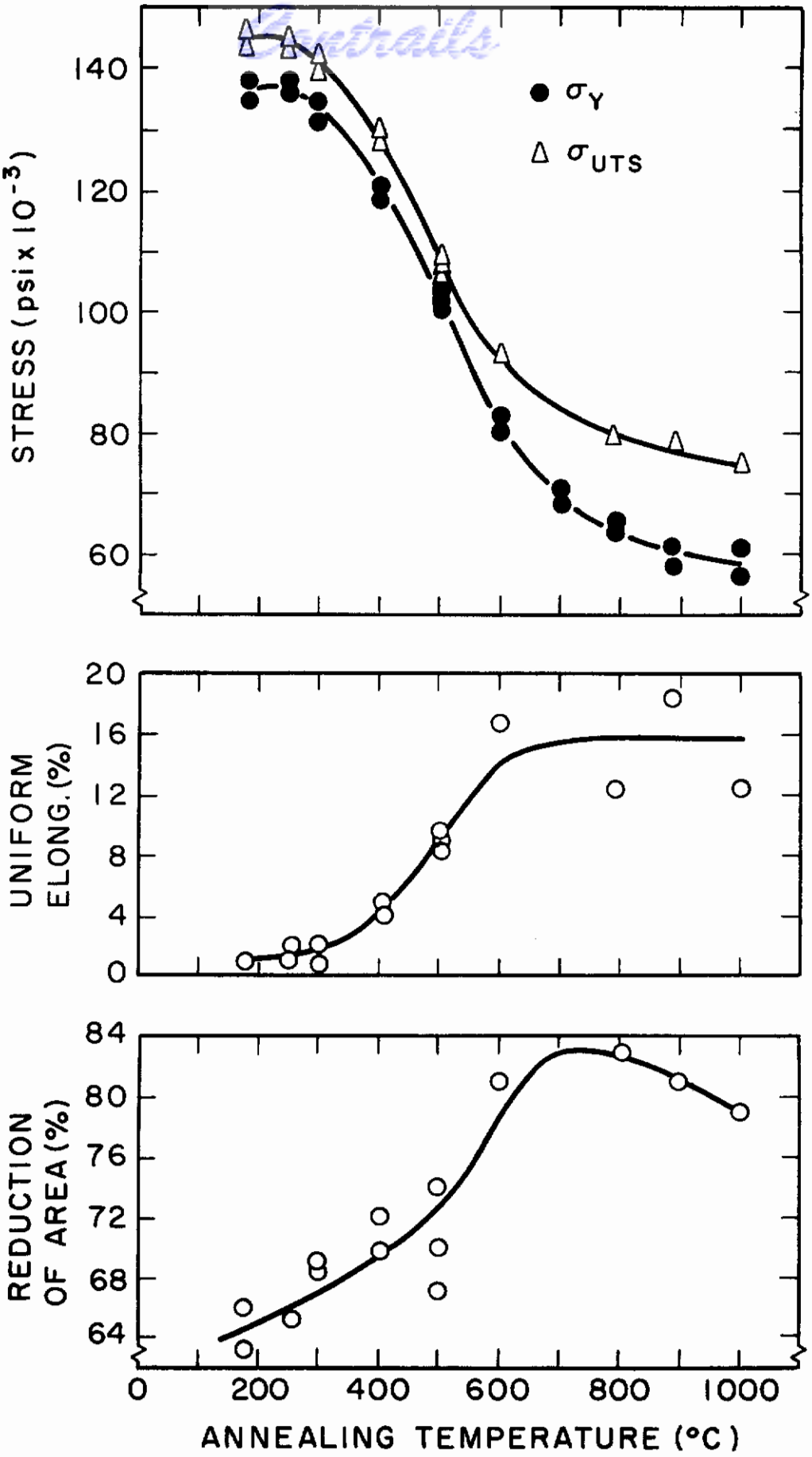

Fig. 78 - Effect of annealing on the mechanical properties of Fe-3.19 Si cold drawn 66%.

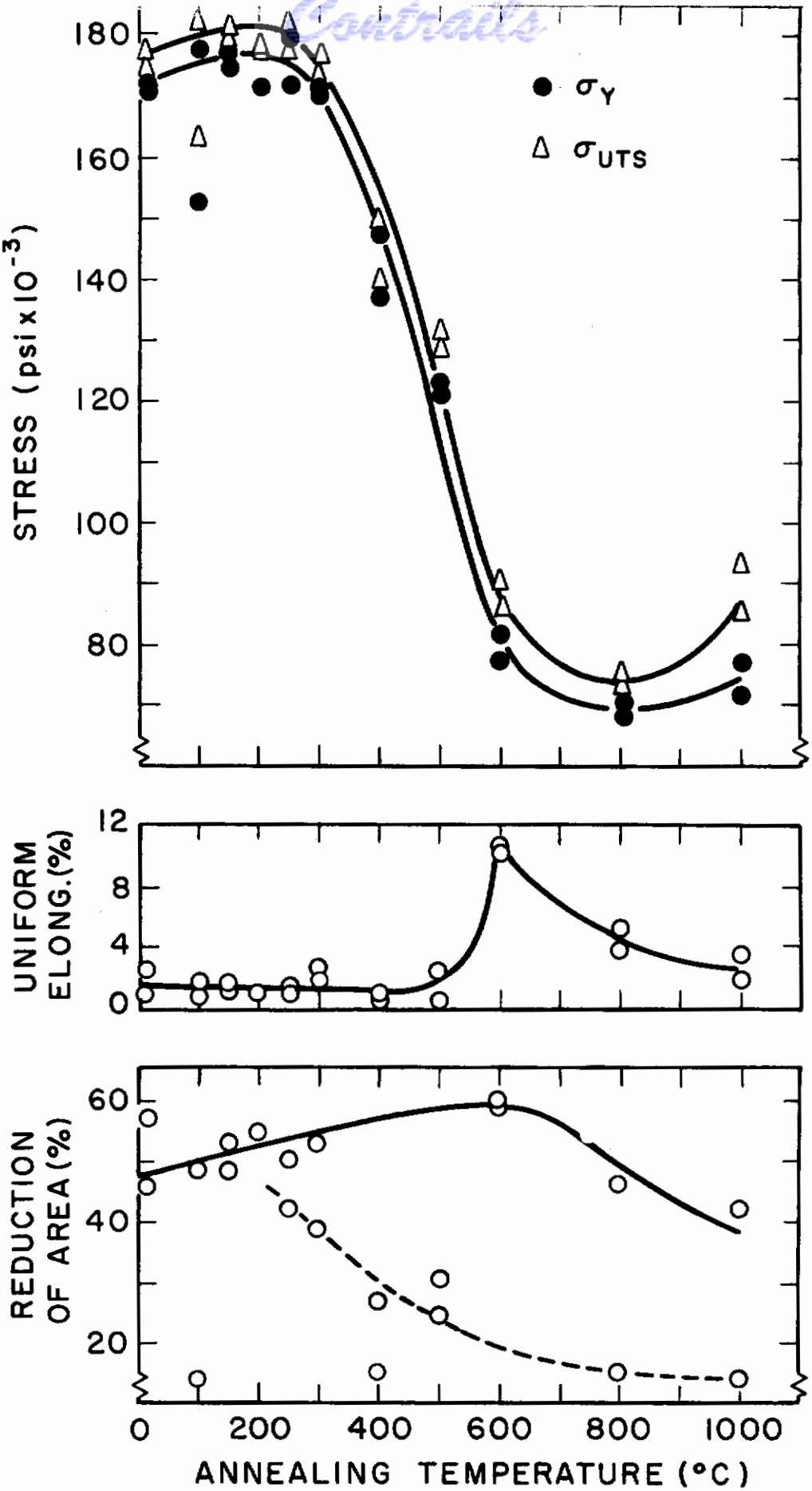

Fig. 79 - Effect of annealing on the mechanical properties of Fe-3.19 Si cold drawn 87%.

The strength in tension of all three series exhibited the same general dependence upon annealing temperature. The principal effects of increased prior deformation were an increase of the yield stress and ultimate tensile strength and a shift in the position, but not in the extent, of the temperature range over which softening occurred. Inspection of the electropolished surfaces of the tensile specimen gauge lengths revealed that the cold worked structure recrystallized to fine, equiaxed grains at 600 - 700°C. Thus, recovery of mechanical properties was essentially complete before the onset of recrystallization. The refractory metals show somewhat similar behavior (4), and examples of other metals in which substantial softening was observed prior to recrystallization have been reviewed by Perryman (13).

The slight increase of strength at low annealing temperatures is probably ascribable to strain aging, although no discontinuous yielding was evidenced by the load-elongation curves of unrecrystallized specimens. The sudden reappearance of the upper yield point coincided with the formation of the recrystallized structure.

All of the as-drawn wire showed a very small uniform elongation, although there was considerable reduction of area due to necking. Both of these parameters increased gradually to their maximum values as the corresponding tensile strengths decreased upon annealing.

Some anomalies can be noted in the data for the wire reduced 87% (Fig. 79). Several specimens showed unusually low ductilities (dashed curved of reduction of area versus annealing temperature) and in some cases this is reflected in lowered values of strength. Consequently, it was suspected that this might have resulted from internal defects introduced during the drawing operation. On the other hand, the yield stress and ultimate tensile strength of wire annealed at 1000°C were unusually high, even though this wire, too, had very limited ductility. These results are difficult to explain solely by postulating internal cracks.

The mode of fracture of the low-ductility specimens was not always the same. Below the temperature at which recrystallized grains were observed to form, the low-ductility specimens failed by shear on a plane approximately 45° from the wire axis. However, after 800 and 1000°C anneals the fracture was of the cleavage type (Fig. 80) and a moderate amount of twinning was observed throughout the 1000°C specimen. Figure 81 shows a typical twinned grain.

A detailed metallographic investigation, including dislocation etch-pit studies, is being conducted to correlate microstructures with recovery of mechanical properties in the extended temperature interval over which these property changes are observed prior to recrystallization and to determine the influence of structure on the fracture characteristics.

Fig. 80 - Room temperature cleavage fracture of Fe-3.19 Si cold worked 87%, annealed 30 minutes at 1000°C and tested in tension. 580X.

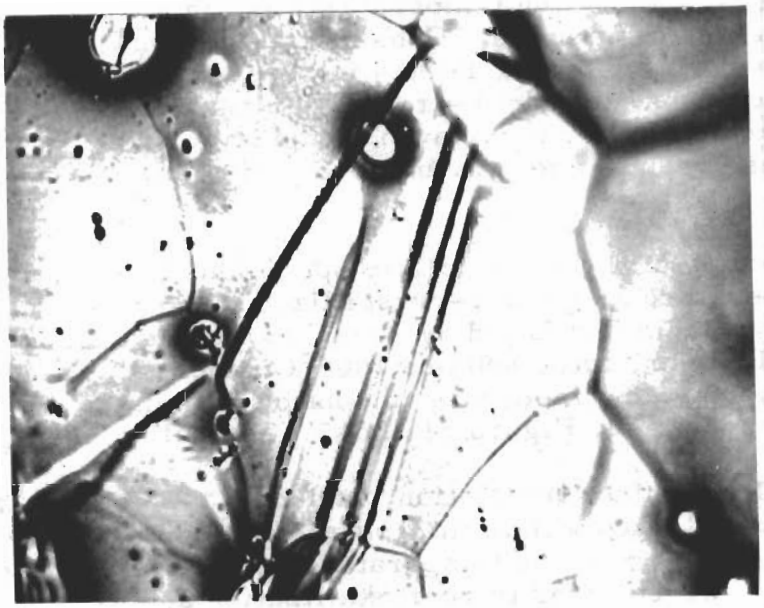

Fig. 81 - Same specimen as above. Twins formed on surface during tensile test. 1000X.

F. Texture Determination in Tungsten Sheet

1. Description of Results

The pole figure technique of Meieran (14) was used to determine the textures of 5-mil W-P5, 30-mil W-P2, and 18-mil W-P3 tungsten sheets in the as-received condition and after vacuum annealing for 30 min. at 900 and 1300°C.

The pole figure for as-received 5-mil W-P5 sheet appears in Fig. 82. It is possible to assign two ideal orientations to the pole figure, the (100) [011] and (112) [1$\bar{1}$0]. However, the sheet was cross-rolled twice and it is thus difficult to ascribe a secondary texture component to the rolling operation.

The texture of the 900°C annealed sample of the W-P5 appears in Fig. 83a, and there is only a slight sharpening as compared with the as-received pole figure. Similarly the microstructure shows little change. Upon annealing at 1300°C the texture again sharpens as seen in Fig. 83b. The microstructure shows a definite tendency toward equiaxed grains.

The pole figure of 30-mil W-P2 sheet showed essentially a (100) [011] texture with a small spread of pole density about the ideal positions. Upon annealing, the textures sharpened slightly about the ideal positions. However, the microstructure showed a change from fibered grains to equiaxed ones at about 1200°C.

The texture of the 18-mil W-P3 sheet in the as-received condition is a mixture of two ideal components, (100) [011] and (112) [1$\bar{1}$0]. The (100) [011] is dominant, but there is a considerable spread of pole density about the ideal positions. After annealing at 900°C for 30 min., two texture components remain evident, and the pole density has slightly sharpened about (100) [011]. After annealing at 1300°C the texture again sharpens about many of the ideal texture positions, and the microstructure shows equiaxed grains.

2. Discussion of Results

The effect of annealing on all pole figures is to cause a slight sharpening of pole density about ideal texture positions. Work at Rutgers has already shown in annealed W-P5 sheet that subgrains or cells of the order of one micron in size increase in perfection with annealing as low at 500°C, and at higher temperatures subgrain boundary motion occurs. It seems likely that the texture sharpening is associated with the growth of subgrains in the ideal texture orientation at the expense of others, thus producing a gradual change in texture. This view is consistent with the more recent observations on the substructural changes during annealing of tungsten wire, presented in Section C of this report.

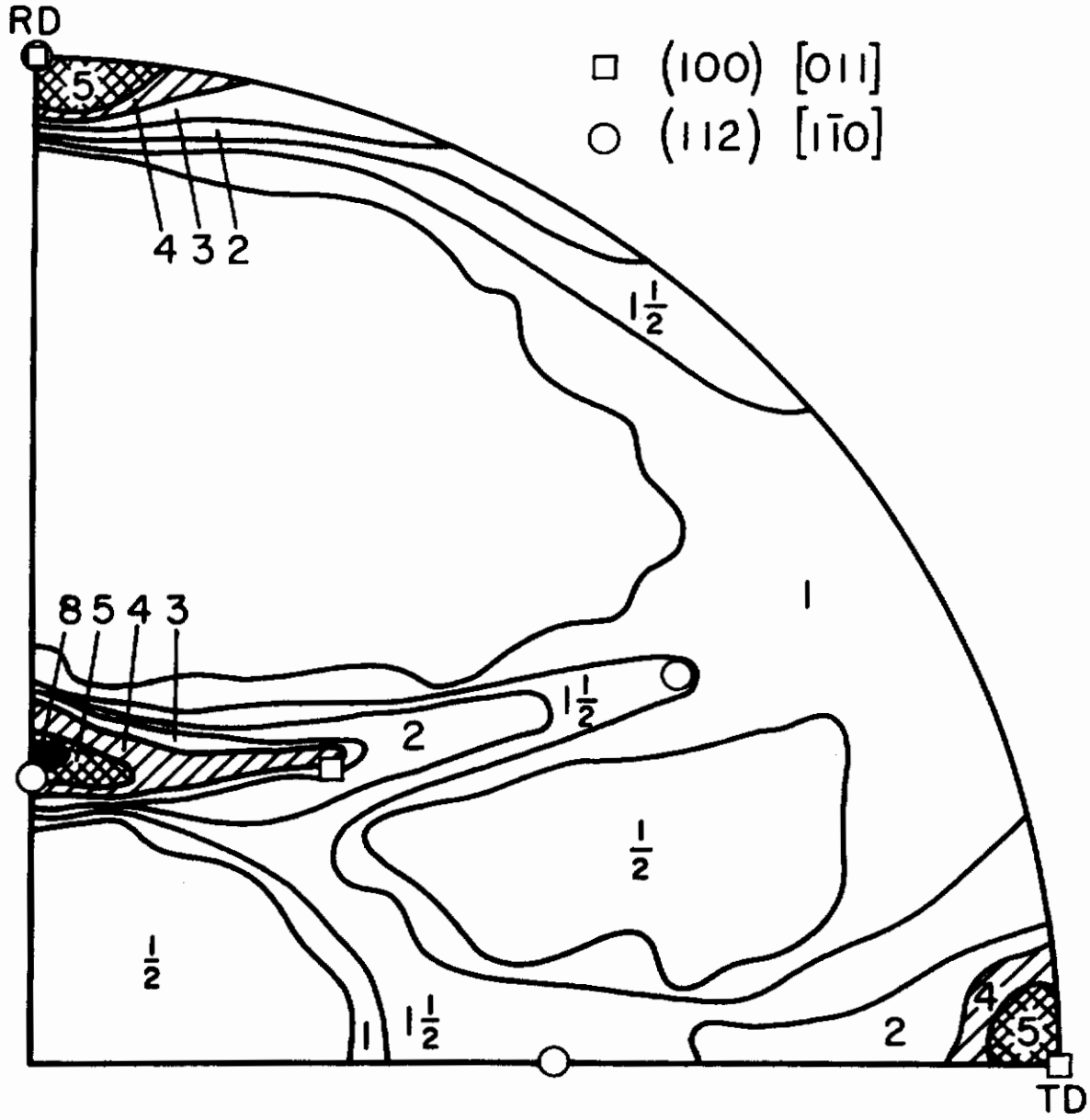

Fig. 82 - Pole figure of W-P5 sheet, as-received.

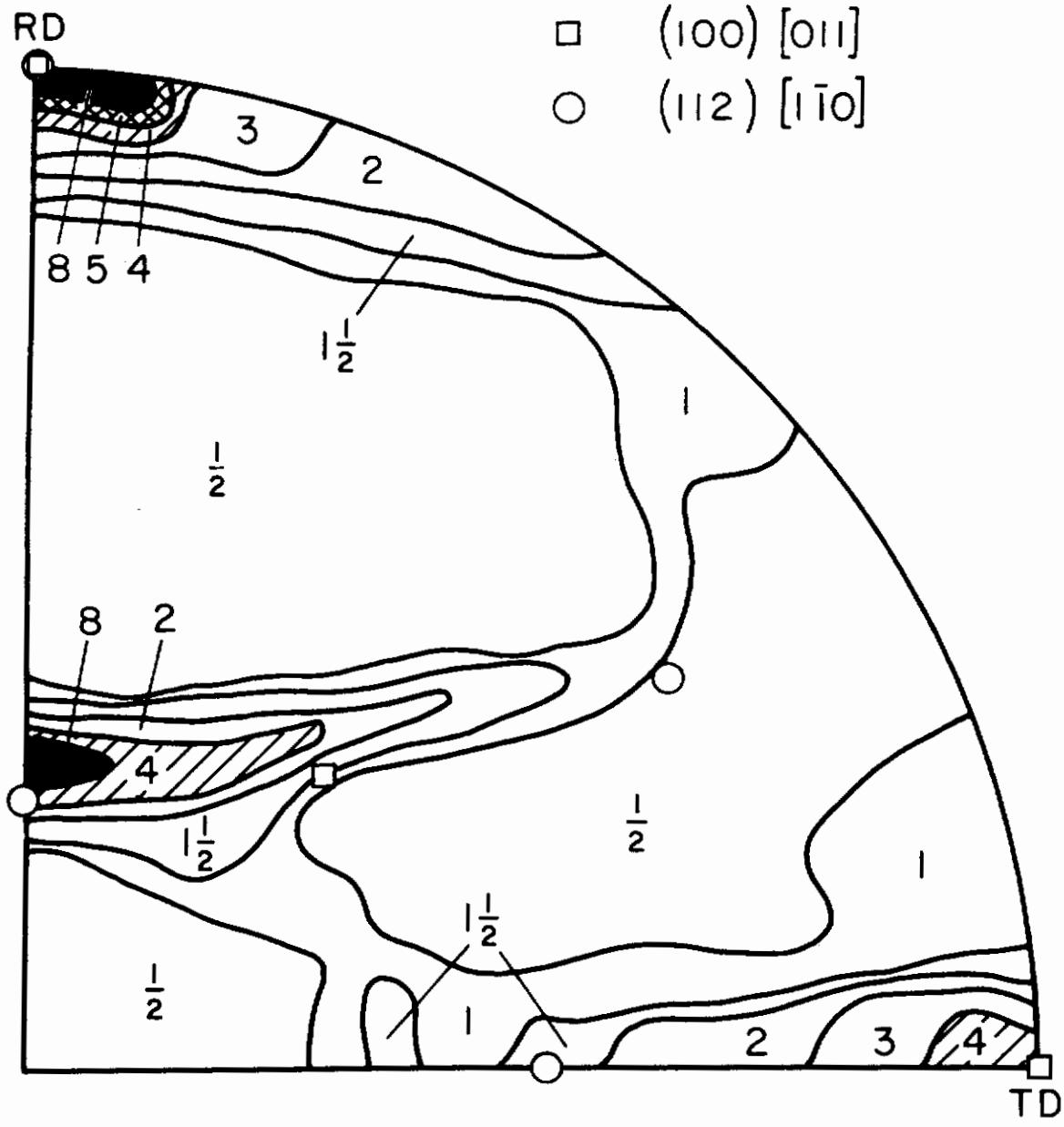

Fig. 83a - Pole figure of W-P5 sheet, annealed 30 minutes at 900°C.

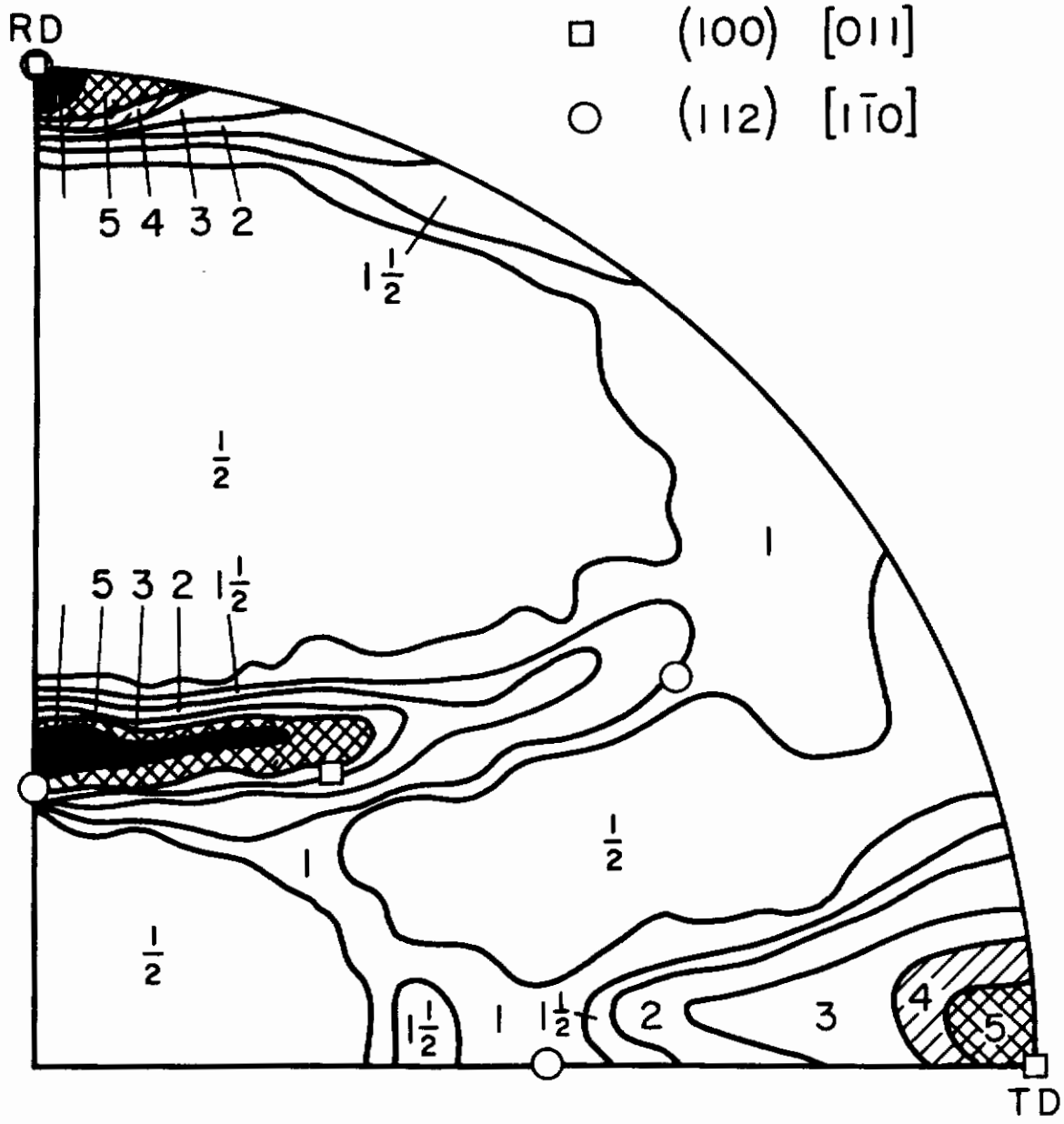

Fig. 83b - Pole figure of W-P5 sheet, annealed 30 minutes at 1300°C.

REFERENCES

(1) Pugh, J. W., "Tensile and Creep Properties of Tungsten at Elevated Temperatures," Proc. ASTM 57 (1957) 906.

(2) Pugh, J. W., "On the Recovery and Recrystallization of Tungsten," 3rd Plansee Seminar, Springer-Verlag (1959).

(3) Michalak, J. T. and Paxton, H. W., "Some Recovery Characteristics of Zone-Melted Iron," Trans. AIME 221 (1961) 860.

(4) WADD Technical Report 61-181 (August, 1961).

(5) Peck, J. F. and Thomas, D. A., "A Study of Fibrous Tungsten and Iron," Trans. AIME 221 (1961) 1240.

(6) Kelly, P. M. and Nutting, J., Proc. Roy. Soc. A259 (1960) 45.

(7) Smithells, C. J., Tungsten, Chemical Publishing Co. (1953).

(8) Jones, F. O., "The Annealing of Worked Tungsten," J. Less-Common Metals 2 (1960) 163.

(9) Koo, R. C., "Recovery in Cold-worked Tungsten," J. Less-Common Metals 3 (1961) 412.

(10) Davis, G. L., "Recrystallization of Tungsten Wires," Metallurgia 58 (1958) 177, 228.

(11) Leber, S., "Cylindrical Textures in Tungsten and Other Body-centered Cubic Metals," Trans. ASM 53 (1961) 697.

(12) Barrett, C. S., Structure of Metals, 2nd Ed., p. 489, McGraw-Hill Co. (1952).

(13) Perryman, E. C. W., in Creep and Recovery, American Society for Metals, Cleveland (1957).

(14) Meieran, E. S., "Use of the Reciprocal Lattice for the Development of a New Pole Figure Technique," Rev. Sci. Inst. 33 (1962) 319.

V. STUDY OF SUPERJOGS, DISLOCATION TANGLES AND CELL STRUCTURE OF REFRACTORY METALS - Work carried out at Rutgers, the State University by S. Weissmann and N. Hosokawa

A. INTRODUCTION

Recent studies by transmission electron microscopy have shed new light on the hardening mechanism of b.c.c. materials. They have shown that the deformation process is associated with the formation of certain structural features, namely, dislocation junctions, superjogs, dislocation loops, tangles, and cell structures[1,2]. Although the occurrence of these structural features is well accepted there is as yet no agreement among various investigators with regard to the mechanism of their formation. Nor does there exist any general agreement as to what roles they play in the work-hardening mechanism.

In order to elucidate the nature and mechanism leading to the formation of these structural features a systematic study has been undertaken on the deformation of single and polycrystalline refractory metals. This study was carried out by combining the qualitative observations of transmission electron microscopy, the semi-quantitative studies of selected area electron diffraction with the quantitative strain analysis of the divergent X-ray beam method[3]. Although the quantitative X-ray analysis is still in progress and can therefore not be reported in full, certain structural features disclosed by transmission electron microscopy as well as by the X-ray divergent beam method have emerged which are worth mentioning and which are the subject of this report.

B. EXPERIMENTAL METHODS AND RESULTS

1. Specimen Preparation

Tantalum (Ta-E1-S0.0101") foils were annealed at 1500° in vacuo to insure complete recrystallization. The temperature of annealing was determined by means of a micropyrometer. The foils were then extended in tension at room temperature to various amounts and subsequently subjected to a chemical etch consisting of a mixture of 50% concentrated HNO_3 and 50% 49.4% HF. Through the action of this etch the foil was nearly uniformly thinned. When a thickness was reached such that the foil was no longer opaque to a light source the etching was interrupted and the foil was then usually adequately prepared for the direct observation of lattice defects by transmission electron microscopy.

In order to study quantitatively the mode of deformation of single crystals, tensile or compression specimens were prepared suitable for subsequent X-ray investigation. For compression tests the zone-refined crystals of tungsten (W-E5), tantalum (Ta-E5), columbium (Cb-E5) and molybdenum (Mo-E5) were cut into small cylinders 1/2" in length and 1/4" in diameter. The gauge dimensions of the tensile specimens were 1/2" x 1/4". Prior to deformation the specimens carefully etched and electrolytically polished. The molybdenum crystal which has been used in this study has been etched with 98% H_2SO_4.

2. Dislocation Structure in Annealed Specimens

As expected the distribution and arrangement of dislocations of the specimens annealed at 1500°C were by no means uniform over the entire specimen. Some areas exhibited dislocation networks characterized by long and straight dislocations such as those shown in Figs. 84 and 85, while other areas showed ill-developed hexagons (Fig. 86). In specimens which have not fully recrystallized the substructure of the unconsumed matrix displayed dislocation networks with well-developed hexagons (Fig. 87). However, in none of the annealed specimens were entangled dislocations observed.

The hexagonal dislocation networks were analyzed by the method used for iron as described by Carrington et al.[3] The results obtained in tantalum were analogous to those obtained by the aforementioned authors, inasmuch as it could be shown that the $\frac{a}{2}[111]$ dislocations interact to yield an a <100> dislocation at the junction, according to the reaction

$$\frac{a}{2}[111] + \frac{a}{2}[1\bar{1}\bar{1}] \rightarrow a[100]$$

3. Effect of Deformation on Microstructures

After 1.1% deformation the dislocation density was considerably increased. Although many dislocations were still straight and uniformly distributed as shown in Figs. 88 and 89, many superjogs and loops associated with screw dislocations could be seen throughout the field. The formation of superjogs and loops became more pronounced after 2% deformation and regions of the specimen such as those shown in Fig. 90 may be visualized as the initial stages of dislocation entanglement.

Fig. 91 shows an electron micrograph after 3% extension. The dislocation density and the density of loops continued to increase with deformation and the formation of cell structure resulting from dislocation entanglement is well advanced.

It should be understood, however, that the distribution of dislocations after deformation was by no means uniform over the entire specimen. Thus one could find in the specimens extended 1.1% regions with relatively high dislocation density resembling those extended to 3% elongation. Conversely, the latter specimens exhibited occasionally regions with low dislocation density resembling those of the 1.1% extended specimens. The examples cited in Figs. 84 to 91 should be taken, therefore, as illustrations which show the typical trend of development and indicate the increased complexity in the configuration of dislocations as a function of deformation.

It is believed that the formation of superjogs and entangled dislocations is intimately linked with the cross-slip mechanism. Indirect evidence to this effect can be obtained if one observes in the microscope the path of the screw dislocations set in motion by the thermal stress created by the electron beam itself.

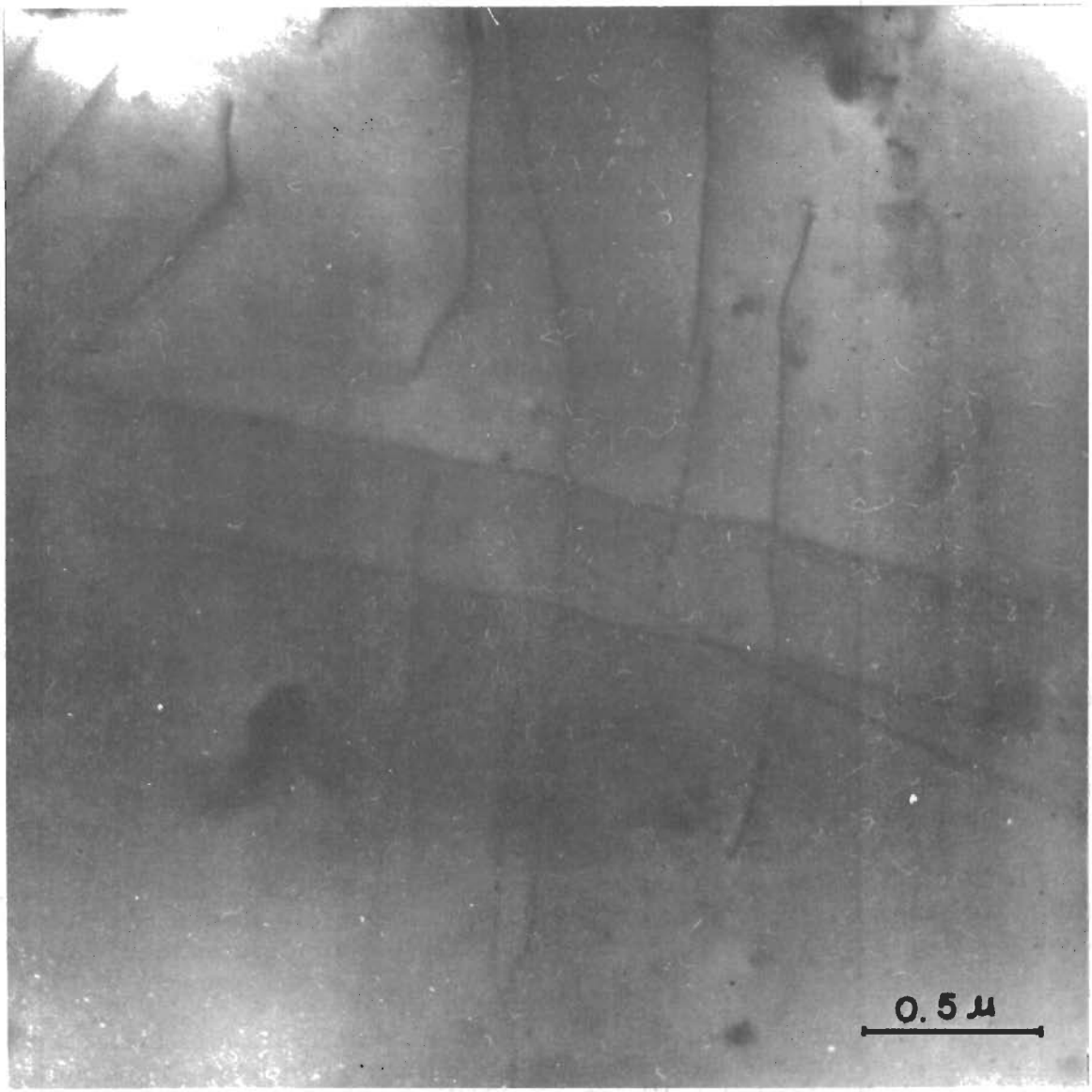

Fig. 84 - Ta-El annealed at 1500°C in vacuo. Note the straight and long dislocation lines.

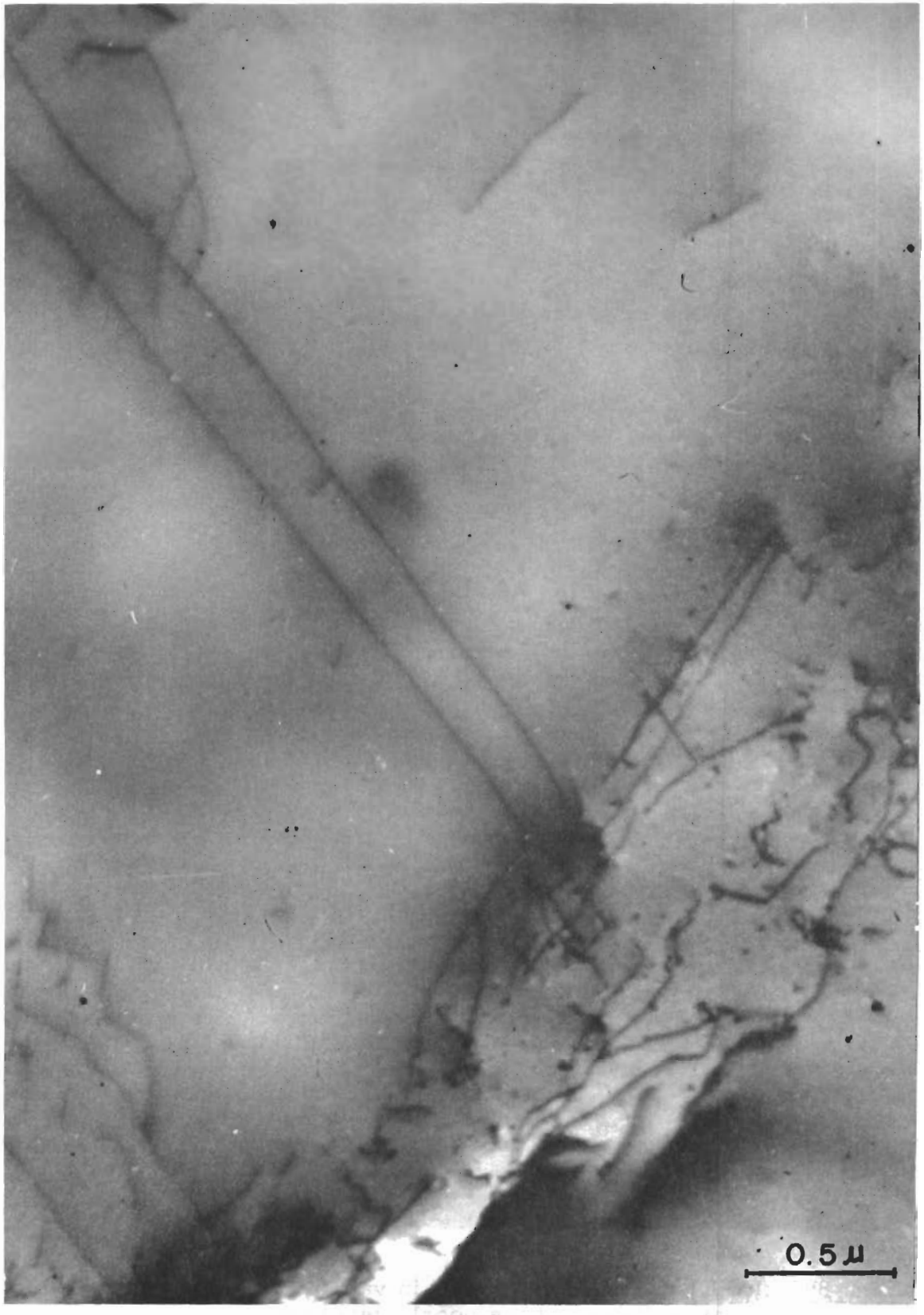

Fig. 85 - Ta-El annealed at 1500°C in vacuo. Note the straight dislocation lines and poorly developed hexagons.

Fig. 86 - Ta-E1 annealed at 1500°C in vacuo. Note the straight dislocation lines and the poorly developed hexagons.

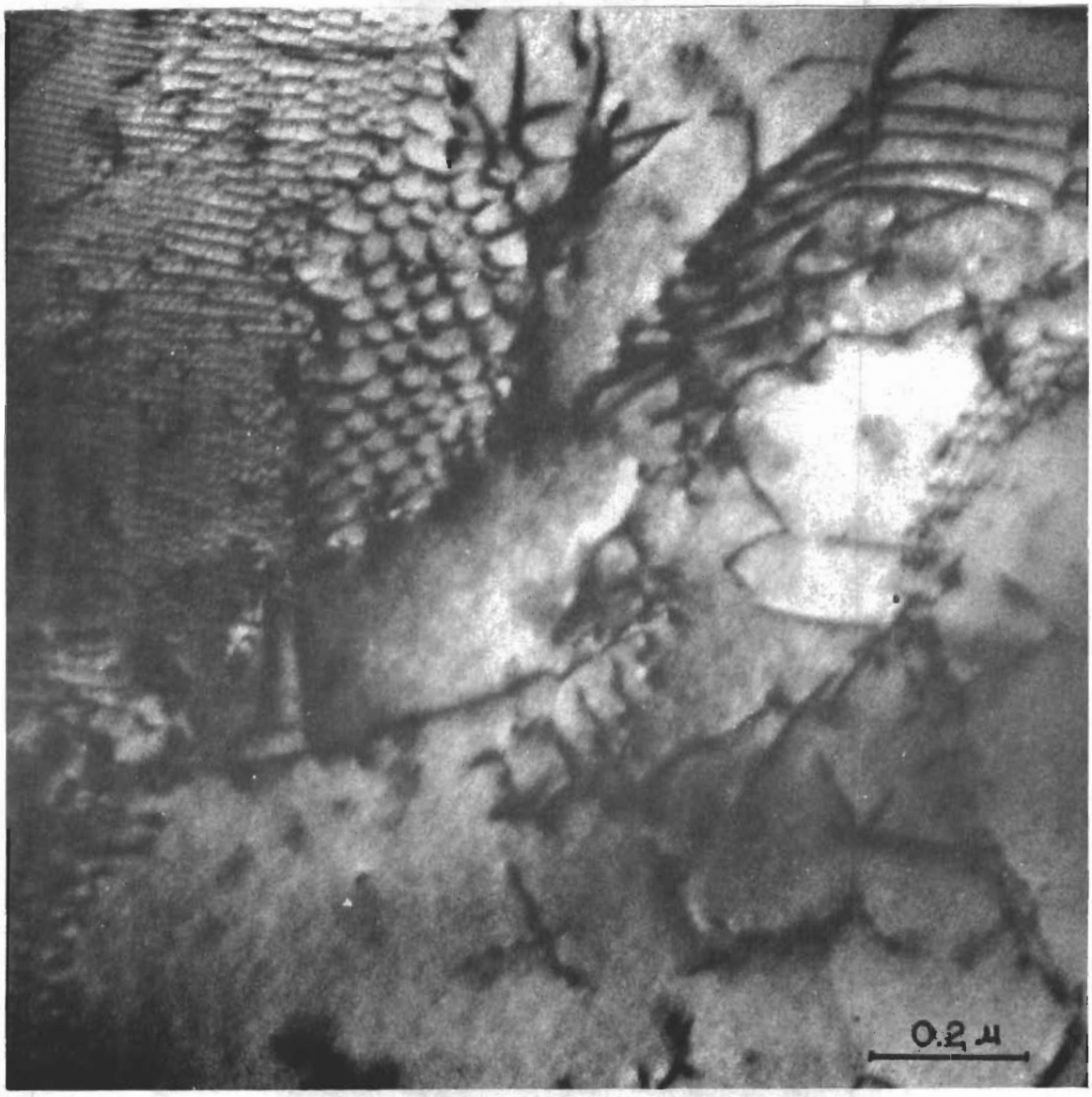

Fig. 87 - **Ta-E1 annealed at 1000°C in vacuo for 20 minutes. Note the well-developed hexagonal dislocation network.**

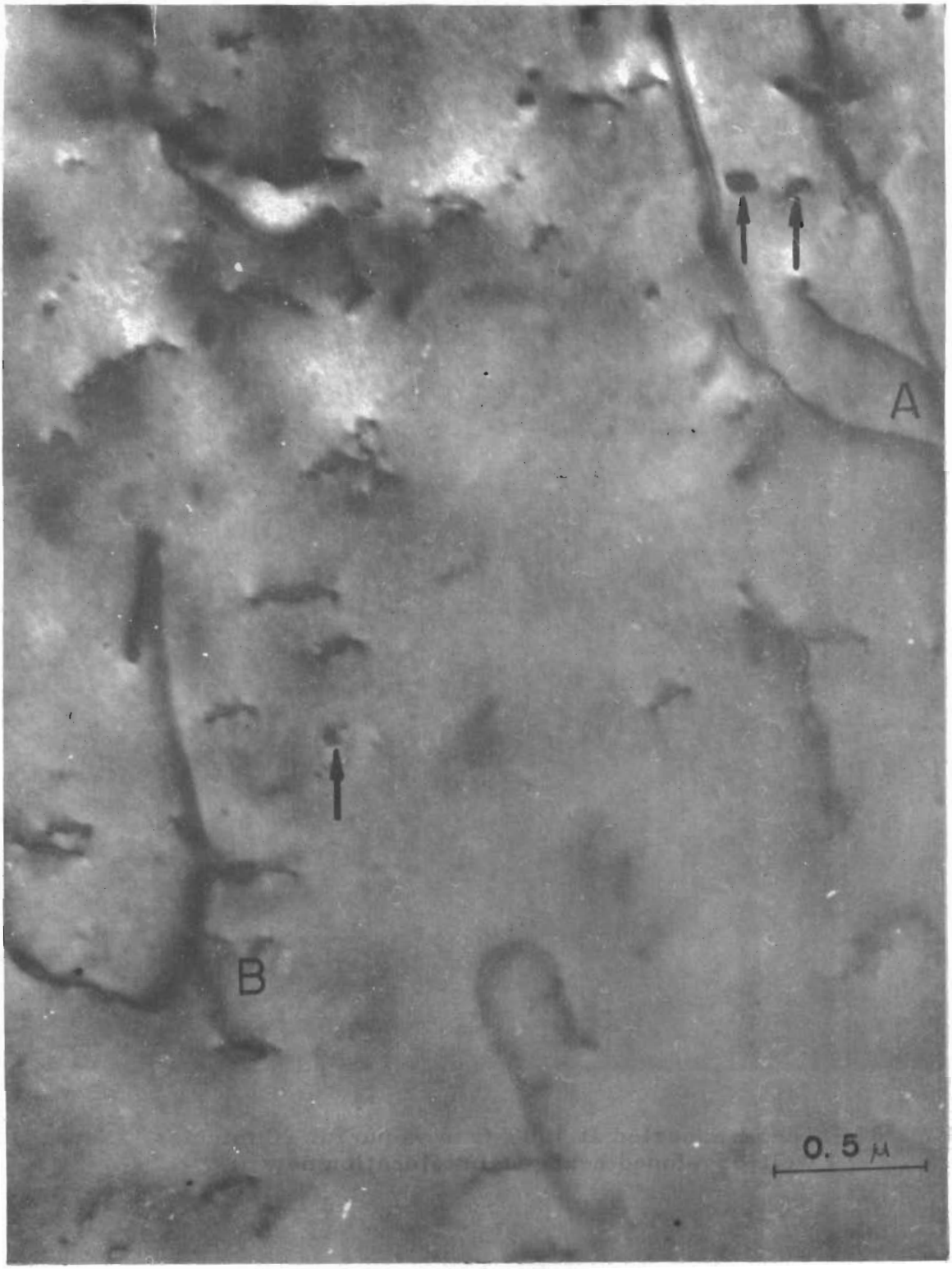

Fig. 88 - Ta-E1 annealed at 1500°C in vacuo and extended 1.1% at room temperature. Arrows point to closed dislocation loops left behind the trails of dislocation dipoles.

Fig. 89 - Ta-E1 annealed at 1500°C in vacuo and extended 1.1% at room temperature. Arrows point to cusps and closed dislocation loops resulting from cross-slip of screw dislocations.

Fig. 90 - Ta-E1 annealed at 1500°C in vacuo and extended 2% at room temperature. Arrows point to cusps and closed loops resulting from cross-slip.

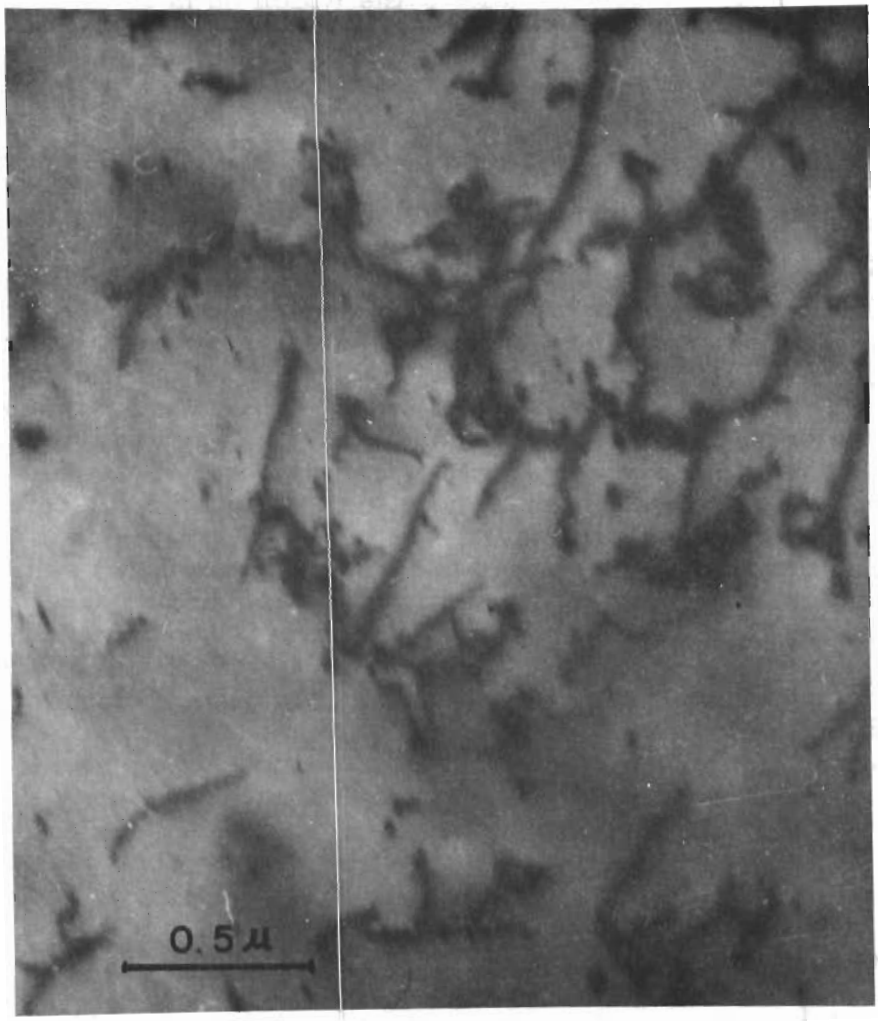

Fig. 91 - Ta-E1 annealed at 1500°C in vacuo and extended 3% at room temperature. Formation of initial stage of cell structure through dislocation entanglements.

Fig.92 shows characteristic zigzag trails left behind the moving screw dislocations on the top and bottom surfaces of the foil. The zigzag trails suggest that screw dislocations cross-slip very frequently; and, in effect, under the influence of local stress fields, may take paths which do not correspond to obvious crystallographic directions. This observation is analogous to those made by other investigators for iron[1].

C. DISCUSSION

1. Formation of Superjogs

The formation of superjogs on screw dislocations as well as the formation of isolated loops during deformation are phenomena observed in many b.c.c. materials. The first observation of such configurations was made by Dash using an etching technique[4]. He found in silicon trails left behind moving screw dislocations. Johnston and Gilmna made similar observations in LiF and they explained these results by a cross-slip mechanism[5]. They asserted that double cross-slip leaves jogs on moving screw dislocations, and these jogs tend to retard the motion of the screws, which leave either trails of point defects or dipoles of plus-minus edge dislocations behind them. Those portions of the screw dislocations which underwent cross-slip can act as Frank-Read sources on the new slip plane and cause profuse multiplication. Washburn et al.[6], studying MgO by transmission electron microscopy, confirmed the existence of plus-minus pairs as suggested by Johnston and Gilman[4]. Fourie and Wilsdorf[7] observed the same type of structure in deformed aluminum single crystals. However, based on an earlier suggestion by Kuhlman-Wilsdorf et al.[8], they considered the formation of superjogs and dislocation loops as being due to the condensation of point defects on gliding screw dislocations and not due to a cross-slip mechanism. The main objection against the cross-slip mechanism which these authors raised[7][9] is the absence of visible barriers or obstacles for the screw dislocations to cross-slip. This objection can be eliminated, if one considers the possibility that cross-slip of one screw dislocation is induced by another locked, parallel screw dislocation. This model was first suggested by Mott[10] and recently analyzed in detail by Li[11]. It appears to offer a plausible mechanism for cross-slip. An illustration for such induced cross-slip may be found near the letters A and B of Fig. 88, where the path of one screw dislocation (established by means of selected area diffraction) is made to deviate by the proximity of another screw dislocation.

Li has shown that if a screw dislocation moving under an applied stress is made to cross-slip by a parallel, locked screw dislocation, the step of cross-slip varies from zero to an upper limit depending on the distance between the two screw dislocations concerned[11]. Let both of the screw dislocations be of the same sign and parallel to the z-axis and let the screw dislocation move originally in a plane parallel to the xz plane, the applied shear stress having only the component σ_{yz}. It can be shown then that the upper limit is $Gb \sin\phi / 2\pi(\sigma^{o}_{\phi} - \sigma_{yz} \cos\phi)$, where G

Fig. 92 - Evidence of cross-slip shown by the zigzag trail of screw dislocation.

is the shear modulus, ϕ is the angle which the second slip plane subtends with the original slip plane and σ_{ϕ}^{o} represents the frictional stress in the cross-slip plane which has to be overcome by the moving dislocation. When the distance between the locked dislocation and the original slip plane of the moving dislocation reaches the value

$$Gb\,(1 + \sin\phi) \;/\; 4\pi(\sigma_{\phi}^{o} + \sigma_{yz}\cos\phi)$$

the step of the cross-slip becomes zero.

One may, therefore, visualize the formation of superjogs and dipole drag, which are associated with the initial stages of dislocation entanglement, by types of mechanism such as those illustrated in Figs. 93 and 94.

Fig. 93a depicts a moving screw dislocation which has acquired jogs as a result of cross-slip. The latter may have occurred either because of obstacles or may have been induced by a locked parallel screw dislocation. The external stress exerted on the screw is here shown to be perpendicular to the screw dislocation, and, therefore, also perpendicular to the Burgers vector b. Under the influence of this stress, segments of the screw dislocation are made to bow out in Fig. 93b, whereby the jogs function as anchoring points. The portions of the screw component near the jogs assume gradually edge character, since they get directed perpendicular to the Burgers vector. The edge components on adjacent slip planes are of opposite sign, forming thus dislocation dipoles and exerting a drag on the moving dislocation. Because of the tension of the dislocation line superjogs may be formed (Fig. 93c) which prevent the edge dislocations of opposite sign from being annihilated should they find themselves in too close a proximity to each other.

In Fig. 94, Washburn et al.[6] have shown a scheme by which trails of dislocation dipoles can be transformed into closed loops or even pinched off into smaller loops. This may presumably occur in the absence of climb via the agency of cross-slip or through the interaction with other dislocations, causing additional jogs and leading finally to closures of the loops. Such closed loops can be seen in Figs. 88 and 89.

2. Formation of Dislocation Tangles and Cell Structure

The formation of dislocation tangles which, as we have seen, is associated with the initial stages of cell structure is undoubtedly intimately connected with the work-hardening mechanism.

The formation of dislocation tangles can be visualized as resulting from the interactions of superjogs created by cross-slip with dislocations of a secondary slip system. It was observed, for instance, that in the deformation of silicon iron single crystals oriented for single slip the formation of cell structure did not

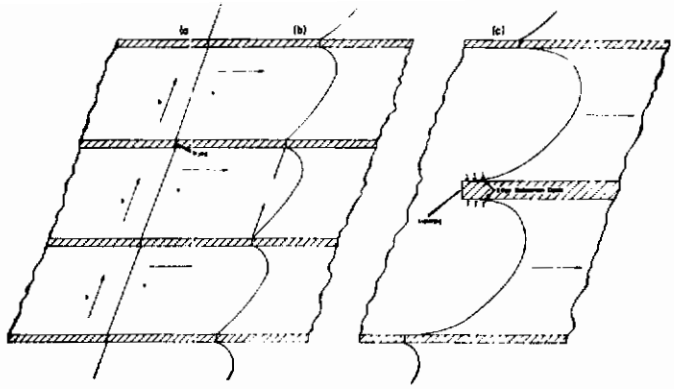

Fig. 93 - Schematic formation of dislocation dipole drag: (a) moving screw dislocation with jog, (b) bowing out of dislocation segments and formation of superjogs due to line tension, and (c) formation of edge dislocation dipoles.

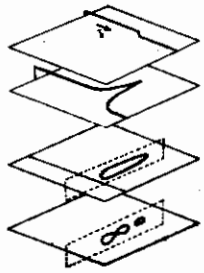

Fig. 94 - Schematic formation of dislocation loops from a moving screw dislocation containing a long jog, ref. (6).

occur and the resulting structure had little effect on the hardening mechanism[2]. This observation suggests that the formation of superjogs alone without the presence of a secondary slip system will not lead to tangle formation.

In a most recent investigation of aluminum Weissmann et al.[12] have shown that the initial stages of cell structure are associated with the formation of a dislocation grid constituted of screw dislocations which derive from different (111) slip planes.

In order to obtain quantitative information concerning the interaction between the dislocation on primary and secondary slip systems strain analyses of Ta single crystals have been carried out. The ultimate aim of these studies lies, therefore, in the quantitative elucidation of the mechanism responsible for the formation of dislocation tangles and cell structure and their interrelationship to the hardening mechanism. Beyond that it is hoped that a better understanding of the fracture mechanism of the b.c.c. materials can be obtained.

D. STRAIN ANALYSIS OF DEFORMED Ta SINGLE CRYSTALS BY THE X-RAY BACK-REFLECTION DIVERGENT BEAM METHOD

1. Description of the Back-Reflection Divergent Beam Method and Strain Analysis

The divergent beam method is essentially a precision method for the determination of lattice parameters and anisotropic lattice distortions of single crystals. Although details of this method have been given elsewhere[13] a brief description pertinent to the latest development of apparatus and method will be offered here.

The divergent beam method utilizes a horizontal capillary X-ray tube in which an electron beam originating from an electron gun is focussed by means of electromagnetic lenses onto the tip of a long capillary tube. This tip, representing the X-ray target, consists of a thin metal foil. By operating the tube at a suitable voltage an X-ray beam with characteristic radiation emerges from the tip of the X-ray tube, exhibiting a divergence of nearly 180°. When this beam impinges on the test crystal, which is placed at a distance of 0-5 mm from the tip of the capillary tube, diffraction patterns of the characteristic spectrum in transmission as well as in the back-reflection are obtained as schematically shown in Fig. 95. These patterns are analogous to the well-known Kossel patterns except that in this case they are produced by an X-ray source located outside instead of inside the crystal. We hav e termed these patterns pseudo-Kossel patterns.

Of particular interest to the study of metal crystals are the back-reflection patterns (Figs. 96,97,98), since these usually offer a sufficiently large number of (hkl) reflections from which the data can be extracted. Referring to Fig. 95, it will be noted that each ellipse of the pseudo-Kossel pattern corresponds to a reflection of a definite (hkl) set of planes. Consequently by indexing the reflections and by

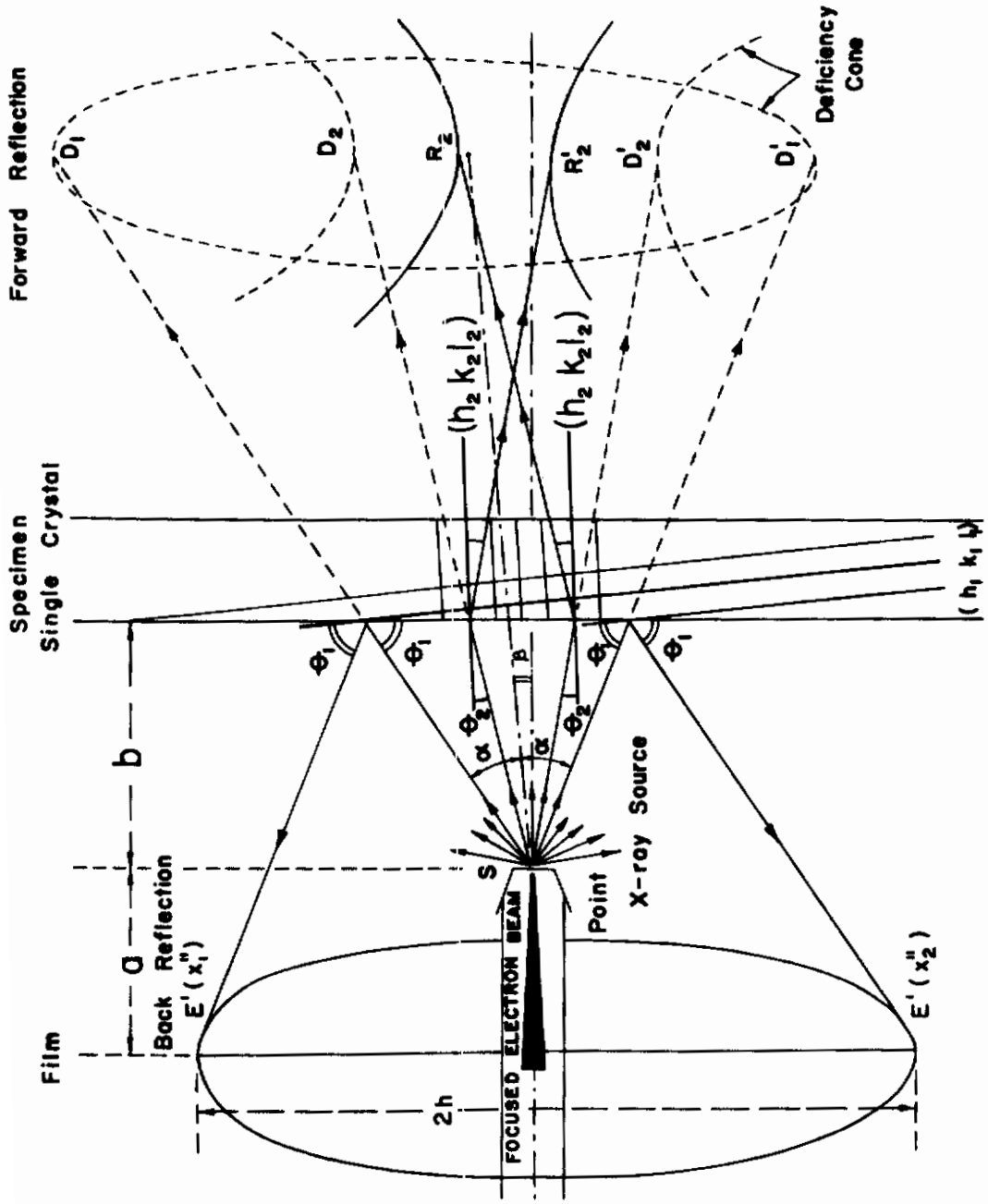

Fig.95– Schematic representation of the generation of pseudo-Kossel patterns by the X-ray divergent beam method

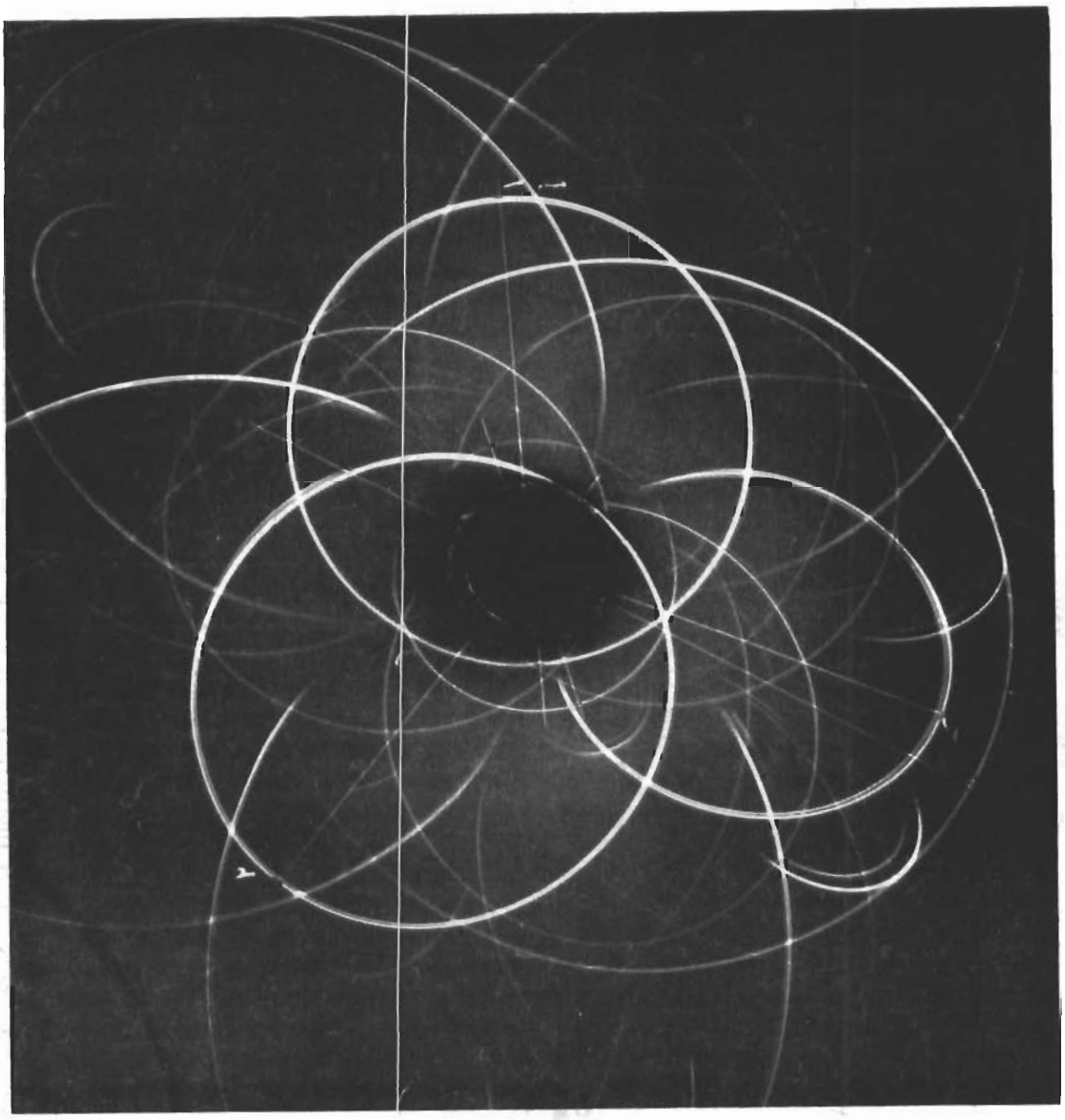

Fig. 96 - X-ray back reflection divergent beam pattern of Ta-E5 crystal compressed 1.44% at room temperature.

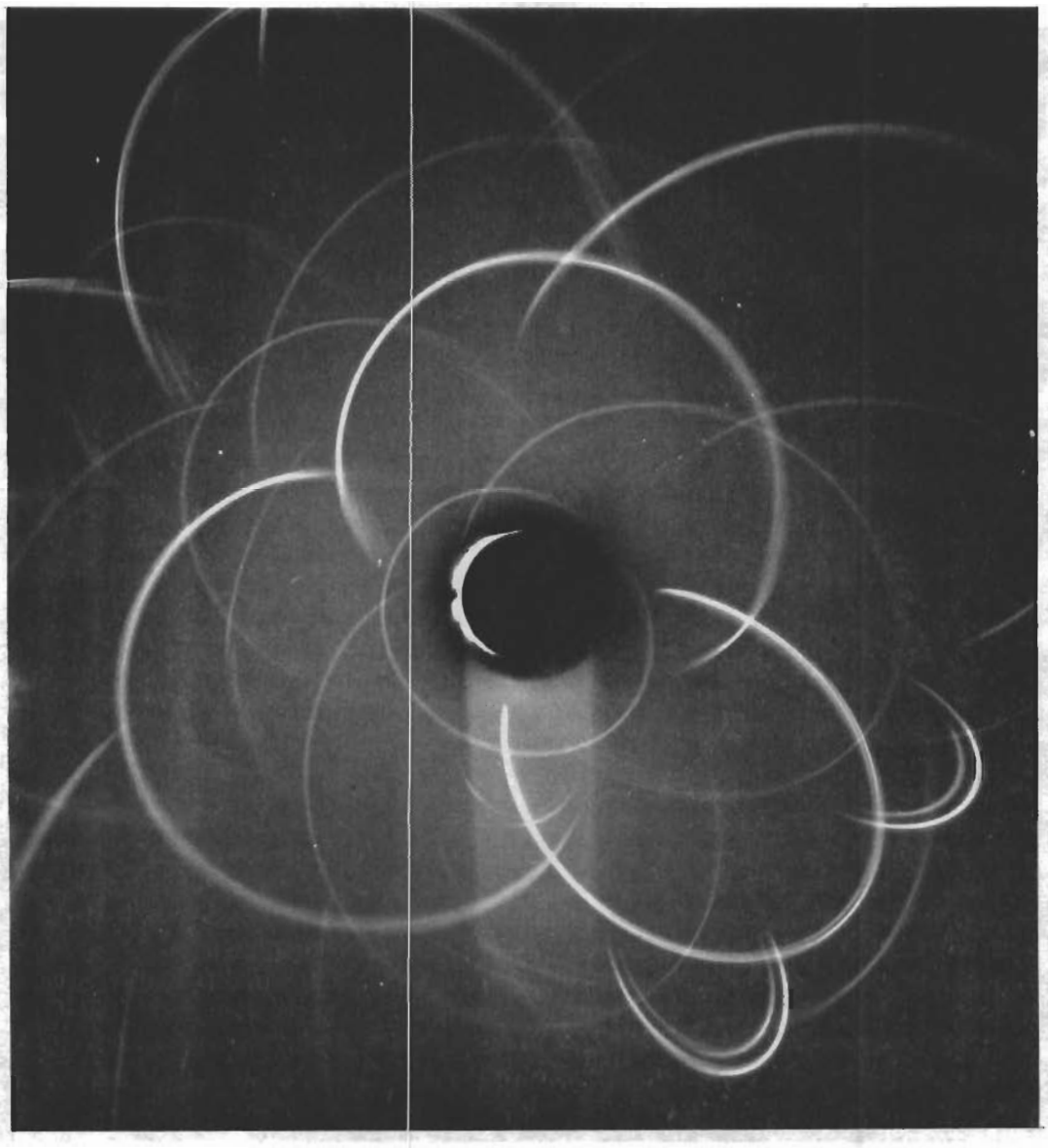

Fig. 97 - X-ray back reflection divergent beam pattern of Ta-E5 crystal compressed 10.25% at room temperature.

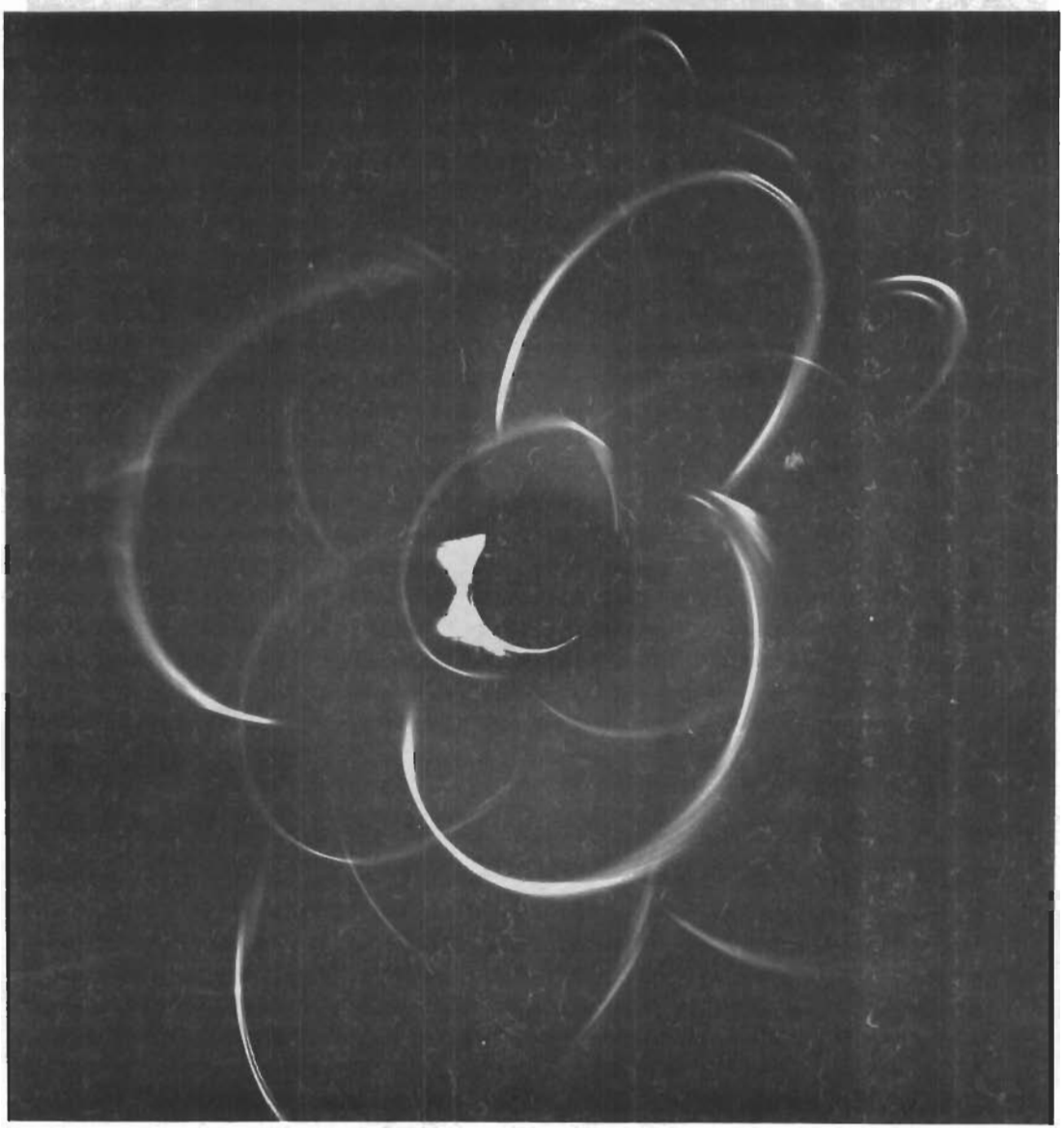

Fig. 98 - X-ray back reflection divergent beam pattern of Ta-E5 crystal compressed 19.04% at room temperature.

measuring the axes of the ellipses the lattice spacings of the individual (hkl) reflections and the lattice parameters can be determined with great precision. These measurements are carried out with the aid of the following relations[13]:

$$F'(x_1'') = \alpha \tan(\alpha - \beta) + \frac{2hb}{a + 2b}$$

$$E'(x_2'') = -\alpha \tan(\alpha + \beta) - \frac{2hb}{a + 2b} \qquad (1)$$

$$\lambda = 2 d \sin\theta$$

where the symbols have the following meanings:

$2h = \overline{E'F'}$ is the long axis of the elliptical pattern,
α is the semi-apex angle of the incident X-ray cone equal to $\pi/2 - \theta$, θ being the Bragg angle,
β is the angle subtended by the normal of the reflecting (hkl) plane and the axis of the capillary X-ray tube (perpendicular to the specimen surface),
a is the film distance from the X-ray source,
b is the specimen distance to the X-ray source,
d is the lattice spacing, and
λ the wavelength of the characteristic radiation concerned.

Since by this method the individual (hkl) reflections can be measured simultaneously, the anisotropic modifications in structure caused by an anisotropic strain distribution can be conveniently studied. Such anisotropic strain distribution is introduced into the crystal by a deformation process and it is expected that progressive deformation will alter progressively the distribution. Imura, Weissmann and Slade[3] have shown that a complete strain analysis can be obtained provided the d-spacings of more than six independent (hkl) reflections are recorded and the corresponding changes in d-spacings, Δd, resulting from strain are determined. The $\frac{\Delta d}{d}$ are used as the raw data for the strain analysis, where d_o represents the corresponding d-spacing of the undeformed crystal. The analysis is carried out by means of a least squares algorithm suitable for use with a digital computer[3]. The strain analysis yields the principal strains, that is, maximum strain E_1, intermediate strain E_2 and minimum strain E_3, as well as the (hkl) planes to which these strains are perpendicular.

2. Strain Analysis

2.1 Precision of Measurements

Single crystal specimens of cylindrical shape having a diameter of 3 mm and a height of 10 mm were prepared from a tantalum single crystal (Ta-E5)

with (210) orientation. The specimens were deformed in compression in the Instron tensile machine and a plot of the critical resolved shear stress vs. strain is shown in Fig. 99. The divergent beam pattern of Fig. 96 corresponds to the deformation stage marked by the letter A in Fig. 99, while Figs. 97 and 98 correspond to the stages D and E respectively. The X-ray patterns corresponding to the latter stages of deformation are not suitable for the strain analysis, since the deformation process has progressed too far. Hence in these patterns the lines are broken up and broadened to such an extent that precision measurements of d-spacings are rendered impossible. However, up to point C on the stress-strain curve (Fig. 99) the patterns are still very sharp and unbroken and, consequently, can be utilized for the strain analysis.

It will be seen from Equation 1 that the precise determination of d-spacings is greatly dependent on the accurate determination of the parameters a and b, that is, on the accurate determination of the specimen-to-film distance. To achieve this end a thin, neutron-irradiated quartz crystal was placed in front of the Ta test specimen for the purpose of internal calibration. Thus, both patterns, that of the quartz and that of the Ta crystal, were simultaneously recorded on the film. The a_o lattice parameter of the quartz crystal was used for the precise determination of the specimen-to-film distance. The reason why a neutron-irradiated quartz crystal was used rather than an unirradiated one lies in the fact that the quartz crystal had to have a thickness of about 5μ in order to permit the registration of the Ta line on the film. Experience has shown that unirradiated quartz crystals cannot be thinned down evenly to the required thickness, whereas neutron-irradiated crystals exhibiting different etching characteristics could be thinned down with concentrated HF to a thickness of 5μ and less.

To obtain a representative sampling of the strain distribution in the crystals it was imperative to obtain $\frac{\Delta d}{d}$ values from various directions. The cylindrical specimens were therfore carefully cut to yield triangular prisms which permitted X-irradiation of the specimens on three different faces. In the most recent development the cutting operation is carried out with the aid of the Servomet spark-erosion machine. The Servomet produces a rapid series of spark discharges of controlled energy between the tool and the specimen. The sparks erode the specimen at a rate dependent on the energy and frequency of the discharges without introducing any measurable distortions into the lattice.

2.2 Results of the Strain Analysis

Table 29 lists the $\frac{\Delta d}{d}$ values and corresponding (hkl) values obtained for the deformation stages A ($\epsilon = 0.077\%$), B ($\epsilon = 0.097\%$) and C ($\epsilon = 1.44\%$) shown in Fig. 99. The results of the strain analysis are given in Table 30 in which the principal strains E_1, and E_2 and E_3 and the corresponding (hkl) planes are listed to which these strains are perpendicular.

The initial orientation of the cylindrical specimens was close to [210] and, therefore, the compression axis was nearly parallel to [210]. It is

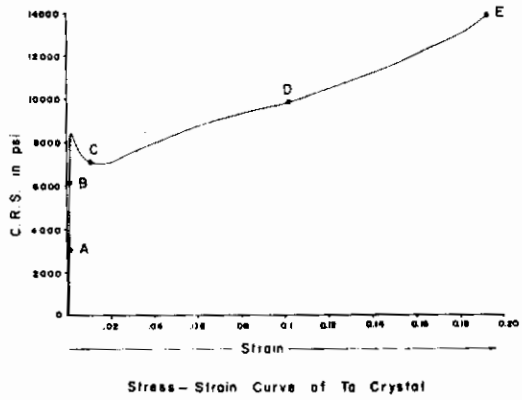

Stress – Strain Curve of Ta Crystal

Fig. 99 - Stress-strain curve of Ta-E5 crystal.

Table 29

Dependence of Strain on Compression

hkl	A* Δd/d%	B* Δd/d%	C* Δd/d%
123	0.00	-0.08	-0.13
$\bar{1}23$	+0.14	-0.07	-0.49
013	+0.08	-0.05	+0.09
024	-0.07	-0.03	-0.14
$3\bar{2}1$	+0.04	-0.08	-0.07
$2\bar{3}1$	+0.23	+0.06	+0.12
$3\bar{1}2$	+0.37	--	--
310	-0.13	+0.18	--
$\bar{3}01$	+0.05	+0.39	---
$4\bar{1}1$	+0.20	--	--
400	+0.08	+0.46	--
$13\bar{2}$	+0.18	-0.24	--
$14\bar{1}$	+0.01	--	--
$03\bar{1}$	+0.61	--	--
$23\bar{1}$	+0.38	--	--
022	--	-0.04	+0.30
$\bar{2}\bar{2}2$	--	-0.03	-0.04
$\bar{3}\bar{2}1$	--	+0.41	+0.07
$\bar{2}31$	--	-0.40	--
$\bar{3}\bar{1}2$	--	+0.02	--
301	--	+0.37	--
$\bar{3}10$	--	+0.41	--
$2\bar{2}2$	--	+0.15	-0.05

*A, B, C refer to compression stages shown in Fig. 99. A corresponds to E = 0.077%; B corresponds to E = 0.097%; C corresponds to E = 1.44%.

Table 30

Effect of Compression on the Principal Strains in Zone-Refined Tantalum Crystals (Ta-E5)

Position on σ - E Curve (Fig.)	% Compression	E_1 (max.) %	(hkl)	E_2 (interm.) %	(hkl)	E_3 (min.) %	(hkl)
A	0.077	0.411	$4\bar{3}\bar{3}$	0.183	$1\bar{2}4$	-0.113	001
B	0.097	0.412	100	-0.371	010	-0.018	001
C	1.44	-0.599	$43\bar{1}$	0.271	$\bar{1}21$	0.175	$1\bar{1}4$

interesting to note that for the deformation stages below the upper yield point, that is, for stages A and B, commonly referred to as the microstrain region, the maximum principal strain E_1 exhibits a positive value. The positive strain value is indicative of lattice expansion. The direction of the principal strain is parallel to $[4\bar{3}\bar{3}]$, that is, nearly parallel to $[1\bar{1}1]$ for compression stage A and shifts to [100] for compression stage B.

The minimum principal strain E_3, on the other hand, exhibits a negative strain value (lattice contraction) and a direction that remains parallel to [001] for both compression stages A and B. The gradual shift in direction of the maximum principal strain towards the [100] direction reflects the activity of two different slip systems. These slip systems are of the 110 <111> type and approximately symmetrical to the [100] direction. Assuming an equal amount of slip on each of these systems the resultant would manifest itself as a maximum principal strain in the [100] direction. It is therefore important to remember that even in the microstrain region, there is some evidence of slip activity on different slip systems which may lead to the formation of the dislocation tangles observed by transmission electron microscopy.

For the compression stage after yielding, that is, for stage C, the maximum principal strain, E_1, takes on a negative value and a direction which results from the activity of many slip systems. This result is quite compatible with the increase in the complexity of dislocation tangles.

It is recognized that the obtained values for the magnitude of the principal strains appear to be still too large, since they do not satisfy completely the requirements that the strains are of the order of σ/G where G is the shear modulus. The strain measurements, therefore, have to be further refined to give complete satisfaction. Nevertheless, the strain analysis is reasonably consistent and certainly gives the right directions for the principal strains as well as the correct signs. The consistency of the data can be checked if it is remembered that the volume change resulting from deformation is negligibly small and that the sum of the magnitudes of the principal strains should be nearly zero. For stages B and C $\Delta(E_1 + E_2 + E_3)$ is 0.032% and 0.153%, respectively.

Finally, it should be pointed out that a close correlation study of the strain distribution by the X-ray divergent beam method and the direct observation of the dislocation structure by transmission microscopy is still in progress. It is hoped that through the combination of these research tools a better understanding of the origin of dislocation tangles and cell structure will be obtained.

E. DEFORMATION OF MOLYBDENUM SINGLE CRYSTAL

A preliminary, semi-quantitative study of zone-refined molybdenum (Mo-E5) deformed at room temperature was carried out. Figure 100 exhibits an X-ray back-reflection divergent beam pattern (pseudo-Kossel pattern) of the undeformed crystal. Each ellipse representing a reflection of a set of (hkl) planes is made up of discrete lines. The discrete lines of the ellipse have been purposely introduced.

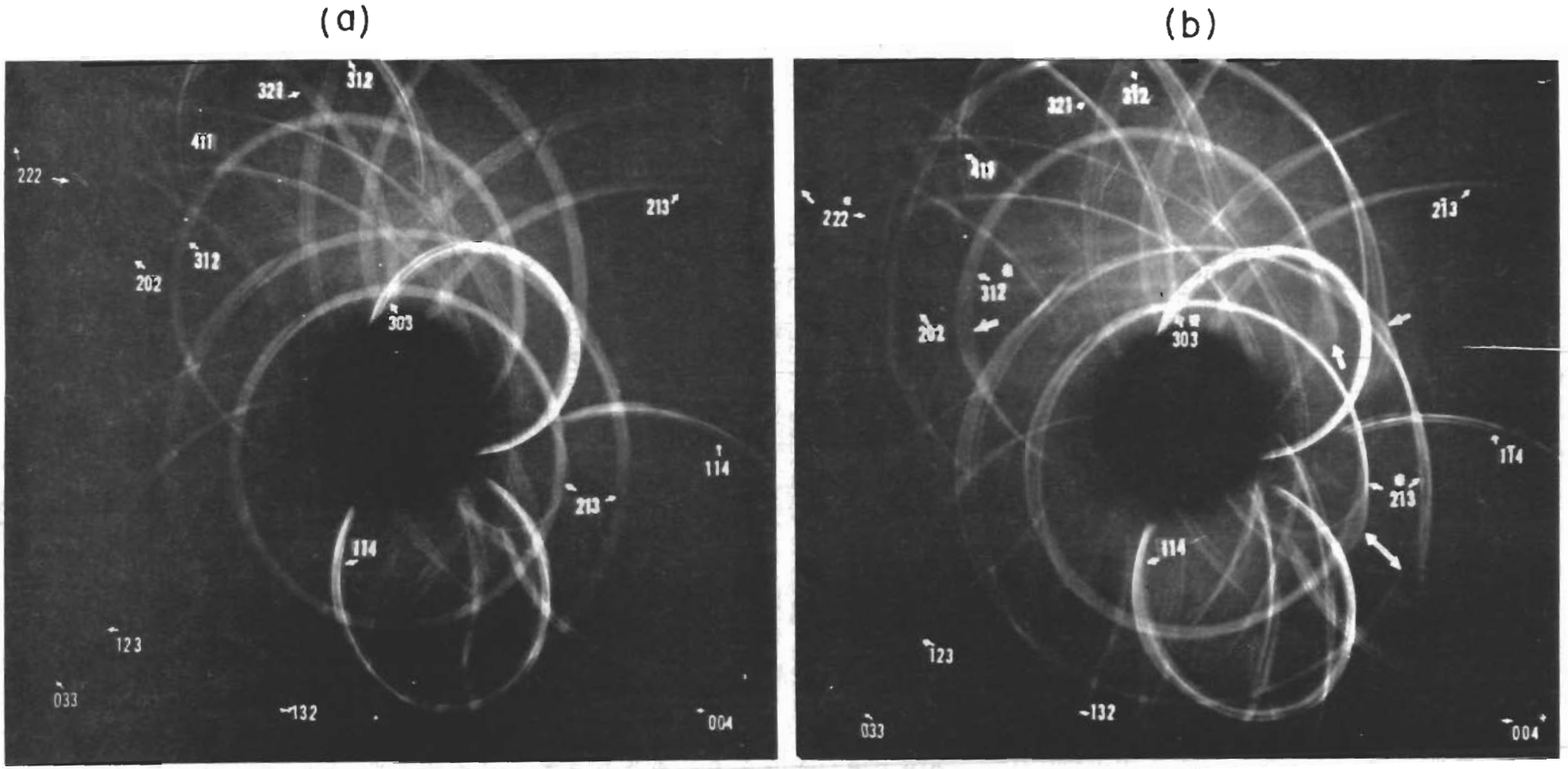

Fig. 100 - X-ray back reflection divergent beam pattern of Mo-E5 crystal: (a) undeformed, (b) deformed 5.8% in tension at room temperature. Note irradiation of adjacent lattice domains by multiple exposure technique. Distorted lattice domains are indicated by arrows.

They resulted from the fact that the specimen was moved closer to the target in discrete intervals in order to irradiate adjacent areas of the specimen. Figure 17b shows the effect of 5.8% extension at room temperature on the pseudo-Kossel pattern. A slight additional extension of the crystal leads to a brittle type of fracture. It may be noted that as a result of the deformation process a blurring and distortion of the discrete line pattern of the ellipses have occurred for some of the (hkl) reflections and that likewise local discontinuities of the pattern became visible. The latter correspond to local lattice misalignment. On the other hand, some other (hkl) reflections appear to have been little affected by the deformation process, since for these reflections the line pattern was still sharp. The sets of planes which exhibited the largest amount of local lattice distortions are the 110 and 112 with the 110 planes more heavily distorted than the 112. This is in good agreement with the frequency of slip planes observed and is characteristic for the mode of deformation of most body-centered cubic structures.[14] Furthermore, the observed anisotropic mode of lattice deformation, that is, the preferential distortion of certain sets of (hkl) planes as contrasted to other, relatively undisturbed, (hkl) planes appears to be characteristic of the deformation of brittle materials. It suggests that during the deformation process severe obstacles to cross-slip are being formed, restricting the lattice defects (dislocations) principally to the active slip planes. By contrast the plastically deformed crystals, such as aluminum crystals, or even tantalum crystals deformed at room temperature, exhibit patterns in which all the (hkl) reflections become severely distorted (Fig. 15). Although anisotropy of deformation becomes also conspicuous for these crystals, it is by no means as distinctly apparent as for the brittle mode of deformation of refractory metals.

REFERENCES

(1) Weissmann, S., Nakayama, Y., and Imura, T., "Substructure and Dislocation Networks in Tungsten," Wright Air Development Division Technical Report Tr-61-19.

(2) Keh, A.S. and Weissmann, S., "Deformation Substructure in Body-Centered Cubic Metals," Proc. Conf. on "The Impace of Transmission Electron Microscopy on Theories of the Strength of Crystals, "Berkeley, Cal., July, 1961 (Interscience Publishers; in press).

(3) Imura, T., Weissmann, S., and Slade, J.J., Jr., "A study of Age-Hardening of Al-3.85% Cu by the Divergent X-Ray Beam Method" (accepted for publication in Acta Crystallographica).

(4) Dash, W.C., "Evidence of Dislocation Jogs in Deformed Silicon," J. Appl. Phys. 29 (1958) 705.

(5) Johnston, W.G., and Gilman, J.J., "Dislocation Multiplication in Lithium Fluoride Crystals," J. Appl. Phys. 31 (1960) 632.

(6) Washburn, J., Groves, G.W., Kelly, A., and Williamson, G.K., "Electron Microscope Observations of Deformed Magnesium Oxide, "Phil. Mag. 5 (1960) 991.

(7) Fourie, J.T. and Wilsdorf, H.G.F., "Production of Dislocation Loops by a Combined Climb and Glide Mechanism," J. Appl. Phys. 31 (1960) 2219.

(8) Kimurs, H., Maddin, R., and Kuhlman-Wilsdorf, D., "Quenched-In Vacancies in Noble Metals--II, Mechanism of Quench Hardening, "Acta Met. 7 (1959) 154.

(9) Kuhlman-Wilsdorf, D., Maddin, R., and Wilsdorf, H.G.F., "Point Defect Hardening in Face-Centered Cubic Metals," to be published in Symposium on "Strengthening Mechanisms in Solids,". A.S.M. (1960).

(10) Mott, N.F., "Mechanical Properties of Metals," Proc. Phys. Soc. (London), B64 (1951) 729.

(11) Li, J.C.M., "Cross Slip and Cross Climb of Dislocations Induced by a Locked Dislocation," J. Appl. Phys. 32 (1961) 593.

(12) Weissmann, S. Imura, T., and Hosokawa, N., "Recrystallization and Grain Growth of Aluminum," Eleventh Technical ONR Report (to appear in the Proceedings of the Symposium on "Recovery and Recrystallization of Metals," A.I.M.E. Annual Meeting, February, 1962).

(13) Imura, T., "The Study of Deformation of Single Crystals by the Divergent X-Ray Beams", Bulletin of Naniwa University, Ser. A 2 (1954) 51.

(14) Maddin, R., and Chen, N.K., "Geometrical Aspects of the Plastic Deformation of Metal Single Crystals, "Progress in Metal Physics 5 (1954) 53.

VI. YIELD PHENOMENA IN REFRACTORY METALS

Work carried out at the University of Liverpool by W. S. Owen, T. Ellis, C. L. Formby, D. Hull, I. D. McIvor, A. R. Rosenfield, A. Gilbert and C. N. Reid.

A. Scope

The primary objective was to understand the mechanism by which yielding occurs in refractory metals and how it is affected by variations in grain size, substructure, and association of interstitial atoms with substructure. Most of the work has been a tantalum although some aspects of the deformation of columbium and molybdenum have also been examined. The work is conveniently subdivided into the following studies:

1) The Yield of Polycrystalline Tantalum - by W. S. Owen, D. Hull, A. Gilbert and C. N. Reid.

2) The Distribution of Dislocations in Annealed Tantalum - by W. S. Owen, D. Hull and I. McIvor.

3) The Significance of the Yield Parameter σ_i - by W. S. Owen and A. R. Rosenfield.

4) The Effect of Quenching Temperature on the Yield Parameters of Tantalum - by W. S. Owen, C. L. Formby and A. R. Rosenfield.

5) The Strain Aging of Tantalum - by W. S. Owen and A. R. Rosenfield.

6) Deformation Structure in Tantalum - by W. S. Owen, D. Hull and I. McIvor.

7) The Deformation of Tantalum Single Crystals - by W. S. Owen, D. Hull and T. Ellis.

8) The Stable-Unstable Plastic-Flow Temperature Transition in Annealed Tantalum - by W. S. Owen and A. R. Rosenfield.

B. General Introduction

The deformation behaviour of ductile body-centred cubic metals tested in uniaxial tension can be described by four relationships:-

1. The elastic equation

$$\sigma = E\epsilon \qquad (1)$$

2. The strain-hardening equation

$$\sigma = K\epsilon_p^n \qquad (2)$$

3. The yield point equation

$$\sigma_y = \sigma_i + k_y d^{-1/2} \quad (3)$$

4. The instability condition

$$\epsilon > n \quad (4)$$

σ is the stress, σ_y the yield stress, ϵ the strain, ϵ_p the plastic strain, n the strain-hardening index, k_y the locking parameter and σ_i the internal frictional stress opposing the propagation of a slip band. Other useful quantities can be defined in terms of these equations. For example, the ultimate tensile stress σ_{UTS} is given by the simultaneous solution of equations 2 and 4:

$$\sigma_{UTS} = Kn^n \quad (5)$$

or in terms of engineering stress:

$$\sigma'_{UTS} = \frac{Kn^n}{1+n} \quad (6)$$

E, Young's modulus and K, the strength constant, are material constants, but σ_i, n, k_y and d can be changed appreciably by changes in composition or thermal treatment. It is shown in Section E that σ_i and n are interdependent and so the number of parameters in the latter class is reduced to three. Measurements have been made of the effects of interstitial solute concentration, annealing treatment, substructure and test temperature on σ_i and k_y for tantalum. σ_i is a function of composition and test temperature and k_y is a function of composition, test temperature and, at low total interstitial content, the annealing temperature which, in turn, determines the substructure. These matters are discussed in Section C and the substructures are described in detail in Section D.

The additional stress required to initiate a slip band in a polycrystalline material in which the dislocations are locked is described by k_y. The large variation in the reported value and the temperature dependence of k_y is due to the variety of dislocation sources which are available for slip nucleation. Possible locations for the start of slip are grain boundaries, virgin crystal or locked dislocations. A small and temperature dependent k_y is thought to be due to slip initiation by the unlocking of weakly pinned dislocations and a large and temperature independent k_y to the operation of the other sources which require a high stress and are not thermally activated. The binding energy of interstitial atoms and dislocations in tantalum was investigated by measuring the variation of k_y with quenching temperature (Section F). The relation between aging time and the yield parameters is discussed in Section G. In Section H electron-transmission electron microscopic evidence for the location of slip sources is described.

The frictional stress σ_i is usually considered to be the stress required to move the slip dislocations through an unaged crystal. The significance of σ_i is discussed in Section E. This stress has been measured by three different methods, by plotting σ_y as a function of $d^{-1/2}$ and extrapolating to infinite d, by extrapolation of the homogeneous strain-hardening part of the stress-strain curve to the elastic strain and by plotting the flow stress σ_f as a function of dislocation density and extrapolating to zero density. The results obtained by the first two methods are presented in Section C, and by the third method in Section H.

The general theory of the ductile instability transition temperature in terms of the yield parameters listed above is developed in Section J and it is used to assess the effect of metallurgical variables on the instability transition temperature for tantalum.

Some observations on the yield and fracture of tantalum single crystals (Section I) are included.

C. The Yield of Polycrystalline Tantalum

1. Abstract

The yield characteristics of three dilute tantalum alloys containing carbon, nitrogen or oxygen are investigated. Annealing cold worked wires between 1140° and 1745°C, to establish a grain-size between $d^{-1/2} = 1.9$ to 11.0 $mm^{-1/2}$, produced dislocation densities between 0.1 and 5.0×10^{10} dislocations cm^{-2}. The parameters σ_i or σ_f^o, the flow stress at zero plastic strain, and k_y which is related to the stress required to unpin a dislocation, were measured by two methods; plotting the lower-yield stress as a function of $d^{-1/2}$ (where 2d is the mean grain diameter) and by extrapolation of the homogeneous strain-hardening stress-strain curve to zero plastic strain. The latter method reveals any dependence of the yield parameters on grain size and sub-structure.

The initial substructure of annealed tantalum has no significant effect on the flow stress, but when the interstitial content is less than 75 ppm increasing the dislocation density decreases k_y. When 50 ppm of carbon is present k_y does not vary with testing temperature. However, oxygen and nitrogen pinning results in a value of k_y which increases with decreasing temperature. It is concluded that in tantalum-carbon pinning is by precipitation of carbides on the dislocations while oxygen and nitrogen probably form Cottrell atmospheres.

2. Introduction

Like all body-centered cubic metals, prestrained and unaged tantalum does not yield discontinuously, plastic flow starting at a stress σ_f^o. Subsequent deformation is homogeneous over the gauge length. However, an aged specimen does not yield until a stress σ_{UY} is reached, plastic strain spreads heterogeneously at a lower stress σ_{UY} and homogeneous strain hardening occurs only after the Luders bands have covered the whole gauge length. It is usual to analyse the yield behaviour in terms of two parameters;[1] σ_f^o, the stress required to cause slip in the unaged specimen and a parameter related to $(\sigma_{LY} - \sigma_f^o)$ which is a measure of the additional stress required to unpin the dislocations in an aged specimen.

Two different experimental methods can be used to obtain these parameters; the grain-size method and the extrapolation method. The former depends upon the fact that in polycrystalline specimens the stress concentration due to the deformation of adjacent grains is proportional to $d^{1/2}$, the mean grain diameter being 2d. The proportionality constant can be written as $k^{-1/2}$. It is found experimentally[2] that at constant testing temperature σ_{LY} is linearly proportional to $d^{-1/2}$ and if it is assumed that the intercept on the stress axis

represents a constant stress σ_i independent of grain size

$$(\sigma_{LY} - \sigma_i) = k_y d^{-1/2} \qquad (1)$$

The parameter k_y, which may be taken as a measure of the additional stress required to initiate slip in an aged specimen, can be written

$$k_y = \sigma_c \ell^{1/2} \qquad (2)$$

Equations (1) and (2) were obtained by Petch from a specific dislocation model[1]; the stress concentration being provided by a pile-up and slip being generated from a Cottrell locked source located a distance ℓ from the tip of the pile-up. However, the form of these equations is not dependent upon the specific model assumed for stress concentration and slip generation.

Since σ_i represents the stress required to initiate slip in an unaged specimen (i.e. when $k_y d^{-1/2} \to 0$) it must be identical with σ_f^o (this is discussed in Section E of this report) and

$$(\sigma_{LY} - \sigma_f^o) = k_y d^{-1/2} \qquad (3)$$

The extrapolation method[3] is an alternative means of determining σ_f^o. It depends upon the extrapolation of the homogeneous strain-hardening portion of the stress-strain curve to zero plastic strain. During homogeneous strain-hardening at constant temperature the relationship between true stress σ and true strain σ is accurately represented by

$$\sigma = K \epsilon^n \qquad (4)$$

where K is a strength constant. Thus, the logarithm of true stress is a linear function of the logarithm of true strain. On such a plot the extrapolation to zero plastic strain can be carried out with confidence and σ_f^o can be determined accurately.

Unlike the grain-size method, the extrapolation method does not require the assumption that σ_f^o be independent of d, but it does depend upon the homogeneous strain-hardening being unaffected by the aging treatment. The latter assumption was tested by comparing the stress-strain curves of prestrained and of prestrained and aged specimens. No difference in the strain-hardening characteristics was detected. In a study of pure iron Mogford and Hull[4] found excellent agreement between the two methods of obtaining the yield parameters.

Since a range of grain size is usually established by annealing cold worked specimens at different temperatures it is probable that the substructure (that is, the density and arrangement of dislocations) also varies with grain size and if substructure affects the yield behaviour significantly the assumption in the grain-size method of a σ_i independent of grain size will be erroneous. Thus, comparing the values of σ_i and k_y obtained by the grain-size method with σ_f^o and k_y by extrapolation provides a means of revealing effects due to substructure. Values of these parameters for tantalum by either method have not been reported. It was found by thin-film electron microscopy that appreciable substructural changes were produced by changing the annealing temperature of cold worked tantalum and consequently in the present work both methods of measuring the yield parameters were used.

3. Experimental Methods

Tantalum of three different impurity levels (Table 31) was tested. The material was obtained in the form of 0.030 inch diameter wire which had been cold drawn to 90 percent reduction. 60cm lengths were annealed by self-resistance electrical heating; a device for keeping the wires taut in a vertical vacuum chamber ensured that the specimens were straight before testing. A cold vacuum better than 10^{-7}mm Hg with a leak rate too small to measure was achieved by using an all-glass vacuum system which was baked before heating the specimen and a 30 litre per second mercury diffusion pump. The specimen temperature was assessed from the value of the heating current which had been calibrated by observing the melting point of a number of different pure metals attached to a tantalum wire specimen. It is estimated that the temperatures recorded are correct to within $\pm 15^{\circ}$C. Many systematic experiments, in which specimens were annealed at different vacuum pressures and heating and cooling rates, clearly showed that reproducible yield stress results could be obtained only when the pressure was kept below 10^{-5}mm Hg throughout the annealing cycle and a standard procedure was adopted which ensured that this was always achieved.

The tensile specimens, 3.8 cm long, were either immersed in a constant temperature bath of liquid refrigerant or cooled to a constant temperature by a Wessel liquid nitrogen evaporator.[5] The specimen temperature was measured with an accuracy of $\pm 1^{\circ}$C and the yield stress measurements on specimens from the same 60 cm length of annealed wire were reproducible to better than 1% and from duplicate anneals to within $\pm 1.5\%$.

4. Results

The grain size increased and the dislocation density decreased on increasing the annealing temperature (Table 32). For each material, increasing the annealing temperature from 1140° to 1745°C decreased the dislocation density by at least an order of magnitude. Low temperature annealing produced well-defined sub-boundary dislocation networks (Fig.101). The subgrain size and the scale of the nets increased with increasing temperature and at high temperatures the dislocations appeared to be randomly dispersed with appreciable volumes free from dislocations (Fig.102).

All specimens tested between 150° and 293°K showed a pronounced yield drop, a Luders plateau and a measurable strain-hardening gradient, but between 78° and 150°K, although a yield drop could be clearly distinguished, necking occurred before the Luders elongation was complete. Thus, it was not possible to apply the extrapolation method to the low-temperature test results. All specimens broke with a fibrous ductile fracture. The Luders elongation increased and the strain-hardening index n (equation 4) decreased with decreasing temperature between 293° and 150°K. Provided the grain size was small no significant variation of n with grain size was found.

When compared at the same grain size and testing temperature, Ta-E2 has the lowest and Ta-E4 the highest yield stress σ_{LY} and the variation of σ_{LY} with temperature is about the same in each case (Fig.103).

Table 31

Interstitial Solute Content of Specimens

Metal	Content in ppm C	N	O	Total
Ta-E2	50	12	12	74
Ta-E3	8	22	14	44
Ta-E4	3	12	147	162

Table 32

The Variation of Grain Size and Dislocation Density with Annealing Temperature

Metal	Annealing Temperature °C	Grain Size, $d^{-1/2}$ $mm^{-1/2}$	Dislocation Density $\times 10^{-10}$ cm^{-2}
Ta-E2	1744	1.9	0.50
	1346	3.4	1.50
	1140	11.0	5.06
Ta-E3	1744	1.3	0.1
	1247	3.9	1.3
	1088	9.0	6.7
Ta-E4	1545	4.6	0.10
	1140	9.3	4.20

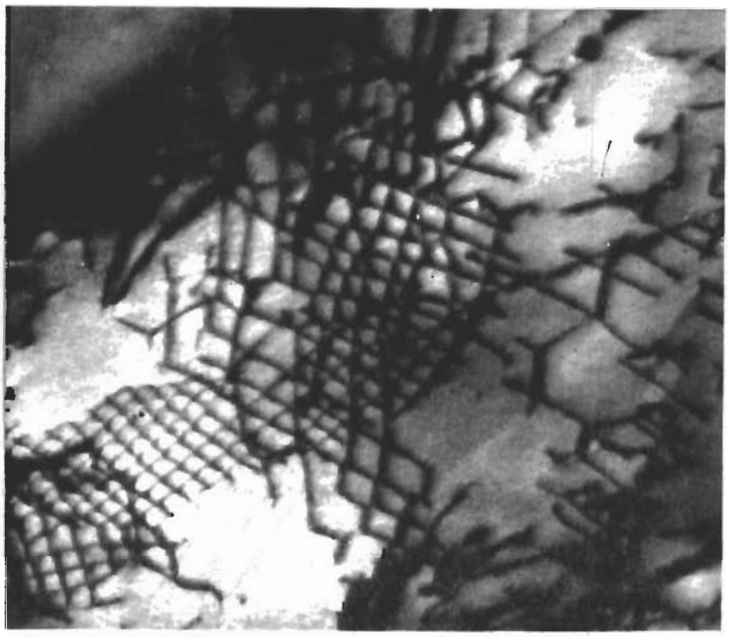

40,000X

Fig. 101 - Subboundary dislocation networks produced in Ta-E1 annealed at 1200°C

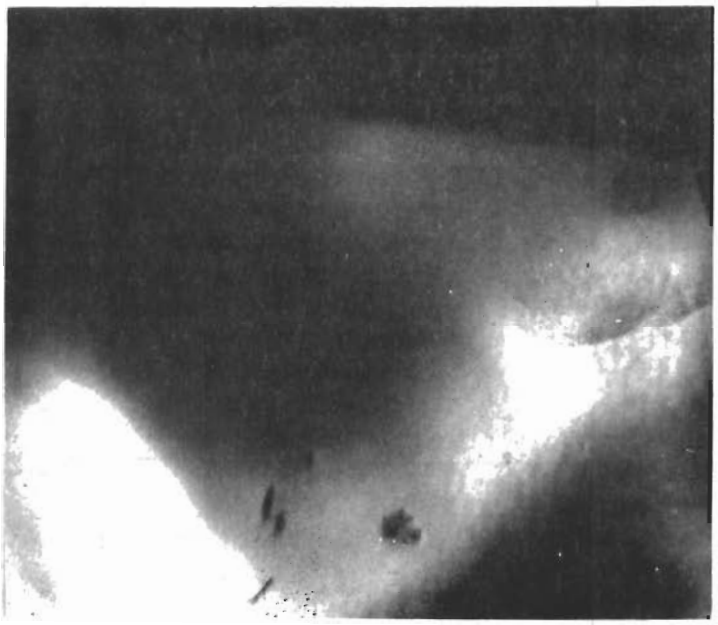

40,000X

Fig. 102 - Ta-E3 annealed at 1745°C

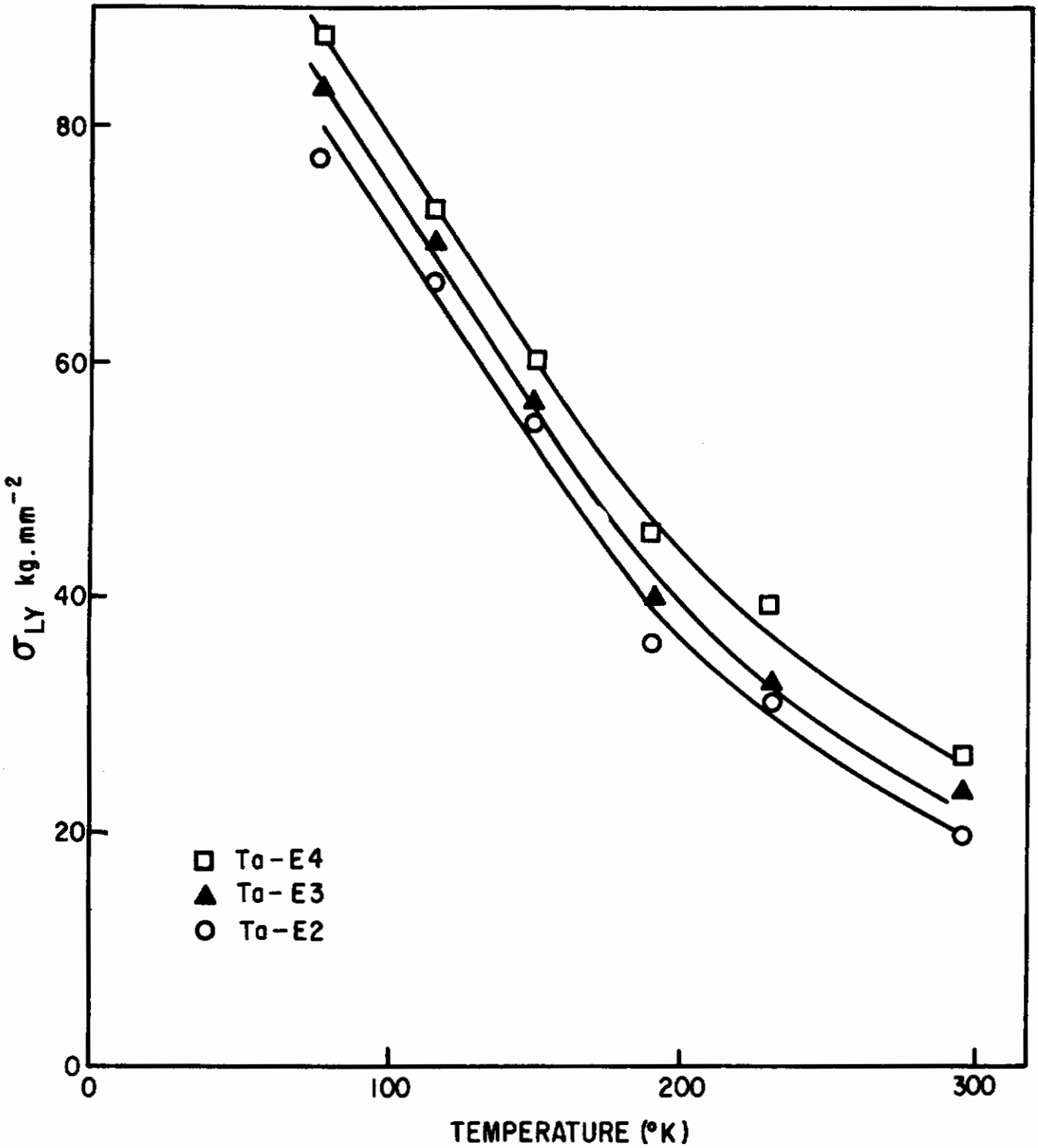

Fig. 103 - Variation of lower-yield stress σ_{LY} with temperature. Grain size $d^{-1/2} = 4.0\ mm^{-1/2}$.

The plots of σ_{LY} at constant temperature as a function of $d^{-1/2}$ exhibited some scatter but by testing numerous duplicates and four different grain-sizes at each temperature it was possible to locate the best straight line with reasonable certainty. The values of σ_i and k_y obtained from these plots are shown in Figs. 104 and 105. Within the limits of experimental error the values of σ_i for the three alloys were identical at each testing temperature (Fig. 104). Thus, the differences in σ_{LY} must be accounted for by differences in k_y and, in fact, k_y increases from Ta-E2 through Ta-E3 to Ta-E4 (Fig. 105). k_y for Ta-E2 is insensitive to variation in temperature, but for Ta-E3 and Ta-E4 k_y increases with decreasing temperature.

In all cases, when tested at the same temperature, the extrapolation method gave smaller values of σ_f^o (equivalent to σ_i) and larger values of k_y than the grain-size method. There does not appear to be any significant variation of σ_f^o with substructure and grain size and so values over the whole grain-size range are grouped together in the data plotted in Fig. 104. Nor is there any significant difference in the values or the temperature dependence of σ_f^o for Ta-E2 and Ta-E3, but σ_f^o for Ta-E4 is appreciably greater, being close to σ_i given by the grain-size method. The extrapolation method reveals that for Ta-E2 and Ta-E3 k_y is markedly dependent upon annealing temperature and consequently upon grain size and substructure (Figs. 106 and 107) In both cases k_y increases with increasing annealing temperature. k_y for Ta-E2 is independent of temperature whereas for Ta-E3 and Ta-E4 this parameter increases with decreasing temperature. The same result was found by the grain-size method. The extrapolation k_y values for Ta-E4 are only a little larger than the values by the grain-size method at the same temperature and no significant variation of k_y with grain size is evident (Fig. 108). The variation with temperature appears to be about the same as that revealed by the grain-size method.

5. Discussion of Results

Although all three alloys were annealed over a temperature range which produced an appreciable variation in substructure with grain size, σ_i (σ_f^o) and k_y by the grain-size and extrapolation methods were in reasonable agreement for the alloy with relatively high oxygen (Ta-E4). No dependence of these parameters on annealing temperature was found. Thus, it appears any effects due to variation in substructure are eliminated by high oxygen content. However, the two alloys with smaller interstitial solute content and low oxygen (Ta-E2 and Ta-E3) exhibited effects which varied with annealing temperature. The parameter affected is k_y. The increase in k_y with annealing temperature revealed by the extrapolation method cannot be due to the increase in grain-size since this is allowed for in equation 3. Thus, the effect must be due to substructure. One possible explanation can be suggested if it is assumed that ℓ is related to the average spacing between dislocations. Coarsening the substructure and decreasing the dislocation density by increasing the annealing temperature will increase ℓ. Consequently, assuming the critical local stress to initiate slip (σ_c in equation 2) is unaffected, k_y will increase with annealing temperature. An alternative explanation could be based on the fact that in Ta-E2 and Ta-E3 the total solute content is small and thus it is unlikely that the dislocations are saturated. As the dislocation density is decreased by increasing the annealing temperature the solute concentration per unit length of dislocation line will increase producing

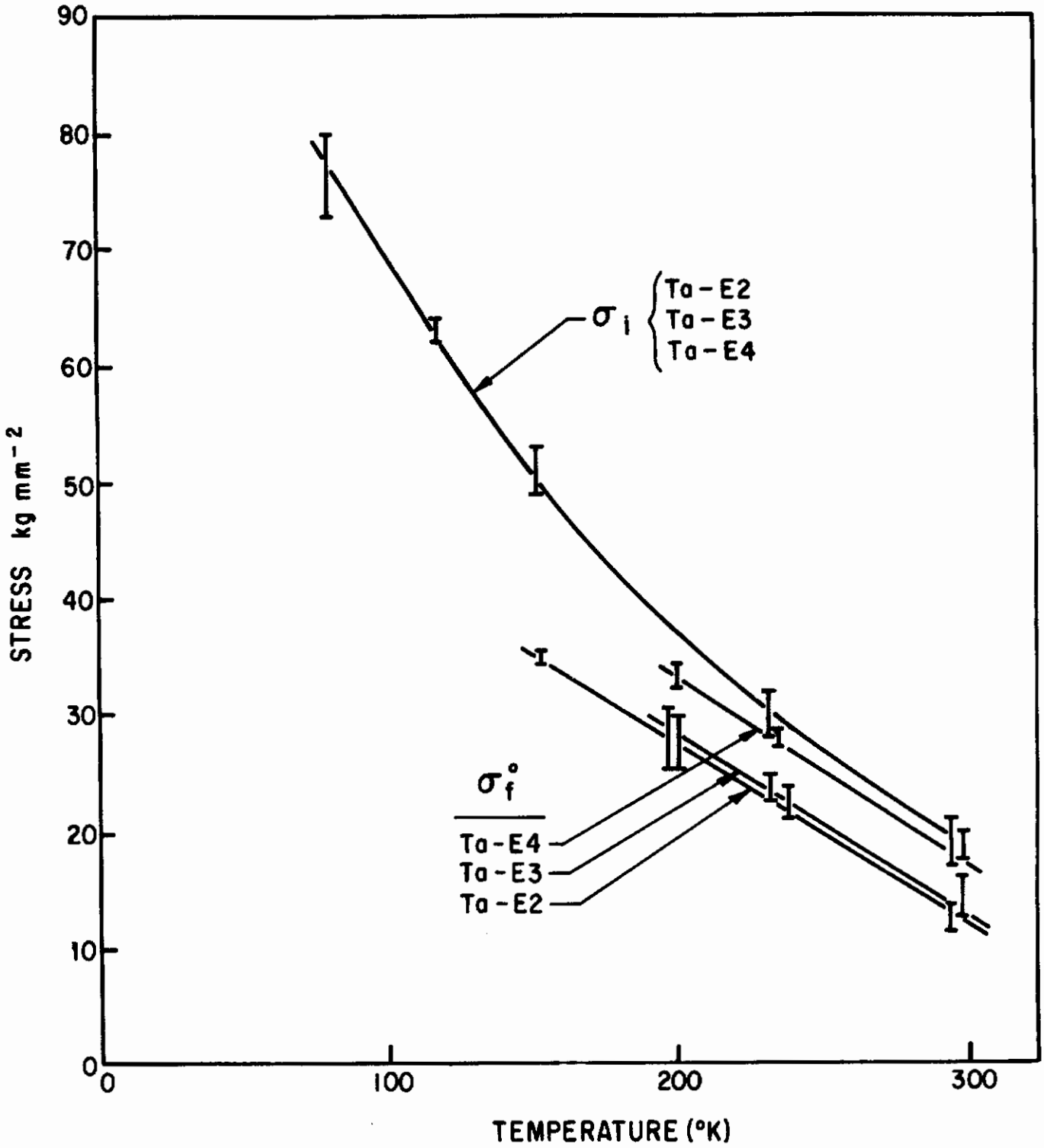

Fig.104 Variation of σ_i (by grain-size method) and σ_f^o (by extrapolation) with temperature. All grain sizes in the range $d^{-1/2}$ = 1.9 to 11.0 included.

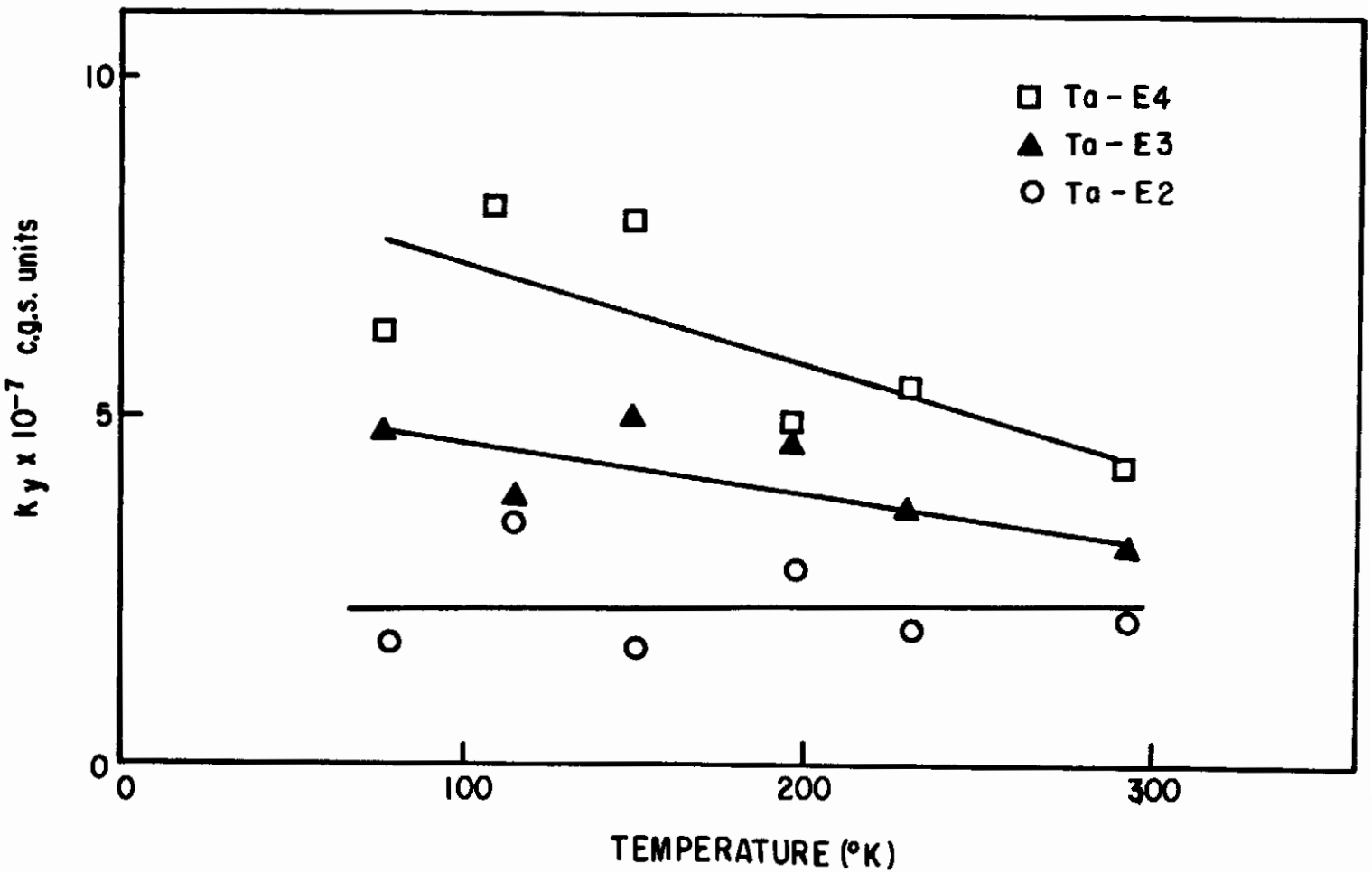

Fig. 105 Variation of k_y by grain-size method with temperature.

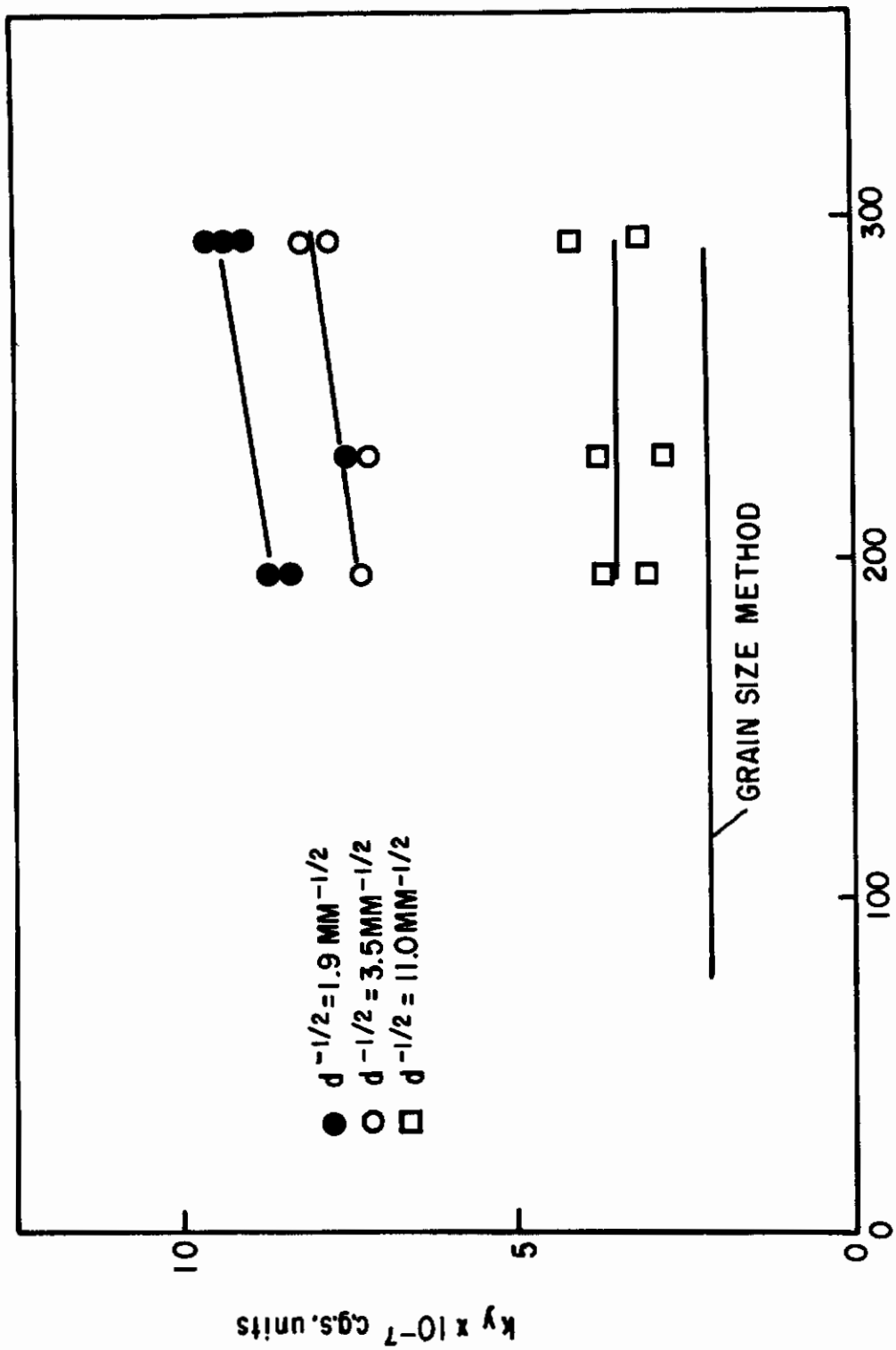

Fig. 106 - Variation of k_y with grain size and temperature, Ta-E2. All results by extrapolation method except where indicated.

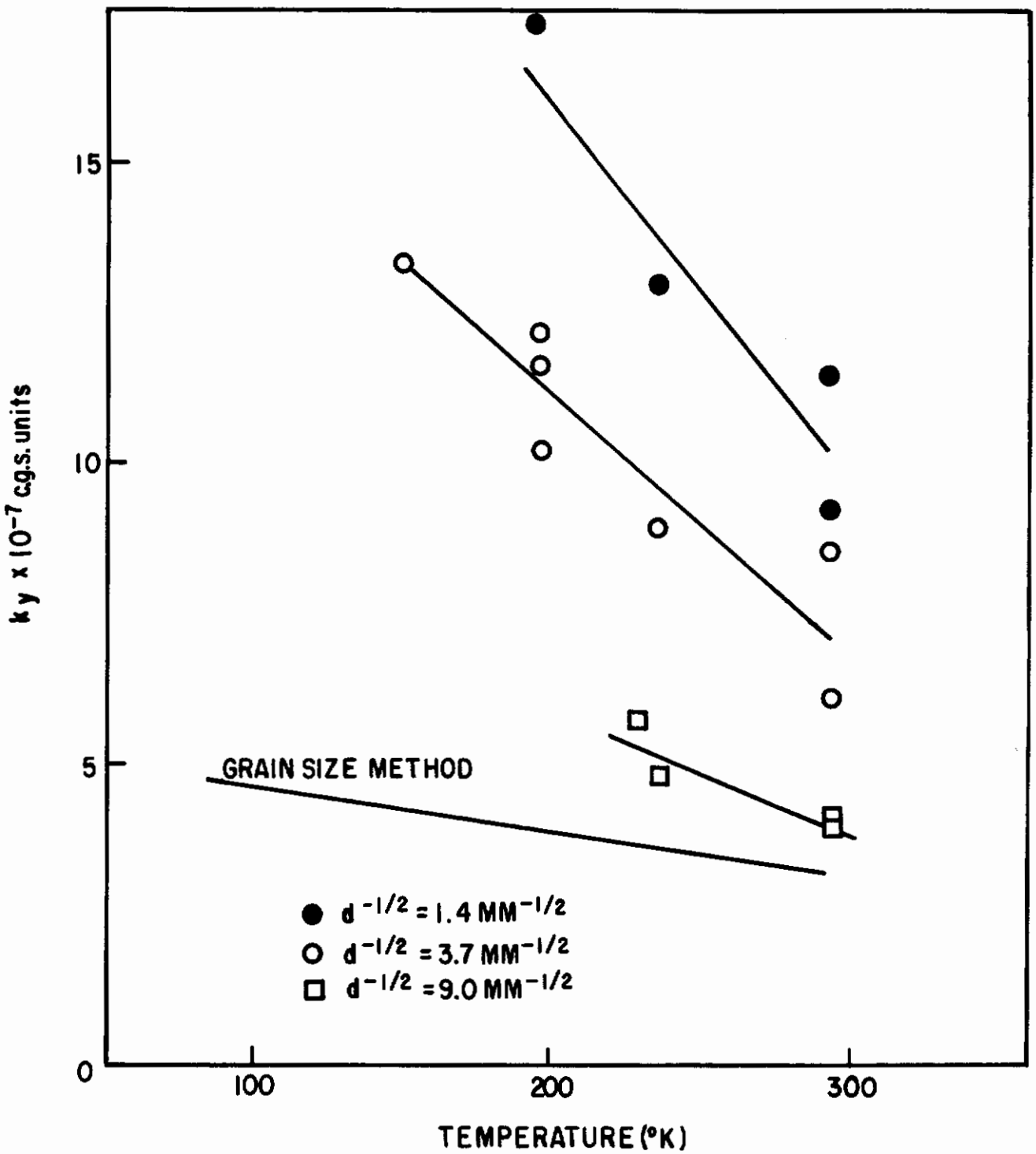

Fig. 107 - Variation of k_y with grain size and temperature, Ta-E3. All results by extrapolation method except where indicated.

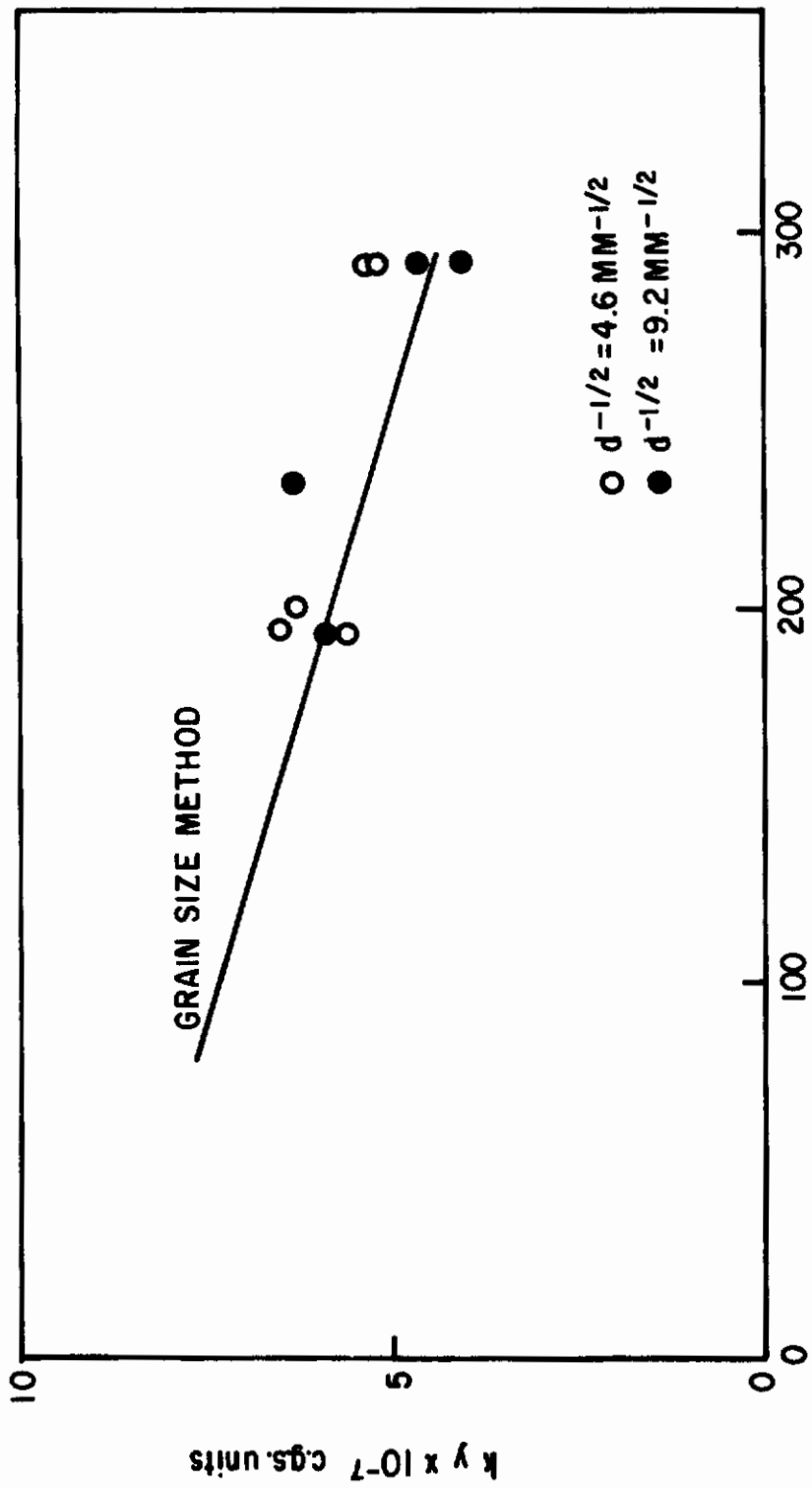

Fig. 108 - Variation of k_y with grain size and temperature, Ta-E4. All results by extrapolation method except where indicated.

stronger pinning. Thus, k_y will increase with increasing grain size. This explanation is the more attractive of the two because it is also consistent with the data from Ta-E4. In this alloy the solute (oxygen) content is twice that in the other alloys and the dislocation density at the same grain size is appreciably lower (Table32). The resulting greater solute concentration at dislocations would be expected to produce stronger pinning and this is revealed by the high value if k_y found experimentally (Fig.105). The insensitivity of k_y in Ta-E4 to dislocation density indicates that the dislocations are completely pinned after all the annealing treatments.

The difference between σ_f^o and σ_i for Ta-E2 and Ta-E3 may mean that the assumption that both these stresses represent the stress required to move unpinned dislocations is incorrect. It seems unlikely that any other significance could be attached to σ_f^o and thus, if the assumption is unjustified the Petch-Cottrell interpretation of σ_i[1, 3] must be questioned. However, it seems more probable that the high value of σ_i results from the grain-size variation of the true k_y as revealed by the extrapolation analysis. The slope of the σ_{LY} versus $d^{-1/2}$ plot is diminished because k_y increases with d; the apparent k_y is too small and σ_i, the intercept at infinitely large grain size, is too large. The variation of k_y with grain size is not revealed as a deviation from linearity of the σ_{LY} versus $d^{-1/2}$ plot because the variation is continuous with grain-size and there is inevitably some experimental scatter in σ_{LY}.

It is notable that when the major interstitial content is carbon (Ta-E2) k_y is not temperature dependent but when only oxygen or nitrogen are present (Ta-E3 and Ta-E4) a pronounced increase with decreasing temperature is observed. Extrapolation of the data of Vaughan, Stewart and Schwartz[6] suggests that the room temperature solubility of nitrogen and oxygen in tantalum is about 0.8a/o (575 ppm) and 2.1a/o (1700 ppm) respectively; that is, far in excess of the solute concentrations in Ta-E3 and Ta-E4. However, the solubility of carbon is too small to detect by X-ray lattice parameter measurements and is certainly less than 50 ppm at room temperature. Thus, it is probable that in the tantalum-carbon alloy (Ta-E2) the dislocations are pinned by carbide precipitates and consequently there is no significant thermally activated contribution to the unpinning process. In the alloys containing nitrogen and oxygen (Ta-E3 and Ta-E4) pinning by Cottrell atmospheres appears more probable.

σ_f^o is not affected significantly by variations in the substructure of the annealed specimens, but this parameter appears to be increased by increasing the total interstitial solute concentration; σ_f^o for Ta-E4 being higher than for Ta-E2 and Ta-E3. Similar effects have been found in iron-base alloys.[7] Because there is no discernable difference in the temperature dependence of σ_f^o, it is concluded that the effect of the interstitial solute is to alter the non-thermally activated component of σ_f^o and thus it is assumed it acts by changing the long-range stress field. In iron-alloys the effect has been attributed to changes in the type and dispersion of precipitates.[7] However, the major interstitial solute in Ta-E4 is oxygen and it is improbable that any precipitation occurs in this case. No evidence of precipitates was found by thin-film transmission electron microscopy. As pointed out by Christian,[8] a measurable change in σ_f^o due to direct solute dislocation interaction would require a very high solute concentration. This problem remains unresolved.

6. References

(1) N.J. Petch, J.I.S.I., 173 (1953) 25.

(2) E.O. Hall, Proc. Phys. Soc., 64B (1951) 747.

(3) A.H. Cottrell, Trans. A.I.M.E., (April 1958) 192.

(4) I. Mogford and D. Hull, private communication.

(5) E. Wessel, Proc. A.S.T.M., (1956) 540.

(6) D.A. Vaughan, O.M. Stewart and C.M. Schwartz, Trans. Met. Soc. A.I.M., 22 (1961) 937.

(7) A. Cracknell and N.J. Petch, Acta Met., 3 (1955) 186.

(8) J.W. Christian, private communication.

D. The Distribution of Dislocations in Annealed Tantalum

1. Abstract

The density and distribution of dislocations in three dilute alloys of tantalum containing oxygen, nitrogen and carbon have been determined by transmission electron microscopy after 90% cold work and subsequent annealing between 900°C and 1750°C. Annealing below 1200°C results in a marked decrease in the dislocation density and the formation of regular arrays of dislocations in sub-boundary networks. Above 1200°C the sub-boundaries are removed. The changes are sensitive to impurity content. The geometry of dislocations in regular networks have been studied using a stereographic method. Over 60% of the networks examined were probably formed by the intersection of two parallel sets of $a/2\langle 111\rangle$ dislocations.

2. Introduction

An understanding of the yield behaviour of body-centered cubic metals requires detailed information on the initial distribution of dislocations in the annealed condition. In iron[1,2,3] dislocations are not uniformly distributed after recovery and recrystallization or during deformation. The most common feature of recrystallization substructure is the formation of sub-boundaries composed of regular arrays of dislocations in a network. These are characteristic of the thermal treatment given to the cold worked metal and may be affected by impurity content. The geometry of dislocation networks has been studied in detail in non-metals[4] and to a limited extent in metals[1]. The theoretical conditions relating to their geometry have been outlined by Frank[5] and Carrington et al[1] have applied some of these principles to the analysis of networks observed in iron by thin film electron microscopy.

3. Experimental Methods

3.1 General

Tantalum wires 0.030 in. diameter containing known amounts of carbon, nitrogen and oxygen (Table 33) were cold rolled to produce foils 0.002 in. thick. The foils were annealed for 1/2 hour between 900° and 1750°C by electrical resistance heating in a vacuum better than 8×10^{-5} mm. Hg., and cooled at a rate of 500°C min^{-1}. Thin foils for examination by transmission electron microscopy (A.E.I., E.M. 6 electron microscope) were obtained by electropolishing in a solution of 10 parts 40% hydrofluoric acid and 90 parts concentrated sulphuric acid, using platinum electrodes. The current density was 0.1 to 0.2 amp. $cm.^{-2}$ and the applied voltage 12 to 20 volts. The orientation of the foils was determined by selected area diffraction.

3.2 Stereographic Analysis of Dislocation Networks

Following the work of Carrington et al[1] on iron it is assumed that the hexagonal networks formed in tantalum (Fig. 109) arise from the intersection of either parallel sets of $\frac{a}{2}$ <111> dislocations (Fig.110), or parallel sets of $\frac{a}{2}$<100> dislocations (Fig.110). Short sections of $\frac{a}{2}$ <100> and $\frac{a}{2}$ <110 > dislocations are formed at these intersections respectively. The geometry of these networks is described by[6]

$$\underline{d} = \underline{r} \times \underline{\ell 2} \sin \frac{\phi}{2}$$

where $\underline{d}$ is the resultant Burgers vector intersected by a line $\underline{r}$ lying in the sub-boundary, $\underline{\ell}$ is the unit vector along the axis of misorientation across the sub-boundary, and ϕ is the angular misorientation. Since $\underline{d}$ and $\underline{r}$ are mutually perpendicular, if each $\underline{r}$ line is drawn to intersect only one set of dislocations in the network it must lie at right angles to the Burgers vector of these dislocations. The three $\underline{r}$ lines are drawn in Fig.110. The essence of the stereographic analysis described by Carrington et al[1] is the determination of the orientation of the three $\underline{r}$ lines so that the Burgers vectors of the dislocations associated with them can be determined.

Fig.111 illustrates the plane of a network ABCD lying at an angle, θ, to the plane of a thin foil which is parallel to (001). A photograph of a network in a foil appears as the projection of the network in the plane of the foil, and similarly the $\underline{r}$ lines drawn on a photograph such as Fig.110 are the projection of these lines in the foil plane. The orientation of the foil is shown stereographically in Fig. 112. The trace AB of the net ABCD (Fig.111) in the foil is shown and from the value of α and θ the pole and great circle representing the orientation of the net is plotted. Similarly, the projected $\underline{r}$ lines $\underline{r}'_1$, $\underline{r}'_2$ and $\underline{r}'_3$ in the plane of the foil have been drawn and the true $\underline{r}$ lines $\underline{r}_1$, $\underline{r}_2$ and $\underline{r}_3$ in the plane of the net determined. The Burgers vectors of the

Table 33

Composition of Tantalum Specimens

Metal	Content in ppm			
	C	N	O	Total
Ta-E1	< 10	18	7	35
Ta-E2	50	12	12	74
Ta-E4	3	12	147	162

Table 34

Effect of Temperature and Impurity on the Spacing of Dislocations in Networks

Metal and Annealing Temperatures	Number of nets Measured	Values of (W) Spacing						
		0 to 200Å	200 to 400Å	400 to 600Å	600 to 800Å	800 to 1000Å	1000 to 1200Å	1200 to 1400Å
TaE1, 1200°C	23	0	6	5	2	2	4	4
	9	1	3	1	0	2	1	1
	5	0	2	3	0	0	0	0
TaE2, 1200°C	16	1	8	3	1	1	1	1
1100°C	24	8	10	4	1	0	0	1
TaE4, 1200°C	1	0	0	1	0	0	0	0
1100°C	4	2	1	1	0	0	0	0
1000°C	4	3	0	1	0	0	0	0
900°C	5	4	1	0	0	0	0	0

40,000X

Fig.109-Hexagonal network in tantalum formed by the intersection of parallel sets of $\frac{a}{2}$ <111> dislocations.

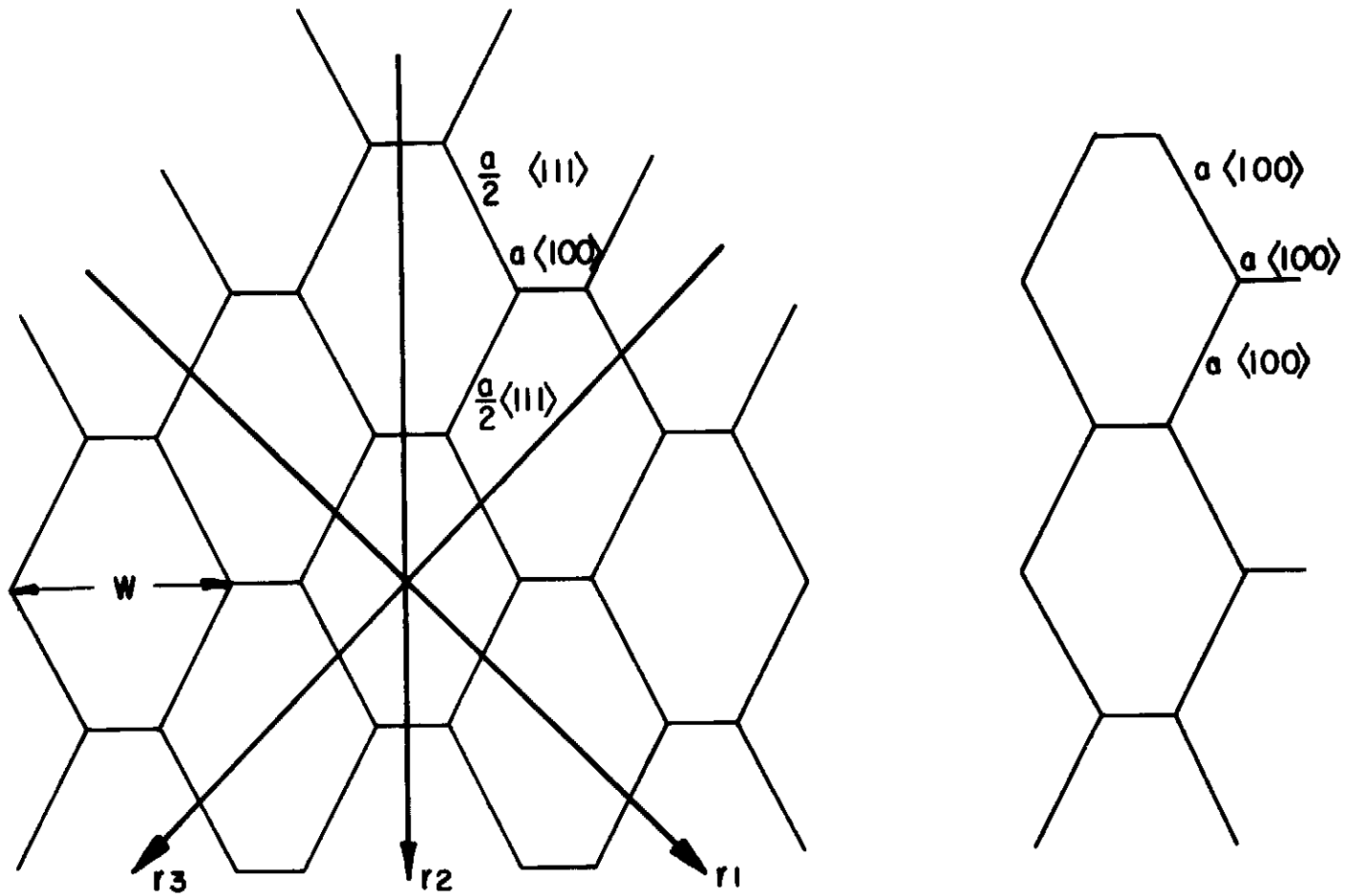

Fig. 110 Diagram of a dislocation networks formed by the intersection of parallel sets of (i) $\frac{a}{2}$ < 111> dislocations, (ii) $\underline{a}$ < 100> dislocations.

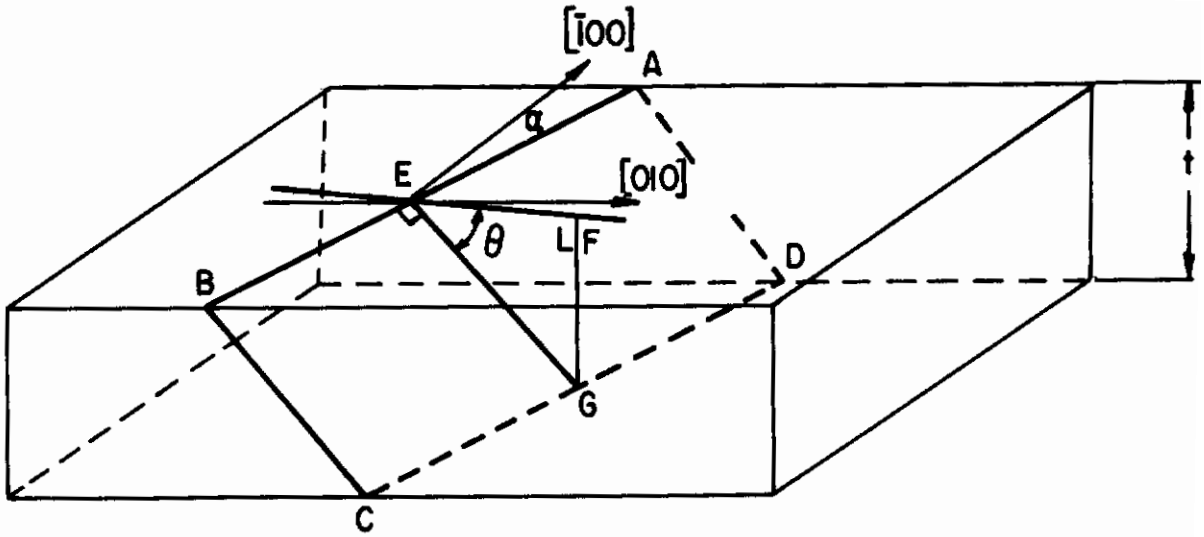

Fig. 111 - Diagrammatic representation of the plane of a network in a thin foil.

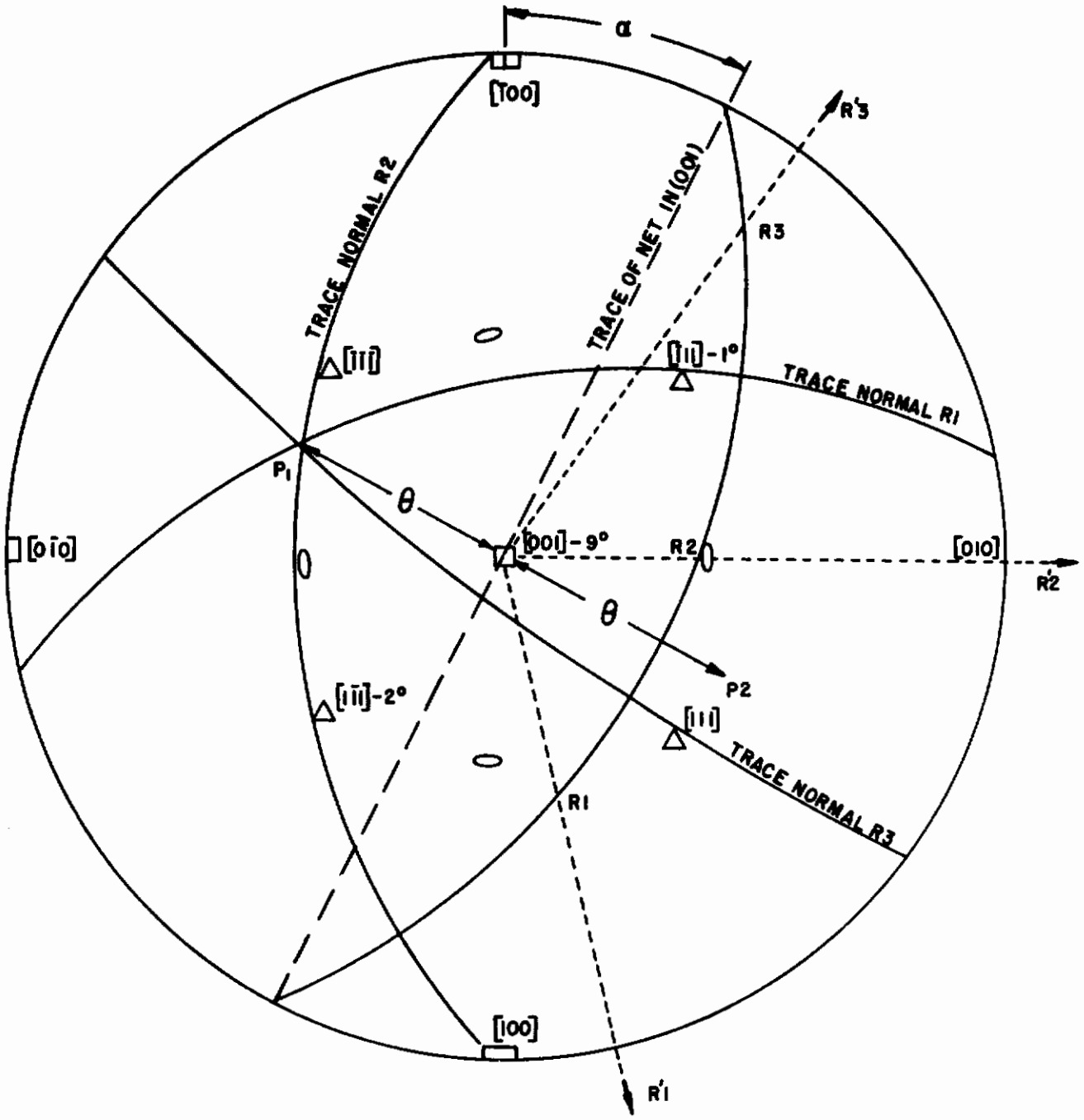

Fig.112 - Stereographic representation of method of determining Burgers vectors of dislocations in a network.

dislocations intersected by the $\underline{r}$ lines lie on the trace normals of $\underline{r}_1$, $\underline{r}_2$ and $\underline{r}_3$ and these have been plotted also. In this example the trace normals $\underline{r}_1$, $\underline{r}_2$ and $\underline{r}_3$ are within 1°, 9°, and 2° of $[\bar{1}11]$, $[001]$ and $[1\bar{1}1]$ respectively, indicating close agreement with a network of the type illustrated in Fig. 110.

The position of the trace normals depends on θ which is determined from the thickness of foil, t, and the projected width of the net EF = d. Experimentally d can be determined accurately, but there is no direct way of determining the thickness of the foil FG for each net examined. It was estimated that the foil thickness would lie between 1000A and 2000A. The analysis was carried out, therefore, for three values of θ calculated using thicknesses of 1000A, 1500A, and 2000A and the best fit was recorded. For a given value of θ, determined from $\tan^{-1}\frac{t}{d}$, there are two possible positions of the network since is is not known whether the line AB is at the top or bottom of the foil i.e. the angle between the foil and the net is either θ or $(\pi - \theta)$. The pole of the net is either p_1 or p_2 in Fig. 112. For the (001) orientation the solution obtained from the network analysis is independent of whether the angle is θ or $(\pi - \theta)$ because of the symmetry. About 50% of the foils examined has an $\{001\}$ orientation and the remainder were parallel to $\{111\}$. In the latter the solutions for the two possible angles are not the same and the best fit was used.

4. Experimental Results

4.1 Effect of annealing temperature and impurity content on density and distribution of dislocations

Prior to annealing all the tantalum alloys had been severely cold-worked at 20°C. The dislocation density, N, measured using a method described by Keh and Weissmann[3] was greater than 3×10^{11} cm.$^{-2}$ and it was difficult to resolve the individual dislocations. The effect of annealing, for 30 minutes at temperatures between 900° and 1750°C, on the dislocation density is shown in Fig. 113. Annealing at 900°C reduced the dislocation density to $\simeq 9 \times 10^{10}$ cm.$^{-2}$ and the density decreased progressively as the temperature was increased although each alloy behaved in a slightly different way.

For Ta-E1 increasing the annealing temperature from 900° to 1200°C resulted in a transition from a random distribution of dislocations with only a few isolated networks to a well ordered array of sub-boundaries surrounding sub-grains $\simeq 1\mu$ diameter almost free from dislocations. The changes are illustrated in Figs. 114, 115 and 116. The networks are often extensive and Fig. 117 shows such a network which was almost parallel to the plane of the foil. Over 90% of the Ta-E1 foils examined by selected area diffraction were parallel to 001. The changes in sub-structure in Ta-E2 were similar to those in Ta-E1. Regular networks were formed at 1100°C and the average sub-grain

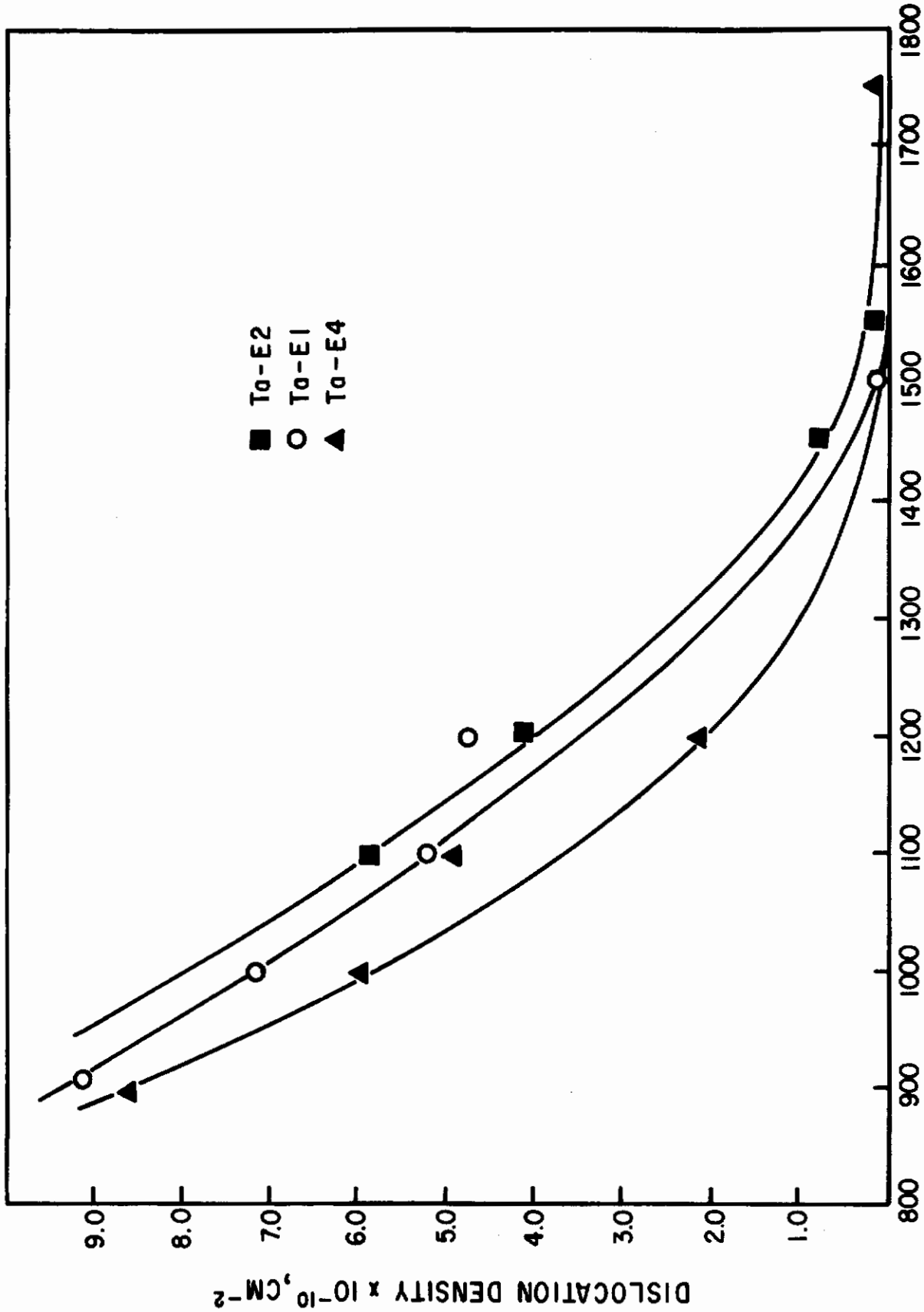

Fig. 113 -Effect of annealing temperature on dislocation density

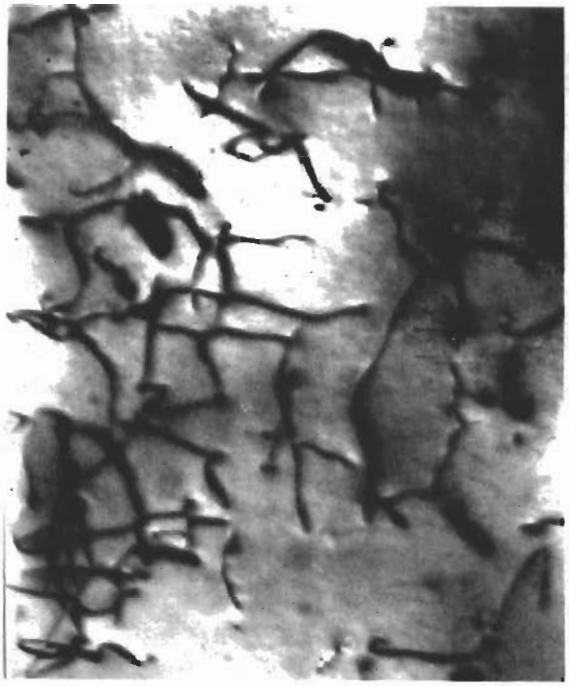

40,000 X

Fig. 114 - Random distribution of dislocations in Ta-E1 annealed at 900°C

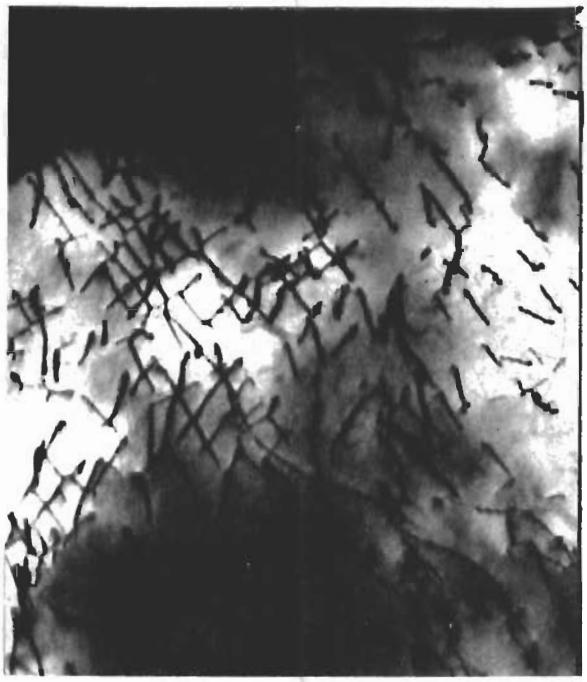

40,000X

Fig. 115 - Dislocation in Ta-E1 annealed at 1100°C

40,000 X

Fig. 116 - Ordered arrays of sub-boundary dislocation networks in Ta-E1 annealed at 1200°C

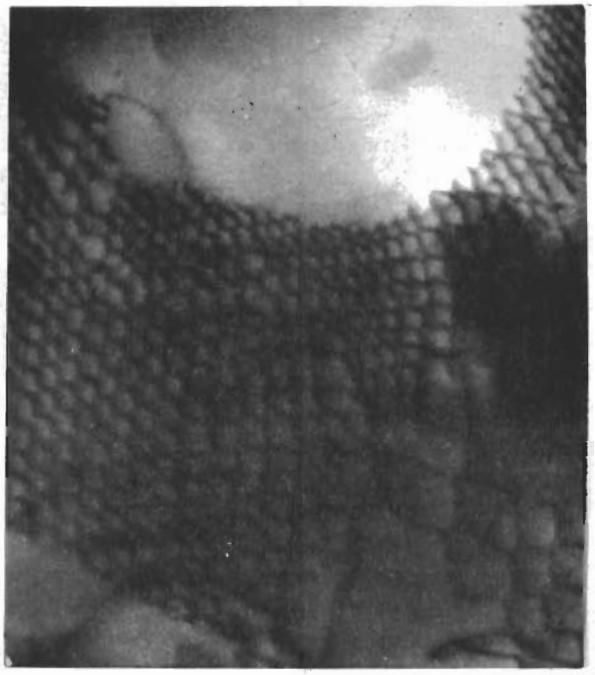

40,000X

Fig. 117 - Dislocation network almost parallel to the plane of the foil in Ta-E1 annealed at 1200°C

size was ~ 0.7μ. The networks were slightly finer than those in Ta-E1. The only outstanding difference between Ta-E1 and Ta-E2 was the preferred orientation of the foils; the majority of the Ta-E2 foils were parallel to {111} . Annealing above 1100°C produced a gradual reduction in the sub-structure and after annealing at 1550°C the dislocation density was less than 0.6×10^{10} cm.$^{-2}$ and no sub-boundary networks were observed. Whereas Ta-E1 and Ta-E2 had similar sub-structures this was not true for Ta-E4 given equivalent annealing treatments. After annealing between 900° and 1200°C the dislocation density was lower than the other alloys and a regular network structure was formed on annealing at temperatures as low as 1000°C. At this temperature the networks were extremely fine (Fig.118). No dislocation networks were observed after annealing at 1200°C, and after annealing at 1750°C the dislocation density was less than 0.1×10^{10} cm.$^{-2}$. Isolated dislocation loops were observed after the latter treatment. The preferred orientation of Ta-E4 foils was {001} .

A quantitative picture of the effect of annealing temperature and impurity on the spacing of dislocations in sub-boundaries and hence the misorientation of adjacent sub-grains was obtained by measuring the value of W, (Fig. 110). The results from measurements of over 100 networks are summarized in Fig.119 and Table 32. Insufficient measurements were made of Ta-E4 to justify plotting a histogram of the distribution of W. However, the general trend can be obtained from Table 32 . Two main points arise from these results: (1) the average value of W increases slightly with annealing temperature in agreement with the reduction in the average dislocation density; and (2) for foils annealed at 1100°C and 1200°C the average value of W for Ta-E1 is nearly the same as for Ta-E2 but significantly larger than for Ta-E4.

4.2 Geometry of Dislocation Networks

Fifty-two (52) networks from the three alloys were analysed to determine whether they agreed with either a <111>/<100> or a <100>/<110> network (Fig. 110). The total angular discrepancy between the three trace normals of the r lines and the directions concerned will be referred to as ψ. Thus ψ for the example given in Fig. 112 is 12°. For the <111>/<100> arrangement 20 networks had ψ less than 15° and for another 12 networks ψ less than 25°. For the <100>/<110> arrangement 13 networks had ψ less than 15° and for another 9 ψ less than 25°. 12 networks gave equally good agreement for both reactions and 9 networks could not be accounted for by either reaction within a total discrepancy of 30°. It was considered that above ψ = 25° no meaning could be placed on the results.

The orientation of the networks was also determined and the poles of the planes are plotted in Fig. 120.

5. Discussion of Results

The analysis of the geometry of the dislocation networks does not give a unique solution to the Burgers vectors of the dislocations because it is essentially a single surface method. The results, therefore, show only whether or not there is agreement with a given set of Burgers vectors. In the present results over 60%

40,000X

Fig. 118 - Fine networks in Ta-E4 annealed at 1000°C

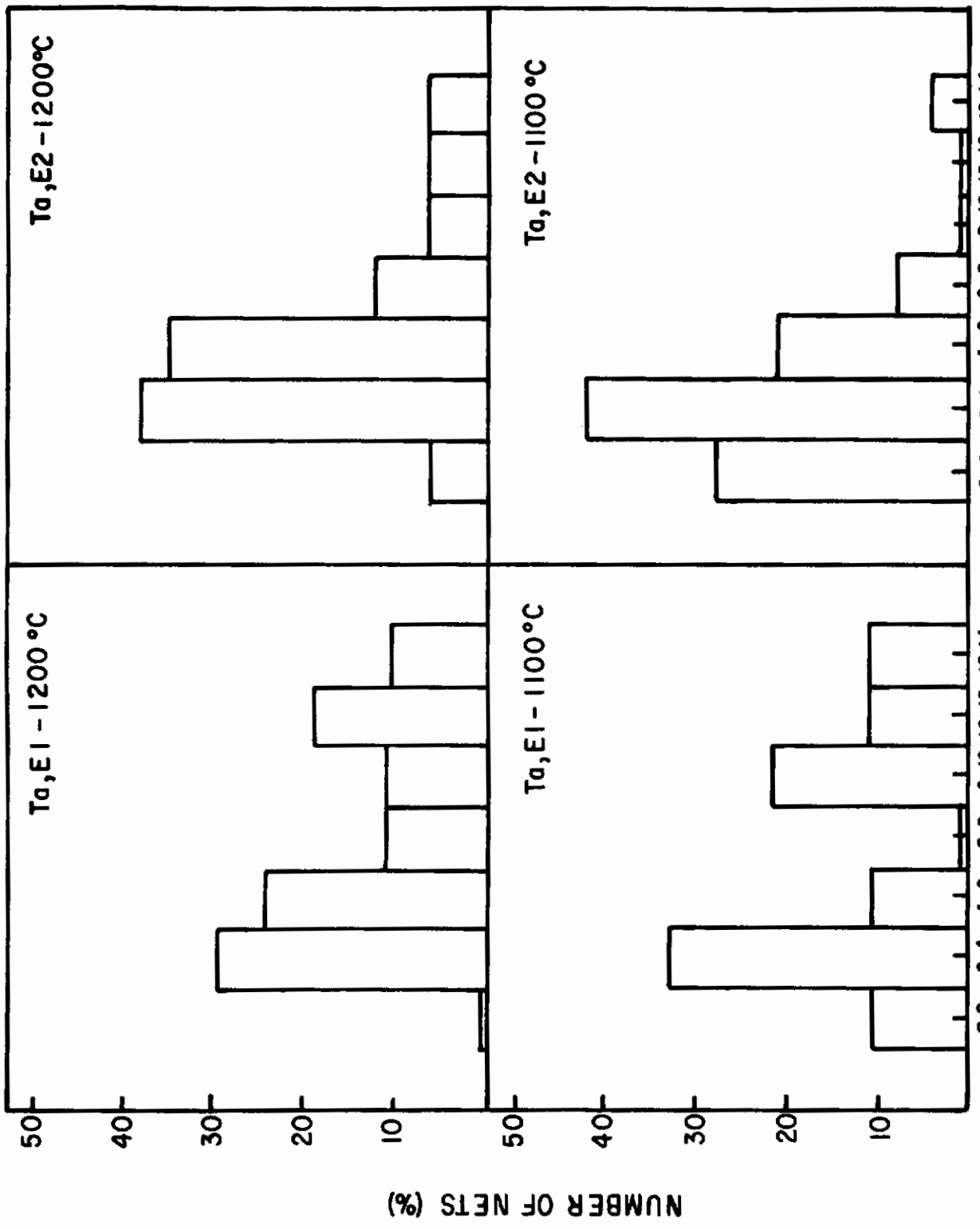

Fig. 119- Histograms of the distribution of the spacing of dislocations in regular networks for Ta-E1 and Ta-E2 annealed at 1100°C and 1200°C

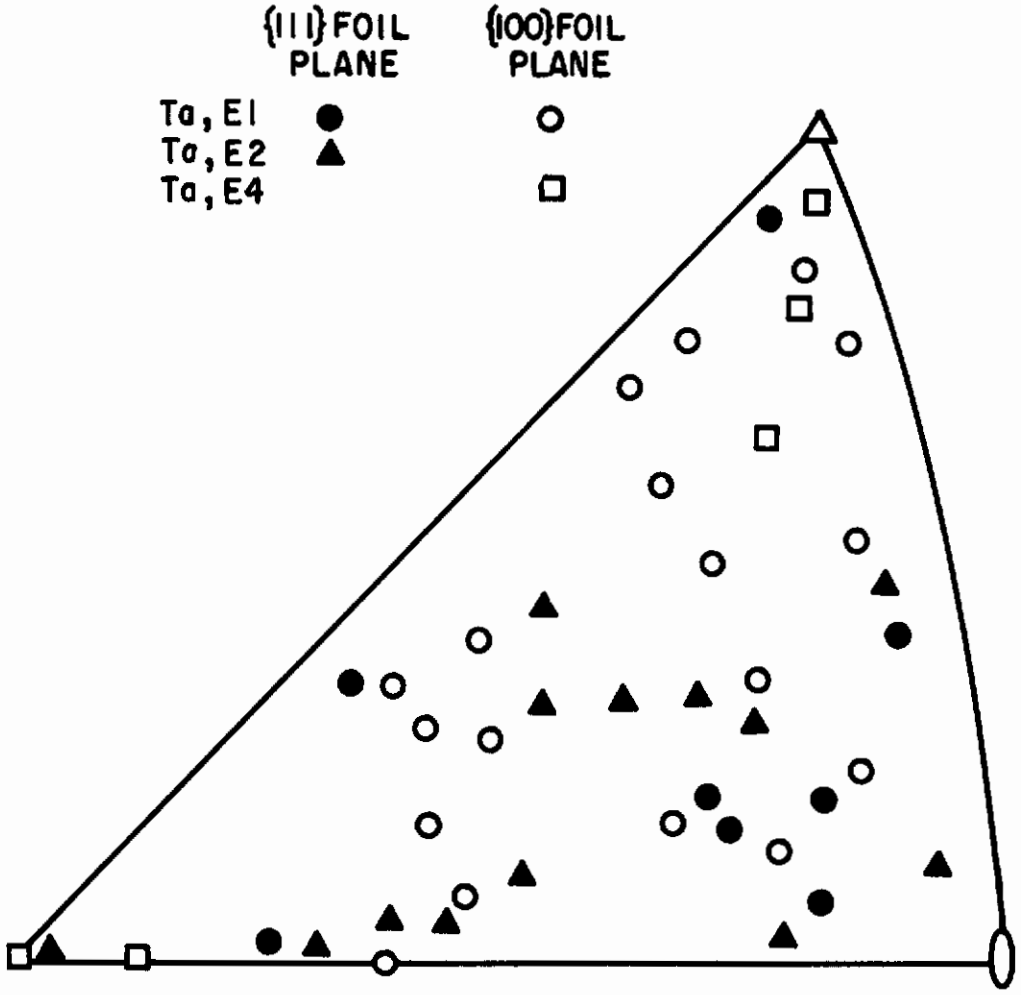

Fig. 120 - Poles of planes of dislocation networks in Ta-E1, Ta-E2 and Ta-E4

of the networks are in agreement with <111>/<100> networks and 40% with <100>/<110> networks. The material after cold rolling contains a high density of tangled dislocations and since these have been formed by plastic deformation it is reasonable to assume that the majority are $\frac{a}{2}$ <111> slip dislocations. During deformation some a <100> dislocations may have formed at the intersection of $\frac{a}{2}$ <111> dislocations but it is unlikely that they would multiply. During annealing the slip dislocations will rearrange themselves by climb and will form networks with segments of a <100> dislocations. Formation of <100>/<110> networks by a similar process would require the creation of a high density of a <100> dislocations. Thus, it is concluded that the most likely type of network is <111>/<100>.

No satisfactory explanation has been found for the observation of <100>/<110>. The overall experimental accuracy of the method is not high, and in particular, it is often difficult to determine the position of the three r lines, for example in the networks in Fig.116 the position of two r lines is readily determined but the position of the third is uncertain because the relevant segment cannot be resolved. It is possible that the observation of <100>/<110> networks arises fortuitously from the experimental uncertainty. Thus, for a completely random distribution of r line trace normals (Figure 112) any set of three trace normals is more likely to give agreement with <100>/<110> than <111>/<100> because there are more <110> poles than <100> poles.

Four distinct effects were observed, after annealing, cold-worked specimens at successively higher temperature, in all the tantalum alloys examined. The processes overlap somewhat but they are conveniently summarized in order of increasing temperature as follows:

1. Rearrangement and annihilation of dislocations; the dislocation density decreased from greater than 3×10^{11} cm^{-2} after cold rolling to 9×10^{10} cm^{-2} after annealing at 900°C. This process occurred without the formation of sub-boundaries.

2. Formation of dislocation sub-boundary networks which became very regular at the higher temperatures.

3. Coarsening of the networks, i.e. an increase in the spacing W (Figure 119) which is equivalent to a decrease in the angle of misorientation ϕ across the boundary. This process was accompanied by a small decrease in the average dislocation density.

4. Removal of the sub-boundaries and a marked decrease in the dislocation density.

The temperature range in which these effects occurred was not the same for each alloy studied. Thus, regular networks formed in Ta-E4 annealed at 1000°C whereas in Ta-E2 and Ta-E1 regular networks were not observed until they were annealed above 1100°C. Similarly, all the sub-boundaries had disappeared from Ta-E4 annealed at 1200°C but Ta-E1 and Ta-E2 annealed at this temperature contained a large number of networks. The changes in the average dislocation density with annealing temperature summarized in Fig.113also shows marked differences between the three alloys. The first three processes listed above involve the climb of dislocations and it follows that climb at a given temperature occurs more rapidly in Ta-E4 than in Ta-E1 and Ta-E2. This is surprising since it suggests that the activation energy for self-diffusion is lower in Ta-E4 although this alloy has a higher total interstitial impurity content.

At the same testing temperature, Ta-E4 has a higher flow stress than Ta-E2 (section C) suggesting that the movement of slip dislocations is impeded by the presence of a high oxygen content. Thus, it appears that oxygen increases the rate of climb and the resistance to the glide of dislocations.

6. References

(1) W. Carrington, K.F. Hale and D. McLean, Proc. Roy. Soc., 259A (1960) 203.

(2) D.G. Brandon and J. Nutting, J. Iron Steel Inst., 196 (1960) 160.

(3) A.S. Keh and S. Weissmann,Conference on the Impact of Transmission Electron Microscopy, California (1961).

(4) S. Amelinckx, Conference on the Impact of Transmission Electron Microscopy, California (1961).

(5) F.C. Frank, Conference on Plastic Deformation of Crystalline Solids, Mellon Inst., (1950) 150.

(6) F.C. Frank, Conference on Defects in Crystalline Solids, Phys. Soc., (1955) 159.

(7) D. Hull, I. McIvor and W.S. Owen, J. Less Common Metals (1962) to be Published.

E. The Significance of the Yield Parameter, σ_i

1. Introduction

At constant temperature, the variation of lower yield stress σ_y, with mean grain diameter 2d, is:(1)

$$\sigma_y = \sigma_i + k_y d^{-\frac{1}{2}} \qquad (1)$$

The parameters σ_i and k_y have been measured for a variety of materials and σ_i has been found to be far more sensitive to external variables than is k_y. All[2] or almost all,[3] of the temperature dependence of σ_y is due to the temperature dependence of σ_i, and such factors as changes in strain rate,[4] neutron irradiation,[4] and interstitial impurity content[5] also affect σ_y mainly through changes in σ_i. For this reason, it has been claimed[6] that σ_i contains a dislocation-unlocking term. The most common methods of measuring σ_i are: -

(a) extrapolation of the strain-hardening portion of the stress-strain curve to its intersection with the elastic line (σ_i^I in Fig.121a). Commonly, as elsewhere in this Report, σ_i^I is designated σ_f^o.

(b) extrapolation of yield stress-grain size curve to infinite grain size (σ_i^{II} in Fig.121b).

It will be shown that both methods of measuring σ_i are equivalent and that σ_i is a work-hardening parameter unconnected with unlocking.

2. The Determination of σ_i

It is obvious that σ_i^I represents a point on the stress-strain curve but it is not so obvious that σ_i^{II} also lies on this curve. Consider the room-temperature stress-strain curves for tantalum Ta-E4 in Fig.122. The specimen with the largest grain size has the lowest yield stress; consequently its value of σ_y is closest to σ_i. In Fig.123 the flow stress σ_f for various strains is plotted according to the relation:

$$\sigma_f = \sigma_i(\epsilon) + k_f d^{-1/2} \qquad (2)$$

Usually, k_f is smaller than k_y,[7] although in the unusual case where the Luders strain is small and relatively insensitive to grain size, k_y is found to be equal to k_f.[8] In accordance with equation 2, curves representing σ_f for various values of ϵ are straight and parallel. The lower yield-stress values (E, F and G) are each points on one of these curves, corresponding to the stresses necessary to produce the Luders strains for the various grain sizes. Taken together, points E, F and G form the lower yield stress versus grain size curve. As $d^{-1/2}$ decreases, the Luders strain decreases and the points on the lower yield stress versus grain size curve represent flow stresses for progressively smaller strains until, in the limit, the intersection of this curve with the ordinate equals σ_i^{II}. This is exactly the process used to determine σ_i^I (that is extrapolation of the flow-stress curve through progressively smaller strains to its intersection with the curve for zero plastic strain.

Thus, it is not coincidental that values of σ_i^I and σ_i^{II} reported in the literature agree fairly well.[9,10] Small differences arise from two sources; the inherent uncertainty of extrapolation methods and the insensitivity of σ_i^{II} to variations in σ_i and k_y resulting from variation in substructure with grain size when specimens are prepared by annealing cold-worked material at different temperatures.

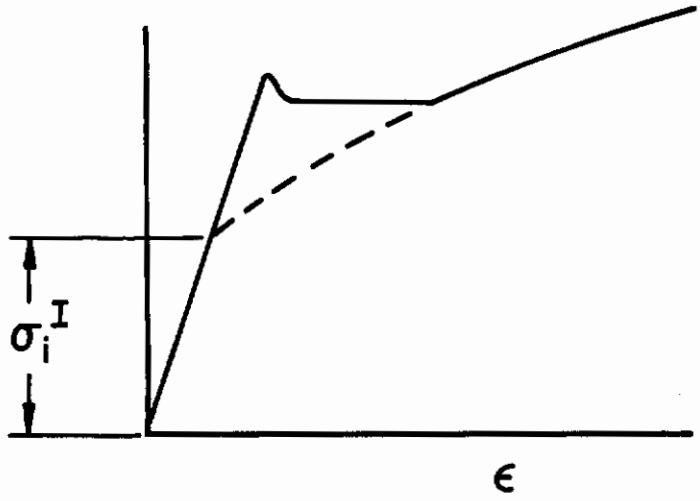

(a) EXTRAPOLATION METHOD

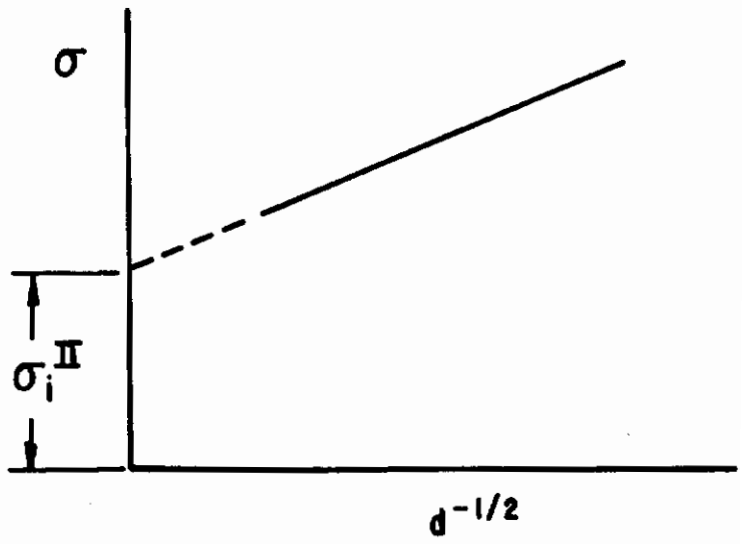

(b) GRAIN-SIZE METHOD

Fig. 121 - Alternative methods of measuring σ_i

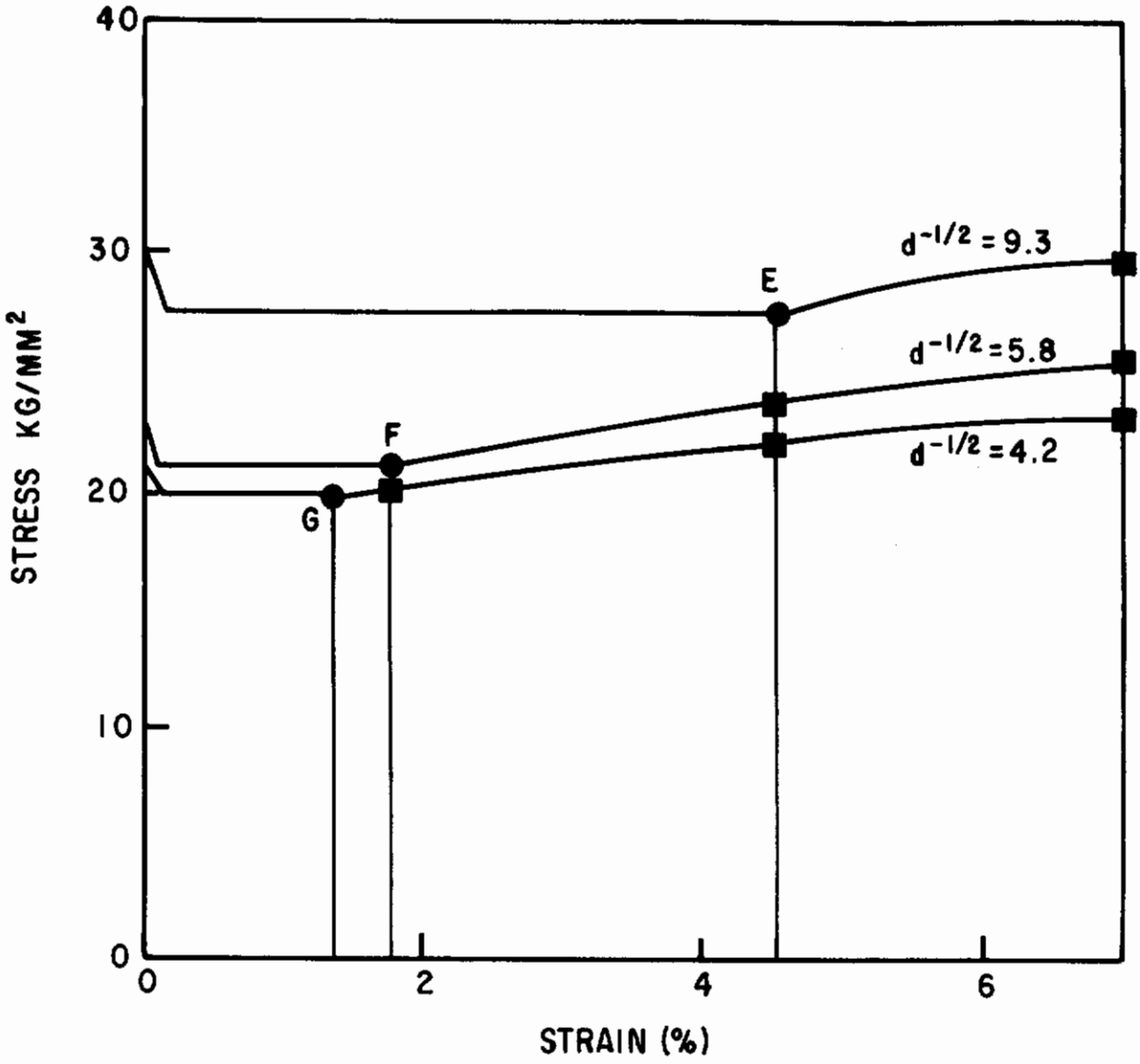

Fig. 122 - Stress-strain curves of tantalum (Ta-E4)

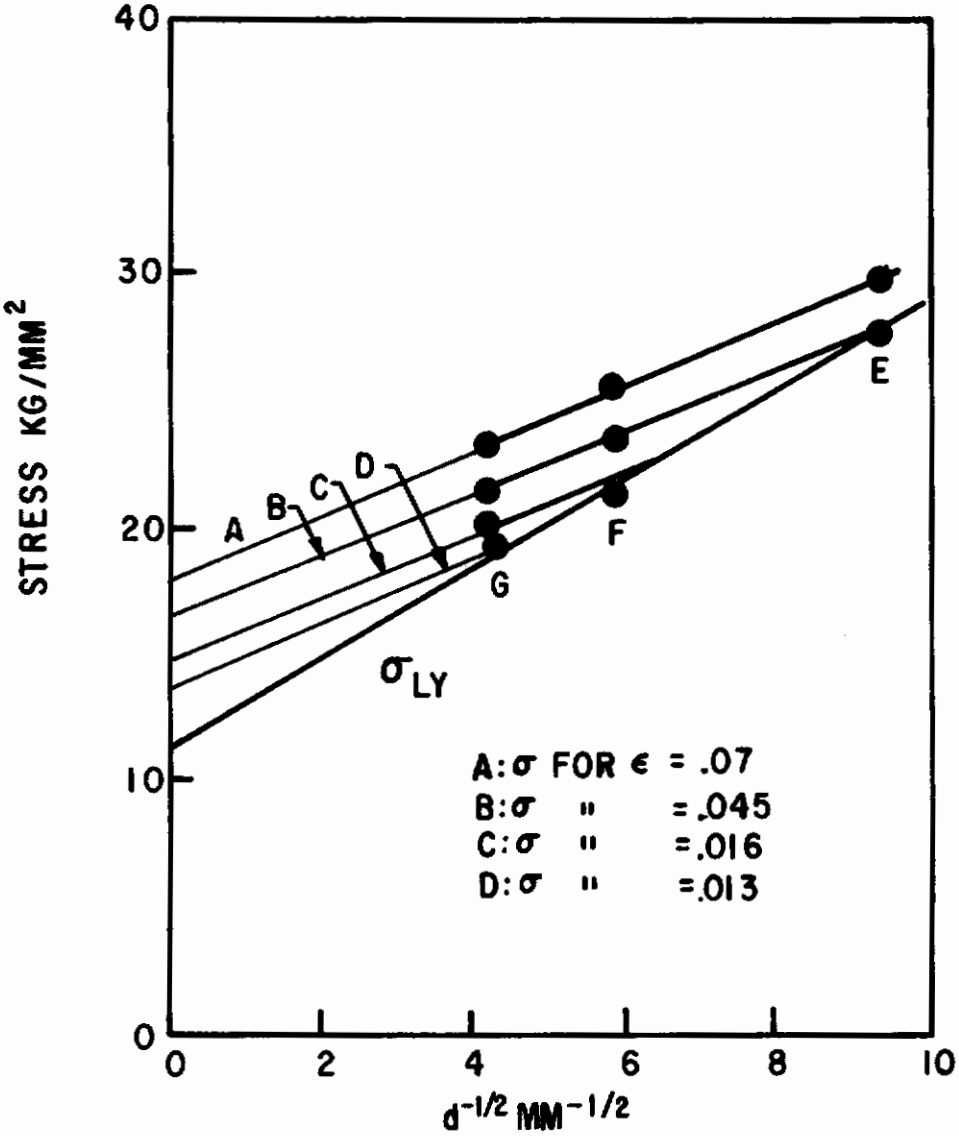

Fig.123- Effect of grain size on flow stress and yield stress of tantalum (Ta-E4)

3. The Relation between σ_i and n

Since σ_i represents a point on the homogeneous strain-hardening curve it must be related to some strain-hardening parameter. For homogeneous strain hardening

$$\sigma_f = K \epsilon^n \tag{3}$$

where K is a material constant and n is a parameter which varies with test temperature[11] and neutron irradiation.[9] The variation of n with annealing temperature and various strain-aging treatments has been measured for Ta-E1 as a function of testing temperature. The values of n have been found to exhibit a unique relation to the values of σ_i independent of testing temperature and aging treatment. This tantalum has a lower impurity content than the material used to obtain the data shown in Figs. 122 and 123 (90 ppm versus 160 ppm) and it has lower room temperature σ_i values. A similar relation is observed in other simultaneous measurements of σ_i and n.[9,10]

Since σ_i represents the simultaneous solution of equation 3 and the elastic equation

$$\sigma = E \epsilon \tag{4}$$

the relation between σ_i and n is

$$\sigma_i^{(1-n)} = KE^{-n} \tag{5}$$

The validity of this expression is demonstrated by Figs. 124 - 127 in which the values of σ_i and n for Ta-E1, Ta-E2, Ta-E3 and Ta-E4 are plotted according to the logarithmic form of equation 5. Data are included for specimens prepared by a variety of annealing and aging treatments and tested over the temperature range 150-300°K. The intercept on the ordinate is log K. Although there is some slight variation in log K from alloy to alloy, it is not considered significant and the value of K for all four alloys may be taken as 75 kg/mm^2.

It has been suggested[6] that the parameter k_y is connected with strain-hardening but a completely random variation of k_y with n was found when a large number of experimental values for tantalum were examined (Fig. 128).

Two important consequences arise from these arguments. First, since σ_i is descriptive of some process governing motion of free dislocations through a specimen, it cannot be related to dislocation-unlocking unless unlocking takes place during the entire plastic-deformation process which is very improbable. Second, there is nothing unique about the Luders strain; this strain is equivalent to the strain produced by homogeneous strain-hardening. The fact that the Luders strain is produced at a different stress and strain rate than homogeneous strain has no significant effect on the extent of strain hardening at the end of the Luders deformation.

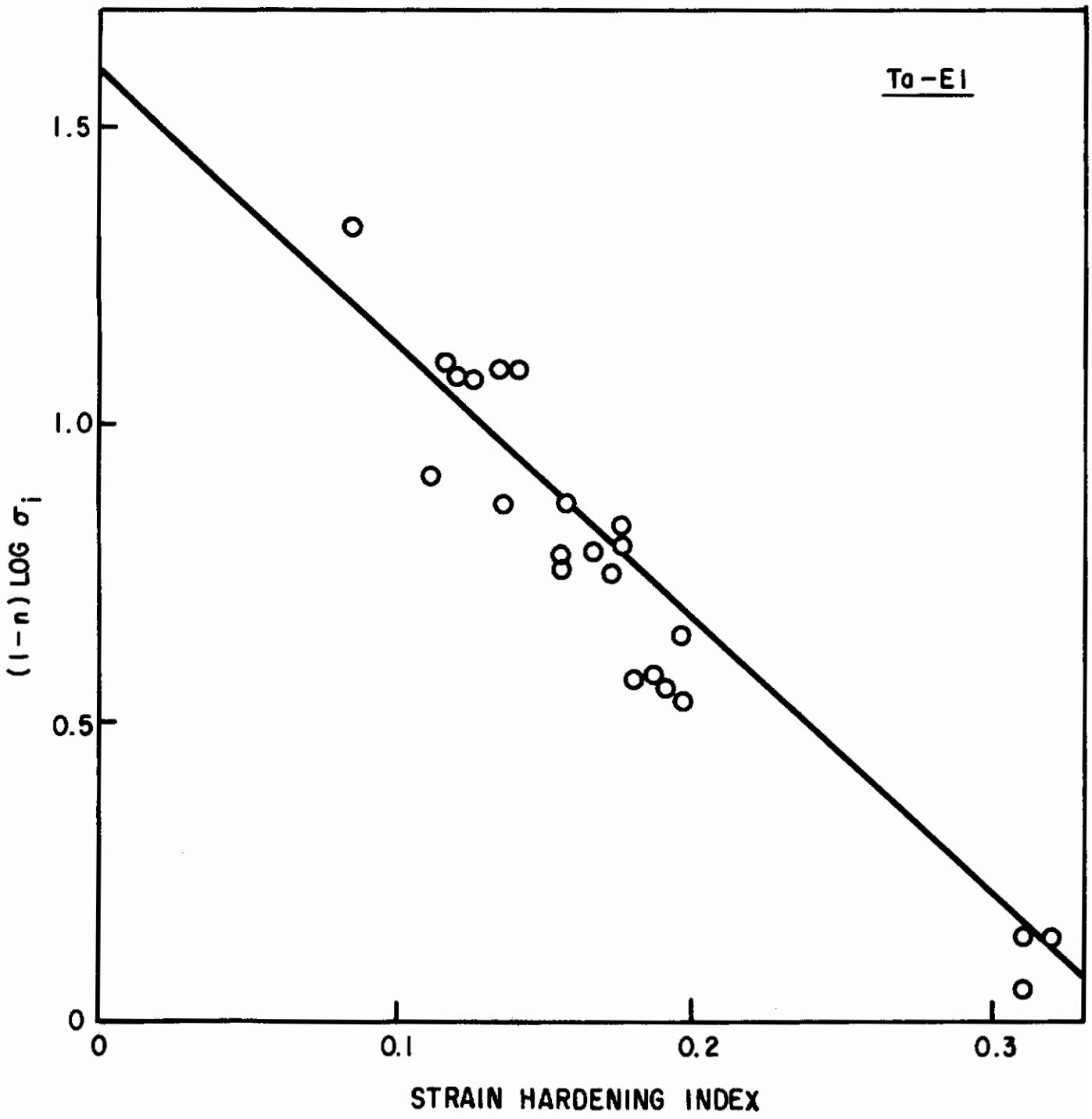

Fig. 124 - Relationship between σ_i and n for Ta-E1, including points for deformed and aged specimens tested at various temperatures

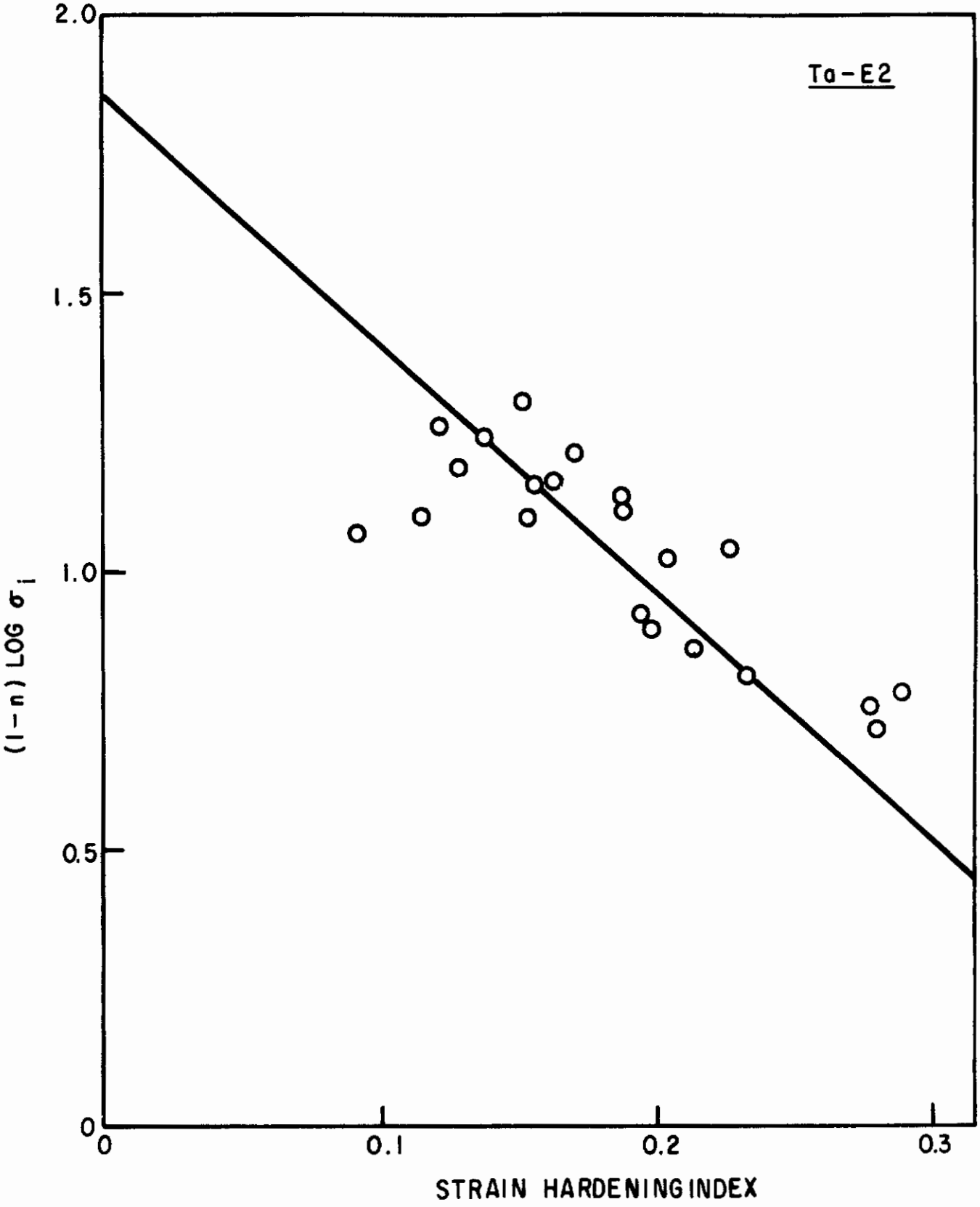

Fig. 125 - Relationship between σ_i and n for Ta-E2.

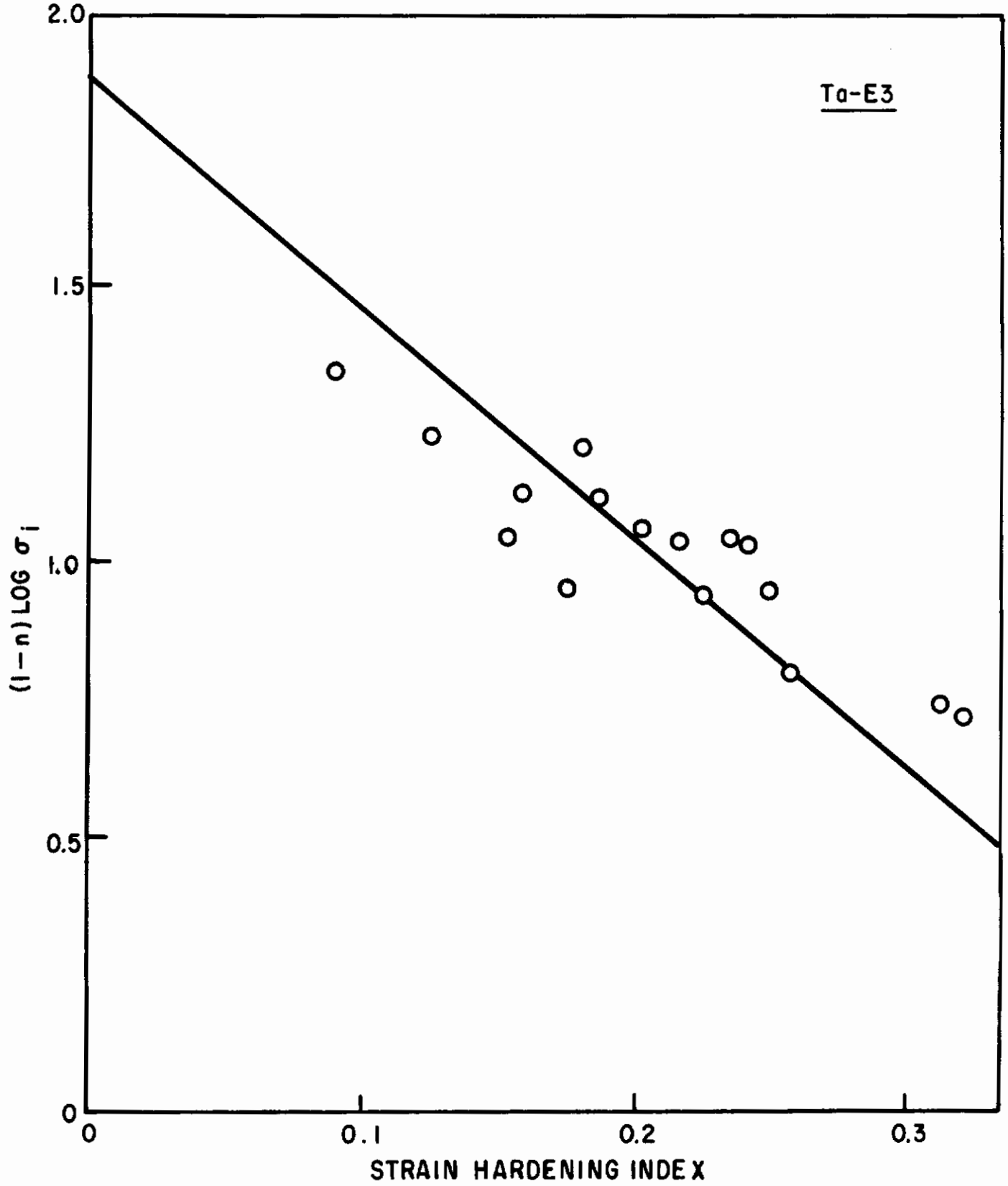

Fig. 126 - Relationship between σ_i and n for Ta-E3

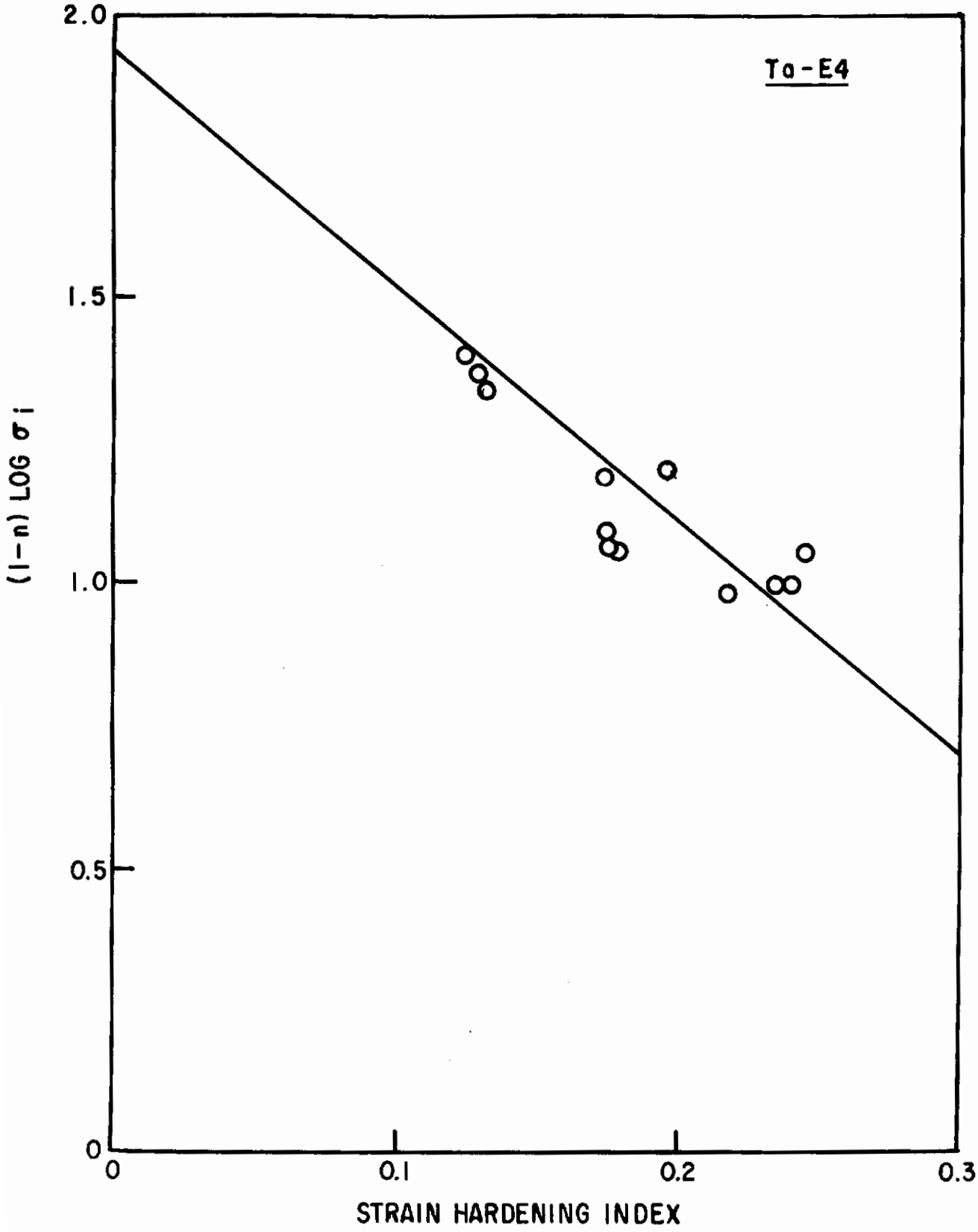

Fig. 127 - Relationship between σ_i and n for Ta-E4.

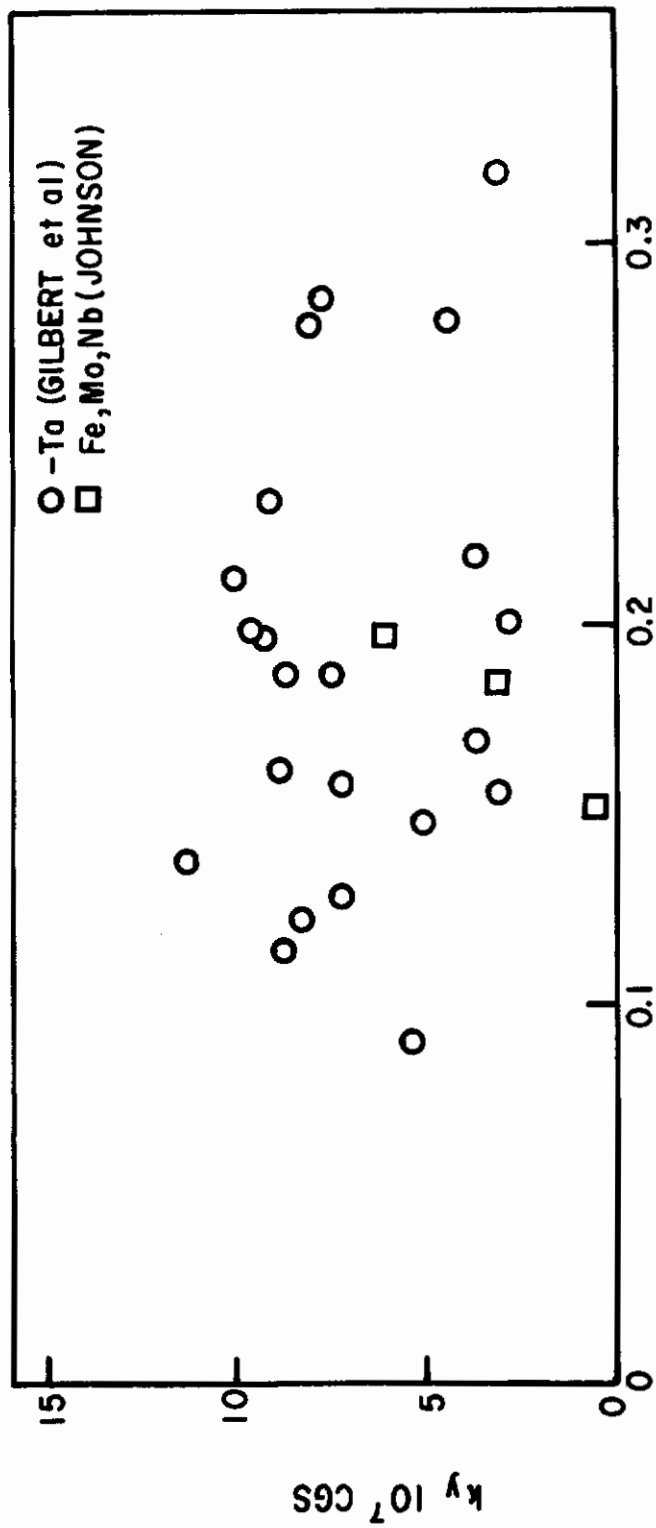

Fig. 128 - Values of k_y and n for several body-centered cubic metals

4. References

1. N. J. Petch, J. Iron and Steel Institute, 174 (1953) 25.
2. F. de Kazinczy, W. A. Backofen and B. Kapadia; "Fracture", New York (1959) 65.
3. D. Hull, Acta Met., 9 (1961) 191.
4. J. D. Campbell and J. Harding "Response of Metals to High Velocity Deformation," New York (1961) 51.
5. A. Cracknell and N. J. Petch; Acta Met., 3 (1955) 186.
6. A. A. Johnson, Phil. Mag., 7 (1962) 177.
7. R. Armstrong, I. Todd, R. M. Douthwaite and N. J. Petch, Phil. Mag., 7 (1962) 45.
8. H. Conrad and G. Schoeck; Acta Met., 8 (1960) 791.
9. I. L. Mogford and D. Hull, to be published.
10. A. Gilbert, D. Hull, W. S. Owen and C. N. Reid, to be published.
11. R. L. Smith, G. Spangler and R. M. Brick, Trans. A.S.M., 46, (1954) 973.

F. Effect of Quenching Temperature on the Yield Parameters of Tantalum

1. Introduction

Segregation of impurity atoms to a dislocation reduces the associated elastic strain energy, thus locking the dislocation in position and a binding energy, U, can be ascribed to the dislocation and its associated impurity atoms[1]. It is assumed that the concentration C of interstitial atoms associated with a dislocation is related to the binding energy and the temperature by the usual Boltzmann expression:

$$C = C_o \, e^{U/kT} \qquad (1)$$

where C_o is the concentration of impurity in the matrix, k is Boltzmann's constant, and T is the absolute temperature. Thus, C increases as the temperature is lowered. Since the stress required to separate a locked dislocation from its atmosphere increases as the concentration of interstitial atoms in the atmosphere increases, k_y also increases with decreasing temperature.

When, on increasing the temperature, $C = C_o$ the discontinuous yield will disappear. In high temperature tensile tests the yield point in iron disappears at 700°K[2] and in commercial tantalum at 815°K[3]. However, in these tests there is an appreciable thermal contribution to unlocking during the test and consequently equation (1) is not directly applicable. Low temperature testing of specimens quenched from high temperatures, so that the impurity distribution of the high temperatures is frozen in , removes this difficulty by ensuring that the thermal contribution is constant from test to test. Thus, any changes observed are due to changes in the impurity distribution. This is the method adopted in the present work.

2. Procedure

Two-foot lengths of 0.030 inch diameter Ta-E2 wire (50 ppm C, 12 ppm N and 12 ppm O) were annealed by resistance heating for 6 minutes at 1000°C (1273°K) in vacuum and cooled by switching off the current. The apparatus is described in Progress Report No. 2. The resulting grain size was 0.0012 mm. Specimens, each four inches long, were cut from the annealed wires and mounted in a specially constructed quenching apparatus (Fig. 129). The electrical leads into the glass vacuum chamber are arranged so that when the specimen is fixed in position a small tension is exerted. The temperature is measured by a thermocouple (0.002 inch diameter wires) welded to the specimen.

In this series of experiments the specimen was slowly heated to 920°C (1190°K) by passing a current through it. The total time to reach 920°C was one hour, during which time appreciable outgassing occurred. The specimen was held at this temperature for one minute. The current was then reduced sufficiently for the specimens to be cooled to the prequench temperature of 520°K, 710°K, 810° K, 860°K, 910°K, 1060°K, or 1190°K. The times held at these temperatures were 4 minutes, 3 minutes, 3 minutes, 2 minutes, 2 minutes, 1 minute and 1 minute respectively.

To quench the specimen the thin aluminum foil diaphragm was broken by means of a plunger and brine at -10°C was sucked into the apparatus. The current was left on during the quench to remove the possibility of some slow cooling occurring just before quenching. The power supplied by the current can be absorbed by the brine with negligible temperature effect. The current was switched off as soon as possible after the foil had been broken. After removing the specimen from the apparatus the center 1.5 inches was carefully cut out and stored in liquid nitrogen.

The specimen was chemically polished and returned to liquid nitrogen to await testing. The tensile test was performed at room temperature with a strain rate of 2.5×10^{-2} min^{-1} using a hard beam Polanyi tensile machine. The gauge length was one inch and the total time at room temperature from quench to yield was about 15 minutes.

3. Experimental Results

Typical load-elongation curves for different quenching temperatures are shown in Fig 130. These curves were analyzed by the extrapolation method[4] and n, σ_i and k_y were measured. The interrelated variables n and σ_i did not change with quenching temperature (Fig. 131).

The graph of k_y versus quenching temperature is shown in Fig. 132. The points marked with open triangles correspond to stress-strain curves with no Luders plateau. The value of k_y in these cases was obtained by taking the offset stresses marked in Figure 130 curves E and F. Consequently, there is some uncertainty and the curve (Figure 132) has not been continued through these points.

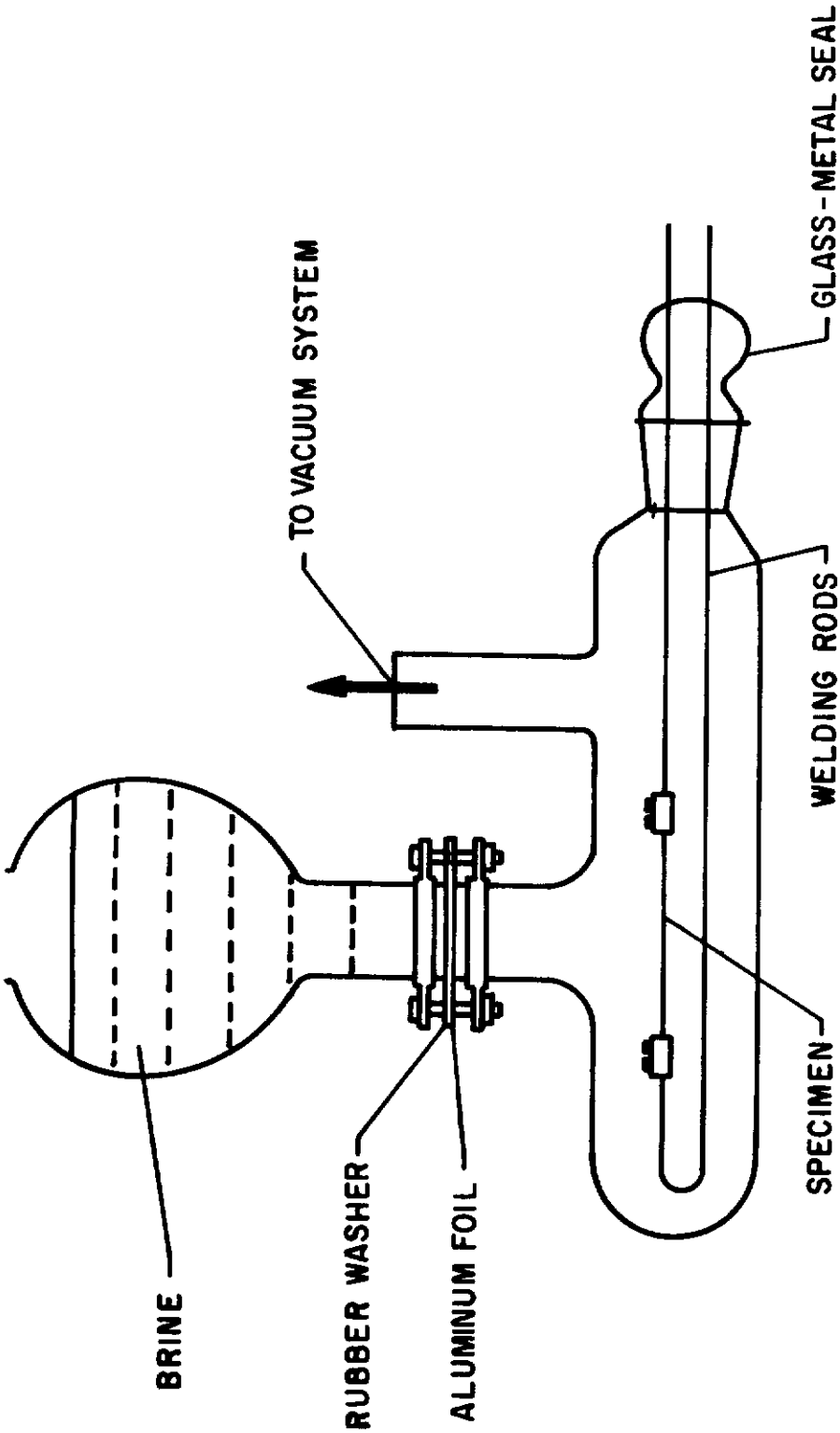

Fig. 129-Diagram of the quenching apparatus

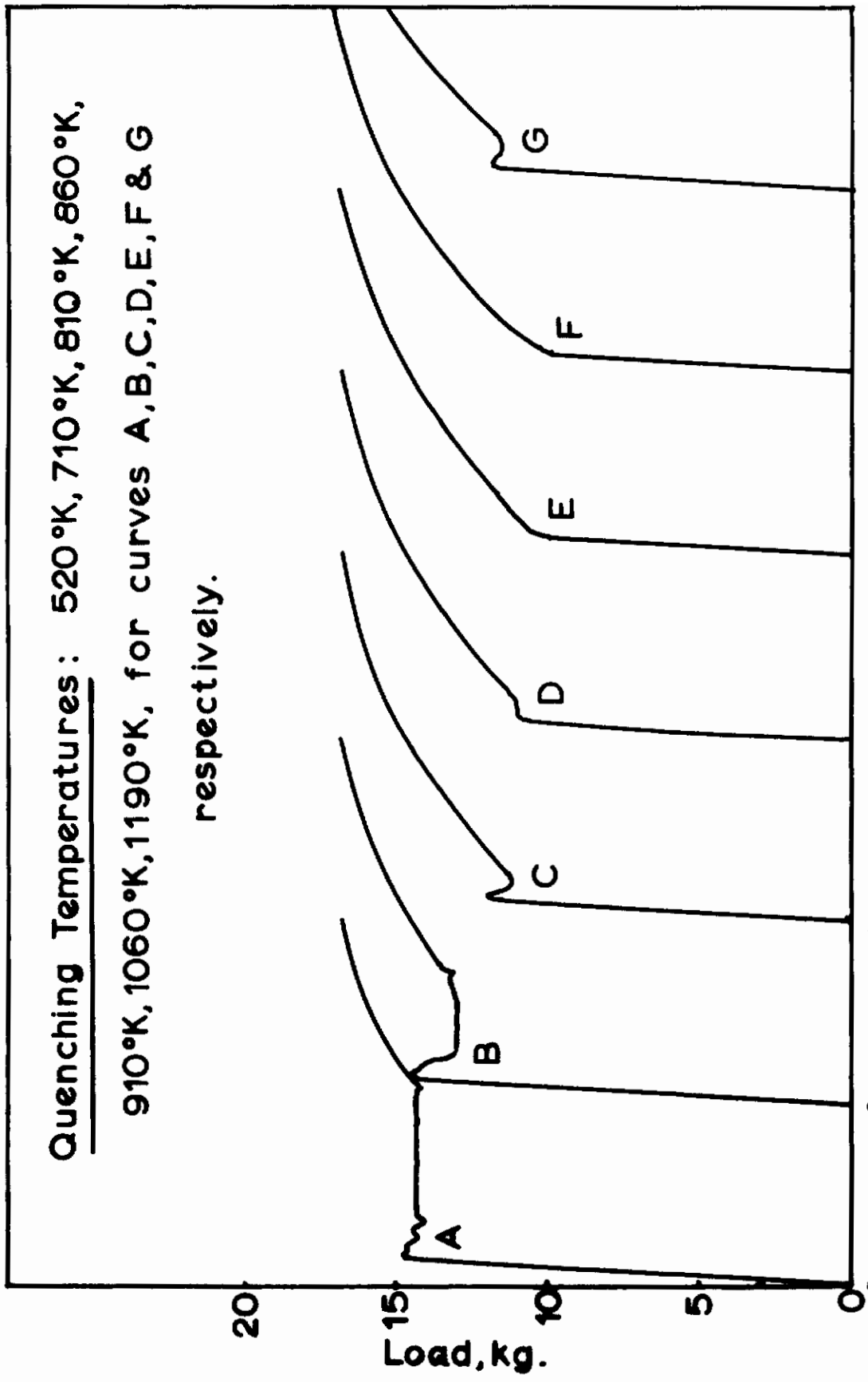

Fig. 130 Load-elongation curves for tantalum quenched from various temperatures

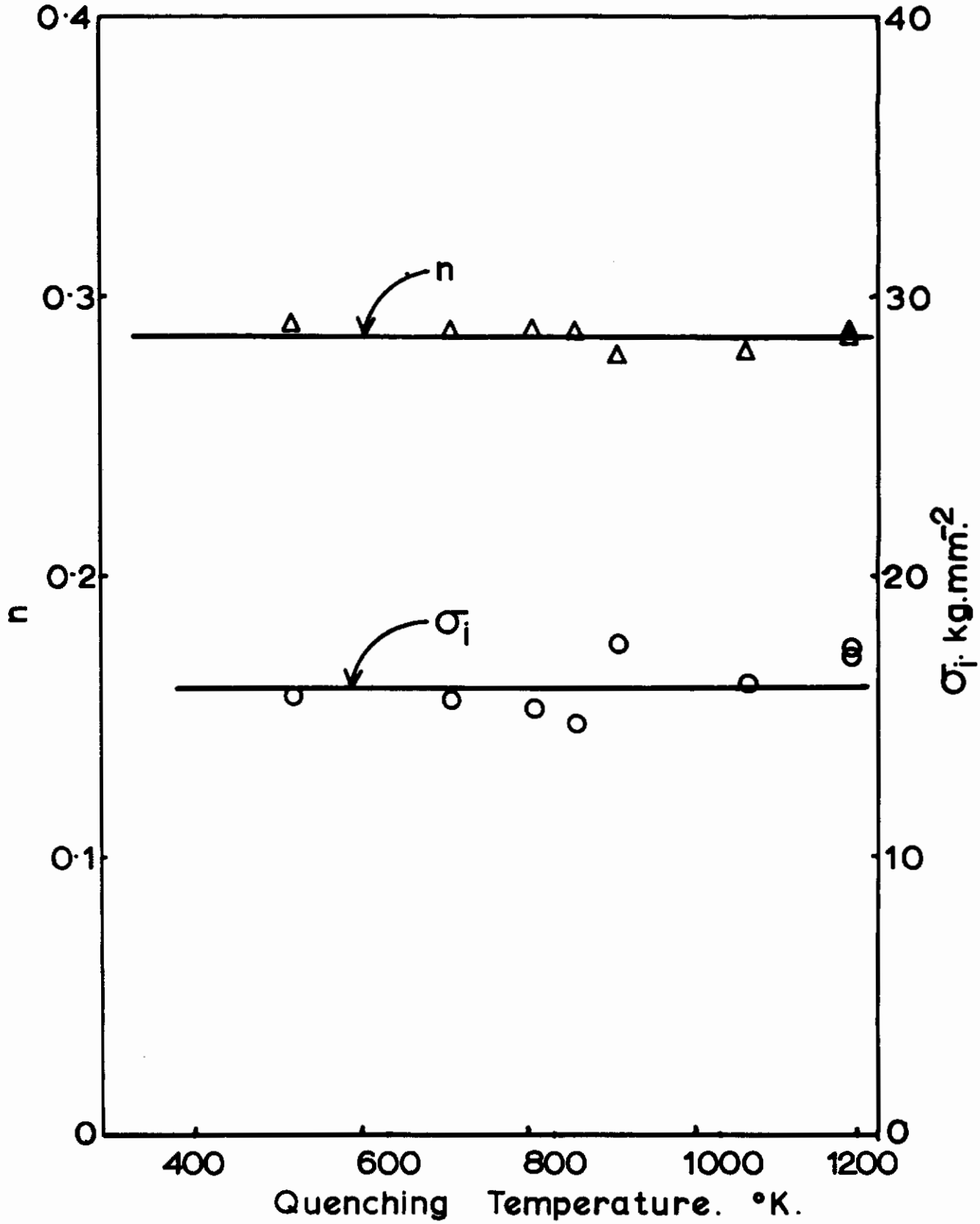

Fig. 131 - Variation of σ_i and n with quenching temperature for tantalum.

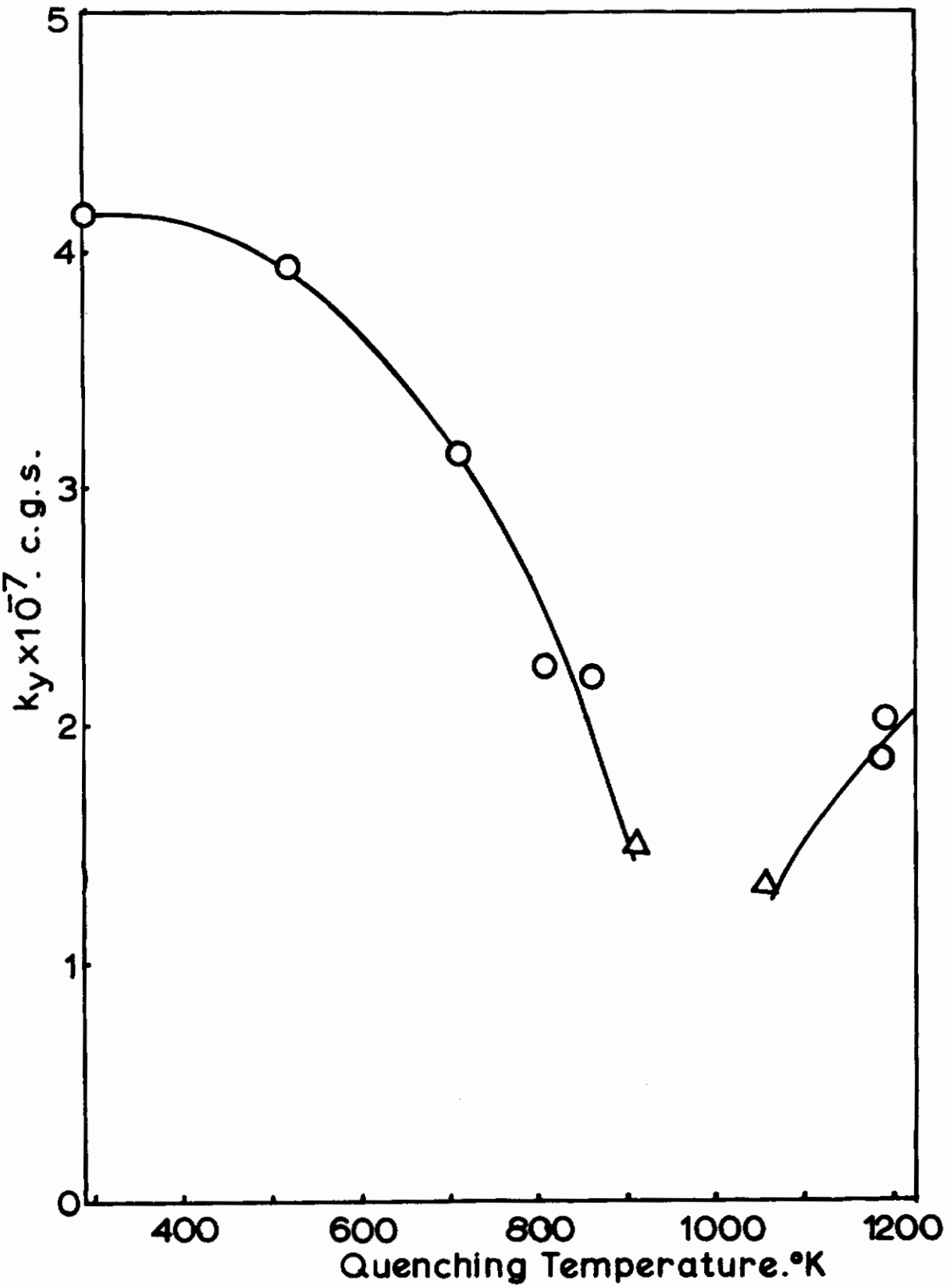

Fig. 132-Variation of k_y with quenching temperature for tantalum.

4. Discussion

The only deformation parameter which changes significantly with quenching temperature is k_y. This parameter is a measure of the difficulty of propagating yield from grain to grain. Modern ideas envisage the stress at the tip of a slip band stopped at a grain boundary generating new dislocations in the next grain. These dislocations then multiply and the grain yields. In slowly cooled material the dislocations are strongly locked, and it is probably easier to generate new dislocations at or near the grain boundary than to unpin the locked dislocations. This process is not thermally activated and k_y does not vary with testing temperature. However, in quenched iron, k_y is markedly temperature dependent [6]. Thus, it seems that thermally activated unpinning is a more probable mechanism for the generation of dislocations in this case. The temperature dependence of k_y in the quenched tantalum specimens has not yet been determined; but, for the present, it will be assumed that the same unpinning mechanism is operative. It is difficult to explain a variation of k_y with quenching temperature on any other basis. The decrease in k_y on increasing the quenching temperature from 293° to 950°K (Figure 132) is probably due to a decrease in the concentration of solute condensed on the dislocation line as the temperature is raised.

However, when the quenching temperature is increased between 1000° and 1200°, k_y increases. A similar effect can be observed on the stress-strain curves obtained by Pugh [3] on testing commercial tantalum at elevated temperatures, although the effect occurs in a somewhat lower temperature range. The reason for the increase in k_y at high temperatures is not known although the following possible reasons for the increase in k_y have been considered:

(1) contamination of the tantalum either during annealing or on quenching. This seems unlikely because σ_i for the quenched specimens does not increase appreciably between 1000° and 1200°K (Fig. 131). Comparing σ_i for annealed Ta-E2 with that for Ta-E4 shows that an increase of about 150 ppm oxygen increases σ_i significantly (section C, this report).

(2) quenched-in vacancies condensing on dislocations to form jogs. This effect would also be expected to increase σ_i. All the specimens were annealed at 1275°K before the quenching treatment and it is unlikely that the jog density established at this temperature would be appreciably modified by subsequent quenching from lower temperatures.

(3) changes in the configuration or composition of the condensed atmosphere. Where three species of interstitial solute with markedly different diffusivity [5] are present, the variation of the composition of the condensed atmosphere with temperature is extremely complex. However, it is unlikely that any change in the atmosphere would produce an increasing k_y with increasing temperature.

The minimum concentration of interstitial which will give effective pinning, and thus a positive value of k_y, is one interstitial atom per atom plane

intersecting the dislocation line i.e., C = 1 in equation 1. k_y approaches zero at 950°K (Fig. 132). Substituting these values in equation 1 and taking C_o as the total interstitial concentration gives the binding energy as 0.53 e.v. per atom. It is not known which of the interstitial elements (carbon, nitrogen or oxygen) is the most effective locking agent at this temperature and consequently the binding energy deduced is some average value. If only one element is condensing on the dislocation the appropriate value of C_o would be appreciably smaller than the total concentration of interstitials. However, the value of the binding energy obtained by the use of equation 1, is insensitive to errors in C_o or in the temperature for zero k_y. For example, if the chosen C_o is in error by a factor of 2 and temperature is incorrectly estimated by 100°C, the binding energy is 0.53 ± 0.1 e.v.

5. References

1. A.H. Cottrell and B.A. Bilby, "Dislocation Theory of Yielding Strain Aging of Iron," Proc. Phys. Soc., 62 (1949) 49.

2. N.F. Mott "Imperfections in Nearly Perfect Crystals," Wiley, New York (1950).

3. J.W. Pugh, "Tensile Properties of Tantalum," Trans. A.S.M. (1956), 48 677.

4. A. Gilbert, D. Hull, W.S. Owen, C.N. Reid, J. Less Common Metals, (1962) in press.

5. R. W. Powers and Margaret V. Doyle, "Diffusion of Interstitial Solutes in the Group V Transition Metals," J. of App. Phys., 30 (1959), 514.

6. R. M. Fisher - private communication.

G. Strain Aging of Tantalum

1. Introduction

It is now realised that dislocation nucleation may occur by a variety of processes, the operative process being determined by the strength of dislocation locking[1], and being characterized by the value of k_y. A small and temperature dependent value of k_y is evidence of slip nucleation being caused by the unlocking of weakly locked dislocations, while a large and temperature independent k_y is evidence of slip nucleation from non-thermally activated sources, such as grain boundaries. Increased resistance to the motion of glide dislocations, which causes changes in σ_i, may also result from the presence of locked dislocations in the lattice. Thus, it is important to examine the progress of ageing in relation to the yield parameters k_y and σ_i.

Wilson and Russell[2] have used the Petch technique[3] to measure the effect of ageing on both σ_i and k_y for a commercial rimming steel. They find a first stage of ageing, characterized by an increase in k_y and later stages characterized by changes in σ_i. The first stage is assumed to be due to the progressive segregation

of impurity atoms to dislocations, increasing the difficulty of unlocking and thus increasing k_y. The later constancy of k_y is due to unlocking becoming more difficult than the other possible nucleation mechanisms and the increase in σ_i is due to the increased interference offered by locked dislocations to the motion of glide dislocations.

Recently, Stein and Low[4] have found an earlier stage of strain ageing in an iron-silicon alloy. They noted that ageing times of about one minute at 100°C were sufficient to restrict the number of dislocations heterogeneously nucleated from a scratch. They did not determine whether this stage was due to an increase in the difficulty of dislocation nucleation (k_y) or dislocation glide (σ_i).

The experiments described in this section were performed in order to determine the ageing stages in tantalum by examining the effect of ageing time on σ_i and k_y. The effect of prestrain without ageing was studied to determine the parameters of the as-deformed material and temperature change tests were included to investigate the effects of various prestrain-induced substructures on σ_i and k_y.

2. Procedure

0.030 inch diameter wires of TaE1C (92ppm oxygen) were vacuum annealed by a procedure described in earlier reports.[5] Unless otherwise noted, all specimens were annealed at 1050°C for 6 minutes to establish a grain size of 0.04-0.06 mm ($d^{-1/2}$ = 4-5 $mm^{-1/2}$).

Three types of experiments were performed:

(1) Extension to fracture of as-annealed wire, carried out at a series of temperatures between 77°K and 293°K, in order to determine the engineering tensile properties of the material. These were carried out in accordance with the procedure used previously[5]. Values of σ_i, n and k_y were determined by the extrapolation technique[5].

(2) 10% prestrain of as-annealed wire followed by restrain to fracture at either the same or a different temperature. When prestrain and restrain were carried out at the same temperature, the interval between the two applications of strain was about 30 seconds. In experiments where restrain was carried out at a different temperature, the interval was about 2 minutes. Only σ_i and n could be calculated for these specimens, since there was no yield drop and as a result, k_y was zero. The cumulative strain was used in determining σ_i and n. Thus, for the purposes of calculation, a point corresponding to 5% strain on the restrain part of the curve was treated as 15% total plastic strain. If this procedure had not been followed, the curves for specimens prestrained and restrained at the same temperature would exhibit different values of σ_i and n. This cannot be the case since examination of the tensile curves shows that unloading has no effect on the restrain curve.

(3) 10% prestrain of annealed wires followed by ageing for various times in an oil bath maintained at 100 ± 1°C. These specimens were then restrained to fracture. Cumulative strain was again used to determine σ_i and n.

k_y was determined from the relationship

$$\sigma_y' = \sigma_f + k_y d^{-1/2} \quad (1)$$

where σ_y' is the strain-aged yield point and σ_f is the flow stress immediately prior to unloading. Thus,

$$\sigma_y' = \sigma_i + K\epsilon_p^n + k_y d^{-1/2} \quad (2)$$

where K is the strength constant and ϵp is the prestrain.

3. Results

Fig. 133 shows the engineering properties of TaE1C wire of an intermediate grain size (0.09 mm) and Fig. 134 shows the same data for a coarse grain size (0.027 mm) tested for comparison. These properties versus temperature curves are the same as noted in previous work on this project. An increase in grain size reduces the Luders strain, uniform elongation, yield stresses and ultimate stresses. An exception is noted in the effect of grain size on yield stress at -196°C, where the coarser grained material has slightly larger yield stresses. This effect has been noted by Adams and Ianucci[6], and is due to the uncertainity in yield stress measurements below the plastic instability transition temperature.

Fig. 135 is a comparison of the lower yield stress and uniform elongation of TaE1C and TaE4 of the same grain size. The main difference between these materials is the oxygen content (92 ppm vs 147 ppm) and the curves show the large effects of this interstitial on the tensile behaviour of tantalum.

Fig. 136 shows the results of the prestrain experiments. Since 77°K is below the plastic instability transition temperature T_{PI}, it was not possible to measure σ_i and n for annealed specimens tested at this temperature. However, since prestrain at room temperature or 195°K suppressed the yield point, it was possible to measure these quantities at 77°K by method 2 as outlined in the procedure section G2. Room temperature prestrain produced a lower value of σ_i and a correspondingly higher value of n at 77°K, as would be expected if the hardening induced by a given amount of strain were more effective the lower the temperature at which the strain was produced. Room temperature prestrain did not alter σ_i and n for specimens restrained at room temperature or at 195°K. However, prestrain at 195°K significantly lowered n for room temperature restrain. The magnitude of the corresponding rise in σ_i is small, due to the small as-annealed value of σ_i and the fact that σ_i bears a logarithmic relation with n.

The kinetics of the yield point return are shown in Fig. 137. These data are quantitatively comparable with results obtained for the ageing of iron-carbon alloys[7]. Such a result is to be expected, since oxygen in tantalum has a diffusion coefficient[8] close to that of carbon in α-iron while diffusion rates of carbon and nitrogen in tantalum are many orders of magnitude slower. It is concluded that oxygen is the principal contributor to the locking of dislocations in tantalum Ta-E1C.

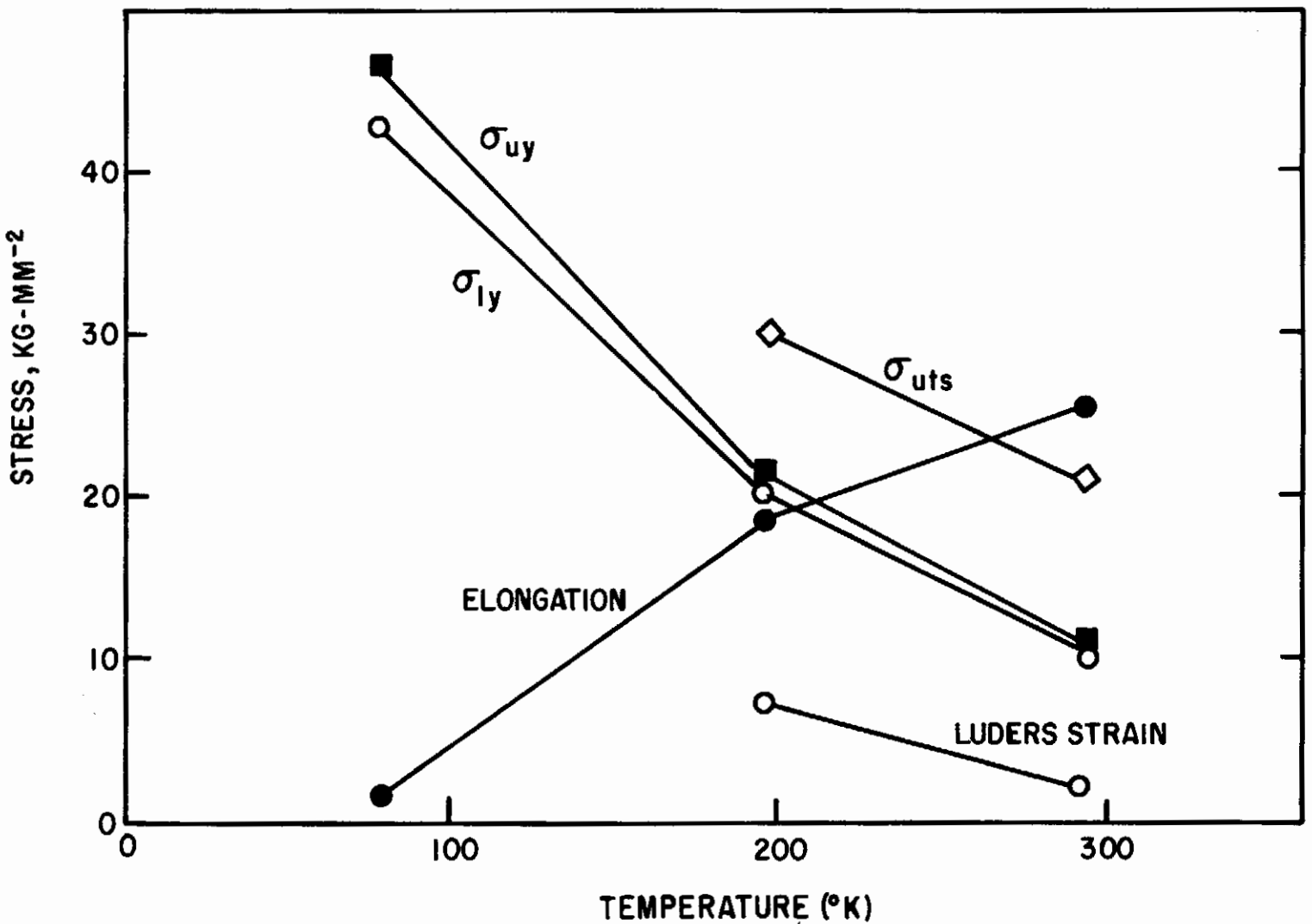

Fig. 133 - Tensile properties of Ta-El C; $d^{-1/2} = 4.7$

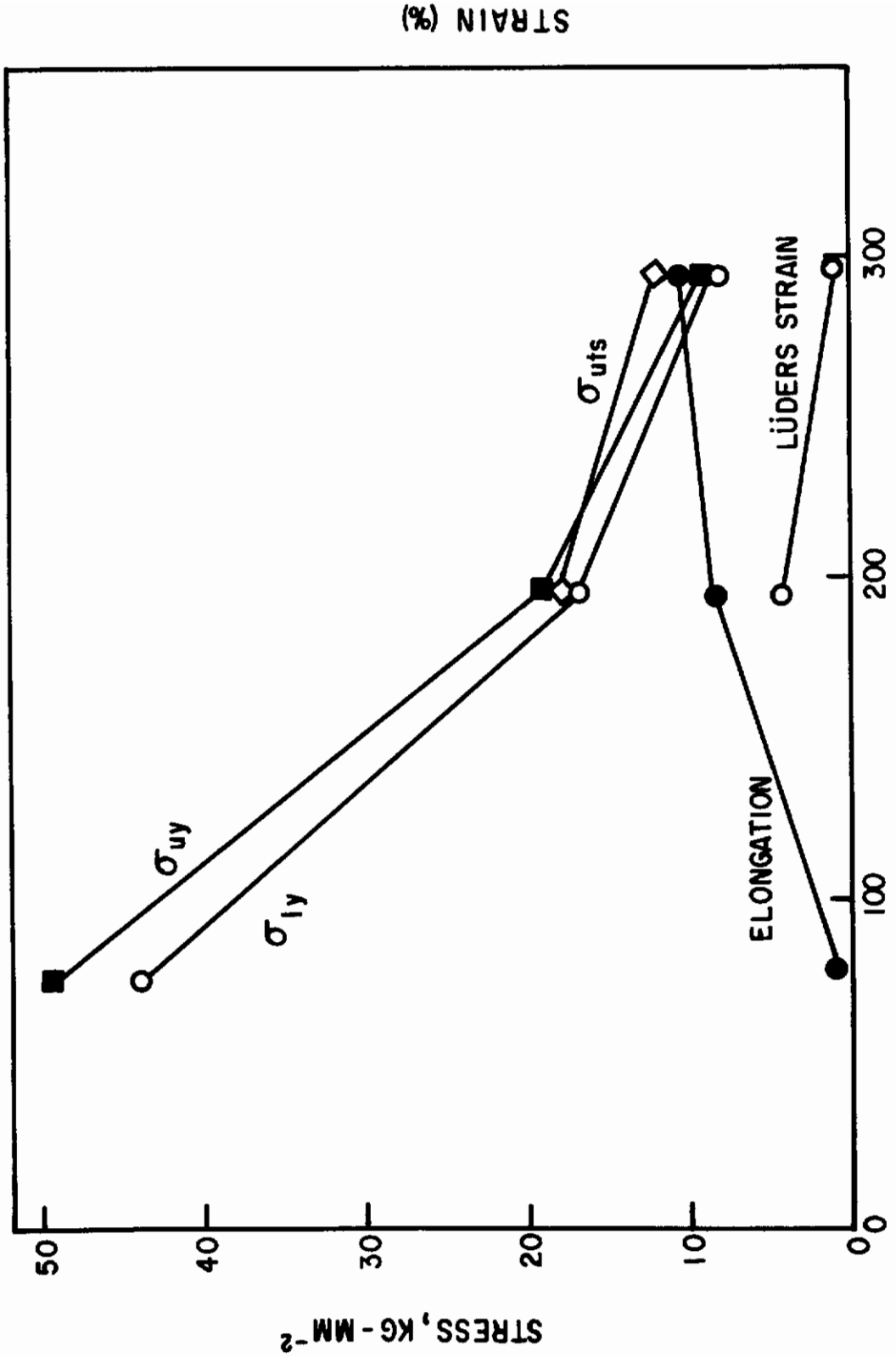

Fig. 134 - Tensile properties of Ta-El C, $d^{-1/2} = 2.6$

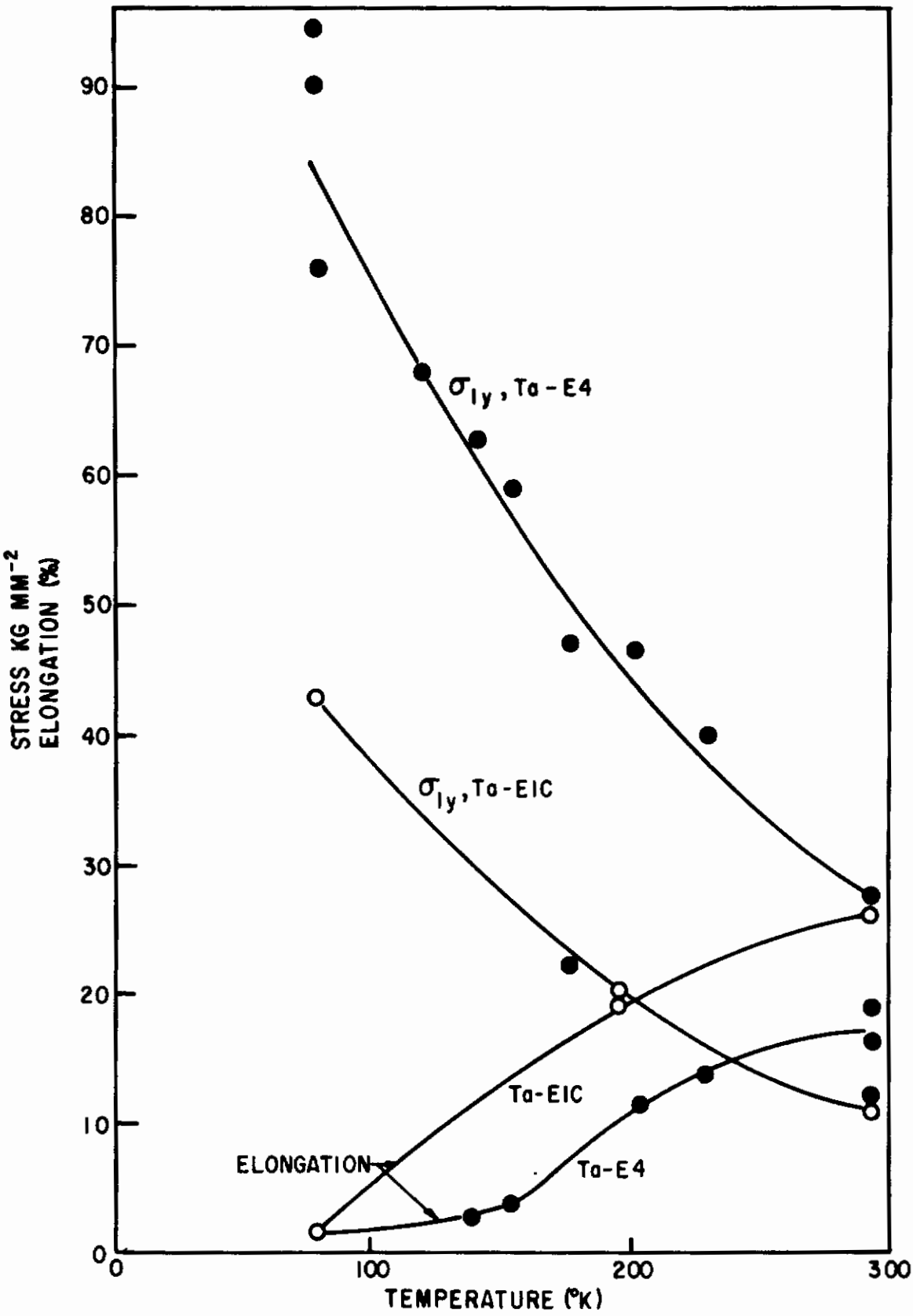

Fig.135 Comparison of tensile properties of Ta-EI C and Ta-E4, $d^{-1/2} = 4.7$

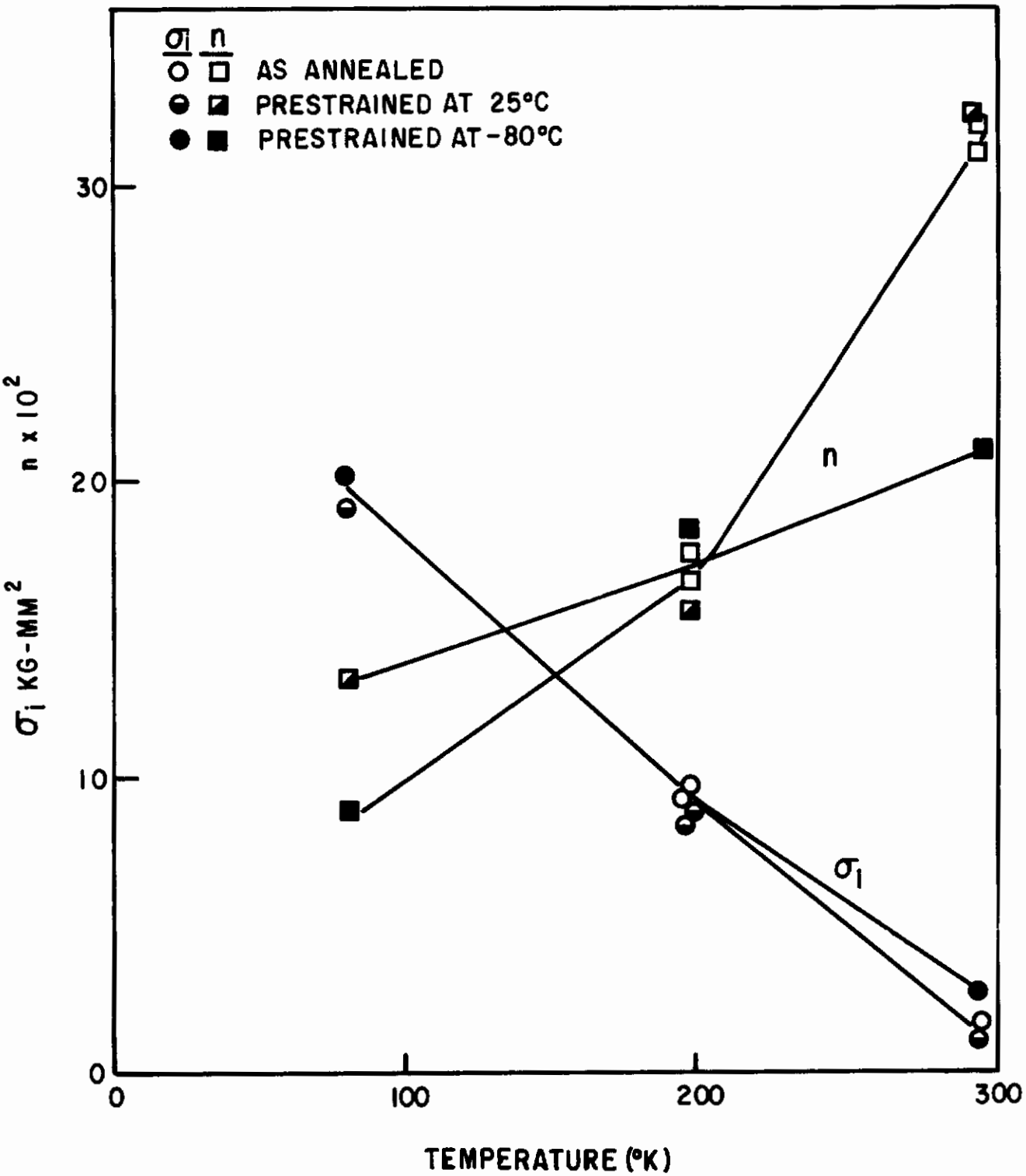

Fig. 136 - Effect of prestrain and temperature on σ_i and n.

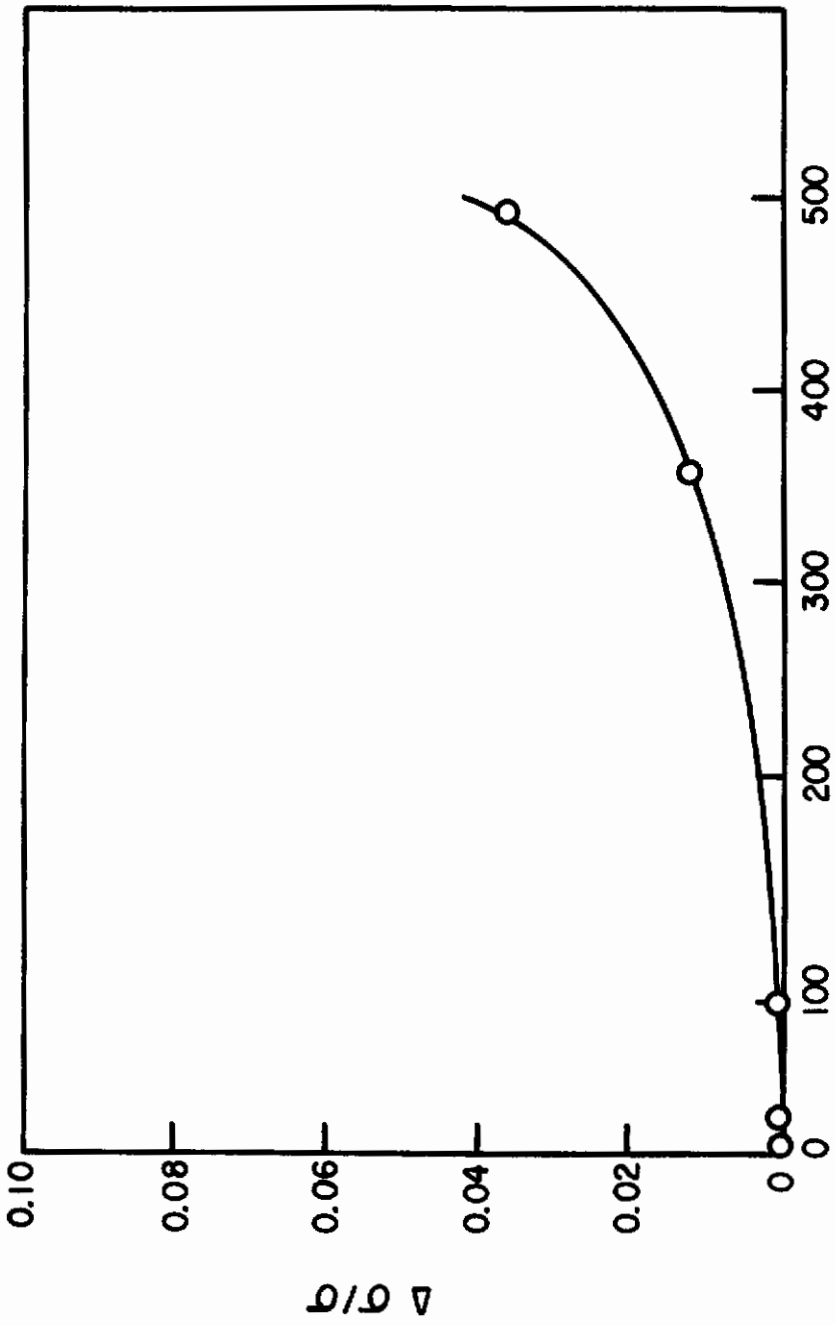

Fig. 137 - Effect of aging time on the magnitude of the yield drop.

Although there was no increase in flow stress until after 10 minutes of ageing, there was a small but measurable change in the shape of the stress-strain curve after only one minute. A typical example is shown in Fig.138 for a specimen prestrained and restrained at room temperature. This change is manifest as an increase in σ_i and a decrease in n and Fig.139 is a plot of the effect of ageing time on these quantities. The change in σ_i in the first ten minutes of ageing is found to be about 15% and σ_i remains constant for the ageing times beyond ten minutes. The next increase in flow stress, which reflects the reappearance of the yield point, was not noted until after 1 hour ageing time (Fig.137).

Specimens aged less than 10 minutes exhibited unstable stress-strain curves soon after the start of plastic deformation. This was especially accentuated in specimens tested at room temperature after prestraining at 195°K. Where aging for only one minute was sufficient to produce the effect. Fig.140 shows the effect of ageing time at 100°C on k_y. Although the first noticeable change in k_y takes place in one hour, the value of k_y reached after 180 minutes was only 10% of the value for slowly cooled (i.e., fully aged) specimens. In contrast, Wilson and Russell[2] were able to age to about 35% of the fully aged value of k_y, at the end of their first stage. Longer ageing times should increase k_y further, since it is likely that 3 hours at 100°C does not represent the end of the Wilson-Russell first stage.

4. Discussion

The presence of a very early stage in the strain-hardening process, as found by Stein and Low[4], has been confirmed. This stage is manifest by an increased difficulty in dislocation propagation (σ_i), and not in dislocation nucleation (k_y). Such an increase can be explained by Snoek ordering of interstitials in the strain field of a dislocation[9]. This mechanism requires only short range diffusion, and thus, short ageing times. Eshelby[10] has calculated the change in yield stress due to Snoek effect. For iron-carbon alloys

$$\Delta \sigma_i = {}^2/_3 \mu C \qquad (3)$$

where μ is the shear modulus, and C is the interstitial content. For tantalum the misfit strain of oxygen atoms is only one-third of that of carbon atoms in iron[11]. Thus, for tantalum:

$$\Delta \sigma_i = {}^2/_9 \mu C \qquad (4)$$

Since $C \cong 10^{-2}$, $\Delta \sigma_i \cong 5$ kg/mm^2, which compares fairly well with the measured $\Delta \sigma_i$ of 3 kg/mm^2. Lautenschlager and Brittain [12] have recently observed an effect of similar magnitude in iron-carbon alloys.

The next stage of strain ageing corresponds to Wilson and Russell's[2] first stage. It is the result of long-range diffusion of interstitials to dislocations, to give weak locking. Currently, longer ageing times are being employed to find the completion of this stage and the extent of the next one, which is expected to be characterized by a rise in σ_i, if the behaviour of tantalum is analogous to that of iron.

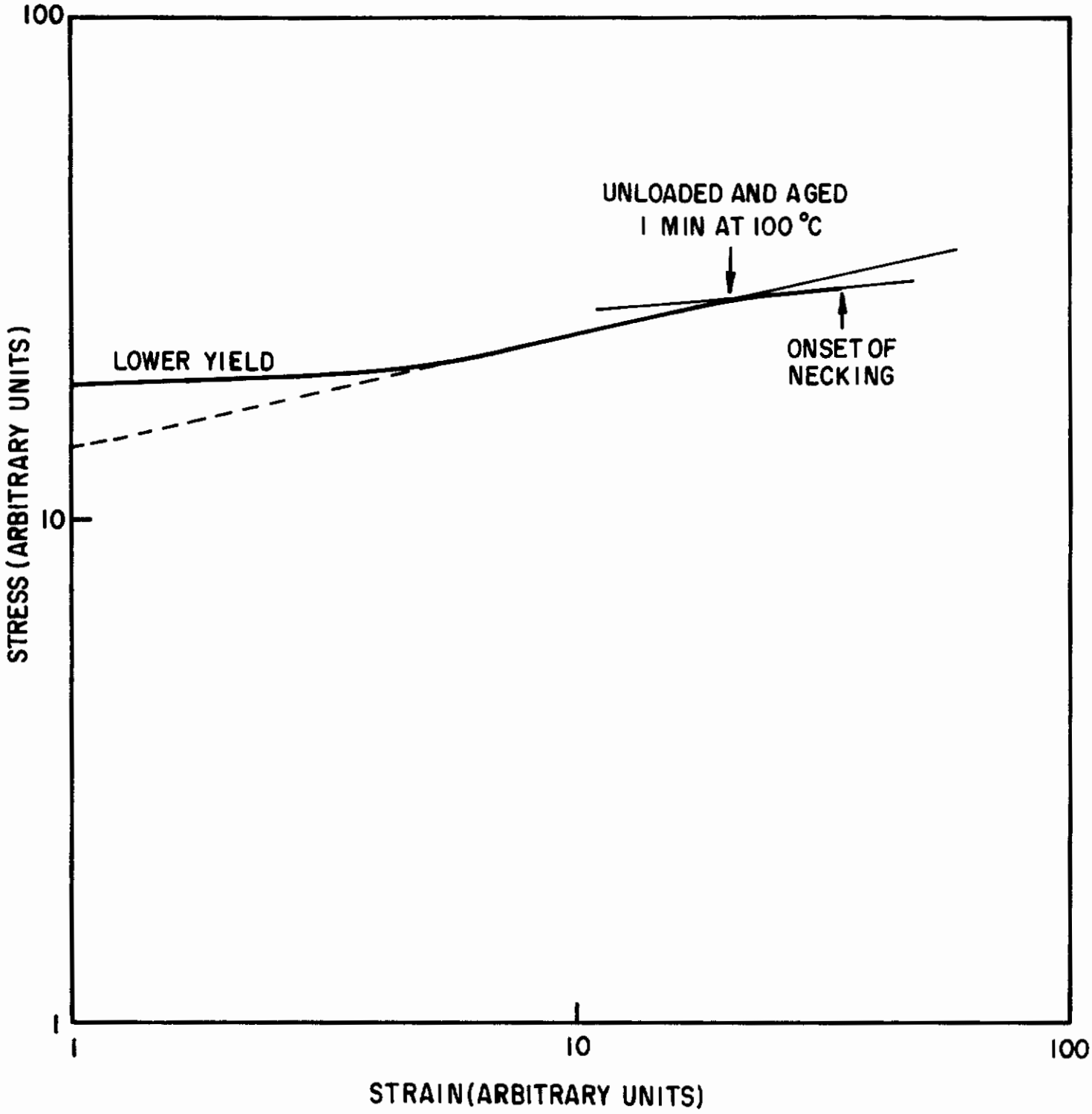

Fig. 138 - Effect of aging in the stress-strain curve

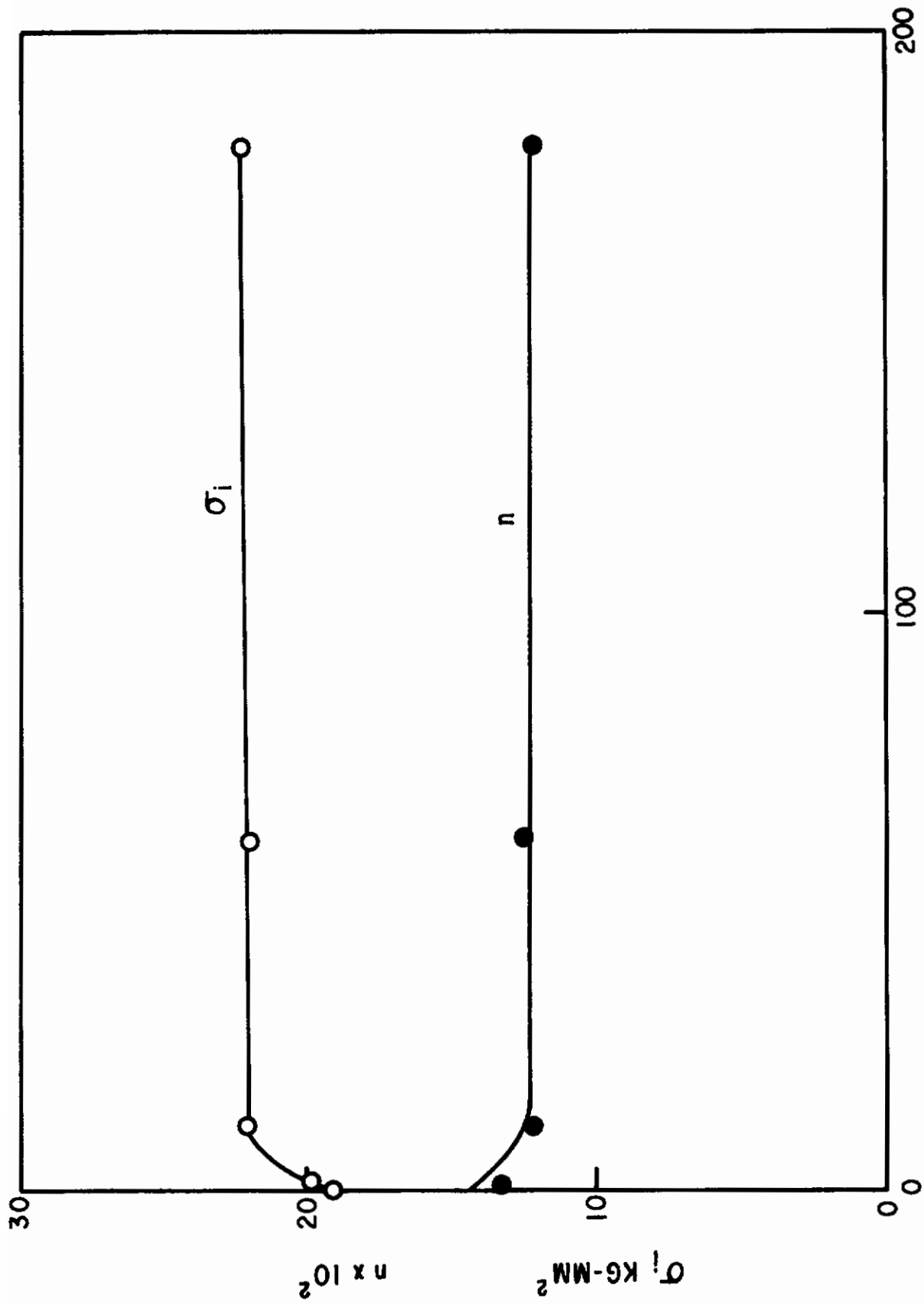

Fig. 139 - Effect of aging on σ_i and n

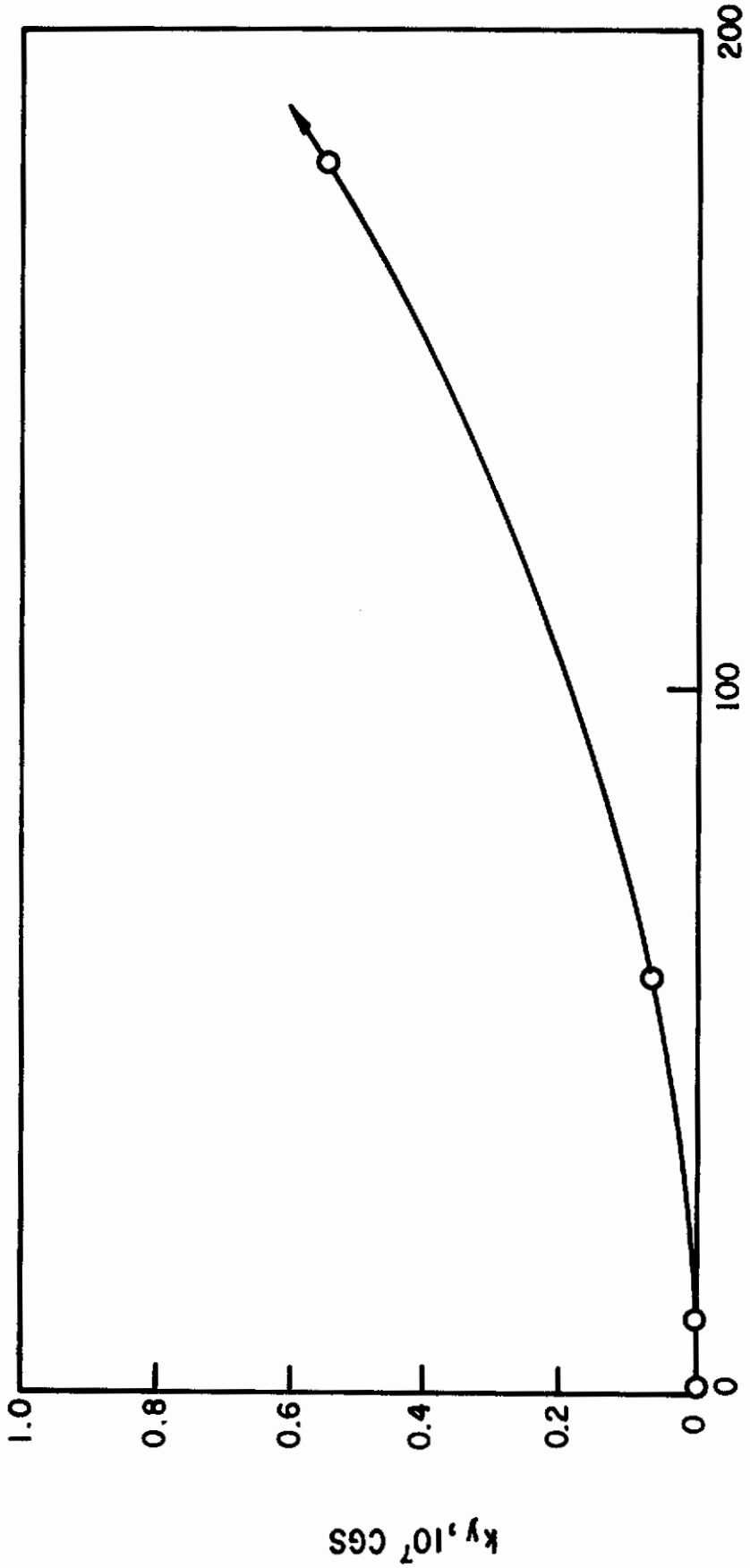

Fig. 140 - Effect of aging on k_y. In fully aged condition $k_y = 5.9 \times 10^7$ c.g.s.

5. References

1. R.W. Fisher, private communication.
2. D.V. Wilson and B. Russell, Acta Met., 8, (1960) 36.
3. N.J. Petch, J. Iron & Steel Institute, 174, (1953) 25.
4. Dale Stein and J.R. Low, to be published.
5. Progress Report II.
6. M.A. Adams, private communication.
7. T. Mura, E.A. Lautenschlager and J.O. Brittain, "Segregation of Solute Atoms During Strain Ageing", Acta Met., 9, (1961) 453.
8. Powers and Doyle, op cit.
9. D.V. Wilson and B. Russell, "Stress Induced Ordering and Strain-Ageing in Low Carbon Steels," Acta Met., 7, (1959) 628.
10. J.D. Eshelby, ibid, appendix October AIME.
11. Dale A. Vaughan, Oliver M. Stewart and Charles M. Schwartz, "Determination of Interstitial Solid-Solubility Limit in Tantalum and Identification of Precipitate Phases", Trans. A.I.M.E., 221, (1961) 937.
12. E. Lautenschlager and J.O. Brittain, "The Influence of the Temperature of deformation on Strain Ageing of Alpha-Iron", Trans. A.I.M.E., 224, (1962) 48.

H. Deformation Substructure in Tantalum

1. Scope

Ta-E4 foils with a low initial dislocation density and a large grain size have been deformed in tension at 293° and 240°K. The results are compared with those obtained from parallel experiments or Ta-E1 with a high initial dislocation density. The substructure produced by different increments of strain was examined by transmission electron microscopy. The role of grain boundaries in dislocation generation during deformation was also examined.

The increase in flow stress with increasing strain is related to the increase in dislocation density

$$\sigma_f = \sigma_o + \alpha\mu b\sqrt{N} \qquad (1)$$

where α is a geometric constant, μ the shear modulus, b the Burgers vector and N the dislocation density. The significance of σ_o in equation 1 is discussed.

2. Experimental Procedure

Thin cold-rolled sheets of Ta-E4 were annealed at 1750°C and 1200°C respectively giving a grain size of $d^{-1/2} = 2.8$ mm$^{-1/2}$ and an initial dislocation density of 1×10^9 cm^{-2} for Ta-E4 and $d^{1/2} = 4.0$ mm$^{-1/2}$, $N = 5 \times 10^{10}$ cm^{-2} for Ta-E1. Tensile specimens approximately 0.4 cm wide, 0.003 in. thick with a gauge length of 2.0 cm were cut from the sheet. Copper foil was stuck to each end of the specimen with opoxy resin and these collars were then soldered into the chucks of the tensile machine with Wood's metal. The specimens were tested in tension at a strain rate of 1.7×10^{-2} mm^{-1} at 293°, 240°, 206° and 78°K.

Separate series of specimens were pulled to selected strains, unloaded, thinned and examined by transmission electron microscopy.

3. Results

3.1 Tensile Results

Typical stress-strain curves are shown in Figs. 141 and 142. The values of σ_f^o and b_y (obtained by the extrapolation method) and σ_y and n are listed in Table 35. In the tests at 206° and 78°K necking occurred before the Luders strain was complete, and, consequently, it was not possible to obtain the yield parameters. The only exception was one Ta-E4 specimen tested at 206°K as shown by the dashed curve in Fig. 142.

3.2 Electron-Microscopy Observations

a) Ta-E4 strained at 293°K - Ta-E4 specimens were strained 0.9, 1.1, 2.2, 2.8, 4.3, 6.2, 7.5 and 10.0 percent. The change in dislocation density with strain is shown in Fig. 143. Typical arrangements of dislocations after 2.8, 4.3 and 10 percent strain are shown in Figs. 144, 145 and 146. A prominent feature was the progressive increase in the number of dislocations near grain boundaries. The tendency to the formation of cellular substructure with increasing deformation was not marked, the main observation being an increase in the dislocation entanglement.

Dense bands of dislocations (slip bands) were occasionally observed, Fig. 147. Fig. 148 shows a slip band blocked at a grain boundary which has generated dislocations in the adjacent grain.

b) Ta-E4 strained at 240°K - Specimens were strained 1.7, 2.5, 3.4, 5.3, 6.9 and 10.0 percent. Optical examination of the surface of specimens strained less than 5 percent revealted well defined boundaries to the Luders bands. Fig. 149 shows the Luders regions in an isolated specimen which fractured at an elongation less than the Luders strain. The change in substructure from yielded to unyielded material is shown in Figs. 150, 151 and 152.

Table 35

Results from Extrapolation of Stress-Strain Curves for Ta-E4 strained at 293°, 240°, 206°K and Ta-E1 strained at 293°K

Specimen	Testing Temperature °K	σ_y Kg.mm^{-2}	σ_f^o Kg.mm^{-2}	n	k_y c.g.s. units	d$^{-1/2}$ mm$^{-1/2}$
Ta-E4	293	22.2	14.7	0.25	8.5×10^7	2.8
Ta-E4	240	25.4	19.6	0.12	6.5×10^7	2.8
Ta-E4	206	42.3	36.0	0.09	7.1×10^7	2.8
Ta-E1	293	17.7	10.2	0.27	5.9×10^7	4.0

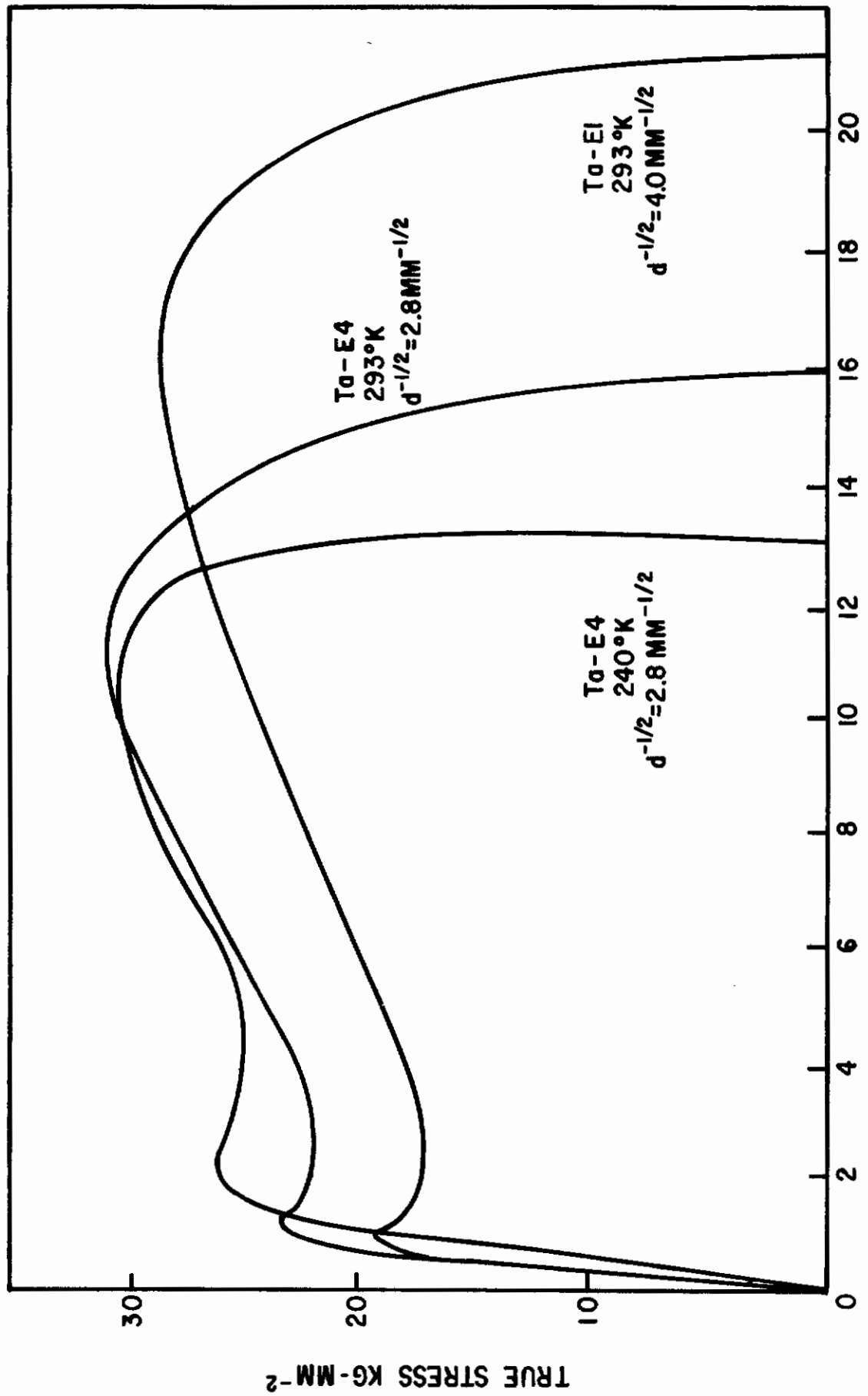

Fig. 141 - Stress-strain curves for Ta-E4 strained in tension at 293° and 240°K and Ta-E1 strained in tension at 293°K

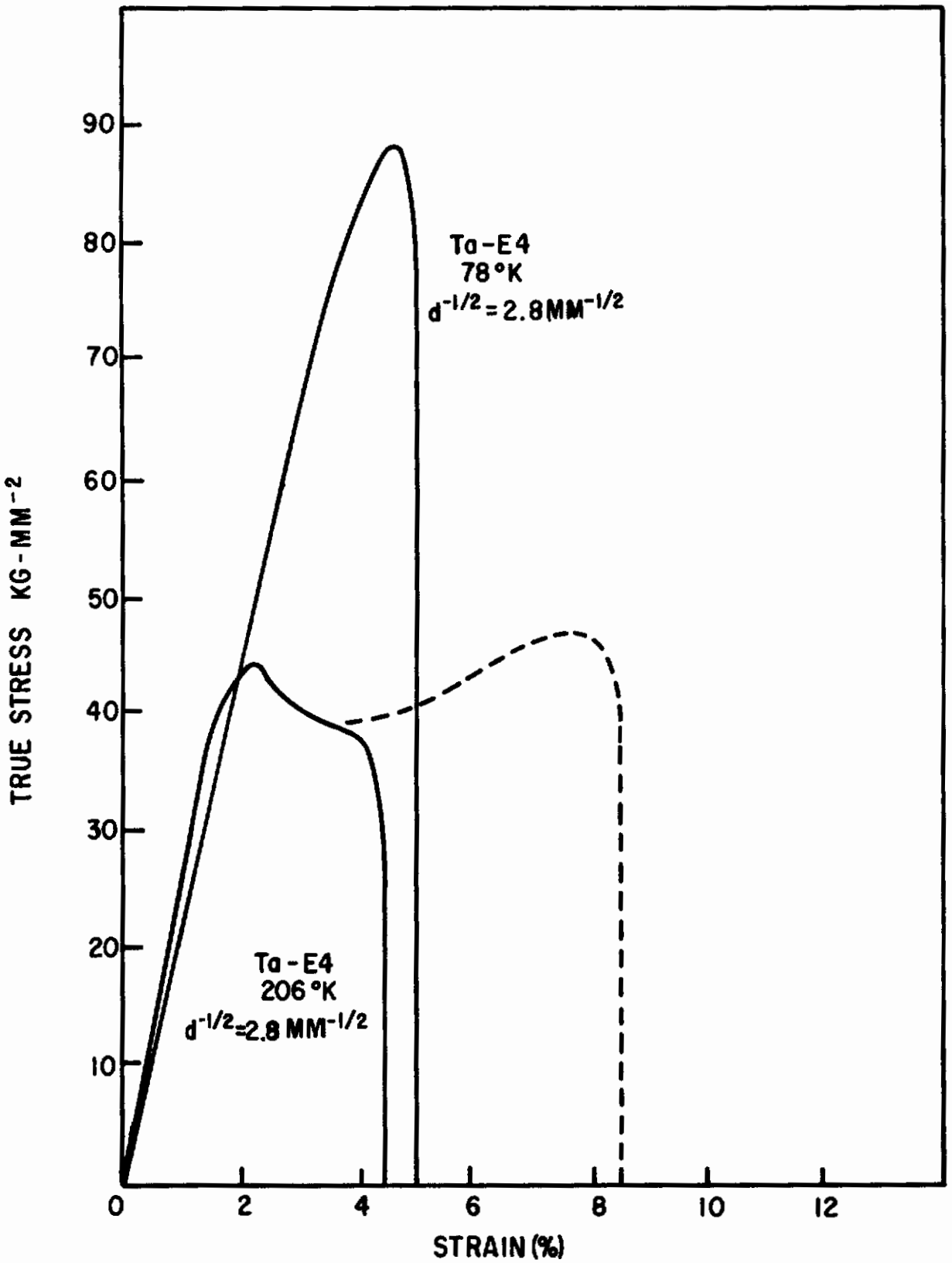

Fig. 142 - Stress-strain curves for Ta-E4 strained in tension at 206° and 78°K.

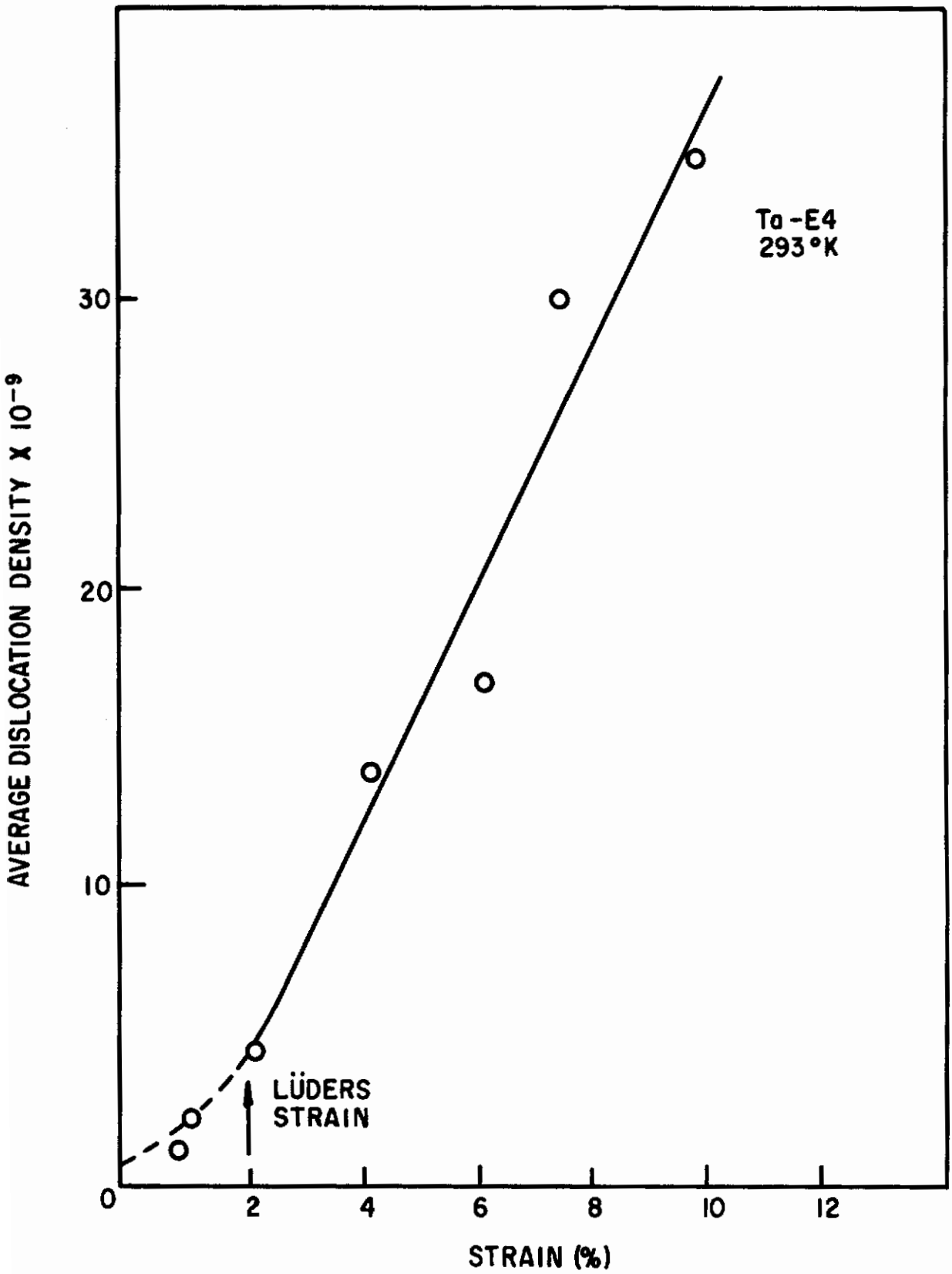

Fig. 143 - Change in dislocation density with strain for Ta-E4 strained at 293°K

40,000 X

Fig.144 - Ta-E4 strained 2.8% in strain at 293°K.

40,000 X

Fig. 145 -Ta-E4 strained 4.3% in strain at 293°K.

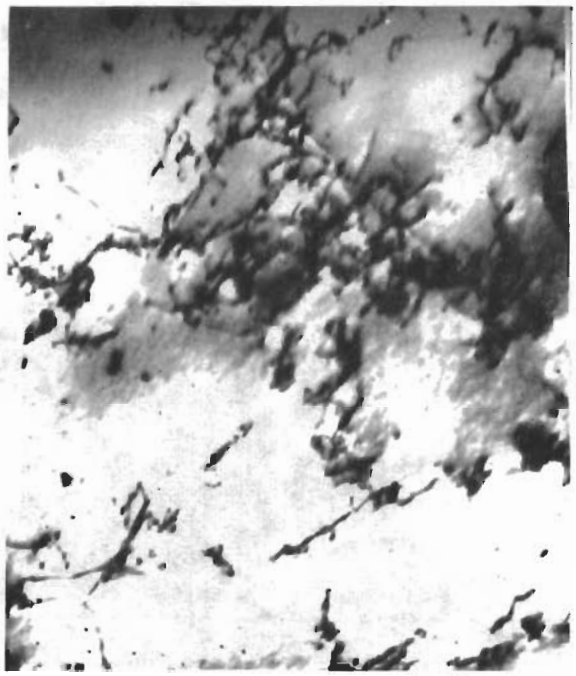

40,000 X

Fig. 146 -Ta-E4 strained 10.0% in strain at 293°K.

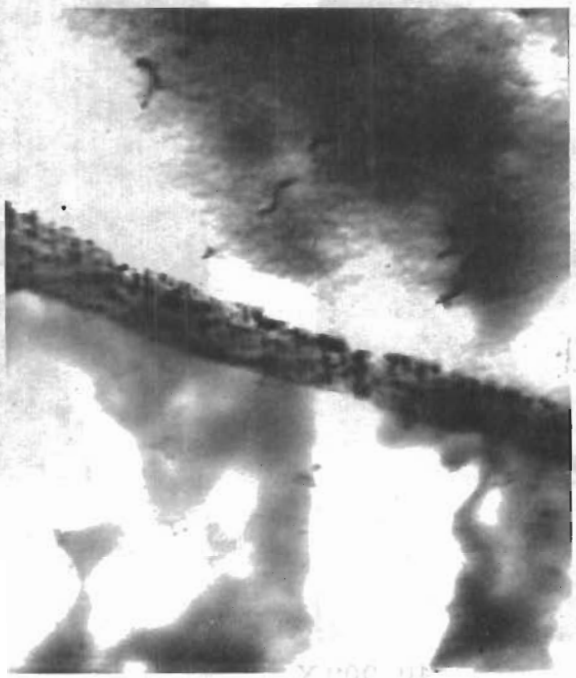

60,000X

Fig. 147-Ta-E4 strained 7.5% in strain at 293°K.

60,000X

Fig. 148 -Ta-E4 strained 4.3% in strain at 293°K.

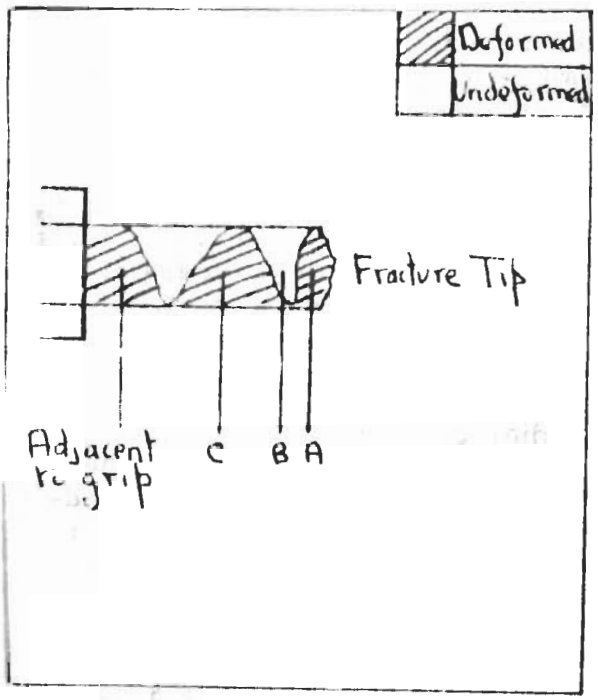

Fig.149- Undeformed and deformed regions on Ta-E4 specimen fractured at 240°K.

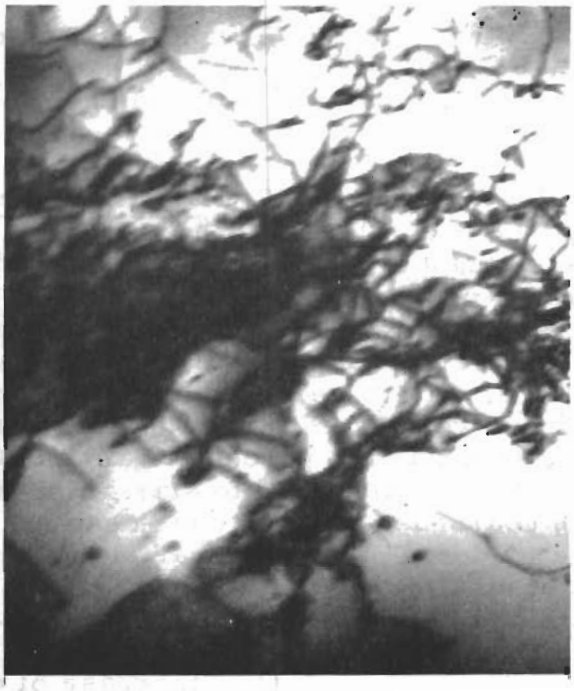

40,000X

Fig.150 - Region A in Ta-E4 strained to fracture at 240°K.

Fig. 151 - Region B in Ta-E4 strained to fracture at 240°K.

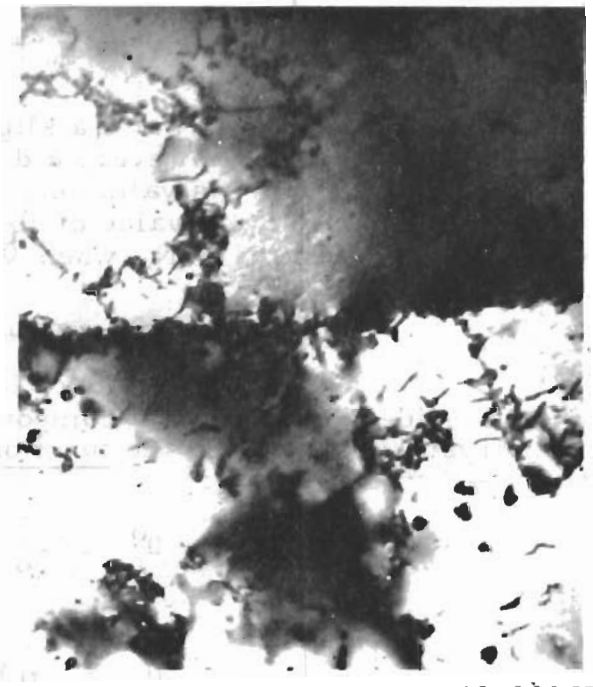

40,000 X

Fig. 152 - Region C in Ta-E4 strained to fracture at 240°K.

The increase in dislocation density with strain is shown in Fig. 153. The limited results suggest that the dislocation density increases with strain more rapidly at 240° than at 293°K. In other respects there was no obvious difference in the substructure developed at the two temperatures.

c) Ta-E1 strained at 293°K - Specimens were strained 1.6, 2.0, 4.6, 7.3, 9.2, 10.6, and 12.2 percent. At 1.6 percent strain most of the dislocations were straight and uniformly distributed but occasional networks in the process of breaking-up were also observed (Fig. 154). Very few regular networks remained at 2.0 percent strain. At this point a number of tangles of dislocations formed and there was some indication of cell formation although it was not possible to estimate the cell size. At 4.6 percent the cell structure was better defined and tangles of dislocations were extensive. The cells were about 0.3μ diameter. This structure was still clearer at 7.3 percent strain and the cell size was about 0.2μ (Fig. 155). The cell structure appeared to start to break-up at 9.2 percent strain. The grain boundaries coarsened and many dislocation loops were observed. At 10.6 percent strain some evidence of cells remained but the dislocation distribution was more uniform than at smaller strains (Fig. 156). The cell structure disappeared at 12.2 percent strain and the dislocation density was uniform throughout the specimen (Fig. 157).

The increase of dislocation density with flow stress is shown in Fig. 158.

4. Discussion

The flow stress σ_f increases linearly with the square root of the dislocation density (Fig. 158) and

$$\sigma_f = \sigma_o + \alpha\mu b\sqrt{N} \qquad (1)$$

σ_o is the stress required to move a slip band through a dislocation-free lattice and when $N = 0$, $\sigma_f = \sigma_o$. However, a dislocation-free specimen is never realised in practice and equation 1 is valid only when N is greater than the initial dislocation density No. The lowest value of σ_f possible is the flow stress of the annealed material σ_f^o. Because $N = N_o$ when $\sigma_f = \sigma_f^o$

$$\sigma_f^o = \sigma_o + \alpha\mu b\sqrt{N_o} \qquad (2)$$

If σ_f^o is considered to have two components, (1) the stress to propagate slip in a virgin crystal, σ_o, and (2) the functional stress due to the initial dislocation frictional substructure, σ_s:

$$\sigma_f^o = \sigma_o + \sigma_s \qquad (3)$$

and

$$\sigma_s = \alpha\mu b\sqrt{N_o} \qquad (4)$$

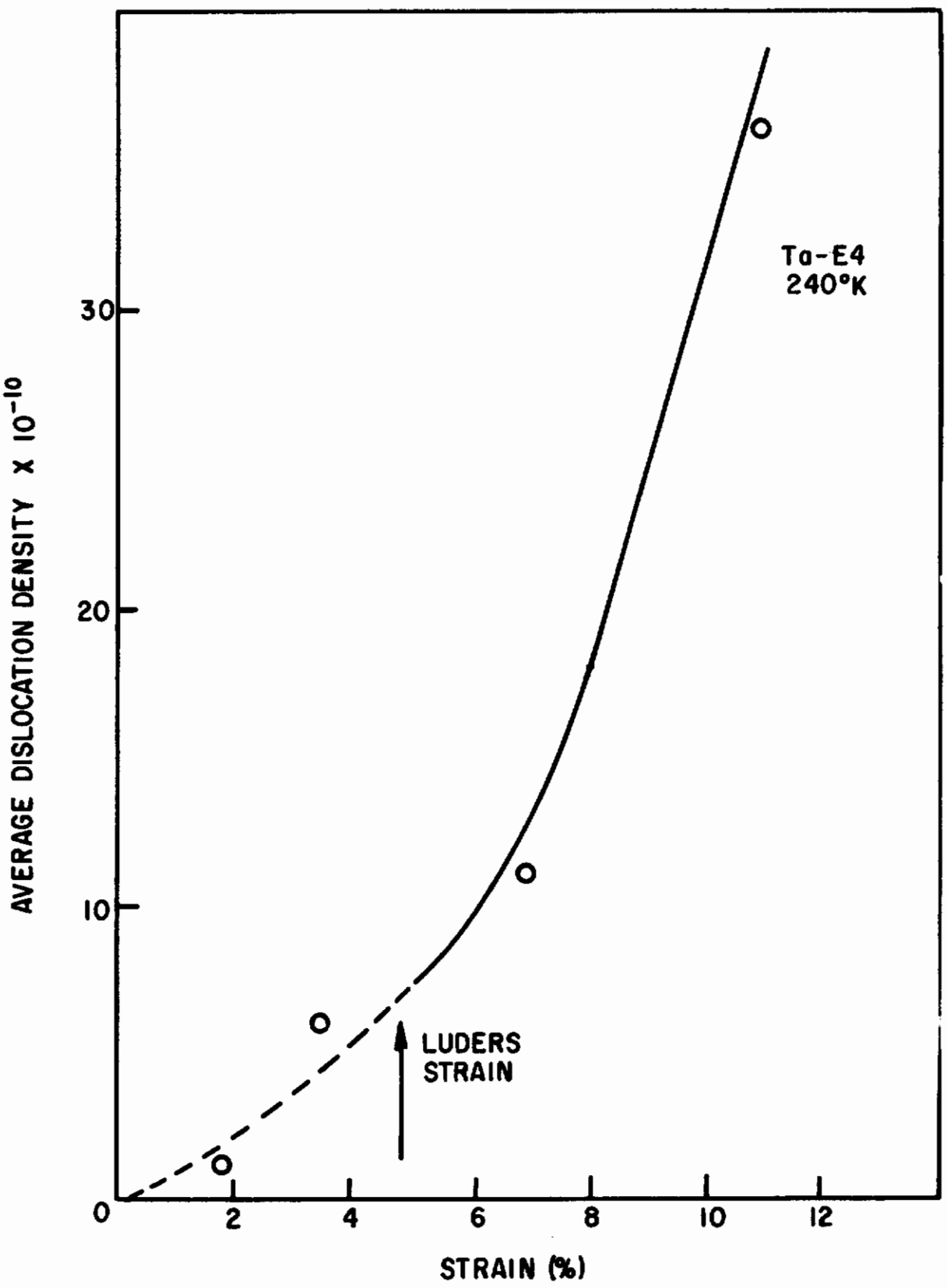

Fig. 153 - Change in dislocation density, with strain for Ta-E4 strained at 240°K

40,000X

Fig. 154 - Ta-El strained 1.6%

40,000X

Fig. 155 - Ta-El strained 7.3%

40,000X

Fig. 156 - Ta-El strained 10.6%

40,000X

Fig. 157 - Ta-El strained 12.2%

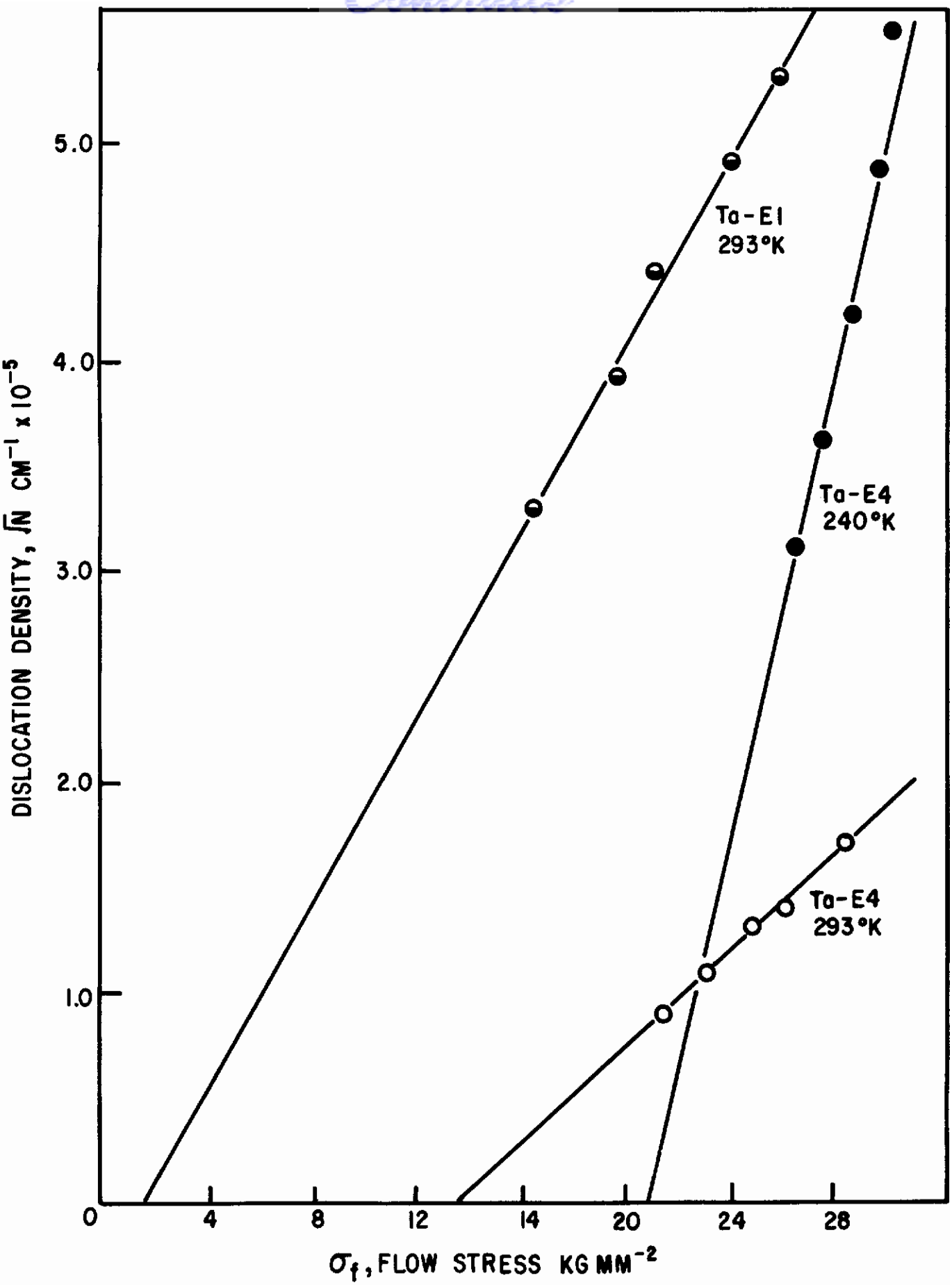

Fig. 158 - Change in dislocation density, $\sqrt{N}$, with flow stress for TaE4 strained at 293° and 240°K and Ta-E1 strained at 293°K.

The values of σ_f^o obtained by the use of equation 2 are a little higher but in fair agreement with the values obtained by extrapolation of the stress-strain curve (Table 36). As expected, the contribution of σ_s to σ_f^o is greatest in the material with the high initial dislocation density (Ta-E1). The most striking feature of these data is the wide variation in the values of σ_o. Clearly, σ_o is not the Peierls-Nabarro stress. More extensive studies of the effect of initial substructure and metallurgical variables on σ_o are required before an attempt can be made to interpret this parameter.

The important role of grain boundaries is the yield phenomena was clearly seen in many of the specimens examined. After some plastic strain, accumulation of dislocations at the boundaries resulting in apparent thickening of the interface was observed. Slip bands which meet a boundary produce new dislocations in the adjacent grain (Fig. 148) although it is not possible to decide whether the new dislocations are generated in the boundary or in virgin crystal close to the boundary.

5. References

(1) A.S. Keh and S. Weissmann, "Deformation Substructure in Body-Centered Cubic Metals", Proc. Conference on the Impact of Transmission Electron Microscopy on Theories of the Strength of Crystals. University of California (July 1961).

(2) A.H. Cottrell, Trans. A.I.M.E., 212(1958)192.

I. The Deformation of Tantalum Single Crystals

The object of these experiments is to determine the effect of temperature on the deformation behaviour of single crystals in tantalum.

1. Procedure

The crystals were produced from electron beam melted tantalum swaged to 0.167 in. diameter. The improved cathode and focusing plate assembly gave a stable molten zone of approximately 0.15 in. length which was passed down the rod at a rate of 0.2 inch per minute. It was not necessary to carry out degassing runs before the final zone passes. However, to facilitate machining at a later stage, single crystals with non-uniform diameter were ground to true cylinders and reannealed for one hour at 2500°C in the electron beam apparatus. This procedure removed any strains imposed on the material during grinding. Many of the crystals were seeded with the object of producing a single orientation but, in fact, there was some scatter. A summary of the orientations produced is shown in Fig. 159.

The crystals were machined chemically in a solution containing 50 cc concentrated sulphuric acid, 20 cc concentrated nitric acid and 20 cc concentrated hydrofluoric acid. The machining time was reduced from 24 hours to less than 3 hours by enclosing the rotation mechanism, the specimen and the hygroscopic acid mixture in a perspex box to prevent free circulation of air.

Mechanical tests were carried out on crystals of orientation shown in Fig. 160, using a strain rate of about 0.02 min^{-1}.

Table 36

Flow Stresses for Ta-E4 strained at 293° and 240°K
and for Ta-E1 strained at 293°K

Specimen	Testing Temperature °K	No cm^{-2}	α	σ_f^o $Kg\ mm^{-2}$ From σ-ϵ curve	σ_f^o $Kg\ mm^{-2}$ From equation 2	σ_o $Kg\ mm^{-2}$	σ_s $Kg\ mm^{-2}$
Ta-E4	293	$1x10^9$	0.34	14.7	16.4	13.6	2.8
Ta-E4	240	$1x10^9$	0.07	19.6	21.4	20.8	0.6
Ta-E1	293	$5x10^{10}$	0.19	10.2	11.8	1.6	10.2

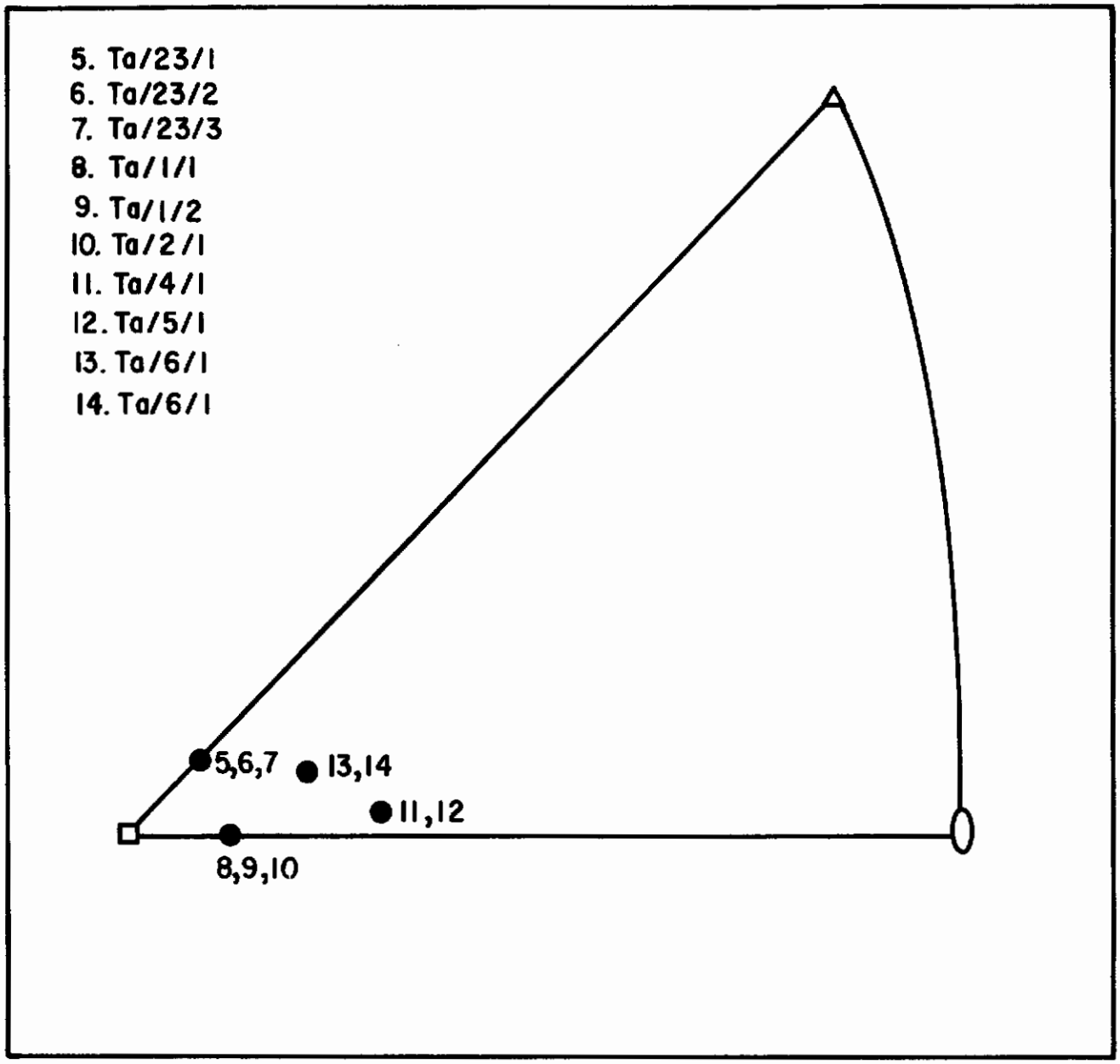

Fig. 159 - Unit stereographic triangle showing orientation of as-grown crystals.

The crystallography of the slip and twinning planes present after deformation was determined by measuring the traces on the crystal surface as described by Barrett[1]. The orientation of the crystal was measured with reference to the tensile axis and a fiducial mark placed on the shoulder at one end of the specimen. The angles α and β (Fig. 161) for a single trace were measured as the crystal was rotated through the angle over which the trace was visible. The values obtained were plotted on a stereographic projection and the pole of the slip or twinning plane determined. The angular measurements were made using a modified goniometer and telescope.

2. Mechanical Tests at 293°K

The data obtained for tests at 293°K on tantalum single crystals are summarized in Table 37 and the stress-strain curves are shown in Fig. 162. All the curves show a well-defined lower yield stress but a small Luders strain.

The resolved shear stress-strain relationship taking the slip system to be {011} <111> for crystals tested at 293°K is shown in Fig. 163. The yield stress of three of these crystals is almost the same, but the yield stress of the remaining crystal is considerably lower. It is possible that Ta/40/1 had a slight irregularity in the cross-section which caused premature yielding.

All the specimens tested showed an appreciable yield drop. This does not agree with the results reported by Ferriss, Rose and Wulff[2] who found the yield drop in tantalum single crystals to be dependent on crystal orientation. Crystals with the tensile axis orientated at the corners or sides of the standard stereographic triangle showed the least yield effect, whereas crystals in the center of the triangle showed appreciable yield drops. The present results show that the yield drop is not orientation dependent. Crystals with orientations on sides of the stereographic triangle (specimens 1 and 7, Fig. 160) as well as crystals with an orientation in the center of the triangle (specimen 4) had a large yield drop. Even specimens with orientation close to the (001) pole show a marked yield.

Specimen Ta/2/1 showed a high degree of work hardening (Fig. 162) compared with the other crystals tested which may be due to multiple slip. It has been found that in face-centered cubic metals, crystals with {001} orientation showed multiple slip and therefore work-hardened to a greater extent than crystals with orientations allowing only single slip to occur.[3]

The slip trace analyses on crystals strained at 293°K gave results consistent with multiple slip on {110} planes.

3. Mechanical Tests at 196°K

One crystal (Ta/43/2) which had been strained about 4 percent at 293°K and then tested at 196°K showed a cleavage fracture. The orientation of this cleavage face is shown in Fig. 164. It is clear that the cleavage plane is {100}. The specimen elongated 23 percent before fracture and the reduction in area at the fracture was about 20 percent. The crack appeared to start at the surface but not from the region of minimum diameter. This initiation point was not associated with any microstructural feature such as twinning but there was some evidence of a very

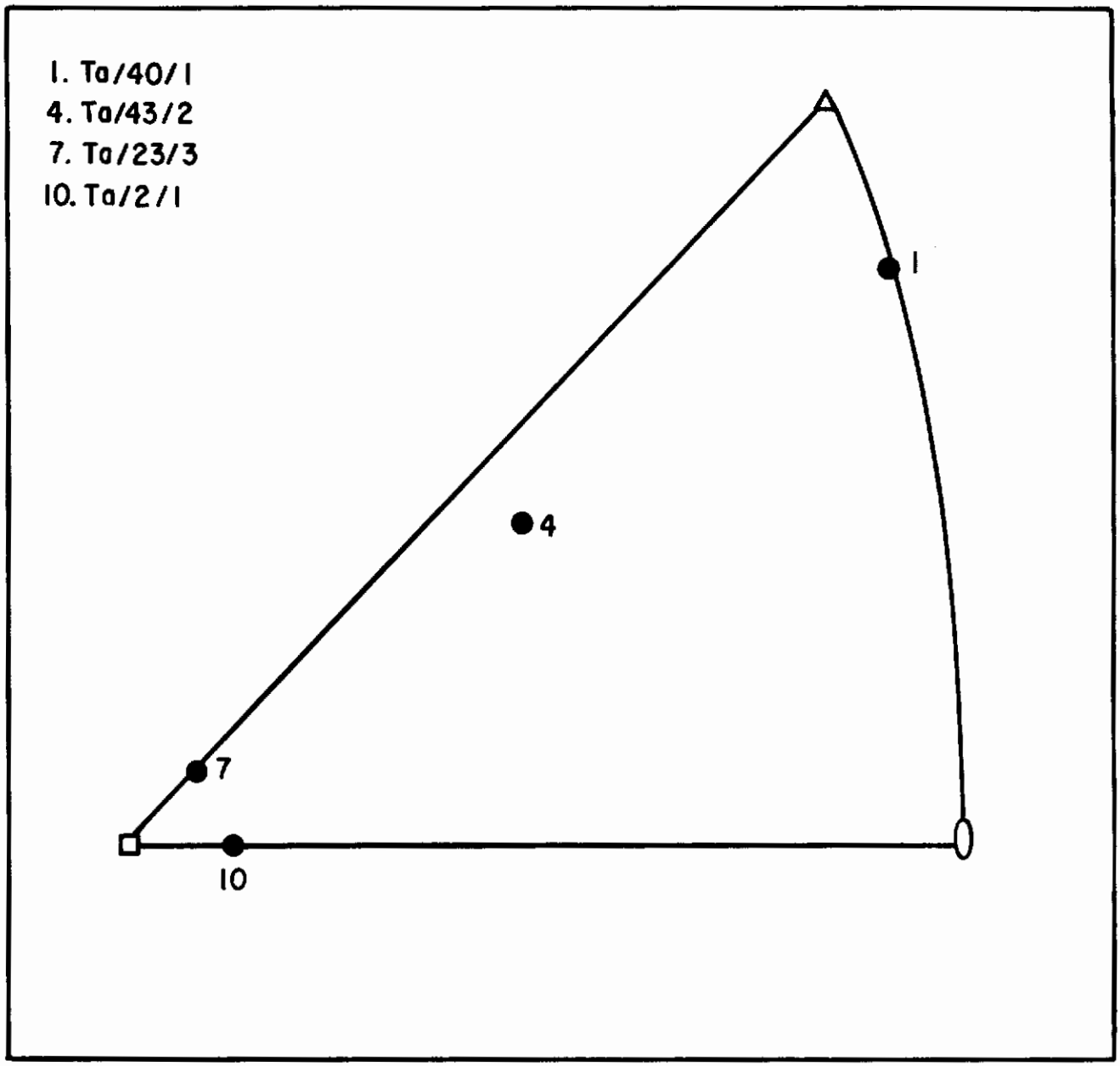

Fig. 160 - Unit stereographic triangle showing orientation of crystals tested.

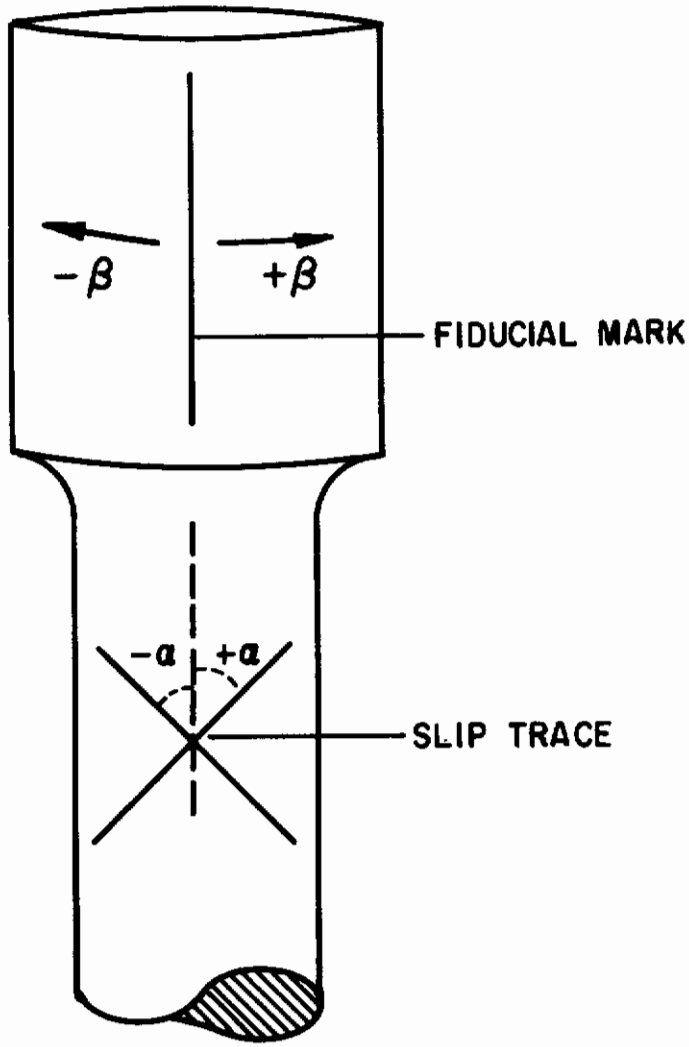

Fig. 161 - Illustration showing angles measured in the determination of the pole of a plane from its surface trace

Table 37

Summary of the Mechanical Properties of Single Crystals Tested at 293°K

Specimen	Upper Yield Stress Kg mm^{-2}	Lower Yield Stress Kg mm^{-2}
Ta/40/1	17.8	15.1
Ta/23/3	17.4	15.8
Ta/43/2	15.2	14.3
Ta/2/1	14.2	13.8

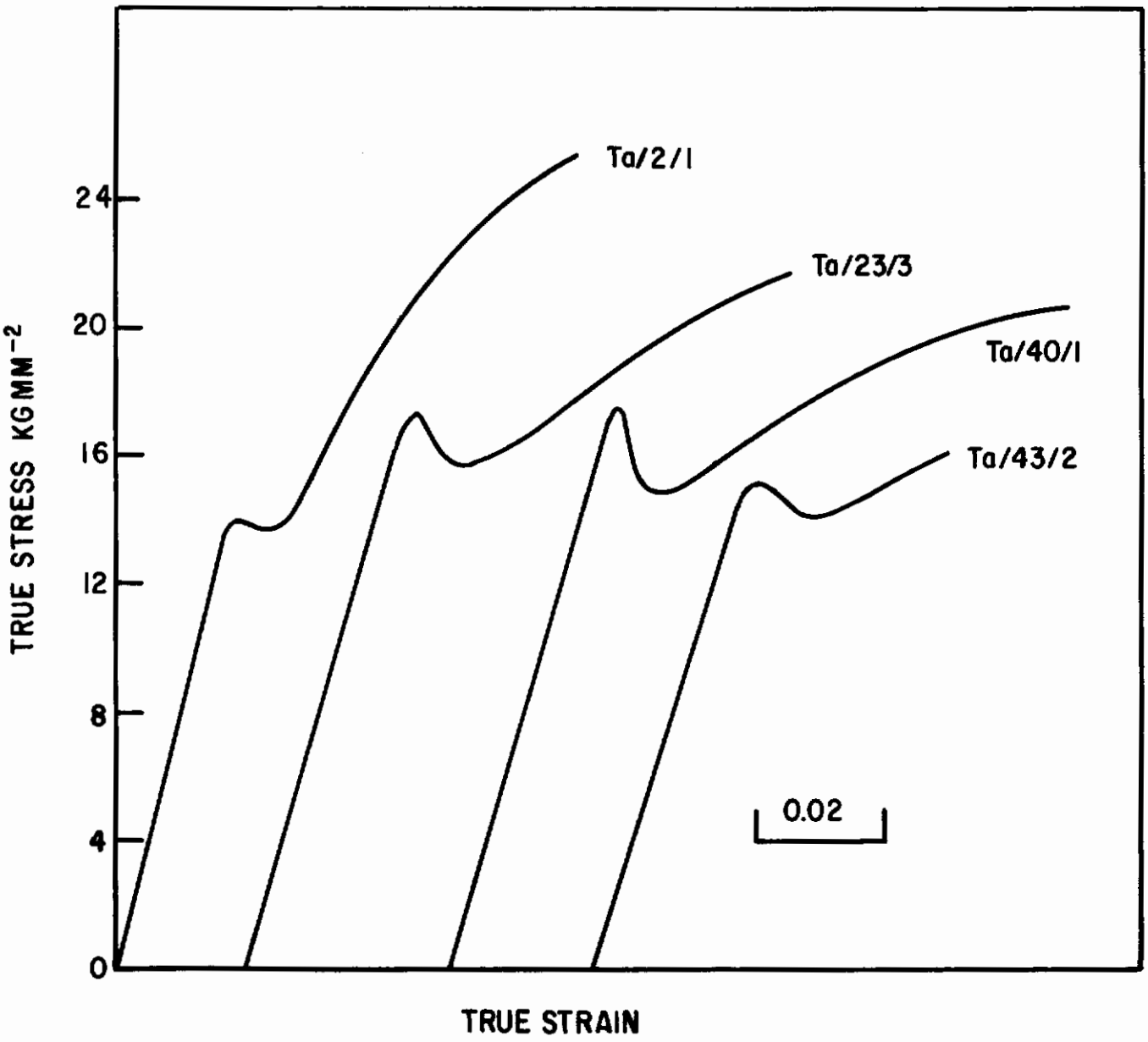

Fig. 162 - Stress-strain curves for tantalum single crystals tested at 293°K

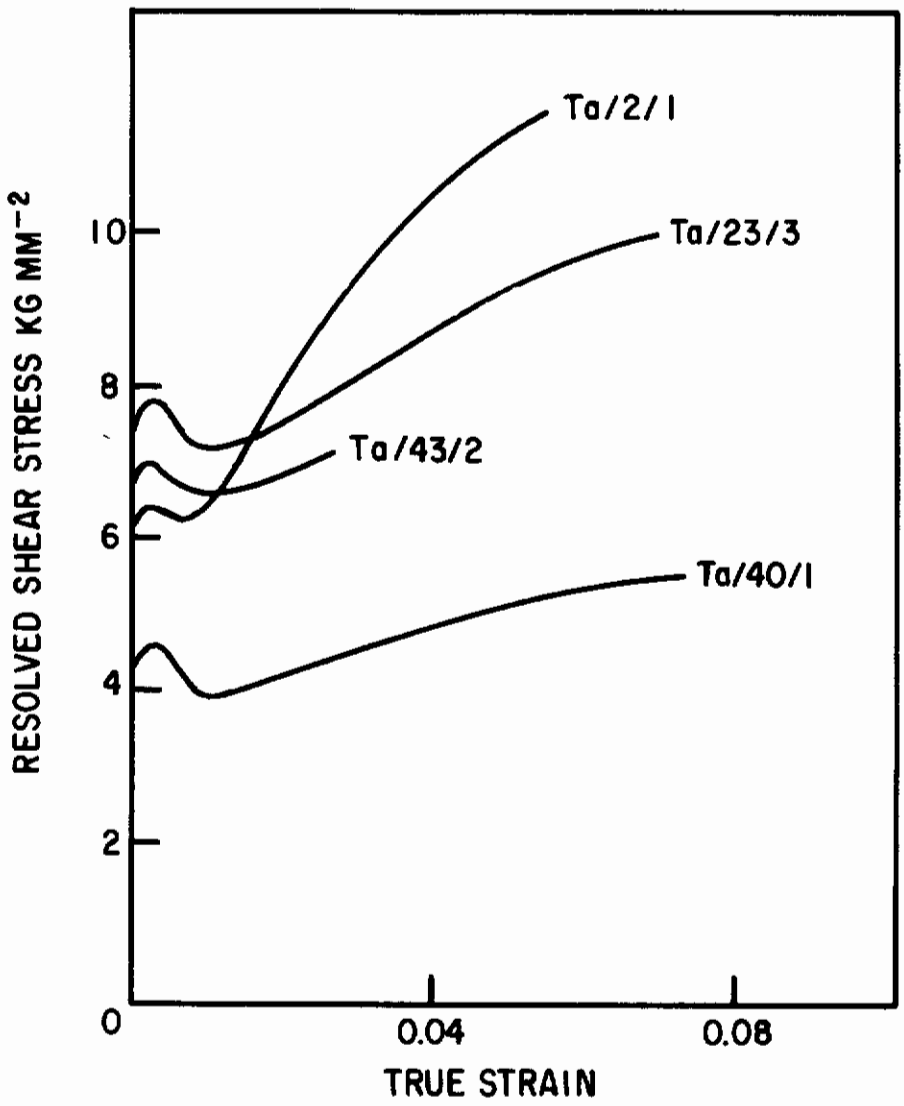

Fig. 163 - Variation of resolved shear stress with strain of tantalum single crystals with different orientations.

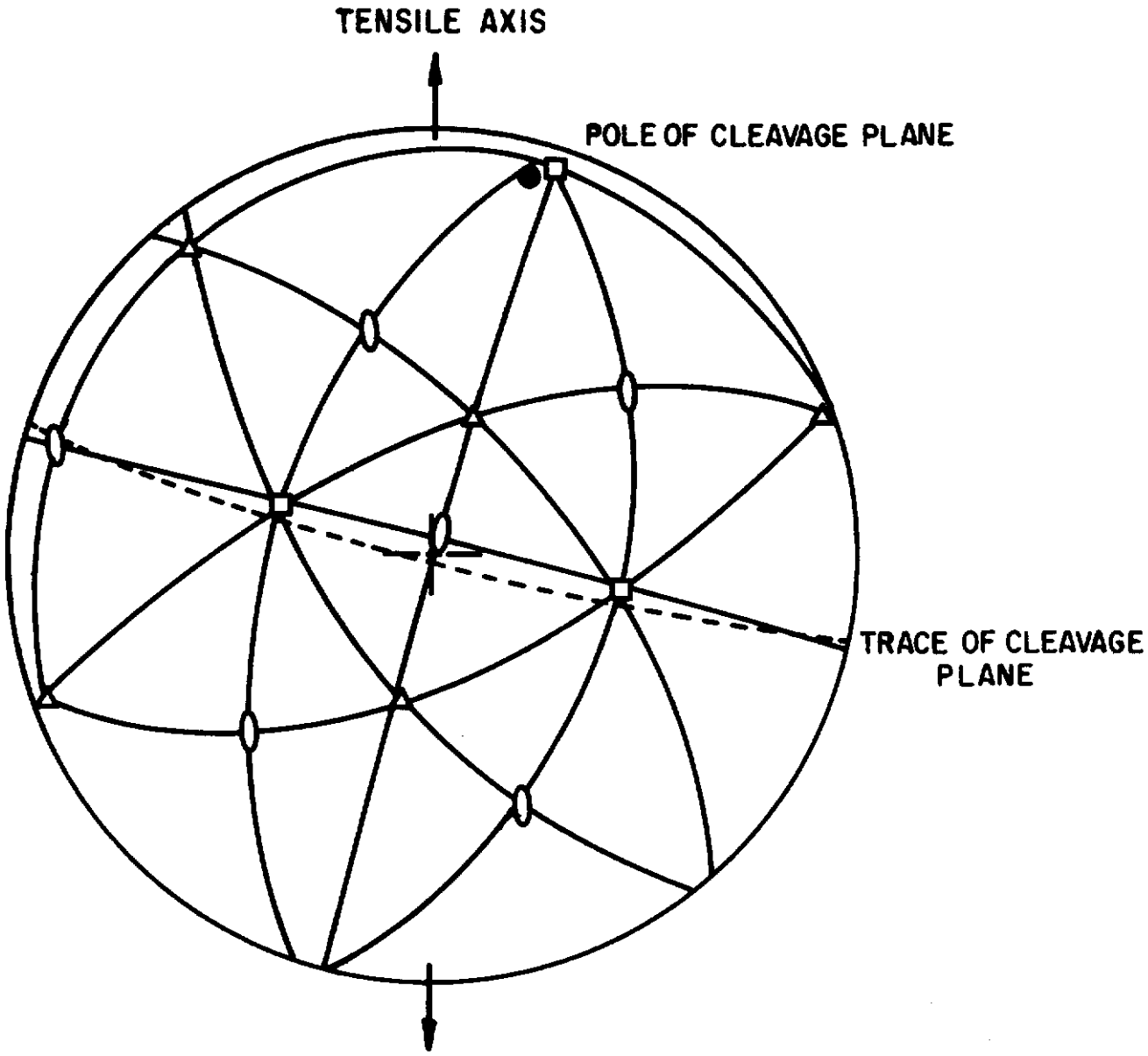

Fig. 164 - Stereographic projection showing orientation of cleavage plane. Ta/43/2 tested at 196°K

small blowhole in the crack initiating region. The propagation of the crack caused fine twinning in one direction only together with a large amount of plastic tearing. River markings were also present on the fracture surface. The appearance of the fracture surface is very similar to that found in iron after cleavage[4,5,6].

The existence of {100} cleavage in tantalum was confirmed by testing four as-grown crystals oriented close to the [100] tensile axis at 196°C. All four crystals fractured by cleavage on a {100} plane.

4. References

(1) C.S. Barrett, "Structure of Metals", McGraw-Hill Book Co., New York 1952, p. 40.

(2) D.P. Ferriss, R.M. Rose and J. Wulff, "Deformation of Tantalum Single Crystals", private communication.

(3) K. Lucke and H. Lange, Zeit Metall., p. 43, 55 (1952).

(4) D. Hull, Acta Met., 8 (1960) 11.

(5) J.M. Berry, Trans. A.S.M., 51 (1959) 556.

(6) C.F. Tipper, A.M. Sullivan, Trans. A.S.M., 43 (1951) 906.

J. The Stable-Unstable Plastic-Flow Temperature Transition in Annealed Tantalum

1. Introduction

It is difficult to induce cleavage fracture in polycrystalline tantalum. Such fractures have been reported only for coarse grained impure specimens subjected to severe plastic deformation at 77°K[1] and specimens containing an appreciable concentration of hydrogen[2]. However, a different form of catastrophic failure is likely to be encountered in this material; the high velocity unstable ductile crack. The essential feature of this type of fracture is that plastic flow immediately ahead of the crack is confined to a small volume in which, at a high local strain rate, shear failure occurs quickly. In a uniaxial tension test this critical condition is revealed by necking of the specimen before homogeneous strain hardening. That is, a local plastic instability resulting in rapid shear fracture occurs before the heterogeneous Luders deformation is complete. The strain rate and stress conditions near the tip of a fast running crack are obviously different from those existing during necking of a tensile bar and thus no simple quantitative correlations can be expected. However, tensile test studies provide a relatively simple means of assessing the effects of metallurgical variables on the plastic instability phenomenon which is an important factor in both situations.

2. The Plastic Instability Condition

For polycrystalline specimens deforming homogeneously the relation

between true stress σ and true plastic strain ϵ is

$$\sigma = K \epsilon^n \tag{1}$$

K is a material constant and n the strain hardening exponent. A tensile specimen necks when[3]

$$\epsilon = n \tag{2}$$

We define the critical instability condition resulting in rapid shear failure as

$$\epsilon_L \geq n \tag{3}$$

where ϵ_L is the Luders strain. Since ϵ_L increases and n decreases with decreasing temperature, there is a critical temperature (the plastic instability transition temperature, T_{PI}) at which this condition will occur. For some materials, such as certain mild steels [7], the cleavage fracture transition temperature, T_{CF}, is higher than T_{PI} so that rapid shear failure is not a serious engineering problem. However, in tantalum and all materials for which $T_{CF} < T_{PI}$, it is desirable to reduce T_{PI} by control of the metallurgical variables.

Because ϵ_L and σ_Y (the lower yield stress) define a point on the homogeneous strain hardening curve (equation 1)

$$\epsilon_L = \left(\frac{\sigma_Y}{K}\right)^{\frac{1}{n}} \tag{4}$$

Thus, plastic instability will occur when

$$\frac{\sigma_y}{K} \geq n^n \tag{5}$$

and introducing the grain-size dependence of σ_y [4]

$$\sigma_y = \sigma_i + k_y d^{-1/2} \tag{6}$$

where σ_i is the frictional stress, k_y the pinning parameter and 2d average grain diameter.

$$k_y d^{-1/2} \geq K n^n - \sigma_i \tag{7}$$

The frictional stress is equal to the flow stress at zero plastic strain[5,6]. Thus, if ϵ_i is the elastic strain at σ_i and E is Young's modulus, simultaneously

$$\sigma_i = K \epsilon_i^n$$

and (8)

$$\sigma_i = E \epsilon_i$$

Inequality (7) can now be written

$$k_y d^{-1/2} \geq \frac{(E n)^n}{\sigma_i^{n-1}} - \sigma_i \qquad (9)$$

and since E is a constant which is relatively unaffected by changes in temperature or metallurgical variables, the plastic instability condition is seen to be dependent upon the magnitude of k_y, d, n and σ_i. k_y and d are independent variables in impure material but k_y increases with increasing d when the impurity is less than about 50ppm[6]. σ_i and n are also interdependent as can be seen by eliminating ϵ_i from the simultaneous equations (8), but each is independent of k_y and d. Thus, the two sides of equation (9) can be varied independently.

3. Application to Tantalum

The parameters k_y, σ_i, n and d have been measured for tantalum over a range of temperature, grain size and impurity content[6] and so it is possible to assess the relative effects of these variables on the instability transition temperature T_{PI}. The extremes of the available data are represented by the results of two alloys (Ta-E2 and Ta-E3) containing less than 50 ppm and an alloy Ta-E4 containing more than 175 ppm total impurity. In Ta-E2 the major impurity is carbon, in Ta-E3 nitrogen and oxygen and in Ta-E4 oxygen. In Fig. 168 $k_y d^{-1/2}$ and $\left[\frac{(En)^n}{\sigma_i^{n-1}} - \sigma_i\right]$ are plotted as a function of temperature. The transition temperature T_{PI} occurs at the point of intersection. σ_i increases rapidly with decreasing temperature and at constant temperature it increases with impurity content. There are corresponding decreases in n. The function $\left[\frac{(En)^n}{\sigma_i^{n-1}} - \sigma_i\right]$ is not significantly different for the two relatively pure materials but at constant temperature it is about 15 kg mm^{-2} lower for the more impure material. The maximum grain size range which can be achieved by annealing cold-worked material is from about $d^{-1/2} = 1.0$ $mm^{-1/2}$ to 10.0 $mm^{-1/2}$. At 295°K, k_y is a function of the type and concentration of impurity and of the annealing treatment. The maximum values found were about 2×10^7 cgs for Ta-E2, 4×10^7 cgs for Ta-E3 and 5×10^7 cgs for Ta-E4. In Ta-E4, k_y is strongly temperature dependent, in Ta-E3 less so and in Ta-E2 there is no variation of k_y with temperature.

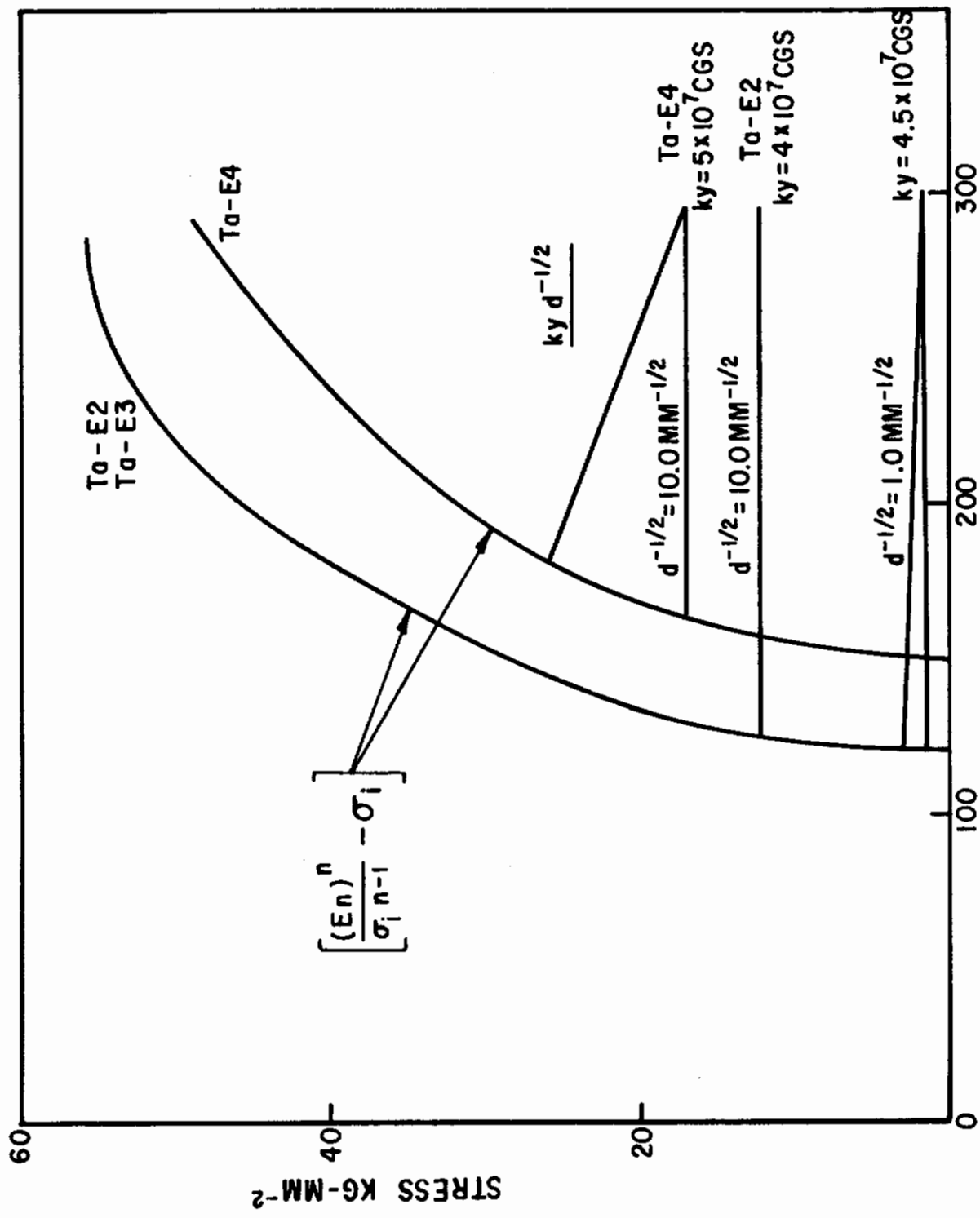

Fig. 165 - $\left[\frac{(En)^n}{\sigma_i^{n-1}} - \sigma_i\right]$ and $k_y d^{-1/2}$ as a function of temperature Ta-E2, Ta-E3 and Ta-E4.

Increasing the grain size alone produces only a small decrease in T_{PI} (maximum decrease about 15°K) but the effect is more pronounced if k_y is large and strongly temperature dependent. The maximum change in T_{PI} for the impure material which can be achieved by controlling d and k_y is about 30°K; for the pure material the variation is appreciably smaller. The change in T_{PI} resulting from the variation of σ_i with impurity content is the largest single effect. Over the range of impurity studied, T_{PI} can be shifted about 30°K. The highest plastic instability transition temperature occurs in fine-grained material with high total interstitial concentration, giving a large σ_i, and high oxygen content, giving a large and temperature dependent k_y. Conversely, the lowest transition temperature is obtained by establishing a coarse grained structure in pure material. It is preferable that any interstitial present should be of the type (such as carbon) which produces a temperature insensitive k_y.

In practice, coarsening the grain size may not be desirable because it results in a decrease in the yield stress and a greater susceptibility to brittle fracture. Fortunately, the increase of the T_{PI} of tantalum with decreasing grain size is small. Thus, in most circumstances it would probably be advisable to use a fine-grained material to minimize the transition temperature by reducing σ_i and the magnitude and temperature dependence of k_y to the smallest value that can be achieved by control of the type and total content of interstitial elements. This compromise may not be satisfactory for other metals.

4. References

(1) M.A. Adams and A. Ianucci, private communication.

(2) A. Clauss and H. Forestier, "La fragilité du tantale en presence d'hydrogene a temperature ambiante" Les Memoires Scientifiques de la Revue de Metallurgie, 56 (1959) 614-616.

(3) G. Sachs and J.D. Lubahn, "Failure of ductile metals in tension", Trans. A.S.M.E. (May 1946) 271.

(4) N.J. Petch, "The Cleavage Strength of Polycrystals," J. Iron and Steel Inst. 174 (1953) 250.

(5) A.R. Rosenfield, submitted to J. Inst. Metals.

(6) A. Gilbert, D. Hull, W.S. Owen and C.N. Reid, "The Yield of Polycrystalline Tantalum", J. Less Common Metals, to be published.

(7) G.T. Hahn, B.L. Averbach, W.S. Owen and Morris Cohen "Initiation of Cleavage Microcracks in Polycrystalline Iron and Steel", Fracture, J. Wiley, New York, 1960.

VII. TRANSMISSION ELECTRON MICROSCOPE STUDY OF DEFECTS IN COLUMBIUM AND TANTALUM - Work carried out at the University of Cambridge by P. B. Hirsch and E. Levin.

A. Scope

The previous annual report contained an account by R. L. Segall of initial observations on the recovery of fatigued columbium. A preliminary value of 3.1 (± 0.4) e.v. for the activation energy of self-diffusion was reported, deduced from the temperature at which dislocation loops anneal out at appreciable rates. This value, which is for diffusion by vacancies or interstitials, is considerably lower than that of 4.33 e.v. obtained by Resnick[1] In view of this discrepancy, and the unexpectedly low value of the activation energy obtained, further study of the recovery of fatigued b.c.c. refractory metals was undertaken.

Following the lines of Segall's experiments, research during the past year has been directed toward further study of the activation energy for the annealing of dislocation loops in columbium. Bulk deformation and annealing studies were carried out, and an attempt was made to observe directly the mechanism of the process of loop annealing by heating stage experiments. Similar studies were carried out for tantalum.

B. Experimental Procedure, Results and Discussion

1. Bulk deformation and annealing of columbium

Zone refined crystals of columbium were cold rolled into foils of about 5-mil thickness, and then annealed at 1200°C in a vacuum of about 5×10^{-6} m.m. Hg. After this anneal, the dislocations are arranged in hexagonal networks forming sub-boundaries within the recrystallized grains; the interior of the sub-grains are essentially dislocation-free.

Dislocation loops were introduced into the annealed foils by fatigue bending at room temperature. Fig.166shows a typical area of a specimen after this deformation. It shows a cross-grid of dislocations in [111] -directions slightly inclined to the plane (120) of the foil, and a considerable density of dislocation loops, some of which are elongated. In other regions the dislocations are very irregular and tangled, and the loops tend to be circular.

The density of loops is observed to decrease after short anneals at temperatures above 600°C, the number of the smallest of them changing most noticeably at first. During the annealing process there is a continual change in distribution of loop sizes with increasing annealing temperature, as previously observed in the f.c.c. metals by Segall, Partridge and Hirsch[2]. Fig.167 shows a typical distribution of loops after annealing at 700°C for 20 minutes. After a short anneal at 750°C most of the loops have disappeared.

These observations essentially confirm those of Segall. Assuming that the process of annealing is climb by volume self diffusion a value of the activation energy can be obtained using the formula of Silcox

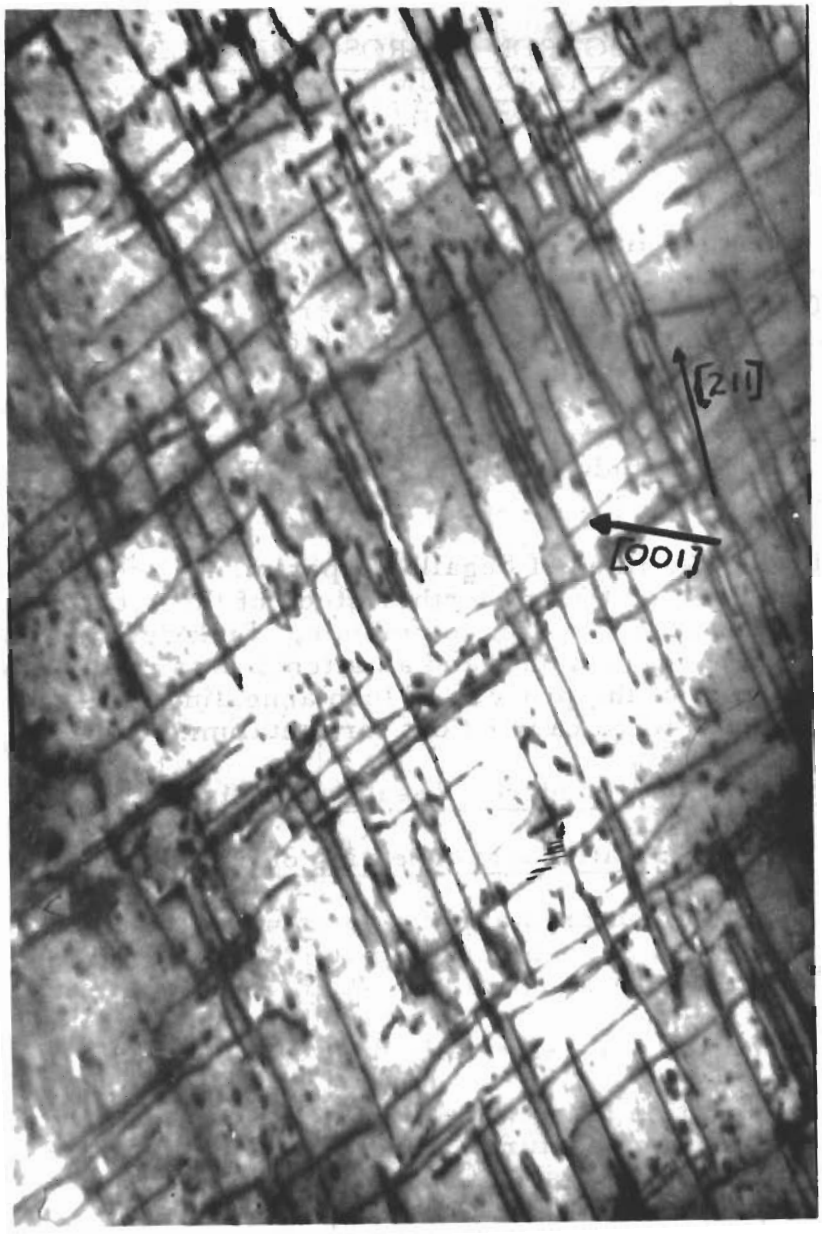

Fig. 166 - Dislocations and loops in columbium deformed in fatigue at room temperature.

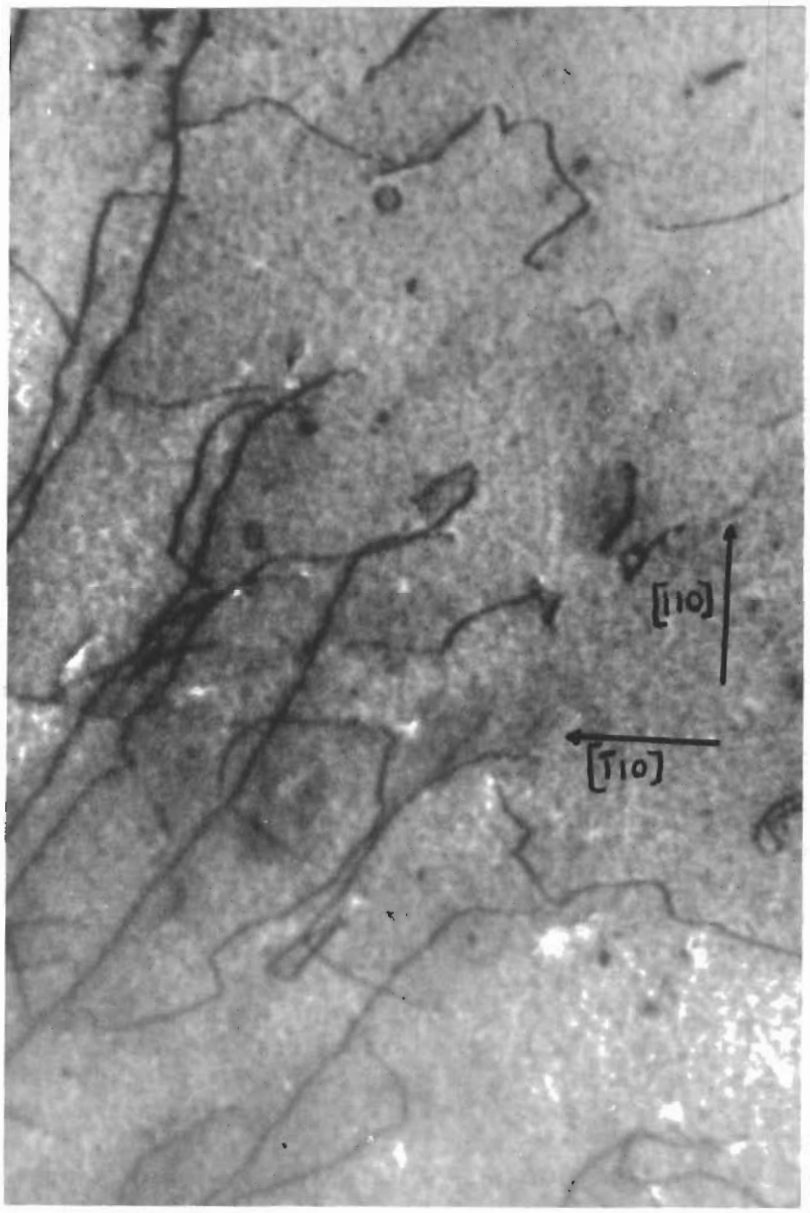

66,000X

Fig. 167 - Fatigued specimen of columbium annealed at 700°C for 20 minutes.

Whelan[3]. A value of ~ 3 e.v. is found in this way, in agreement with that derived by Segall. However, because of uncertainties in some of the parameters in the Silcox and Whelan formula, this value may be in error by 15%. In spite of this relatively large margin of uncertainty this value is low compared with the published value of the activation energy of self diffusion, due to Resnick[1] (4.33 e.v.). The question arises therefore as to whether the recovery process could be of a different type. It is possible for example that the loops might coalesce with each other and with other dislocations by a process of "conservative climb" controlled by dislocation pipe diffusion[4,3], a mechanism which should involve a smaller activation energy. It was decided therefore to try to observe the annealing process directly using a heating stage in the electron microscope, and these experiments are described in section 3.

2. Bulk deformation and annealing of tantalum

Experiments parallel to those described for columbium in section 2 were carried out for tantalum. The starting material consisted again of zone refined single crystals, cold rolled into foils and annealed at 1100°C in vacuo. The foils were then deformed by fatigue bending at room temperature.

The dislocation arrangements observed in tantalum were similar to those described for columbium, before and after deformation, except that after fatigue bending there were fewer larger loops than in columbium.

The dislocation loops were found to anneal out in the same temperature range as for columbium. Specifically, there is no change in loop density or distribution after short anneals at temperatures up to about 600°C. Above this temperature the loops anneal with increasing rapidity, until about 750°C most of them anneal out in 15 minutes.

An important difference between the behaviour of tantalum and columbium is that in the former marked precipitation occurs above 600°C. On cooling from this temperature rows of dislocation loops and helices are punched out, due to stresses arising from differential thermal contraction on cooling. Fig.168 shows rows of loops formed in this way, along [111] directions, and Fig.169 shows helices at precipitates. Such effects were not observed in columbium.

Assuming again that the annealing process is climb by volume self diffusion, the activation energy for self diffusion in tantalum obtained from the annealing data is similar to that for columbium, i.e. ~ 3 e.v. $\pm$ 15%.

3. Heating Stage Experiments

The relatively low activation energy obtained in the bulk annealing experiments makes it rather important to investigate closely the nature of the process by which loops anneal out in the b.c.c. refractory metals. A concerted attempt was therefore made to observe the annealing mechanism directly using a heating stage in the electron microscope.

Initially, the stereo heating stage designed by J.S. Lally was employed for this purpose. This stage employs a single heated grid, to which

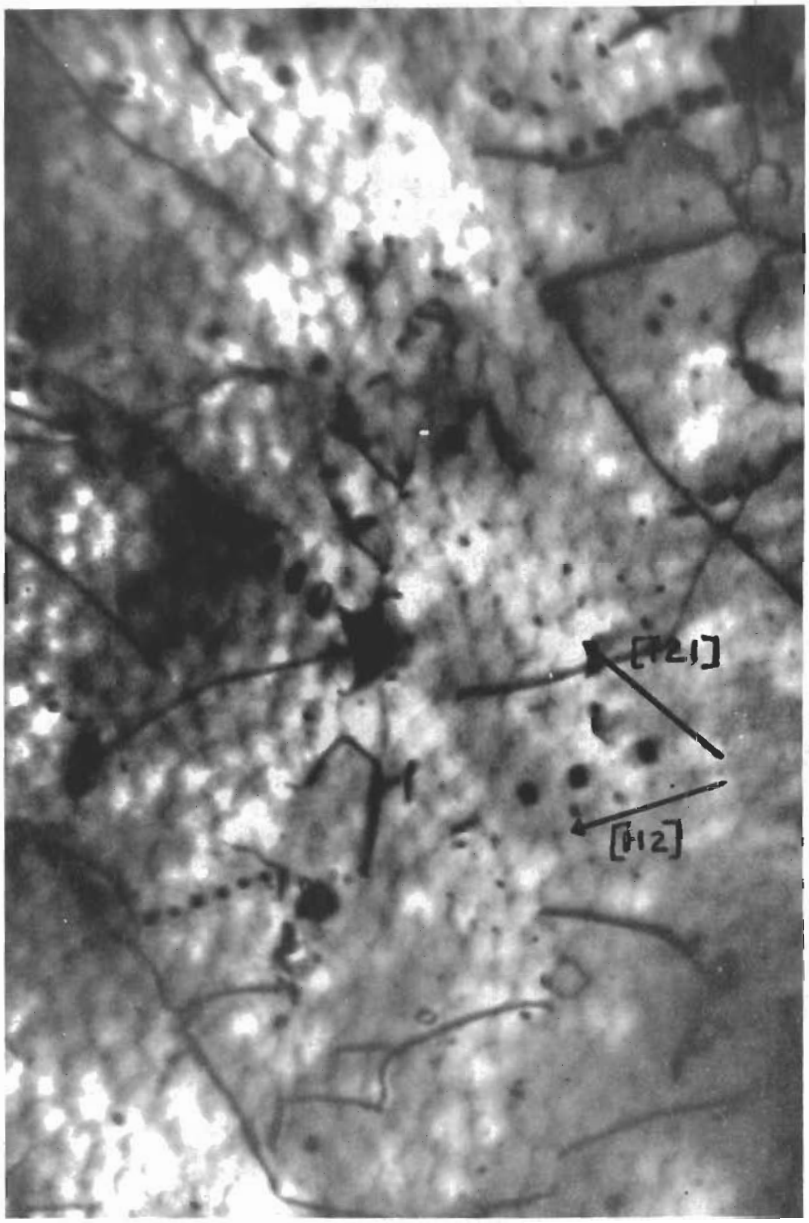

46,000X

Fig. 168 - Rows of loops punched out from precipitates in tantalum, formed on annealing at 600°C.

59,000X

Fig. 169 - Helical dislocations formed at precipitates in tantalum, formed on annealing at 600°C.

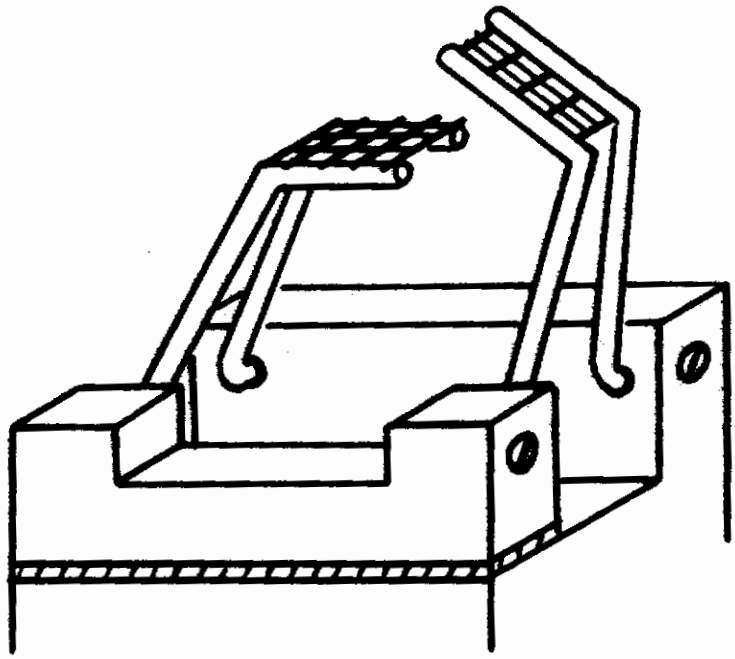

Fig. 170 - Heating stage for electron microscope.

the specimen is usually attached with a small quantity of a soluble adhesive. Such a procedure proved to be wholly inadequate at the relatively high temperatures required for annealing tantalum and columbium, and the specimen heating and supporting arrangements had to be modified. The modification employed is shown in Fig. 170. This arrangement utilizes two separate heated grids, between which the specimen is closely sandwiched, in the same manner in which specimens are normally mounted for transmission microscopy.

The modified grid arrangement of the electron microscope heating stage, has been found to be satisfactory for supporting and heating specimens. However, it has not been possible so far to observe the annealing process in either tantalum or columbium. At temperatures above 600°C the specimens become rapidly opaque and large scale precipitation appears to occur. These effects occur within one minute of heating the specimen to this range of temperatures, and prevent any observations of the annealing process to be made. It appears unlikely at the present time that observations of this type will prove successful, unless drastic improvement of the vacuum in the microscope is first achieved.

REFERENCES

(1) Resnick, R., Abs. J. Met., 11 (1957), 4.

(2) Segall, R. L., Partridge, P. G., and Hirsch, P. B., Phil. Mag. 6, (1961), 1493.

(3) Silcox, J., and Whelan, M. J., Phil. Mag. 5 (1960), 1.

(4) Price, P. B., Phil. Mag. 5 1960, Phil. Mag. 6 (1961), 449.

Appendix A
List of Publications

The reports and papers (published, submitted, or to be submitted) that have resulted at least partly from the work accomplished so far on the current program are listed below:

1. Lement, B. S. et al., "Substructure and Mechanical Properties of Refractory Metals", Contract No. AF33(616)6838, Progress Report I (April 30, 1960).

2. Lement, B. S. et al., "Substructure and Mechanical Properties of Refractory Metals", Contract No. AF33(616)6838, Progress Report II, (October 31, 1960).

3. Lement, B. S., Thomas, D. A., Weissman, S., Owen, W. S., and Hirsch, P. B., "Substructure and Mechanical Properties of Refractory Metals", WADD T. R. 61-181, (August 1961).

4. Lement, B. S. et al., "Substructure and Mechanical Properties of Refractory Metals", Contract No. AF33(616)6838, Progress Report 3, (November 15, 1961).

5. Lement, B. S. and Perlmutter, I., "Mechanical Properties Attainable by Alloying of Refractory Metals", Journal of the Less-Common Metals, 2 (April-August 1960) 253.

6. Weissmann, Sigmund, Passmore, Edmund, and Allen, Steven, "Changes in Mechanical Properties and Dislocation Structure During Recovery Annealing of Tungsten", to be submitted.

7. Cohen, Morris, Weissman, S., and Lement, B. S., "Substructure in Refractory Metals", AIME Chicago Section Presentation, (April 12-13, 1962).

8. Thomas, David, A. and Peck, J. F., "A Study of Fibrous Tungsten and Iron", Trans. AIME, 221 (December 1961) 1240.

9. Weissmann, S., "Substructure and Dislocation Networks in Tungsten", submitted as Chapter in Imperfections in Crystals, Interscience Publishers, Inc. (1962).

10. Weissman, S. and Imura, T., Discussion to chapter on Tungsten and Tungsten-Base Alloys, in Refractory Metals and Alloys, Interscience Publishers (1961), 349.

11. Keh, A. and Weissmann, S., Dislocation Structure in B.C.C. Metals, Prec. 1961, Submitted to International Conference on Impact of Electron Microscopy on Strength on Crystals, Interscience Publishers (1962).

12. Gilbert, A., Hull, D., Owen, W. S., and Reid, C. N., "Yield of Polycrystalline Tantalum", to be submitted.

13. Hull, D., McIvor, I. D., and Owen, W. S., "Substructure of Annealed Polycrystalline Tantalum", to be submitted.

14. Segall, R. L., "Annealing Twins and Stacking Faults in Niobium", Acta Metallurgica, 9 (October 1961) 975.

Appendix B
Definitions of Terminology Related to Substructures

Boundary, Asymmetric - A low-angle boundary consisting of both edge and screw dislocation.

Boundary, Tilt - A low-angle boundary consisting of edge dislocations.

Boundary, Twist - A low-angle boundary consisting of screw dislocations.

Cells - An advanced stage of dislocation entanglement characterized by relatively defined dislocation boundaries.

Dislocation Bowed Out - Partial loop due to anchoring of dislocation.

Dislocation, Edge Dipoles - Edge dislocation segments associated with bowed out screw dislocations. These anchored segments have a direction perpendicular to the Burgers vector of the screw dislocation.

Dislocation, Isolated Loops - Pinched off dislocation dipoles probably arising from considerable cross-slip or condensation of vacancies on such dipoles.

Dislocation Jogs - Local displacements of dislocation lines.

Dislocation Superjogs - Enlarged jogs arising from either cross-slip of screw dislocations or from the process of anchoring edge dislocation dipoles.

Dislocation Tangles - A non-uniform mesh of dislocations probably due to interaction of dislocation on more than one slip system.

Polygonization - The process in which dislocations collect into a more-or-less regular boundary, providing a geometric transition between the two orientations on either side of the boundary. Usually, the disorientation between the two lattices on either side of this low-angle boundary is less than a few degrees.

Recovery - A general increase in lattice perfection resulting from a decrease in point and line defects, without change in the primary grain boundary configuration.

Recrystallization in situ - The formation and growth of subgrains (or grains in extreme case) through polygonization in a plastically deformed matrix.

Recrystallization (Primary Recrystallization) - The formation and growth of relatively strain-free grains in a plastically deformed matrix.

Secondary Recrystallization - Discontinuous grain growth resulting from the migration of some grain boundaries while the others are still immobile.

Strain-Induced Boundary Migration - Occurrence of grain growth at the expense of strain-hardened material. For primary grains, such growth usually takes place during recrystallization, in contrast to that which occurs after recrystallization is complete. For subgrains, such growth usually takes place during recovery.

Subgrains - Portions of a crystal separated by low-angle boundaries.

Subgrain Growth - Increase in subgrain size by migration of subboundaries.

DISTRIBUTION LIST

Aero Corp.
Materials Research Dept.
Attn: Dr. S. R. Maloof
Wilmington, Mass.

Aeronautical Research Laboratory
Attn: ARZ (Mr. E. J. Hassell)
Wright-Patterson AFB, Ohio

Aeronautical Systems Division
Attn: ASRCE (Mr. J. Teres)
Wright-Patterson AFB, Ohio

Aeronautical Systems Division
Attn: ASRCMD (Mr. W. J. Trapp)
Wright-Patterson AFB, Ohio

Aeronautical Systems Division (15 copies)
Attn: ASRCMP-2 (Lt. J. D. Bitzer)
Wright-Patterson AFB, Ohio

Aerospace Corp.
Materials Sciences Laboratory
Attn: Mr. Hans Conrad
2400 E. El Segundo Blvd.
El Segundo, California

Armetco Corp.
Attn: A. E. Franks
776 Kemrow Ave.
Wooster, Ohio

Battelle Memorial Institute
Attn: R. Jaffee
505 King Ave.
Columbus 1, Ohio

Dr. R. W. Cahn
(Dept. of Metallurgy
University of Birmingham
Birmingham Eng.)
c/o Commander
Aeronautical Systems Division
Attn: ASYF (Mr. J. M. Troyan)
Wright-Patterson AFB, Ohio

University of California
Dept. of Metallurgy
Attn: Dr. J. E. Dorn
Berkeley, Calif.

Dr. A. H. Cottrell
(Dept. of Metallurgy
University of Cambridge
Cambridge, Eng.)
c/o Commander
Aeronautical Systems Division
Attn: ASYF (Mr. J. M. Troyan)
Wright-Patterson AFB, Ohio

Dr. P. B. Hirsch
(University of Cambridge
Cavendish Lab.
Cambridge, England)
c/o Commander
Aeronautical Systems Division
Attn: ASYF (Mr. J. M. Troyan)
Wright-Patterson AFB, Ohio

Convair
Physics Group
Attn: Mr. R. J. Sneed
Pomona, Calif.

Crucible Steel Company of America
Central Research Laboratory
Attn: Mr. E. J. Dulis
234 Atwood St.
Pittsburgh 13, Pennsylvania

Battelle Memorial Institute
DMIC
505 King Ave.
Columbus 1, Ohio

University of Florida
Metallurgical Research Lab.
Attn: Prof. F. N. Rhines
Gainesville, Florida

General Electric Co.
FPLD
Attn: Dr. W. Chang
Evendale, Ohio

General Electric Co.
Attn: Mr. Sam Leber
21800 Tungsten Rd.
Cleveland 17, Ohio

General Electric Co.
Lamp Division
Attn: J. W. Pugh
1331 Charden Rd.
Cleveland 17, Ohio

General Electric Co.
Research Laboratory
Attn: G. D. Oxx
P. O. Box 1088
Schenectady, N. Y.

General Electric Co.
Research Lab.
Attn: Mr. D. Lillie
P. O. Box 1088
Schenectady, N. Y.

General Telephone and Electronics Labs, Inc.
Bayside Labs.
Attn: Dr. C. D. Dickinson
Bayside 60
Long Island, N. Y.

University of Illinois
Dept. of Metallurgical Engineering
Attn: Prof. P. A. Beck
Urbana, Ill.

Dr. Walter S. Owen
(Dept. of Metallurgy
University of Liverpool
Liverpool 3, England)
c/o Commander
Aeronautical Systems Division
Attn: ASYF (Mr. J. M. Troyan)
Wright-Patterson AFB, Ohio

Lockheed Aircraft Corp.
MSVD Research Lab.
Attn: Dr. T. E. Tietz
Palo Alto, Calif.

MIT
Dept. of Metallurgy
Attn: Dr. Morris Cohen
Cambridge 39, Mass.

Massachusetts Institute of Technology
Dept. of Metallurgy
Attn: Prof. N. J. Grant
Cambridge, Mass.

MIT
Dept. of Metallurgy
Attn: Dr. David A. Thomas
Cambridge 39, Mass.

Materials Research Corp.
Attn: Dr. M. Adams
47 Buena Vista Ave.
Yonkers, N. Y.

Materials Research Lab., Inc.
Attn: Dr. E. J. Ripling
22333 Governors Highway
Richton Park, Ill.

National Academy of Sciences
MAB
Attn: Dr. J. R. Lane
Washington 25, D. C.

University of Michigan
Research Institute
Attn: Dr. J. W. Freeman
2211 East Engineering Bldg.
Ann Arbor, Mich.

National Research Corp.
Attn: Dr. M. L. Torti
70 Memorial Drive
Cambridge 42, Mass.

Chief, Bureau of Naval Weapons
Department of the Navy
Attn: Mr. N. E. Promisel
Washington 25, D. C.

Chief
Office of Naval Research
Attn: Dr. Salkowitz
Metallurgy Branch
Washington, D. C.

Nuclear Metals, Inc.
Attn: Dr. Stanley Gelles
Concord, Mass.

Oak Ridge National Labs.
Metallurgy Laboratory
Attn: Dr. C. J. McHargue
P. O. Box 212
Oak Ridge, Tenn.

Office of Scientific Research
Attn: Mr. C. Yost
Washington, D. C.

The Ohio State University
Dept. of Metallurgical Engineering
Attn: Prof. J. W. Spretnak
Columbus, Ohio

Pratt and Whitney Aircraft
Metallurgy Dept.
Attn: Mr. G. H. Rowe
CANEL
Middletown, Conn.

E. D. Weisert
Research and Engineering
Rocketdyne
Canoga Park, Calif.

Rutgers, The State University
Bureau of Engineering Research
Attn: Dr. S. Weissmann
New Brunswick, N. J.

Sandia Corporation
Department 5130
Attn: Mr. J. R. Holland
Sandia Base
Albuquerque, New Mexico

Prof. A. G. Quarrell
(Department of Metallurgy
St. George's Square
Sheffield 1, England)
c/o Commander
Aeronautical Systems Division
Attn: ASYF (Mr. J. M. Troyan)
Wright-Patterson AFB, Ohio

Commanding Officer
Springfield Armory
Attn: TIU
Springfield 1, Mass.

Stanford University
Department of Materials Science
Attn: B. A. Wilcox
Stanford, Calif.

Thompson-Ramo Wooldridge
Attn: Dr. A. Nemy
23555 Euclid Ave.
Cleveland 17, Ohio

Union Carbide Metals Co.
Metals Research Labs.
Attn: Dr. R. W. Fountain
P. O. Box 580
Niagara Falls, N. Y.

Westinghouse Electric Corp.
Lamps Division
Attn: Dr. R. H. Atkinson
Bloomfield, N. J.

Westinghouse Electric Corp.
Research Labs.
Attn: R. T. Begley
Beulah Road
Pittsburgh 35, Penn.

Aerojet-General Corporation
Attn: J. E. Herring
Technical Library
Bldg. 2015 Dept. 2410
P. O. Box 1947
Sacramento 9, California

Professor B. A. Bilby
Department of Metallurgy
The University
St. George's Square
Sheffield 1, England

General Electric Co.
Attn: Mr. D. P. Petarra
Large Lamp Division
Advance Engineering #437
Nela Park
Cleveland 12, Ohio

Martin-Marietta Company
Attn: Dr. Irving Kramer
Baltimore 3, Maryland

Sandia Corp.
Attn: J. Read Holland
Div. S132
Physical Research Dept.
Sandia Base
Albuquerque, New Mexico